LEVEL II (12)

(6) MOMENT METHOD CALCULATION OF REFLECTION COEFFICIENT FOR WAVEGUIDE ELEMENTS IN A FINITE PLANAR PHASED ANTENNA ARRAY

(10) A. J. Fenn
G. A. Thiele
B. A. Munk

The Ohio State University
ElectroScience Laboratory
Department of Electrical Engineering
Columbus, Ohio 43212

(9) Doctoral thesis,

TECHNICAL REPORT 784372-7

(15) Contract N00014-76-C-0573

(11) September 1978

(12) 249 p.

(14) ESL-784372-7

Department of the Navy
Office of Naval Research
800 N. Quincy Street
Arlington, Virginia 22217

NOTICES

When Government drawings, specifications, or other data are used for any purpose other than in connection with a definitely related Government procurement operation, the United States Government thereby incurs no responsibility nor any obligation whatsoever, and the fact that the Government may have formulated, furnished, or in any way supplied the said drawings, specifications, or other data, is not to be regarded by implication or otherwise as in any manner licensing the holder or any other person or corporation, or conveying any rights or permission to manufacture, use, or sell any patented invention that may in any way be related thereto.

UNCLASSIFIED

SECURITY CLASSIFICATION OF THIS PAGE (When Data Entered)

REPORT DOCUMENTATION PAGE | READ INSTRUCTIONS BEFORE COMPLETING FORM

1. REPORT NUMBER
2. GOVT ACCESSION NO.
3. RECIPIENT'S CATALOG NUMBER

4. TITLE (and Subtitle)
MOMENT METHOD CALCULATION OF REFLECTION COEFFICIENT FOR WAVEGUIDE ELEMENTS IN A FINITE PLANAR PHASED ANTENNA ARRAY

5. TYPE OF REPORT & PERIOD COVERED
Technical Report

6. PERFORMING ORG. REPORT NUMBER
ESL 784372-7

7. AUTHOR(s)
A. J. Fenn
G. A. Thiele
B. A. Munk

8. CONTRACT OR GRANT NUMBER(s)
Contract N00014-76-C-0573

9. PERFORMING ORGANIZATION NAME AND ADDRESS
The Ohio State University ElectroScience Laboratory, Department of Electrical Engineering, Columbus, Ohio 43212

10. PROGRAM ELEMENT, PROJECT, TASK AREA & WORK UNIT NUMBERS
Project No. NR 371-108/12-29-77 (427)

11. CONTROLLING OFFICE NAME AND ADDRESS
Department of the Navy, Office of Naval Research
800 N. Quincy Street
Arlington, Virginia 22217

12. REPORT DATE
September 1978

13. NUMBER OF PAGES
242

14. MONITORING AGENCY NAME & ADDRESS (if different from Controlling Office)

15. SECURITY CLASS (of this report)
Unclassified

15a. DECLASSIFICATION DOWNGRADING SCHEDULE

16. DISTRIBUTION STATEMENT (of this Report)

17. DISTRIBUTION STATEMENT (of the abstract entered in Block 20, if different from Report)

18. SUPPLEMENTARY NOTES
The material contained in this report is also used as a dissertation submitted to the Department of Electrical Engineering, The Ohio State University as partial fulfillment for the degree Doctor of Philosophy.

19. KEY WORDS (Continue on reverse side if necessary and identify by block number)
Phased arrays
Waveguide
Moment Method
Reflection coefficient

20. ABSTRACT (Continue on reverse side if necessary and identify by block number)

A technique is presented for determining the aperture reflection coefficients for E-plane and H-plane scanned finite planar phased antenna arrays. The array elements are rectangular waveguide-fed apertures arranged in either a rectangular or triangular lattice and are located in an infinite ground plane. The formulation is such that an iris may be present at the waveguide-half space junction and the waveguides may be completely filled with dielectric. The method of moments is used to solve an integral equation for

over

DD FORM 1473, 1 JAN 73 EDITION OF 1 NOV 65 IS OBSOLETE

UNCLASSIFIED

SECURITY CLASSIFICATION OF THIS PAGE (When Data Entered)

20.

the unknown equivalent magnetic current distribution of each aperture.

For arrays with elements located in a rectangular lattice the block Toeplitz admittance matrix property is used in solving the system of equations. The expansion functions that are used to approximate the equivalent magnetic current in each aperture are a column of adjacent rectangular surface patches with piecewise sinusoidal-uniform distribution for arrays with apertures of lengths less than $.6\lambda$.

Numerous results are presented that illustrate how the various elements in a finite array behave during various scan conditions. Rectangular grid arrays of size 3x3 to 27x27 are analyzed for various numbers of expansions. The results show that the aperture distributions of the edge elements differ greatly from that of the TE_{10} mode. The coupling due to the edge elements is shown to significantly affect the center element reflection coefficient.

ACKNOWLEDGMENTS

The authors wish to express their sincere gratitude to Professor J. H. Richmond and Dr. N. N. Wang for their many helpful and interesting discussions, as well as to Professor W. H. Peake for reviewing the manuscript.

The material contained in this report is also used as a dissertation submitted to the Department of Electrical Engineering, The Ohio State University as partial fulfillment for the degree Doctor of Philosophy.

TABLE OF CONTENTS

CHAPTER I
INTRODUCTION

A periodic planar phased array antenna is made up of radiating elements that are identical in geometry and are arranged in a planar and doubly periodic lattice. The periodic nature of phased arrays lends itself to radiation patterns which can be scanned electronically in microseconds. This is accomplished by exciting adjacent elements of the array with appropriate constant incremental phase shifts. Phased array antennas have the important property that the beam pattern of the array is the same whether it is operating as a transmitter or receiver. This feature makes phased array antennas a practical device for radar systems. Due to the agility of the phased array beam, the number of targets which a radar system can detect and track is increased over that of conventional antennas. Improvements in phase shifters such as semiconductor diodes offers increased accuracy and reliability of the array[1].

Most phased array analysis to date has used infinite array techniques to analyze "large" finite arrays. In large planar arrays the majority of the inner core elements behave nearly uniformly. Important characteristics of the large array can be approximated well by modeling it with an infinite array whose elements exhibit a uniform behavior throughout the array[2]. As the large finite array becomes smaller the infinite array model will tend to be invalid. This is due to the radiation and reflection characteristics of elements of the array being strongly dependent on their location. An approximation to the behavior of a finite array can be obtained by using infinite array techniques when only a finite number of elements are excited in an infinite array environment, as done by Amitay, Galindo, and Wu[3]. In "classical" array theory finite arrays are analyzed by neglecting the mutual coupling between array elements. The resulting array beam pattern is expressed as a product of the array factor and the pattern function of an array element[4]. In general, mutual coupling between array elements cannot be ignored.

This paper considers the effects of mutual coupling in finite rectangular grid phased arrays of rectangular and square waveguides in an infinite ground plane. The problem is formulated using the equivalence principle and the method of moments to obtain an approximation to the aperture distribution of each element of the array. The aperture distribution is then used to obtain the scattered field in the waveguide from which the aperture reflection coefficient of a single element can be obtained. Chapter II first discusses the general formulation for single aperture coupling.

In Chapter III the formulation is specialized to the case of a single probe-fed cavity-backed slot antenna in an infinite ground plane. Reflection coefficients for square and rectangular waveguide-fed apertures are computed and compared against data in the literature. In Chapter IV the formulation is extended to analyze a finite array of waveguide-fed apertures in an infinite ground plane. A recent paper by Luzwick and Harrington has also considered this problem[5]. Results are presented for the reflection coefficients of elements in finite phased arrays of size M x M, where M is odd. The reflection coefficient data presented will be for arrays with zero waveguide wall thickness. Since the method is not restricted to zero waveguide wall thickness, the effect of finite wall thickness is also examined.

CHAPTER II
GENERAL FORMULATION FOR ANALYZING APERTURE COUPLING BETWEEN TWO REGIONS

A. Introduction

In this chapter a formulation for determining the aperture coupling between two arbitrary regions will be presented. The formulation closely follows work done by Harrington and Mautz[6] on general aperture coupling and is included for completeness. The problem is formulated using the equivalence principle to obtain an operator equation for the unknown aperture distribution. The method of moments is then used to solve the operator equation for an approximate solution to the aperture distribution. A discussion of the method of moments[7,8] (also referred to as the method of weighted residuals) is presented in Appendix F for completeness. The importance in determining the aperture distribution is that from it the reflection and transmission properties of the aperture can be determined. It is inherent in the formulation that the aperture coupling is represented by the sum of two independent admittance matrices, one for each region. Some examples of problems that can be solved using this formulation are apertures in a conducting screen, waveguide-fed apertures, cavity-fed apertures, waveguide-to-waveguide coupling, waveguide-to-cavity coupling and cavity-to-cavity coupling.

B. Theory

In this section the general problem of aperture coupling between two regions is considered. Figure 2-1 shows two regions a and b coupled by an aperture. Region a contains impressed electric and magnetic sources $(\bar{J}_i, \bar{M}_i)$ and region b is assumed source free (if sources were present in both regions the problem could be analyzed by using superposition). Region a is shown closed and region b is shown open, but in general each region may be open or closed. By the equivalence principle[9] the total field in region a is produced by the impressed sources $(\bar{J}_i, \bar{M}_i)$, plus the equivalent magnetic current

$$\bar{M}_s = \bar{E} \times \hat{n} \qquad (2\text{-}1)$$

over the aperture region, with the aperture covered by a perfect electric conductor. In Equation (2-1) $\bar{E}$ is the total electric field and n is the unit normal to the aperture. The total field in region b is generated by the equivalent magnetic current $-\bar{M}_s$ over the aperture region, with the aperture covered by a perfect

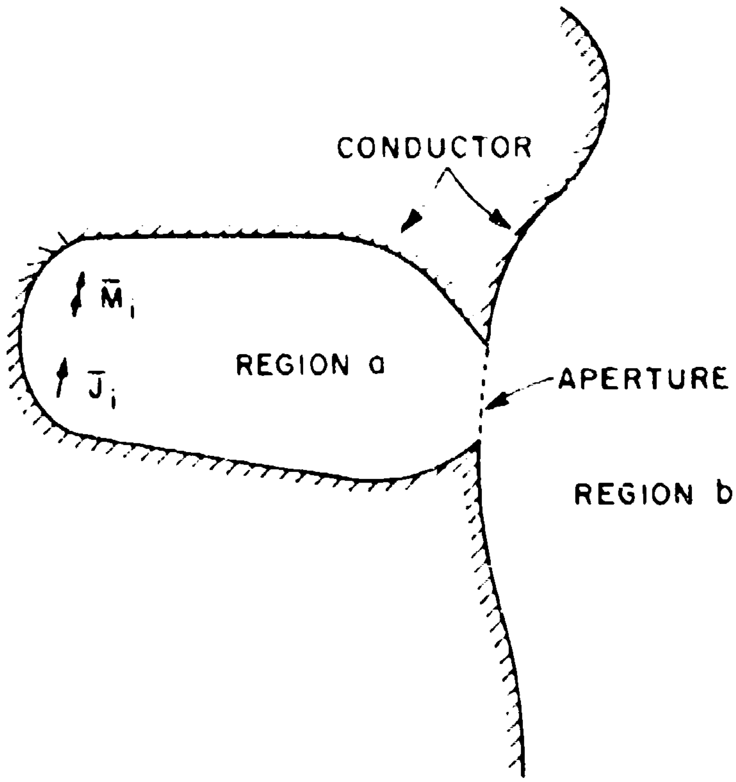

Figure 2-1. General aperture coupling between two regions.

electric conductor. The equivalent situations for regions a and b are shown in Figure 2-2. The magnetic currents $\bar{M}_s$ and $-\bar{M}_s$ satisfy the condition that the tangential component of the electric field be continuous across the aperture. An operator equation involving the unknown current $\bar{M}_s$ can be obtained by satisfying the remaining boundary condition that the tangential component of the magnetic field be continuous across the aperture.

The contribution to the tangential component of the magnetic field in region a, denoted by $\bar{H}_t^a$, over the aperture is from the incident field $\bar{H}_t^i$ due to the impressed sources $(\bar{J}_i, \bar{M}_i)$ and the scattered field $\bar{H}_t^a(\bar{M}_s)$ which is found by some operation on the equivalent source $\bar{M}_s$, that is,

$$\bar{H}_t^a = \bar{H}_t^i + \bar{H}_t^a (\bar{M}_s) \quad . \qquad (2-2)$$

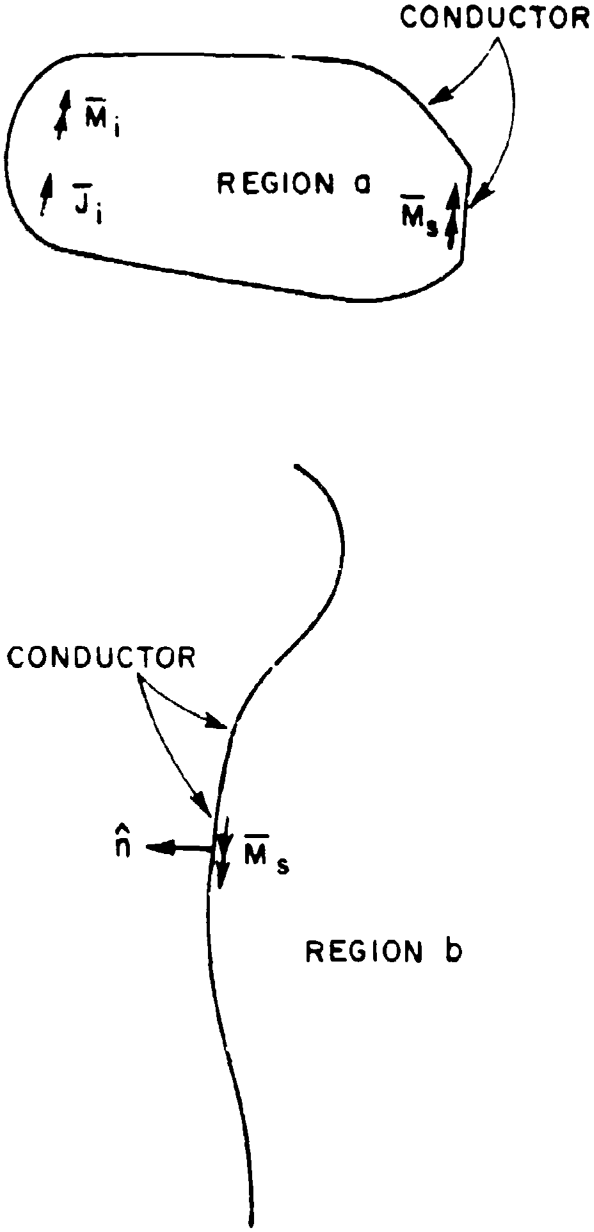

Figure 2-2. Equivalent situations for regions a and b.

In Equation (2-2) the incident and scattered fields are both computed with a perfect electric conductor covering the aperture. In region b the tangential component of the magnetic field over the aperture is due to the equivalent source $-\overline{M}_s$, that is,

$$\overline{H}_t^b = \overline{H}_t^b(-\overline{M}_s) = -\overline{H}_t^b(\overline{M}_s) \quad . \tag{2-3}$$

In Equation (2-3) linearity of the $\overline{H}_t^b$ operator was used and $\overline{H}_t^b(\overline{M}_s)$ is calculated with a perfect electric conductor covering the aperture. Enforcing the boundary condition that the tangential component of the magnetic field be continuous across the aperture is done by setting Equation (2-2) equal to Equation (2-3) resulting in

$$\overline{H}_t^a(\overline{M}_s) + \overline{H}_t^b(\overline{M}_s) = -\overline{H}_t^i \quad . \tag{2-4}$$

Equation (2-4) is the desired operator equation for determining the equivalent magnetic current $\overline{M}_s$.

The true solution for the magnetic current $\overline{M}_s$ would be obtained if the equality in Equation (2-4) were satisfied exactly. As shown in Appendix F, the method of weighted residuals can be used to solve operator equations of the form of Equation (2-4) approximately. An approximation for the current $\overline{M}_s$ is obtained by using the trial function expansion

$$\overline{M}_a = \sum_{n=1}^{N} V_n \frac{\overline{M}_n}{K^{(n)}} \simeq \overline{M}_s \tag{2-5}$$

where $\overline{M}_n$ is referred to as a trial function, expansion function, or basis function,

$K^{(n)}$ is the terminal current in volts which normalizes $\overline{M}_n$ and is found by integrating over the width of $\overline{M}_n$ at it's terminals (thus, $\overline{M}_n/K^{(n)}$ is a "normalized" basis function),

V_n is the unknown coefficient in volts associated with $\overline{M}_n$ to be determined, and

N is the number of unknowns.

Substituting Equation (2-5) into Equation (2-4) and using linearity, the residual is now defined over the aperture region as

$$\overline{R} = \sum_{n=1}^{N} V_n \frac{\overline{H}_t^a(\overline{M}_n)}{K^{(n)}} + \sum_{n=1}^{N} V_n \frac{\overline{H}_t^b(\overline{M}_n)}{K^{(n)}} + \overline{H}_t^i \quad . \tag{2-6}$$

Define a set of normalized weighting or testing functions $\overline{M}_m/K^{(m)}$, $m=1,2,\ldots,N$ equal to the normalized expansion functions (Galerkin's method[10]) and an inner product

$$\langle \overline{M}, \overline{H} \rangle = - \iint_{\text{aperture}} \overline{M} \cdot \overline{H}\, ds. \tag{2-7}$$

The residual is now minimized by taking the inner product of the normalized weighting functions $\overline{M}_m/K^{(m)}$ with the residual and setting it equal to zero. This results in the simultaneous equations

$$\sum_{n=1}^{N} V_n \frac{\langle \overline{M}_m, \overline{H}_t^a(\overline{M}_n) \rangle}{K^{(m)}K^{(n)}} + \sum_{n=1}^{N} V_n \frac{\langle \overline{M}_m, \overline{H}_t^b(\overline{M}_n) \rangle}{K^{(m)}K^{(n)}} = - \frac{\langle \overline{M}_m, \overline{H}_t^i \rangle}{K^{(m)}}$$

$$m=1,2,\ldots N. \tag{2-8}$$

Recognizing the quantities $\frac{\langle \overline{M}_m, \overline{H}_t^a(\overline{M}_n) \rangle}{K^{(m)}K^{(n)}}$ and $\frac{\langle \overline{M}_m, \overline{H}_t^b(\overline{M}_n) \rangle}{K^{(m)}K^{(n)}}$ as admittances (since they have units of mhos) and the quantity $- \frac{\langle \overline{M}_m, \overline{H}_t^i \rangle}{K^{(m)}}$ as current (since it has units of amperes) enables Equation (2-8) to be written as

$$\sum_{n=1}^{N} V_n (Y_{mn}^a + Y_{mn}^b) = I_m \qquad m=1,2,\ldots,N \quad . \tag{2-9}$$

In matrix notation the solution for the coefficients V_n in volts becomes, by matrix inversion,

$$(V) = [\,[Y^a] + [Y^b]\,]^{-1}\,(I) \quad . \tag{2-10}$$

These coefficients are then substituted into Equation (2-5) to determine $\overline{M}_s$. Once $\overline{M}_s$ has been found, standard methods can be used to compute the fields in regions a and b.

Due to the way the problem was formulated the two admittance matrices in Equation (2-10) are independent. Thus, $[Y^a]$ is computed from the characteristics of region a and $[Y^b]$ is computed from the characteristics of region b.

In Chapter III the above formulation will be applied to the problem of calculating the aperture reflection coefficient of probe-fed cavity-backed slot antennas. In Chapter IV the method will be extended to handle finite arrays of waveguide-fed apertures in an infinite ground plane.

CHAPTER III
APERTURE REFLECTION COEFFICIENT OF A SINGLE WAVEGUIDE-FED APERTURE IN AN INFINITE GROUND PLANE

A. Introduction

This chapter considers a calculation of the TE_{mn} aperture reflection coefficient for a probe-fed rectangular waveguide opening into an infinite ground plane, as shown in Figure 3-1. In this paper the long dimension of the rectangular aperture is referred to as the aperture length (H-plane), while the narrow dimension is referred to as the aperture width (E-plane). Using the theory discussed in Chapter II the induced aperture distribution can be found due to the probe source. This aperture distribution is used to calculate the scattered field in the waveguide. The reflection coefficient is found by taking the ratio of the reflected and incident fields at the midpoint of the aperture. First, the theory for analyzing the general case of a waveguide with an iris at the aperture will be presented. Reflection coefficient data and aperture distributions will then be shown for waveguides of various sizes with no iris and compared against data in the literature.

B. Theory

Figure 3-2 shows a probe-fed rectangular waveguide with an iris in an infinite ground plane. The probe is a linear monopole with height h and is located a distance d from the aperture and c to the back wall. With reference to Figure 2-1 the rectangular waveguide is designated by region wg (a) and the half space by region hs (b). As was done in Chapter II (for general aperture coupling) the rectangular aperture is first covered with a perfect conductor. Next, applying the equivalence principle and boundary conditions at the aperture results in the equivalent situations for regions wg and hs shown in Figure 3-3. The equivalent magnetic surface current is related to the total electric field in the aperture by

$$\overline{M}_s = \overline{E} \times \hat{n} \qquad (3\text{-}1)$$

where $\hat{n}$ is the unit normal to the aperture. Since the electric field is z-directed and the unit normal y-directed the equivalent magnetic current will have only a x component. Due to the probe orientation the tangential component of the magnetic field is x-directed. It is desired to solve for the unknown magnetic current $\overline{M}_s$ in order to calculate the scattered magnetic field in the waveguide $\overline{H}^{wg}(\overline{M}_s)$. The magnetic current is approximated by

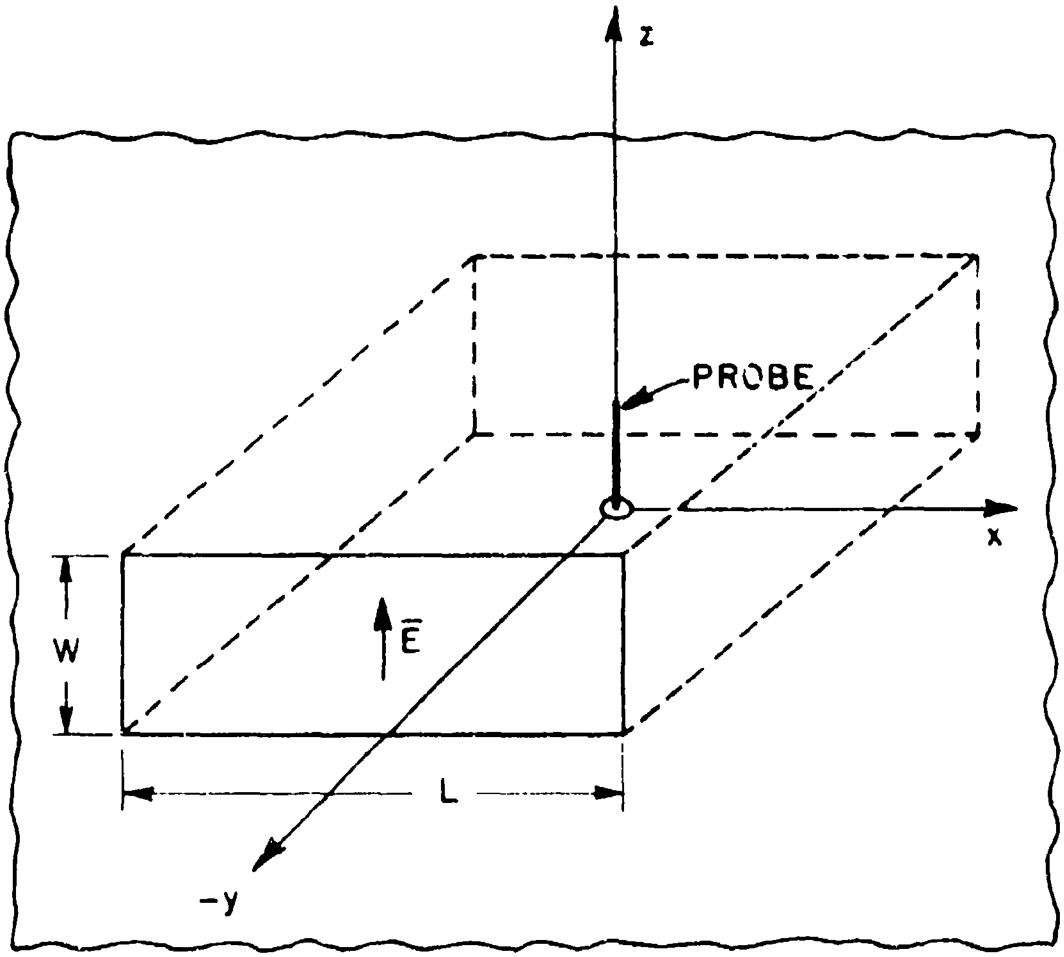

Figure 3-1. A probe-fed cavity-backed slot antenna in an infinite ground plane.

$$\bar{M}_s = \sum_{n=1}^{N} V_n \frac{\bar{M}_n}{K^{(n)}} \qquad (3\text{-}2)$$

where,

$\bar{M}_n$ is an expansion (or basis) function,

$K^{(n)}$ is the terminal current value which normalizes $\bar{M}_n$,

V_n is the unknown complex coefficient associated with $\bar{M}_n$, and

N is the number of expansion functions used to approximate $\bar{M}_s$ in the aperture.

A good choice for the expansion functions is one that satisfies the boundary conditions of $\bar{M}_s$ at the edges of the aperture. In Figure 3-2 at $x = \pm L_i/2$ the equivalent magnetic current must be zero since the incident electric field is parallel to the edge (total tangential $\bar{E}$ is zero at a perfect electric conductor). At $z = d_i$ and $z = d_i + W_i$ the equivalent magnetic current is parallel to the edge and has a singularity inversely proportional to the square root of the distance to the edge. Over the rest of the aperture region the expansion functions should be able to approximate higher order modes if the need arises. A set of basis functions, which is a good approximation to the above conditions, is overlapping rectangular surface dipoles with piecewise-sinusoidal current distribution along the direction of current flow and uniform (also referred to as rectangular pulse) distribution in the direction transverse to current flow. Figure 3-4 shows an example expansion of $\bar{M}_s$ where three rows of five overlapping piecewise-sinusoidal uniform basis functions cover the aperture. The overlapping piecewise-sinusoidal functions can provide a current distribution which is zero at the ends and arbitrary over the remaining interval (if enough functions are used). The adjacent uniform functions yield a current distribution which is an approximation to the singularity at the edge and arbitrary over the remaining interval (if enough functions are used). A typical expansion function with half-length ℓ and width w can be expressed as

$$\bar{M}_n = \hat{x} K_n \frac{\sin \beta(\ell - |x'|)}{\sin \beta\ell} \qquad \begin{matrix} -\ell < x' < \ell \\ 0 < z' < w \end{matrix} \qquad (3\text{-}3)$$

where K_n is a complex coefficient. Using the definition of terminal current $K^{(n)}$ in Chapter II, it follows from Equation (3-3) that

$$K^{(n)} = \int_0^w \bar{M}_n(0)dz = wK_n .$$

Now that a suitable set of expansion functions have been determined Equation (2-8) can be applied. This results in the set of simultaneous equations involving V_n

$$\sum_{n=1}^{N} V_n \left(\frac{\langle \bar{M}_m, \bar{H}_x^{wg}(\bar{M}_n) \rangle}{K^{(m)}K^{(n)}} + \frac{\langle \bar{M}_m, \bar{H}_x^{hs}(\bar{M}_n) \rangle}{K^{(m)}K^{(n)}} \right) = - \frac{\langle \bar{M}_m, \bar{H}_x^{i} \rangle}{K^{(m)}} \qquad (3\text{-}4)$$

$$m = 1,2,\ldots N$$

where

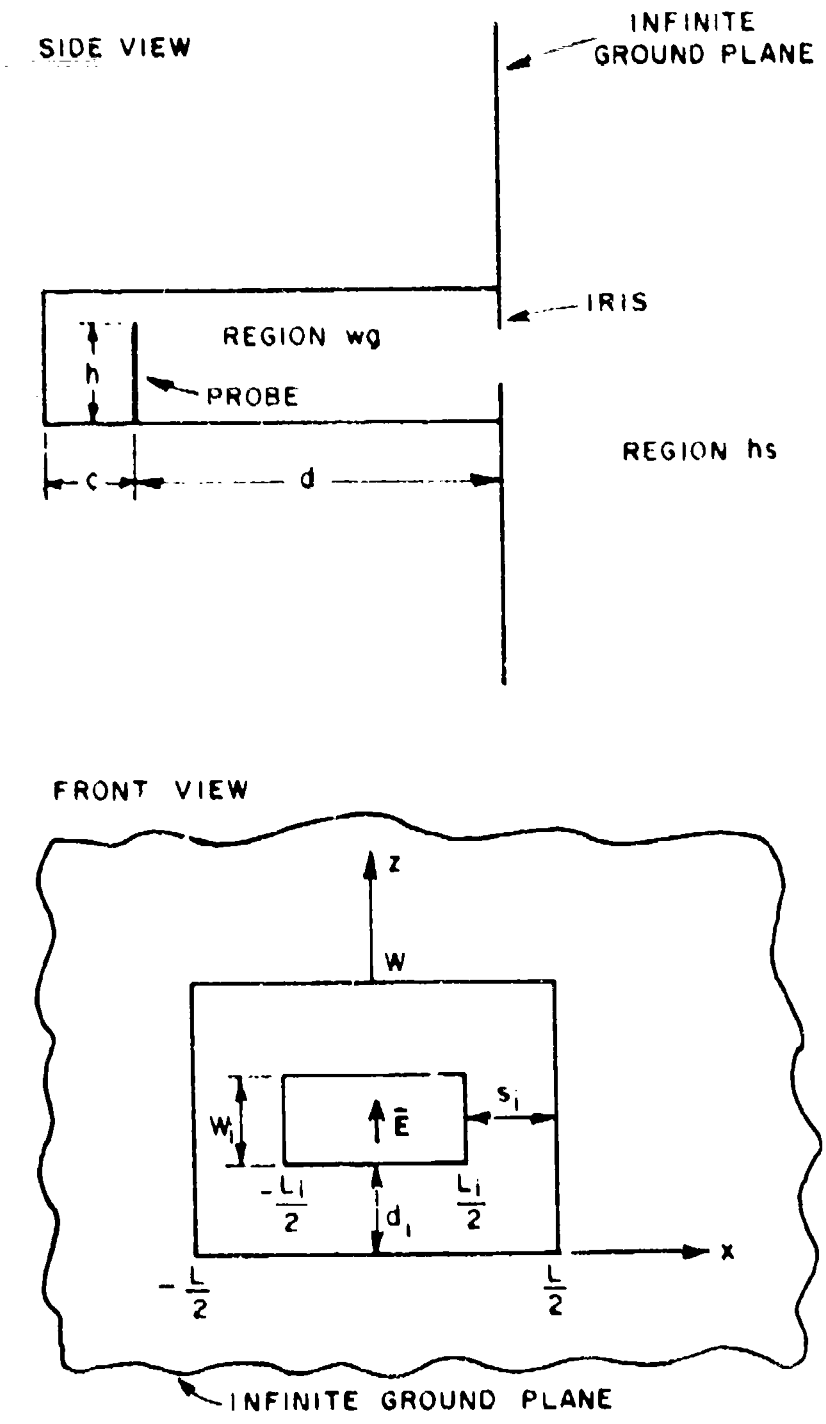

Figure 3-2. Rectangular waveguide-fed aperture with an iris.

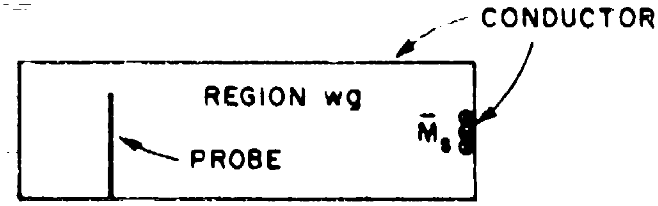

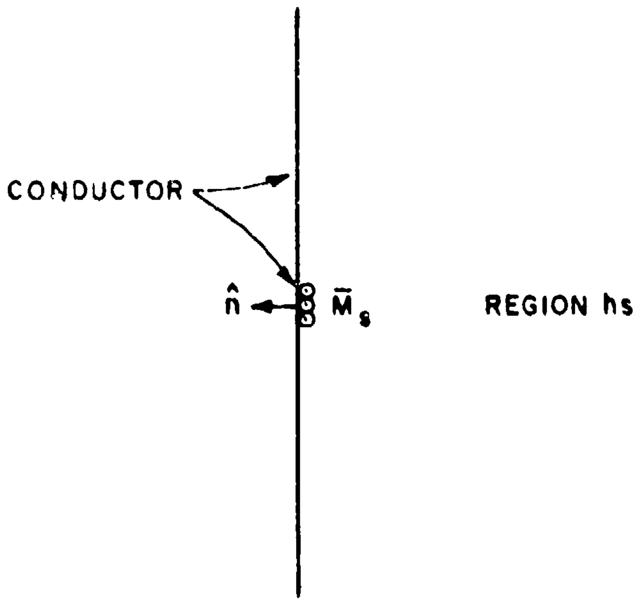

Figure 3-3. Equivalent situations for regions wg and hs.

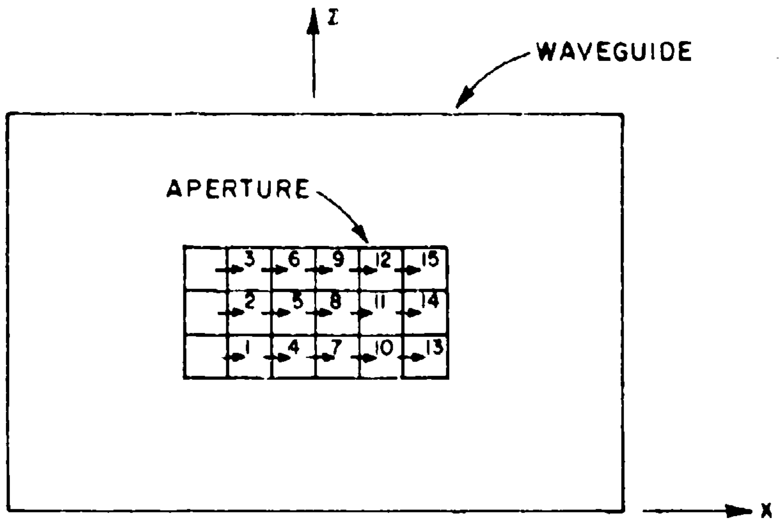

Figure 3-4. Expanding the unknown magnetic current $\overline{M}_s$ into three adjacent rows of five overlapping piecewise sinusoidal-uniform functions.

$$\langle \overline{M},\overline{H} \rangle = - \iint_{\text{surface}} \overline{M} \cdot \overline{H} \; dx\, dz, \qquad (3\text{-}5)$$

$Y^{wg}_{mn} = \dfrac{\langle \overline{M}_m, \overline{H}^{wg}_x(\overline{M}_n) \rangle}{K^{(m)}K^{(n)}}$ is the mutual admittance between basis functions m and n in the presence of the waveguide walls with the aperture covered by a perfect conductor,

$Y^{hs}_{mn} = \dfrac{\langle \overline{M}_m, \overline{H}^{hs}_x(\overline{M}_n) \rangle}{K^{(m)}K^{(n)}}$ is the mutual admittance between basis functions m and n in the half-space region with the aperture covered with a perfect electric conductor,

$\overline{H}^i_x$ is the incident field due to the probe source in the rectangular cavity-backed waveguide, and

$I_m = - \dfrac{\langle \overline{M}_m, \overline{H}^i_x \rangle}{K^{(m)}}$ is the current excitation.

An expression for the current excitation is derived in detail in Appendix E. The result is, from Equation (E-15)

$$I_m = \frac{I_0}{2\beta^3 LWw} \sum_{n_2=-\infty}^{\infty} \sum_{n_1=-\infty}^{\infty} P_1(n_1) P_2^t(n_1,n_2)\, e^{-j\beta d r_y^i} \left(1 - e^{-j\beta 2 c r_y^i}\right)$$

$$\cdot\, e^{j2\pi(n_2 + \frac{1}{2}) \frac{x'}{L}}\; e^{j n_1 \pi \frac{z'}{W}} \qquad (3\text{-}6)$$

where x' and z' are the shifts of expansion m from $x=0$ and $z=0$, respectively,

I_0 is the terminal current for the probe and is assumed to be one ampere,

$$r_y^i = \sqrt{1 - \left(n_1 \frac{\lambda}{2W}\right)^2 - \left((n_2 + \tfrac{1}{2}) \frac{\lambda}{L}\right)^2},$$

$$[illegible]_1) = \frac{2\left[\cos\left(n_1 \pi \frac{h}{W}\right) - \cos\beta h\right]}{1 - \left(n_1 \frac{\lambda}{2W}\right)^2}, \text{ and}$$

$P_2^t = P_2^*$ (means conjugate)

$$P_2(n_1,n_2) = \frac{4}{\sin \beta \ell}\, e^{j n_1 \pi \frac{w}{2W}} \frac{\sin\left(\beta \frac{w}{2}\left(n_1 \frac{\lambda}{2W}\right)\right)}{n_1 \frac{\lambda}{2W}}$$

$$\cdot \frac{\left[\cos\left(2\pi \frac{\ell}{L}(n_2 + \frac{1}{2})\right) - \cos\beta\ell\right]}{1 - \left(\frac{\lambda}{D_x^i}(n_2 + \frac{1}{2})\right)^2}$$

where $w = \frac{W_i}{N_w}$,

$\ell = \frac{L_i}{N}$,

$\beta = \frac{2\pi}{\lambda}$ is the propagation constant,

$N_\ell - 1$ is the number of overlapping piecewise sinusoidal expansion functions chosen along the length (H-plane) of the aperture, and

N_w is the number of adjacent rectangular pulse expansion functions chosen along the width (E-plane) of the aperture.

Equation (3-6) represents a plane wave expansion for the current excitation due to all modes, both propagating and evanescent, that are incident upon the aperture. The two infinite sums on the integers n_1 and n_2 include all these contributions. Values of n_1 and n_2 which make r_y real and imaginary correspond to propagating and evanescent modes, respectively. The TE_{mn}th mode current excitation can be identified by observing the phase factor

$$e^{j2\pi\left(n_2+\frac{1}{2}\right)\frac{x'}{L}} \quad e^{jn_1\pi\frac{z'}{W}}$$

in Equation (3-6) and choosing the proper pair of plane waves. For example, $n_1=0$ and $n_2=0,-1$ corresponds to the TE_{10} mode current excitation. Other mode contributions are found similarly.

The half-space mutual admittances in Equation (3-4) are found by taking the dual[11] of the mutual impedance between two electric surface sources in free space (divide Z_{mn} by η_o, η_o is the free space impedance) and multiplying the result by two. The factor of two arises because the magnetic surface sources exist on a perfect electric conductor which (by image theory) doubles their field contributions. Thus,

$$Y_{mn}^{hs} = \frac{2Z_{mn}^{\text{free space}}}{\eta_o^2} \qquad (3\text{-}7)$$

where $\eta_o = 120\pi$ ohms.

The mutual impedance $Z_{mn}^{\text{free space}}$ between two piecewise sinusoidal-uniform electric surface sources is derived in Appendix C and can be calculated from Equation (C-21). The calculation is done by a single integration which can be performed numerically on the computer.

The calculation of the waveguide mutual admittance in Equation (3-4) is more involved than the half-space mutuals b[illegible]ause position in the waveguide is important. By using image theo[illegible] the waveguide mutual admittance calculation can be handled with infinite array techniques. (There are other equivalent ways of calculating the waveguide mutual admittance, for example by modal expansion as done

by Mautz and Harrington[13].) The calculations are done using a quickly converging series that is derived in Appendix D. To demonstrate the method consider the waveguide with an iris shown in Figure 3-2. The unknown magnetic current $\overline{M}_s$ is expanded in nine unknowns, three along the length and three along the width. For this case the waveguide admittance matrix will be a 9 x 9 symmetric matrix. For the mutual Y^{wg}_{mn} the subscript m will refer to the observation exterior element. The subscript n will refer to the reference source element. To show how infinite arrays are introduced into the problem, three representative calculations of the waveguide mutual admittances will now be given. First, consider the calculation of element $Y^{wg}_{1,9}$ shown in Figure 3-5. The reference element is imaged into the waveguide walls (the walls are then removed) resulting in four infinite arrays of rectangular magnetic surface sources. These equivalent sources satisfy the boundary conditions for the fields where the waveguide walls were located. Elements of the four arrays are identified by the Roman numeral I, II, III, or IV. The exterior element is shown circled for emphasis. By superposition it follows that

$$Y^{wg}_{1,9} = 2\left[Y_{1I} + Y_{1II} + Y_{1III} + Y_{1IV}\right] \qquad (3\text{-}8)$$

where $Y_{1(I,II,III,IV)}$ is the mutual admittance between the exterior element and infinite array (I,II,III,IV). The factor of two is used to account for the perfect conductor. Thus, an expression for calculating the mutual admittance between an exterior magnetic surface source and infinite array of magnetic surface sources is required. Such an expression is derived in detail in Appendix D, the result given by Equation (D-11). The direction cosines s_x and s_z in Equation (D-11) are determined for this case in the following manner: Since the current direction along elements does not change, set the Floquet current factor

$$e^{-j\beta k D_z s_z} = 1 \qquad \text{(see Equation (A-7))}$$

or $\quad \beta k D_z s_z = 0$

so $\quad s_z = 0$

where D_z is the interelement spacing in the z direction. Similarly set the Floquet current factor

$$e^{-j\beta n D_x s_x} = 1 \qquad \text{(see Equation (A-7)}$$

or $\quad nD_x s_x = 0$

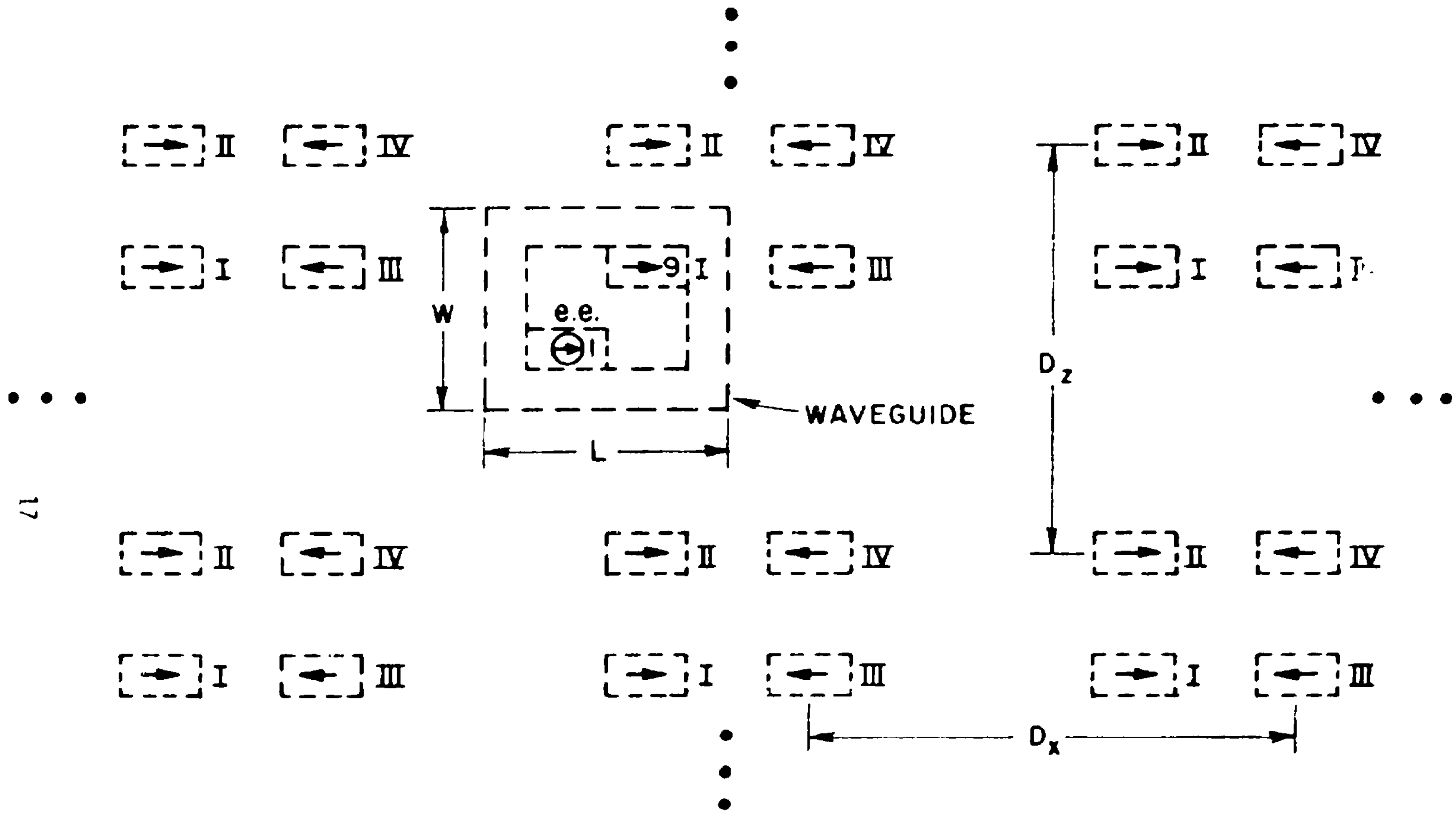

Figure 3-5. Imaging reference element number nine in the waveguide walls results in four infinite arrays.

so $s_x = 0$

where D_x is the interelement spacing in the x direction. From Figure 3-5 it is observed that $D_x = 2L$ and $D_z = 2W$. Note that Equation (D-11) was derived for an exterior element and a reference source with the same current vector sign. Thus, in the calculation of Y_{1III} and Y_{1IV} using Equation (D-11) the final result must be multiplied by -1. Next, consider the calculation of element $Y^{wg}_{1,6}$ shown in Figure 3-6. Since the reference element is located at the midpoint along the length of the waveguide, only two infinite arrays arise this time when image theory is used. Elements of the two arrays are identified by the Roman numerals I or II. By superposition it is clear that

$$Y^{wg}_{1,6} = 2\left[Y_{1I} + Y_{1II}\right] \qquad (3\text{-}9)$$

Equation (D-11) applies with $D_z = 2W$ and $s_z = 0$ as before. For this case $D_x = L$ and since the current vector changes sign periodically set $e^{-j\beta n D_x s_x} = (-1)^n$

or $\beta n D_x s_x = n\pi$

so $s_x = \dfrac{\lambda}{2D_x}$.

As a final example consider the calculation of $Y^{wg}_{1,5}$ shown in Figure 3-7. Since the reference element is located at the midpoint of the waveguide cross section only one array arises when image theory is used. Equation (D-11) is applied with $D_x = L$, $D_z = W$, $s_z=0$, and $s_x = \lambda/2D_x$. The remaining elements of the waveguide admittance matrix are calculated similarly. As a check on the waveguide mutual admittance (given by Equation (D-11) an infinite waveguide can be used as a test case. In Appendix G it is shown that for the TE_{10} mode propagating in an infinite waveguide the reflection coefficient is zero, as it should be.

Upon calculating all the elements of the admittance matrix $[Y]=[Y^{wg}]+[Y^{hs}]$ the unknown coefficients V_n in Equation (3-4) can be found by matrix inversion, that is,

$$(V) = \left[[Y^{wg}]+[Y^{hs}]\right]^{-1}(I) \ . \qquad (3\text{-}10)$$

After the voltage response matrix (V) has been determined, and the coefficients substituted into Equation (3-2), the magnetic field scattered by $\bar{M}_s$ into the waveguide can be determined. The

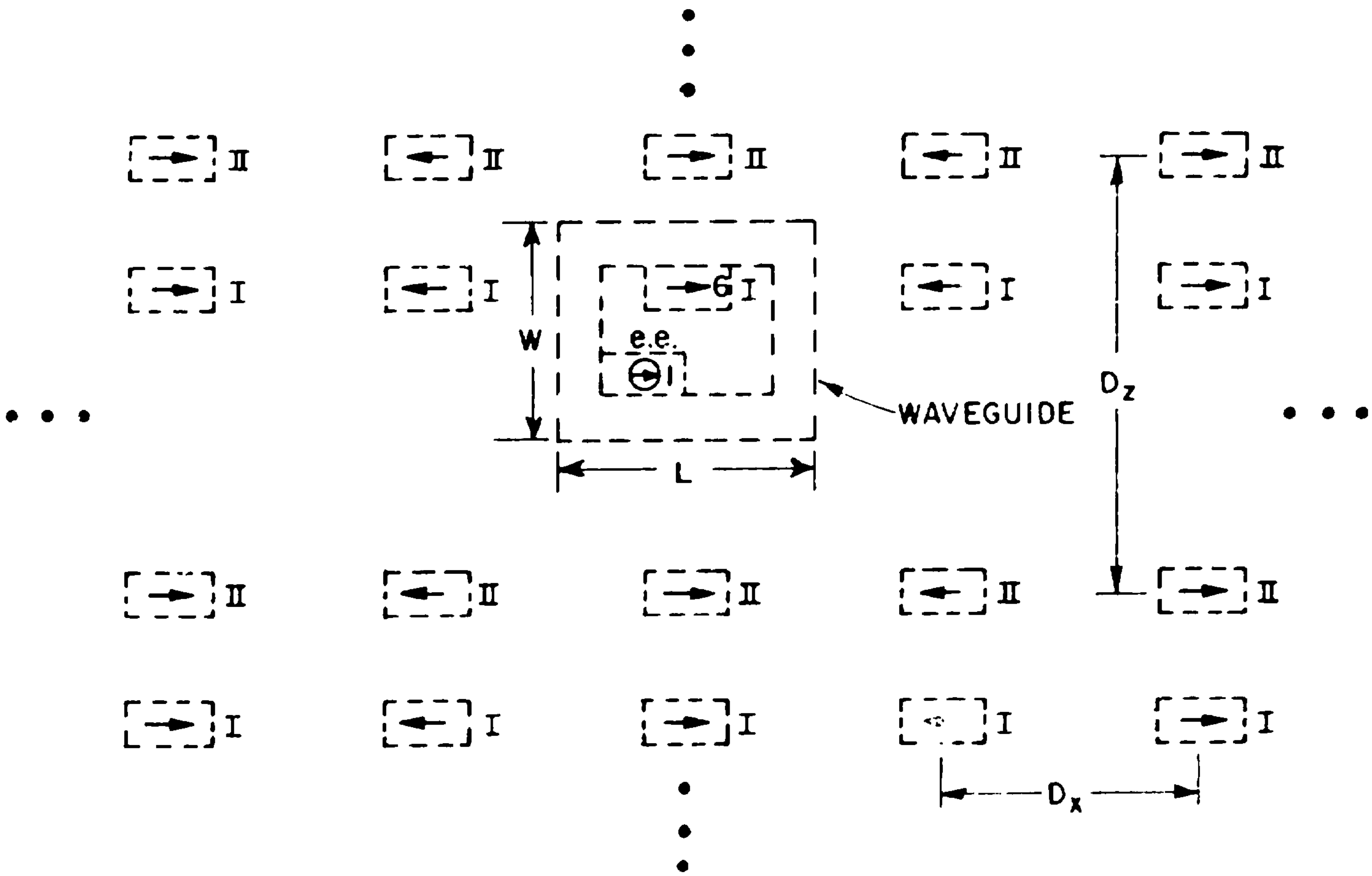

Figure 3-6. Imaging reference element number six in the waveguide walls results in two infinite arrays.

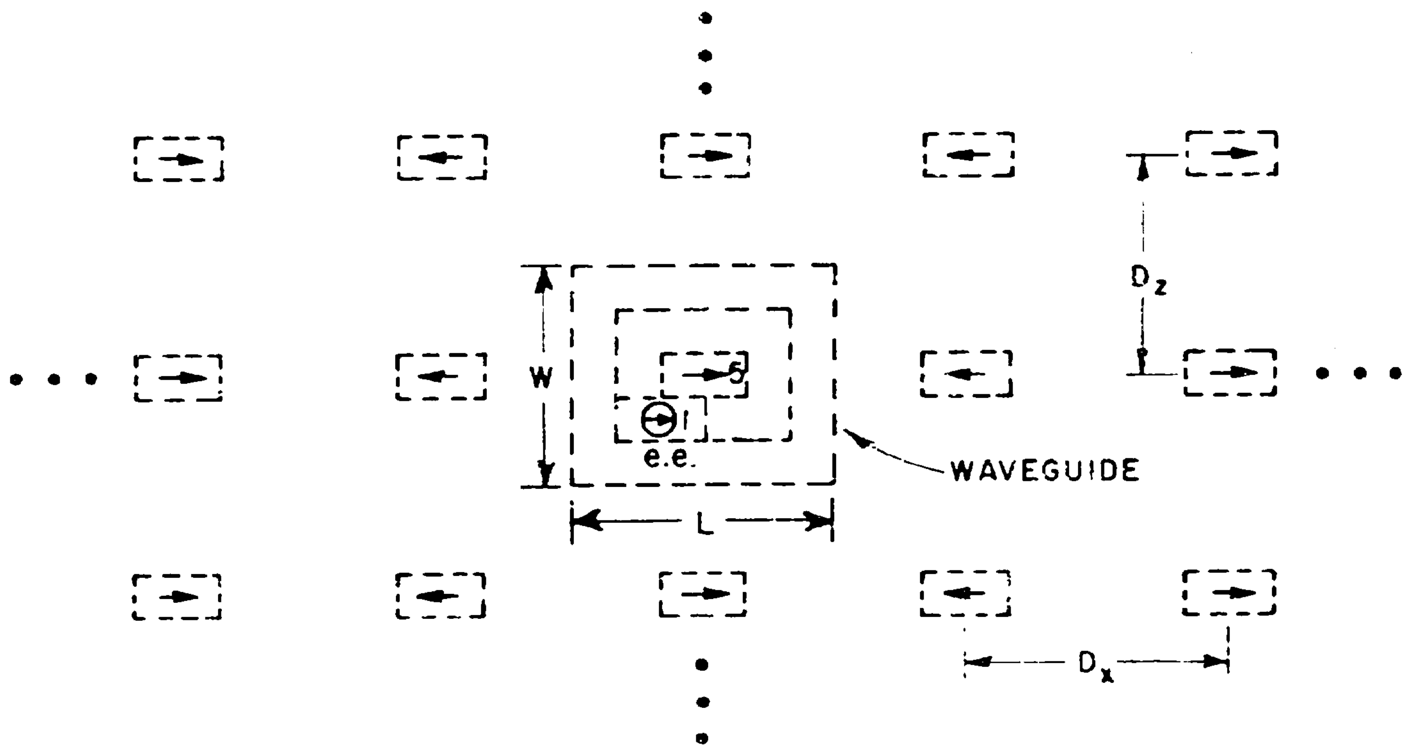

Figure 3-7. Imaging reference element number five in the waveguide walls results in one infinite array.

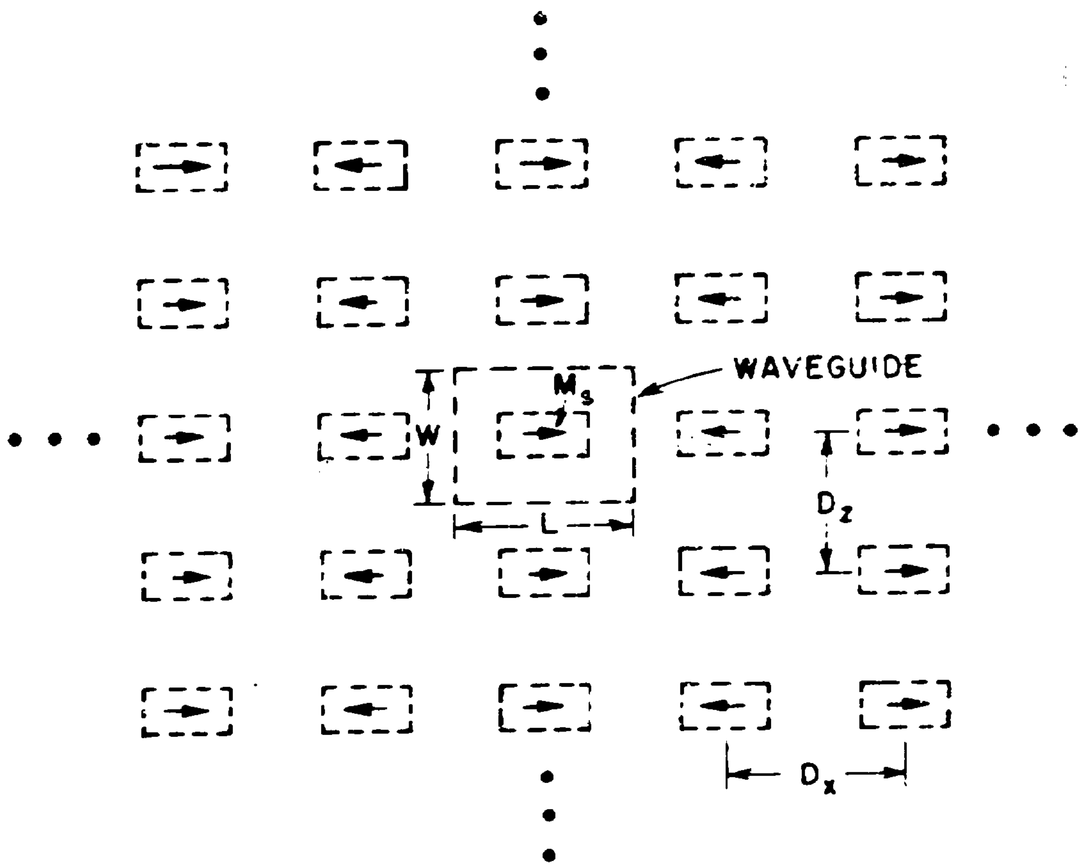

Figure 3-8. Method of images is used to remove the waveguide walls. This results in an infinite planar array of rectangular magnetic surface sources.

scattered field $\bar{H}^{wg}(\bar{M}_s)$ at the midpoint of the aperture is required in calculating the aperture reflection coefficient. A method for obtaining $H^{wg}(\bar{M}_s)$ is to image $\bar{M}_s$ in the waveguide walls. This again results in an infinite array of rectangular magnetic surface sources, as shown in Figure 3-8, which produce a field at the wall position that satisfy the waveguide boundary conditions. Appendix A gives a derivation for the magnetic field radiated by an infinite array of rectangular magnetic surface sources with arbitrary (but periodic) current distribution. The result is given by Equation (A-33). Let the TE_{mn}th aperture reflection coefficient be defined as

$$\Gamma_{mn} = -\frac{H^{wg}_{x_{mn}}(\bar{M}_s) + H^{image}_{x_{mn}}}{H^{i}_{x_{mn}}} \qquad (3\text{-}11)$$

where H_x^{image} is the image of the incident field due to the perfect conductor covering the aperture.

For convenience the reflection coefficient is calculated at the midpoint of the aperture, that is, x=0 and $z = W/2$. At the aperture ($y=-d$) the incident magnetic field doubles because of the perfect electric conducting cover. Thus,

$$H_x^{image} = H_x^{i} \text{ at } y=-d \quad .$$

From Equation (A-33), with $D_x=L$, $D_z=W$, $s_z=0$, and $s_x=\lambda/2D_x$, at the aperture midpoint the x component of the scattered magnetic field due to $\bar{M}_s$ is

$$H_x^{wg}(\bar{M}_s) = -\frac{1}{2\eta\beta^2 LW}\sum_{n_2=-\infty}^{\infty}\sum_{n_1=-\infty}^{\infty}\frac{1-\left(\frac{\lambda}{L}\left(n_2+\frac{1}{2}\right)\right)^2}{\Gamma_y}$$

$$\cdot\, P_2(n_1,n_2)\,e^{-jn_1\pi}\sum_{\ell=1}^{N}\frac{V_\ell}{w}\,e^{j2\pi\frac{x_\ell}{L}\left(n_2+\frac{1}{2}\right)}\,e^{j2\pi n_1\frac{z_\ell}{W}} \qquad (3\text{-}12)$$

where (from Equation (B-9))

$$P_2(n_1,n_2) = \frac{4}{\sin(\beta\ell)} \; e^{jn_1\pi \frac{w}{W}} \; \frac{\sin\left(\beta\frac{W}{2} - n_1\frac{\lambda}{W}\right)}{n_1\frac{\lambda}{W}}$$

$$\cdot \; \frac{\cos\left(2\pi\frac{\ell}{L}\left(n_2+\frac{1}{2}\right)\right) - \cos\beta\ell}{1-\left(\frac{\lambda}{L}\left(n_2+\frac{1}{2}\right)\right)^2} \quad , \qquad (3\text{-}13)$$

$$r_y = \sqrt{1-\left(n_1\frac{\lambda}{W}\right)^2-\left(\frac{\lambda}{L}\left(n_2+\frac{1}{2}\right)\right)^2} \quad , \text{ and}$$

x_ℓ and z_ℓ are the shift factors of expansion function ℓ from $x=0$ and $z=0$ respectively.

Equation (3-12) is a plane wave expansion representing all the propagating and evanescent modes that exist in the aperture region of the waveguide. The TE_{mn}th mode can be identified by observing the phase factor

$$e^{j2\pi\frac{x_\ell}{L}\left(n_2+\frac{1}{2}\right)} \; e^{j2\pi n_1\frac{z_\ell}{W}}$$

in Equation (3-12) and choosing the proper pair of plane waves. For example choose $n_1=0$ and $n_2=0,-1$. The sum of the above phase factor for the two cases is

$$e^{j\pi\frac{x_\ell}{L}} + e^{-j\pi\frac{x_\ell}{L}} = 2\cos\frac{\pi x_\ell}{L}$$

which is the TE_{10} mode. Next, choose $n_1=0$ and $n_2=1,-2$ with the result

$$e^{j3\pi\frac{x_\ell}{L}} + e^{-j3\pi\frac{x_\ell}{L}} = 2\cos\frac{3\pi x_\ell}{L}$$

which represents the TE_{30} mode. Other desired modes are determined similarly.

C. Results

In order to test the theory presented in Section B of this chapter, calculations for the reflection coefficient of the TE_{10} mode for a waveguide-fed aperture antenna with no iris (see Figure 3-1) are made in this section. Two different shapes of waveguide are used, square and rectangular, and results using the moment method are compared against data in the literature.

As a first test case a rectangular waveguide with length to width ratio $L/W = 2.25$ was analyzed. The unknown magnetic current distribution $\bar{M}_s$ was first expanded using 1, 3, 5 and 7 piecewise-sinusoidal expansions along the direction of current flow (H-plane) and one rectangular pulse in the transverse direction (E-plane). The results for the magnitude and phase of the reflection coefficient are shown in Figure 3-9. Agreement between the above formulation (with seven piecewise sinusoids) and the variational formulation of Cohen, Crowley, and Levis[14] and the moment method solution of Mautz and Harrington[15] is quite good. When the above formulation is applied with one expansion function in the aperture agreement is good up to about $L/\lambda = .6$ as shown in Figure 3-9. Three and five piecewise-sinusoidal expansion functions both yielded good reflection coefficient data up to $L/\lambda = 1.0$. In order to check the approximation of one pulse expansion function along the direction transverse to magnetic current flow the region $L/\lambda < .6$ was chosen. This check is also important because the finite arrays that will be dealt with in Chapter IV have elements with $L/\lambda = .5714$. Figure 3-10 shows the TE_{10} aperture reflection coefficient for $L = .5714\lambda$ as a function of pulse expansion functions N_w used to approximate $\bar{M}_s$. The magnitude of the reflection coefficient changes by only about two percent in going from one to nine rectangular-pulse expansion functions. The phase changes by only thirteen degrees correspondingly. The normalized magnetic current for nine expansion functions is shown in Figure 3-11 to illustrate the U-shaped distribution that exists due to the edge condition.

The second test case chosen was a square waveguide. Results for the reflection coefficient as a function of L/λ when seven overlapping piecewise-sinusoidal expansion functions along the direction of current flow were used is shown in Figure 3-12. The agreement with Cohen, Crowly, and Levis is good. The reflection coefficient magnitude agrees fairly well with Mautz and Harrington, however, there is a substantial difference in the phase for $L/\lambda > .7$. This can probably be attributed to their using four rectangular-pulse expansion functions along the direction transverse to current flow instead of only one. This seems to be the case, because when the aperture was chosen to be fixed at $L/\lambda = .5714$ and more pulse expansion functions were used along the transverse direction (see

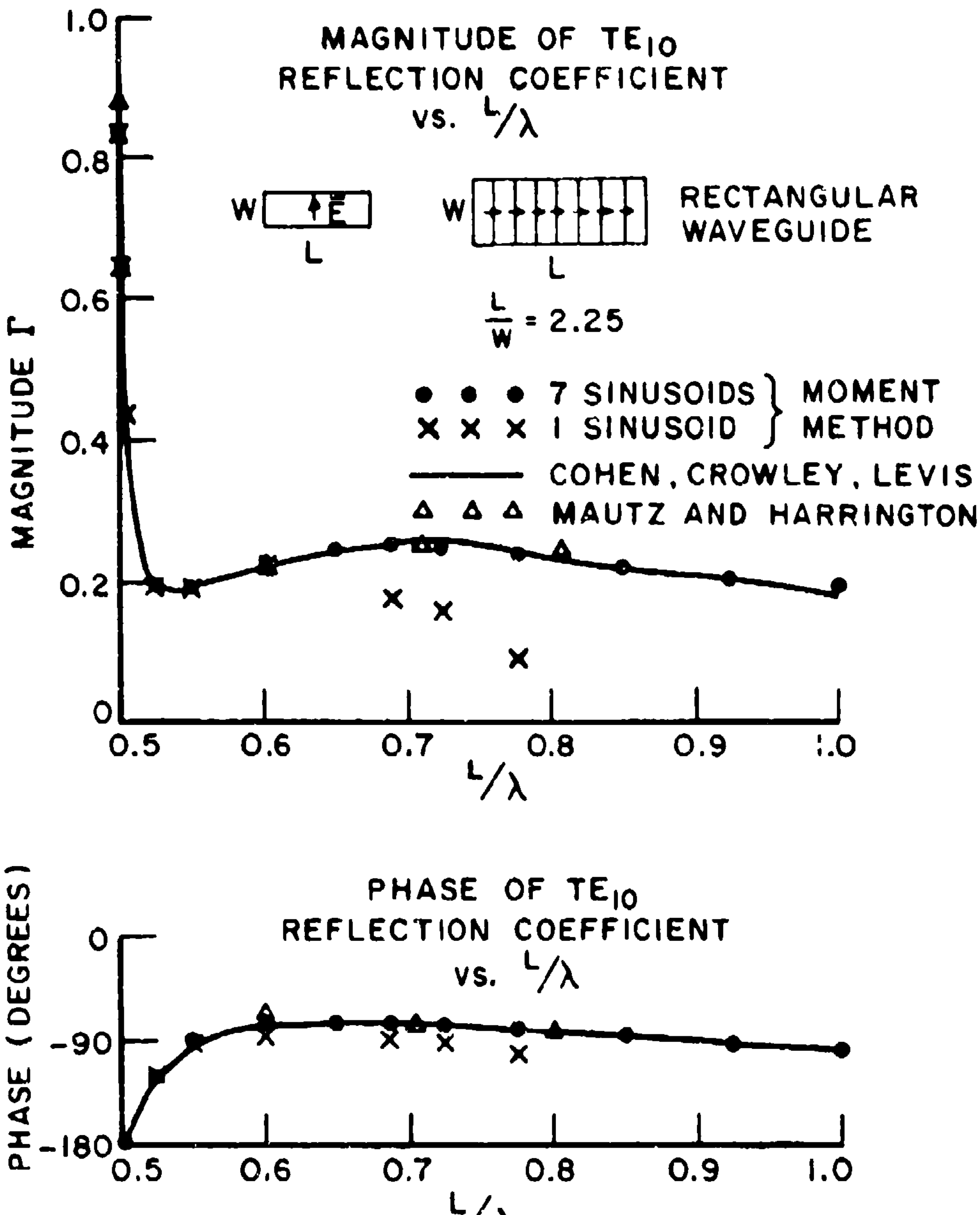

Figure 3-9. Comparison between the reflection coefficient calculated by the theory of this chapter and data in the literature for a rectangular waveguide-fed aperture of size L/W = 2.25 in an infinite ground plane.

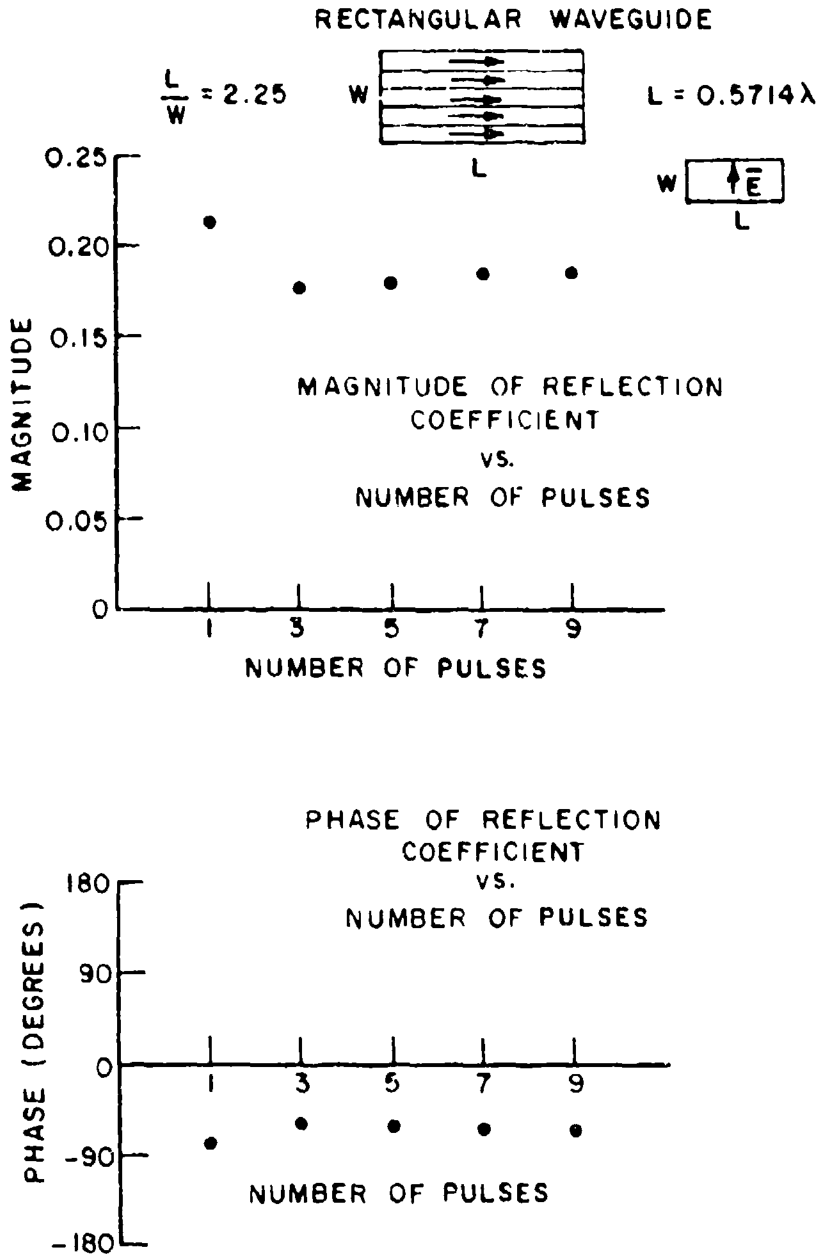

Figure 3-10. Convergence of reflection coefficient for a rectangular waveguide-fed aperture of size L/W = 2.25 in an infinite ground plane.

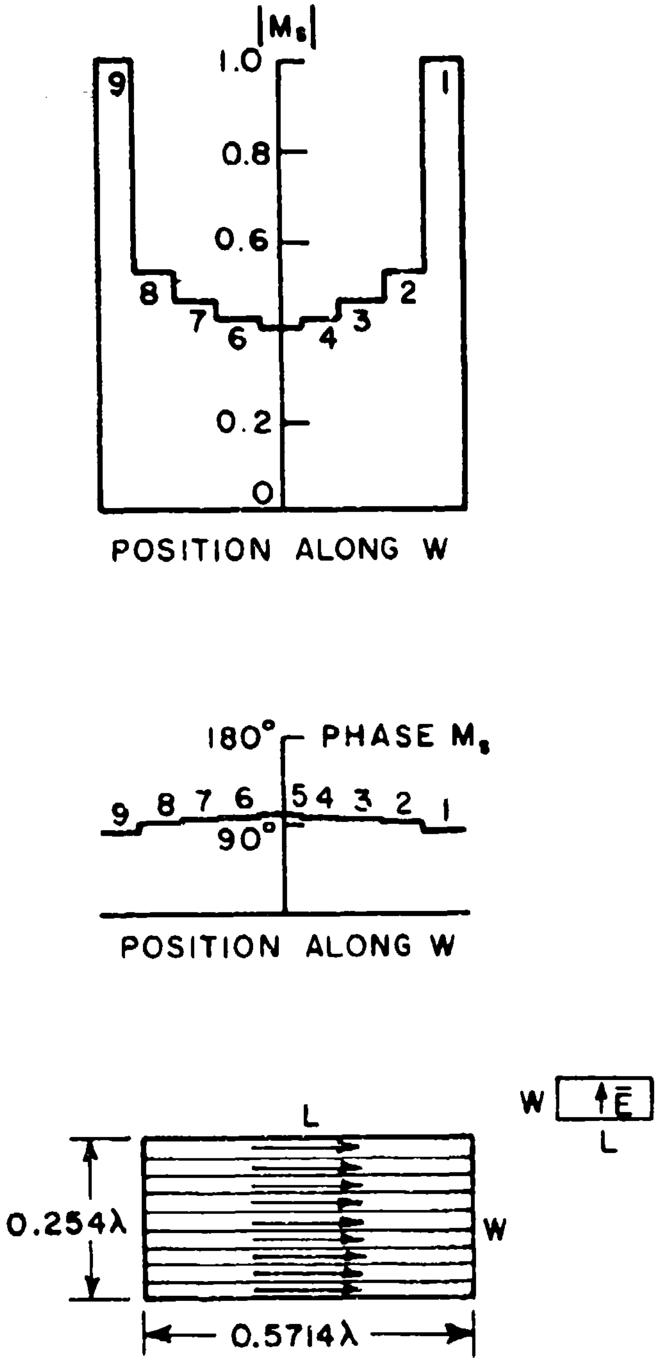

Figure 3-11. Aperture distribution for a rectangular waveguide of size L/W = 2.25 opening into an infinite ground plane.

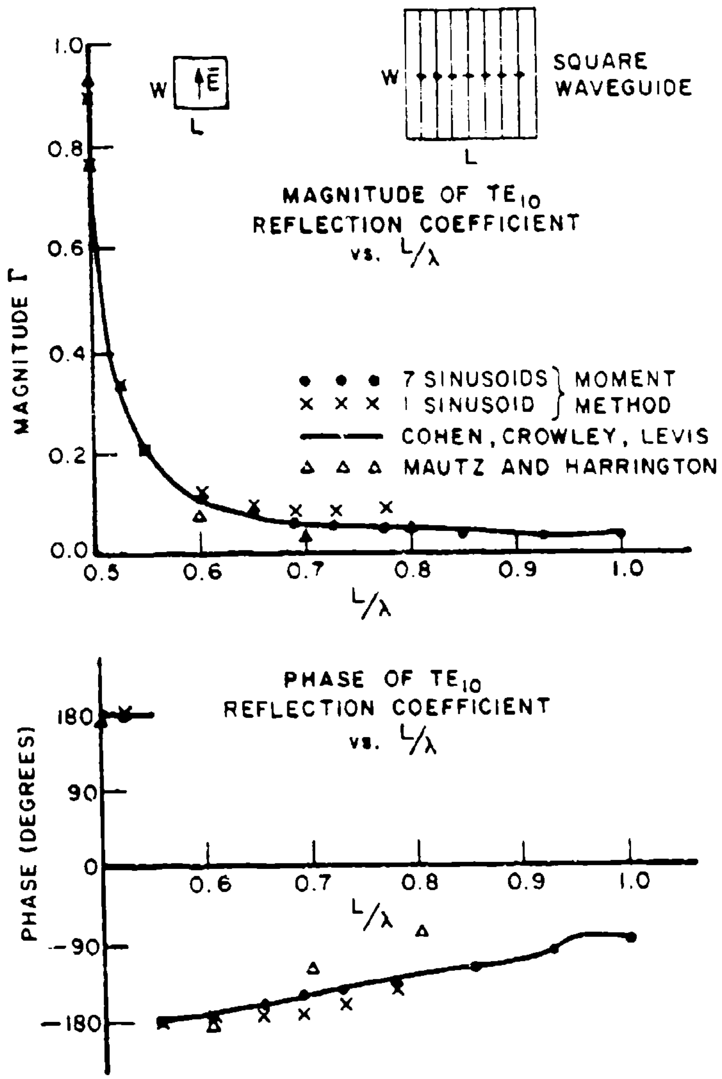

Figure 3-12. Comparison between the reflection coefficient calculated by the theory of this chapter and data in the literature for a square wa\ guide-fed aperture in an infinite groun l plane.

Figure 3-13) there was about a seven percent change in the reflection coefficient magnitude and a twenty degree change in the phase. For larger electrical sizes of apertures similar changes should be expected because the one rectangular pulse approximation becomes poorer. The normalized equivalent magnetic current for nine pulse expansion functions is shown in Figure 3-14.

In the next chapter finite planar phased antenna arrays will be analayzed. The arrays will be made up of the square and rectangular waveguide elements that were discussed in this chapter.

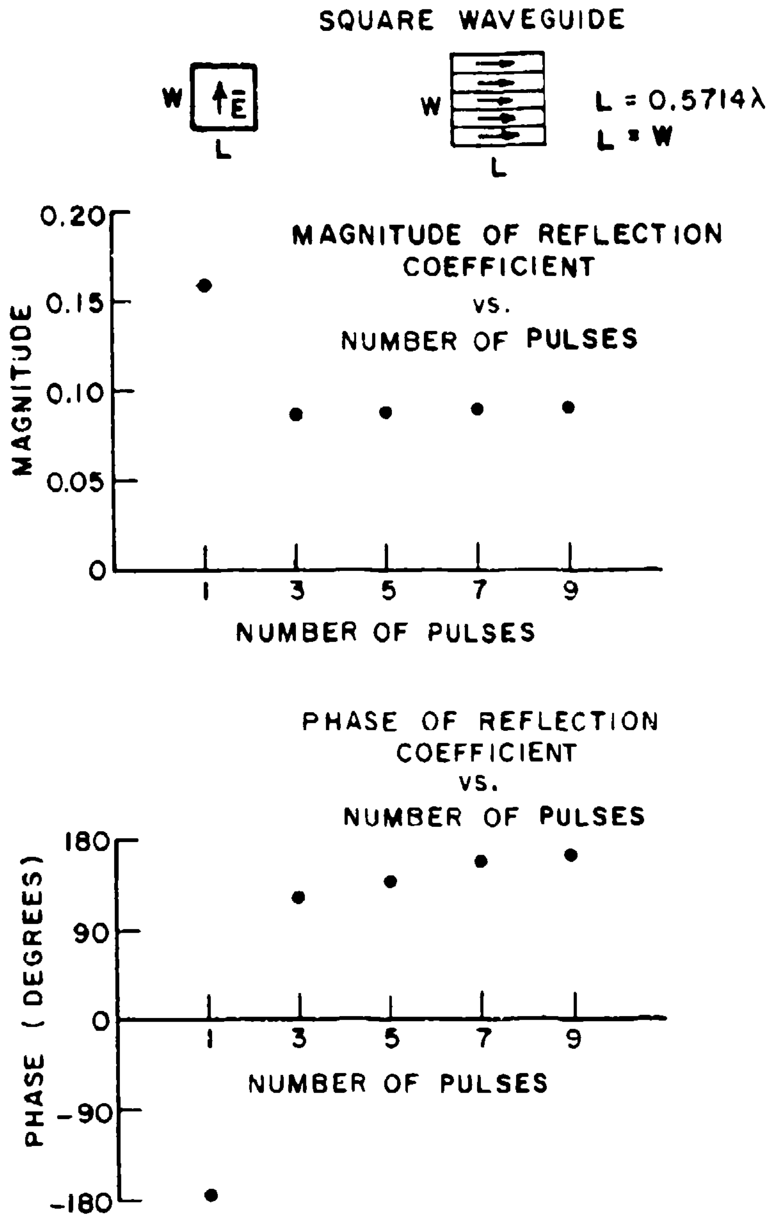

Figure 3-13. Convergence of reflection coefficient for a square waveguide-fed aperture in an infinite ground plane.

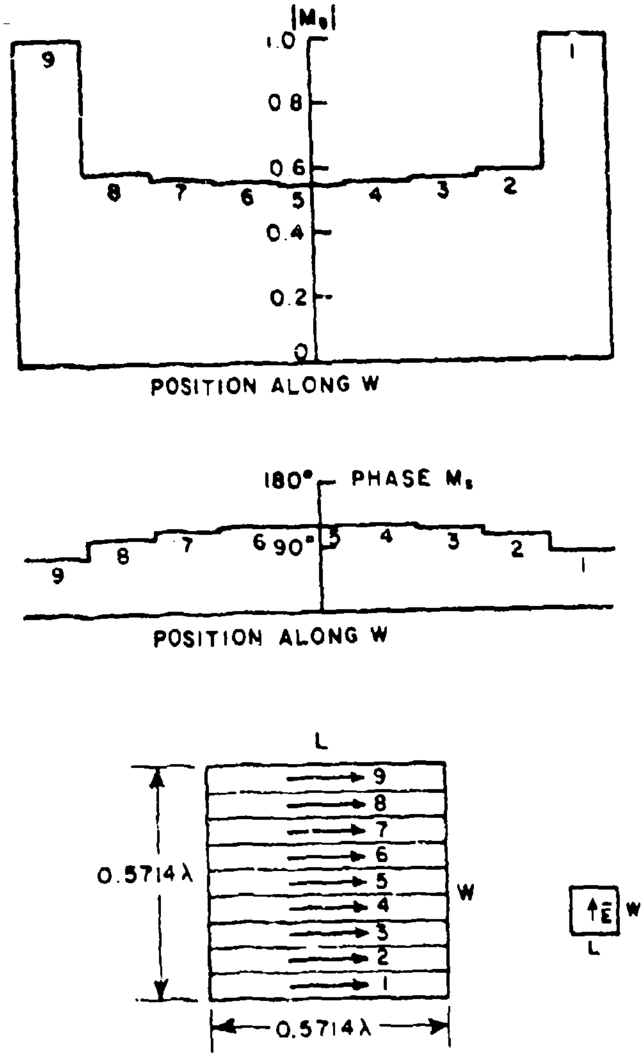

Figure 3-14. Aperture distribution for a square waveguide opening into an infinite ground plane.

CHAPTER IV
APERTURE REFLECTION COEFFICIENTS OF WAVEGUIDE ELEMENTS IN FINITE PLANAR PHASED ARRAYS

A. Introduction

As discussed in Chapter I, when a small finite phased array is analyzed, it is necessary to include the effects of mutual coupling between elements. This chapter considers the effect of mutual coupling in finite phased arrays in which the radiating elements are closely spaced waveguide-fed apertures. The method of analysis involves extending the moment method formulation for the single waveguide-fed aperture that was presented in Chapter III.

In designing phased arrays it is important to know the pattern of the array as a function of scan angle. It is of equal importance to know how much power is being reflected and transmitted by elements of the array as the scan angle varies. For example, the pattern of an array may meet design requirements but the transmitted power may not. For certain sizes and spacings of arrays the Wood's anomaly (also known as the blindness effect)[16,17] occurs in which magnitudes of the reflection coefficients of the elements of the array become unity. In this case the array will be incapable of transmitting any power. Thus, it is necessary to calculate the reflection or transmission coefficients of the elements of the array in order to determine the amount of power that the array can transmit. In the next section the theory for performing such a calculation will be discussed.

B Theory

Figure 4-1 shows a front view of the MxN phased array of rectangular waveguide-fed apertures in an infinite ground plane which will be analyzed in this chapter. A side view of the array, as depicted in Figure 4-2, shows the probe excitation used for each waveguide. A constant current of one ampere is assumed at the terminals of each probe along with the desired phase to achieve a particular scan angle. Taking θ as the E-plane scan angle measured from the normal to the array, the required constant phase shift between apertures is

$$\alpha_s = -2\pi d_s \sin \theta, \qquad (4\text{-}1)$$

where d_s is the center-to-center spacing between apertures in the strong-coupled ($\bar{E}$-plane) direction. Next, letting ϕ be the H-plane scan angle measured from the normal to the array, as shown in Figure 4-3, the required constant phase shift between apertures is

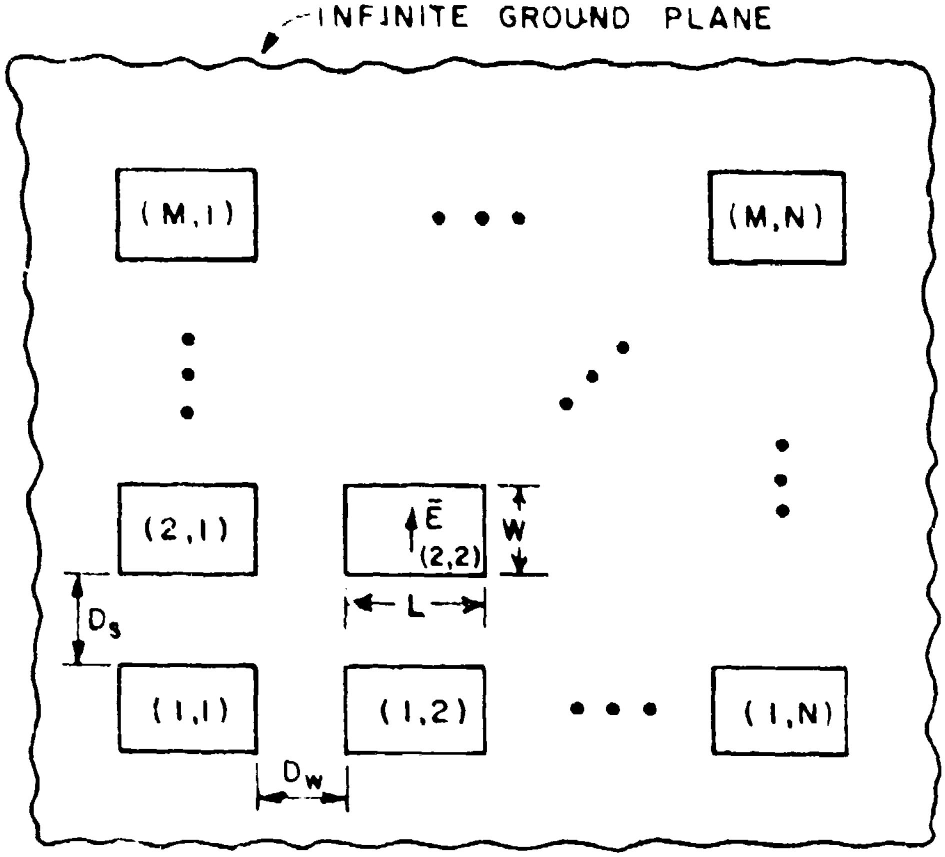

Figure 4-1. MxN array of waveguide-fed apertures in an infinite ground plane.

$$\alpha_w = -2\pi d_w \sin \phi, \tag{4-2}$$

where d_w is the center-to-center spacing between apertures in the weak ($\bar{H}$-plane) direction. Thus, the terminal current of probe (m,n) in the array for a particular scan angle (θ,ϕ) is given by

$$I_{t_{m,n}} = e^{-j2\pi(m-1)d_s \sin\theta}\, e^{-j2\pi(n-1)d_w \sin\phi} \tag{4-3}$$

$$m = 1,2,\ldots,M;\ n=1,2,\ldots,N.$$

Having defined the geometry of the array to be analyzed, the next step is to modify the single slot formulation of Chapter III.

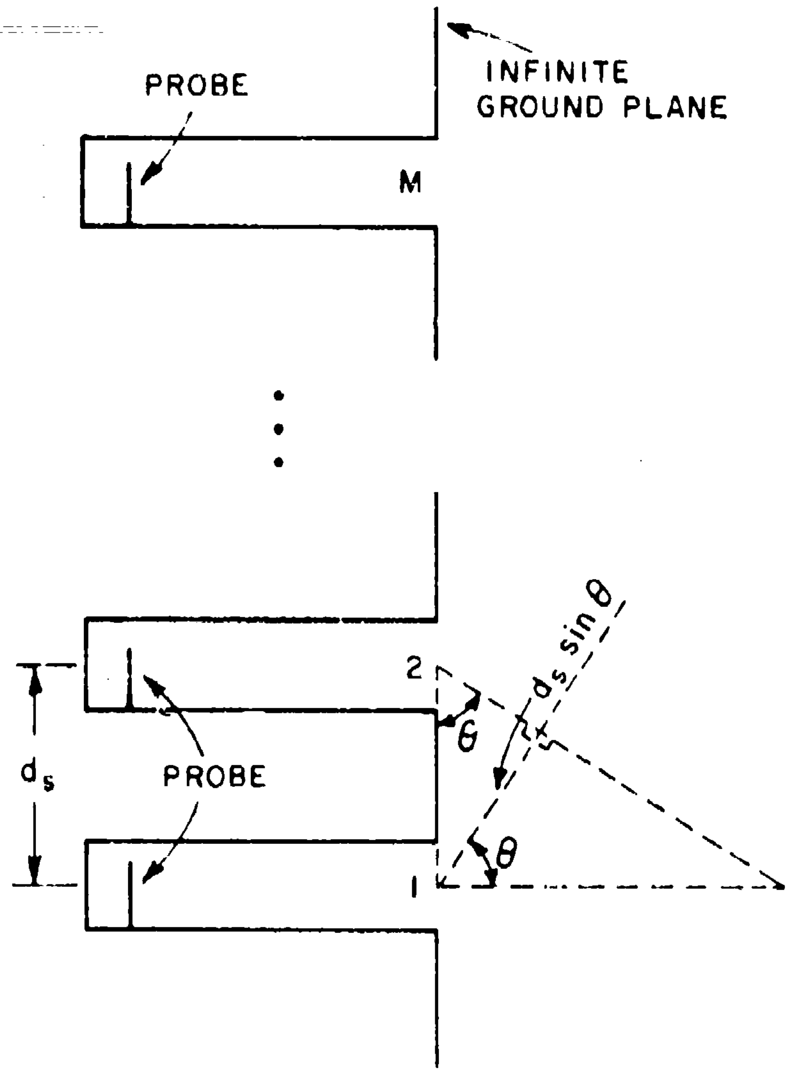

Figure 4-2. Side view of the MxN array shown in Figure 4-1: E-plane scan.

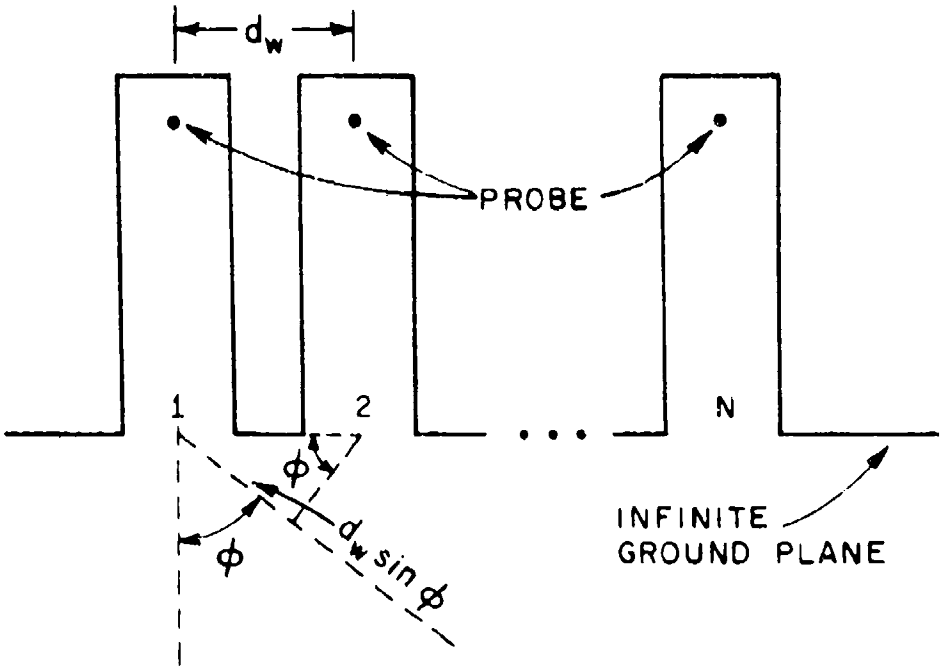

Figure 4-3. Top view of the MxN array shown in Figure 4-1: H-plane scan.

The matrix equation for the unknown coefficients, V_n of the aperture, is given by Equation (3-10) as

$$(V) = \left[\left[Y^{wg}\right] + \left[Y^{hs}\right]\right]^{-1} (I) \tag{4-4}$$

where $\left[Y^{wg}\right]$ is the waveguide admittance matrix,

$\left[Y^{hs}\right]$ is the half-space admittance matrix,

(I) is the excitation current matrix.

For the case of an MxN array of apertures in an infinite ground plane each aperture is covered by a perfect electric conductor and the equivalent magnetic current $+\overline{M}_{s(m,n)}$ is placed on the left side of the conductor and $-\overline{M}_{s(m,n)}$ on the right side. In this manner the boundary condition, that tangential $\overline{E}_{(m,n)}$ be continuous across each aperture, can be enforced. Enforcing the boundary condition that tangential $\overline{H}_{(m,n)}$ be continuous across each aperture results in the new matrix equation

$$(V)_{array} = \left[\left[Y^{wg}\right]_{array} + \left[Y^{hs}\right]_{array}\right]^{-1} (I)_{array} \qquad (4\text{-}5)$$

$(I)_{array}$ is the array excitation matrix composed of M·N sub-matrices corresponding to the M·N elements of the array, thus

$$(I)_{array} = \begin{pmatrix} (I_1) \\ (I_2) \\ \cdot \\ \cdot \\ \cdot \\ (I_{M\cdot N}) \end{pmatrix} \qquad (4\text{-}6)$$

where the elements of $(I)_{array}$ are column vectors of length $(N_\ell - 1)\cdot N_w$ (recall from Chapter II that $N_\ell - 1$ and N_w are the number of expansion functions used in the aperture) due to each element of the array. Since the waveguides have been effectively isolated from each other (due to the perfect electric conducting cover) there is no coupling between apertures by means of the waveguide admittances. There will be an identical waveguide self admittance matrix of size $((N_\ell - 1)\cdot N_w) \times (N_\ell - 1)\cdot N_w)$ for each of the waveguides in the array. The array waveguide admittance matrix will thus be a diagonal block matrix,

$$\left[Y^{wg}\right]_{array} = \begin{bmatrix} \left[Y^{wg}\right] & & & 0 \\ & \left[Y^{wg}\right] & & \\ & & \ddots & \\ 0 & & & \left[Y^{wg}\right] \end{bmatrix} \qquad (4\text{-}7)$$

The number of blocks on the main diagonal is equal to M·N. In the half-space region the magnetic current sheets $-\overline{M}_{s(m,n)}$ (m=1, 2, ..., M; n=1,2,...,N) radiate in the presence of each other. Thus, the coupling that takes place between apertures is done solely by the array half-space admittance matrix.

Calculation of the array half-space admittance matrix elements is done by using Equation (3-7). The array half-space admittance matrix will be a block matrix with every entry being non-zero. For certain array interelement spacings and number of expansion functions used, various symmetries can be used to reduce the number of calculations necessary to fill the array half-space admittance matrix. The same symmetries can be used to reduce the amount of computer storage required for the total array admittance matrix as well as reducing the amount of time required to invert it. These symmetries will be discussed next.

As an example of symmetries that are typically present in analyzing rectangular grid arrays consider a 3x3 array with three pulse expansion functions used to approximate $\bar{M}_s$ per element, as shown in Figure 4-4. In this case the separation between strong-coupled (E-plane) apertures is zero and the spacing between weak-coupled (H-plane) apertures is arbitrary. The resulting array half-space admittance matrix is block Toeplitz[18,19]. A block Toeplitz matrix is symmetric and is composed of symmetric sub-matrices (blocks) with the following property: Let $A_{i,j}$ represent the ij^{th} block of a block Toeplitz matrix, then the elements of the block will depend only on the difference of the subscripts, that is, $|j-i|$.

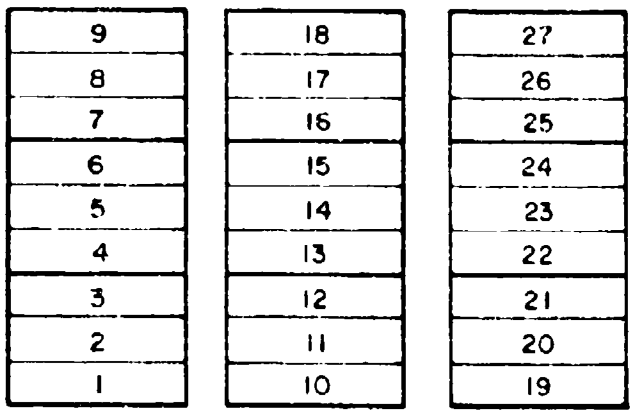

Figure 4-4. 3x3 array with three pulse expansion functions in each aperture gives rise to a block Toeplitz half-space admittance matrix when the separation between strong-coupled apertures is zero.

In the above example the half-space admittance matrix has nine blocks (three in each row and three in each column) of dimensions 9x9 each and in the above notation,

$$[Y^{hs}]_{array} = \begin{bmatrix} [Y^{hs}]_0 & [Y^{hs}]_1 & [Y^{hs}]_2 \\ [Y^{hs}]_1 & [Y^{hs}]_0 & [Y^{hs}]_1 \\ [Y^{hs}]_2 & [Y^{hs}]_1 & [Y^{hs}]_0 \end{bmatrix} \qquad (4\text{-}8)$$

(note that $[Y^{wg}]_{array}$ is also block Toeplitz and thus the total admittance matrix is block Toeplitz). The above block Toeplitz matrix is important for two reasons. First, although the matrix is of size 27x27 (729 elements) only the elements $Y^{hs}_{1,1}$, $Y^{hs}_{1,2}$, ..., $Y^{hs}_{1,27}$ need to be calculated. Since the remaining elements of the matrix repeat, the rest can be filled in (from the above 27) by an algorithm.[20] Second, a computer program for solving a block Toeplitz system of simultaneous equations has been developed by Sinnot[21] which greatly reduces the amount of storage required for the admittance matrix.

Another important geometry that will be analyzed is an array where the separation between strong-coupled (E-plane) apertures is non-zero. An example of this is the 3x3 array with three expansion functions per element as shown in Figure 4-5. For this case the half-space admittance matrix is now double-block Toeplitz. A double-block Toeplitz matrix is defined to be a block Toeplitz matrix with sub-matrices that are also block Toeplitz. In the above example the elements $Y^{ns}_{1,1}$, $Y^{ns}_{1,2}$, ..., $Y^{ns}_{1,27}$ need to be calculated and then only certain of the elements in the second and third rows. The rest of the matrix can be filled in by an algorithm which uses the double-block Toeplitz properties.

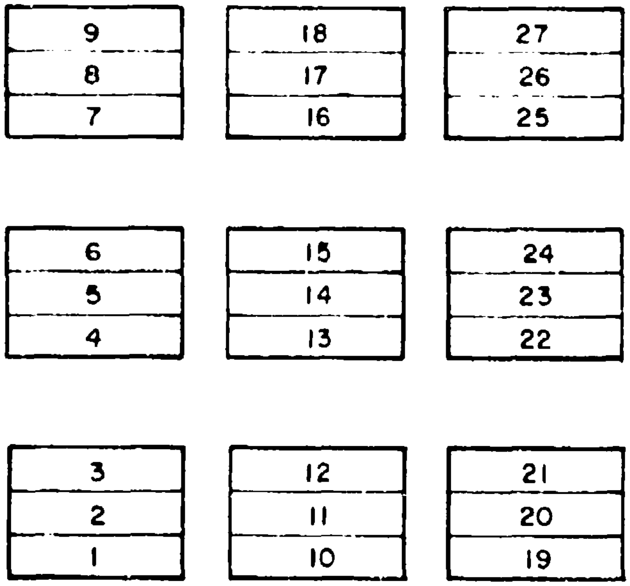

Figure 4-5. 3x3 array with three pulse expansion functions in each aperture yields a double-block Toeplitz half-space admittance matrix when the separation between strong-coupled apertures is non-zero.

Now that a method for analyzing finite arrays has been presented it will be applied in the next section to some specific cases.

C. Results

In this section plane MxM arrays (where M is odd) of square and rectangular waveguides, in an infinite ground plane, will be analyzed. The moment method formulation for finite arrays in the preceding section is utilized. Results will be given for the reflection coefficients of elements in the array, as well as representative aperture distributions, for various scan angles. First, however, the required number of piecewise-sinusoidal expansion functions along the length (H-plane) per aperture in a small

finite array will be determined. This will be done for E, H, and quasi-E-plane (which will be discussed shortly) scanning using a 5x5 array of square apertures as a representatative case. Next, quasi-E-plane scanning with zero wall thickness will be used as a test case to determine the required number of rectangular pulse expansion functions along the width ($\bar{E}$-plane) per aperture. After having determined the proper number of expansion functions per element, E-plane and H-plane scanned arrays of various sizes will then be analyzed. The results will show that one piecewise sinusoidal expansion function per aperture is adequate along the length (H-plane) for $L \leq .5714\lambda$ while more than one pulse expansion function is necessary along the width (E-plane) for both rectangular and square apertures.

E-plane and H-plane array scanning were discussed in the last section (see Figures 4-2 and 4-3). The quasi-E-plane scan differs from E-plane scanning in that the E-vector changes direction by 180° periodically along the x-direction of the array, as shown in Figure 4-6. As discussed in Appendix H, the reflection coefficients in a 5x5 array of square elements ($L=0.5714\lambda$) have almost converged when only one piecewise-sinusoidal expansion function is used. This is true for all three types of scanning. It can

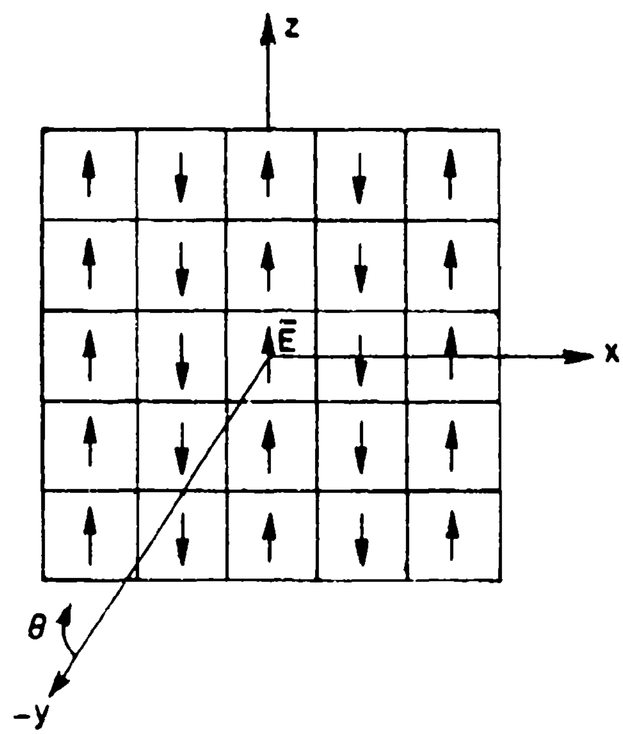

Figure 4-6. Quasi-E-plane scanning in the yz plane.

be assumed that small finite arrays of size similar to the 5x5 array will have about the same type of convergence. Thus, in all the arrays that follow, one piecewise-sinusoidal basis function will be used to expand the unknown equivalent magnetic current in the direction of current flow. This approximation represents a significant savings in computer storage required for the admittance matrix in Equation (4-4) as well as greatly reducing the cpu time required to solve the system of equations. In general, for arrays with apertures having $L > 0.6\lambda$ several overlapping-piecewise sinusoidal expansion functions will be required.

The quasi-E-plane scan provides a good check of the dependence of the reflection coefficient convergence upon the number of pulse expansion functions along the aperture width (E-plane). This is true because for an infinite array, with zero wall thickness between waveguide elements, the reflection coefficient for every element will be zero at broadside scan[22]. This can be explained simply by noting that due to the periodic 180^{0} phase shift in the $\bar{E}$-field along the x-direction of the array and the $\bar{E}$-field being orthogonal to the top and bottom walls of each waveguide, the fields will be unperturbed if the waveguide walls are extended to infinity. Thus, the reflection coefficient of every element in the infinite array must be zero. For a large finite array the reflection coefficient of the center element should be close to zero.

By using the quasi-E-plane broadside scan and observing the center element reflection coefficient, as a function of array size and number of pulse expansion functions, it can be determined whether or not it is converging to the correct value ($\Gamma=0$). Reflection coefficients for elements of arrays of sizes 3x3 to 27x27 as a function of the number of rectangular pulse expansion functions for square and rectangular apertures were computed. Calculations were done on an IBM-370 digital computer with 2048K bytes of storage. Seven pulses per aperture could be run for arrays up to size 9x9. Due to storage limitations only five pulses per aperture were used for an 11x11 array. Three pulses per element could be used for the 13x13 and 15x15 arrays. For larger arrays only one rectangular pulse could be used. The results for square apertures are presented in Table 4-1 and Figure 4-7. In Figure 4-7 the magnitude and phase of the center element reflection coefficient is conveniently plotted on an expanded scale Smith chart as a function of array size and the number of pulse functions used. The family of curves clearly indicate that one pulse function is insufficient for arrays up to size 13x13. In the limit of an infinite array one rectangular pulse expansion function should fit the uniform distribution along the width (E-plane) of the aperture for the TE_{10} mode exactly. Figure 4-8 shows the center element reflection coefficient for one expansion function per aperture as a function of array size. The curve shows a spiral type behavior. Whether or not it would converge to $\Gamma=0$ for a large enough array is not clear.

QUASI-E-PLANE 0° (BROADSIDE) SCAN

ARRAY SIZE

NUMBER OF PULSES	3x3	5x5	7x7	9x9	11x11	13x13	15x15	17x17	19x19	21x21	23x23
1	.088 129.3°	.223 82.6°	.276 59°	.277 40.5°	.239 26.3°	.183 19.4°	.134 24.7°	.120 43.2°	.142 55.8°	.171 57°	.191 53°
3	.089 -153.9°	.150 123.6°	.183 84.5°	.180 56.6°	.148 33.4°	.099 16.1°	.048 13.7°				
5	.105 -142.8°	.130 135.7°	.160 91.2°	.150 59°	.124 31.7°						
7	.113 -138.8°	.135 141.7°	.150 94.5°	.141 60.2°							

ARRAY ELEMENT

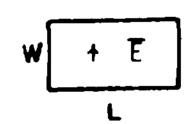

$\frac{L}{W} = 2.25$

$L = 0.5714\lambda$

Table 4-1. Center element reflection coefficient as a function of array size and number of pulse bases along W when the elements are rectangular waveguide-fed apertures with zero wall thickness between elements.

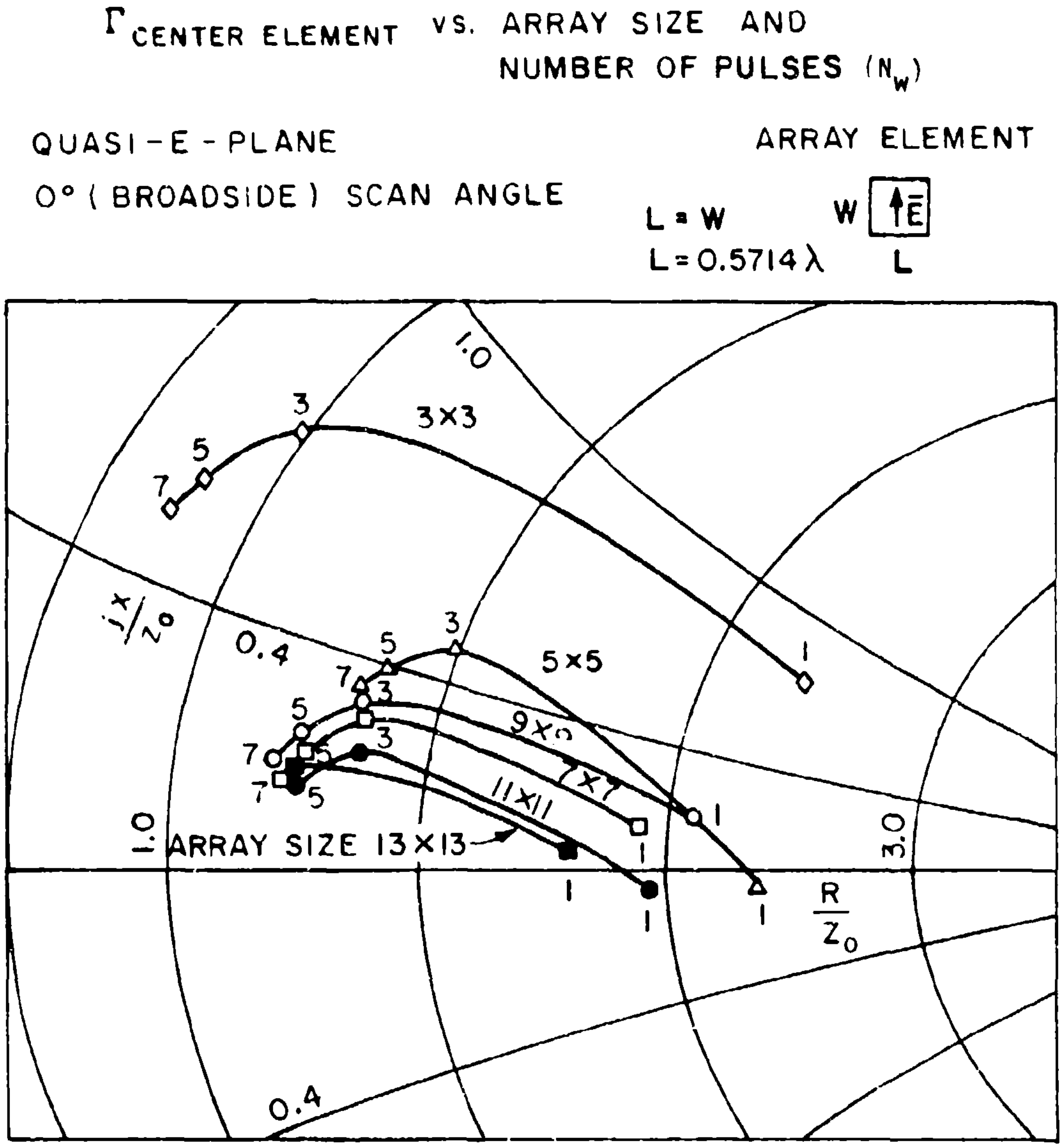

Figure 4-7. Center element reflection coefficient for various sizes of arrays and number of pulses per array element. Array elements are square waveguide-fed apertures. Data points are plotted in the center portion of a Smith chart.

$\Gamma_{\text{CENTER ELEMENT}}$ VS. ARRAY SIZE FOR ONE EXPANSION FUNCTION/ELEMENT

QUASI-E-PLANE

0° (BROADSIDE) SCAN

ARRAY ELEMENT

W E L

L = 0.5714λ

L = W

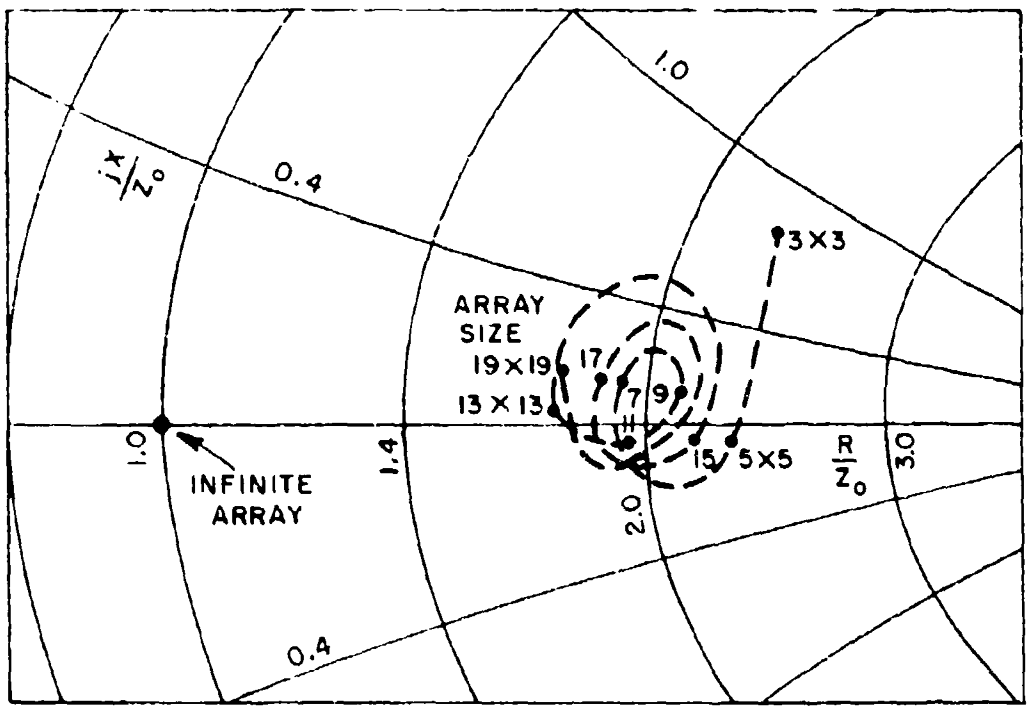

Figure 4-8. Center element reflection coefficient as a function of array size. Array elements are square waveguide-fed apertures. Data points are plotted in the center portion of a Smith chart.

For the case of the 11x11 array with square elements ($L=0.5714\lambda$) and five pulse expansion functions per aperture, the center element reflection coefficient was calculated for a quasi-E-plane scan in ten degree increments. The magnitude of the center element reflection coefficient is plotted as a function of scan angle in Figure 4-9. The results are compared against data calculated by Amitay, Galindo, and Wu for the center column of an infinite array in which all elements of the array are excited and for when only eleven columns of elements are excited.[53]. Although the geometries are quite different the results are similar. Reflection coefficients of all the elements in arrays of sizes 3x3, 5x5, 7x7, 9x9, and 11x11 for various scan angles are presented in Appendix I.

For quasi-E-plane scanned arrays in which the elements are rectangular with length to width ratio 2.25, the results for the center element reflection coefficient as a function of array size and number of pulse expansion functions per element are presented in Table 4-2 and Figure 4-10. Figure 4-10 shows that one pulse expansion function is inadequate for arrays up to size 15x15. It is also clear that as the array size increases fewer pulses are required. This is to be expected because as the array gets larger the aperture distribution of the center element approaches that of the TE_{10} mode. Figure 4-10 also shows that seven pulse bases per element are desirable for arrays up to size 9x9. Figure 4-11 shows the center element reflection coefficient for one expansion function per element as a function of array size. The curve is observed to be a spiral. The reflection coefficient changes less and less as the array becomes larger, as expected. Whether or not the calculated reflection coefficient will converge to zero for a large enough array is not obvious from Figure 4-11. Figure 4-12 shows a similar spiral curve when three pulses per aperture are used. This curve seems to indicate a convergence of the reflection coefficient towards zero. For a very large array the difference between one and three pulses should be very slight as far as the center element reflection coefficient is concerned. Therefore, for large enough arrays it appears that the array formulation will yield converged reflection coefficient data ($\Gamma=0$) for the central elements when only one expansion function is used. This will not be true for the edge and near edge elements. Reflection coefficients for all the elements of finite arrays with rectangular elements of sizes 3x3, 5x5, 7x7, and 9x9 are presented in Appendix J for various scan angles when 7 pulse expansion functions per element are used. For the array of size 11x11, 5 pulses are used. Now that the formulation has been shown to yield accurate reflection data for quasi-E-plane scanning, E-plane scanning will next be considered.

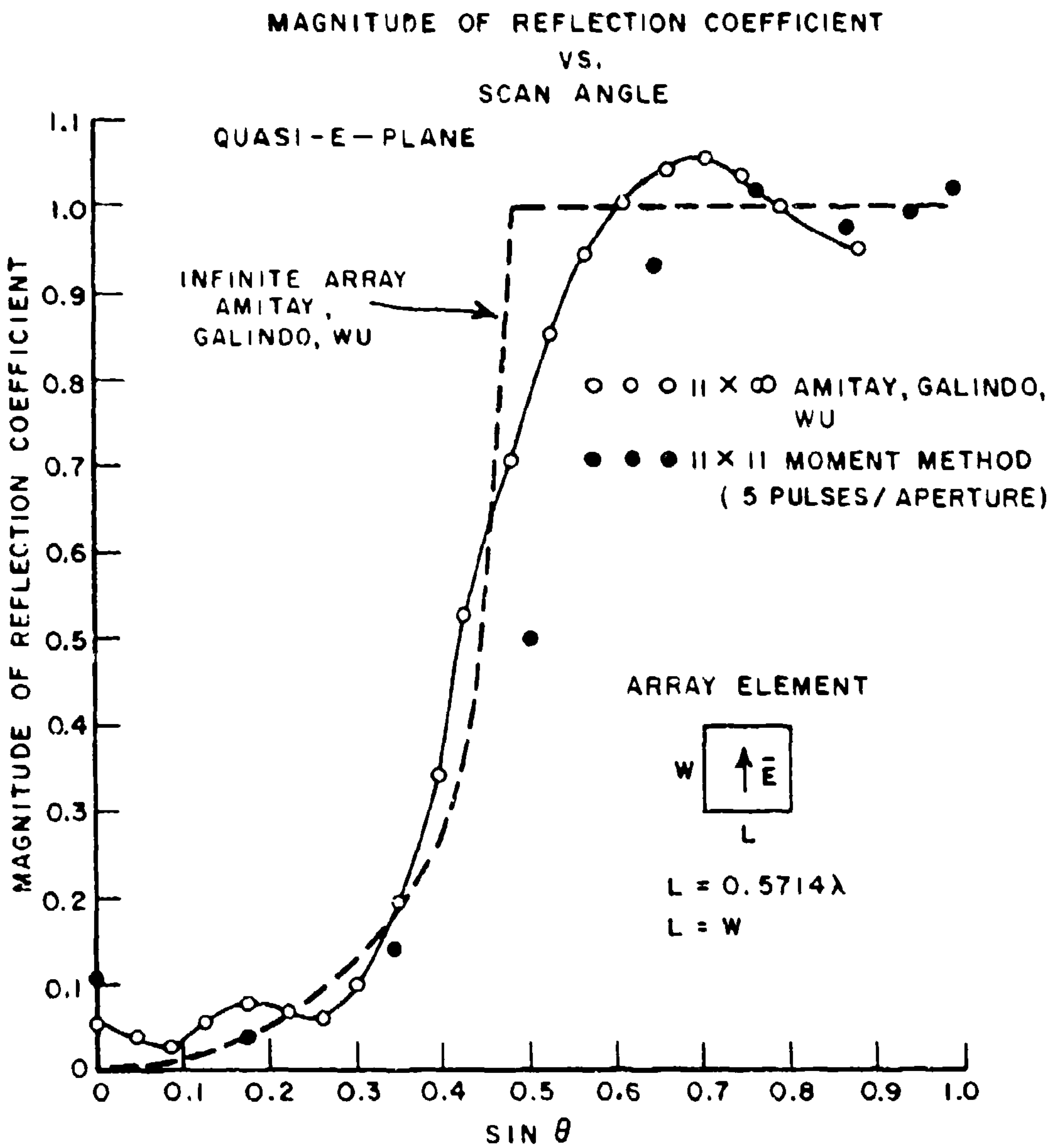

Figure 4-9. Reflection coefficient of the center element in finite and infinite arrays of square waveguide-fed apertures.

QUASI – E – PLANE 0° (BROADSIDE) SCAN

ARRAY SIZE

NUMBER OF PULSES	3x3	5x5	7x7	9x9	11x11	13x13	15x15	17x17	19x19	25x25	27x27
1	.471 16.8°	.399 -1.5°	.315 4.1°	.357 5.4°	.323 -2.9°	.270 2.0°	.370 -1.7°	.304 5.7°	.278 6.8°	.311 7.9°	.306 10.2°
3	.312 73.4°	.245 37.8°	.165 37.5°	.171 40.3°	.148 31.1°	.111 40.6°					
5	.268 84.5°	.202 42.3°	.122 40.1°	.125 45.1°	.105 33.1°						
7	.247 89.5°	.182 43.4°	.100 39.4°	.102 46.2°							

ARRAY ELEMENT

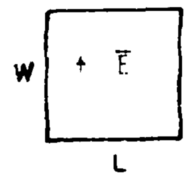

L = 0.5714λ
L = W

Table 4-2. Center element reflection coefficient as a function of array size and number of pulse bases along W when the elements are square waveguide-fed apertures with zero wall thickness between elements.

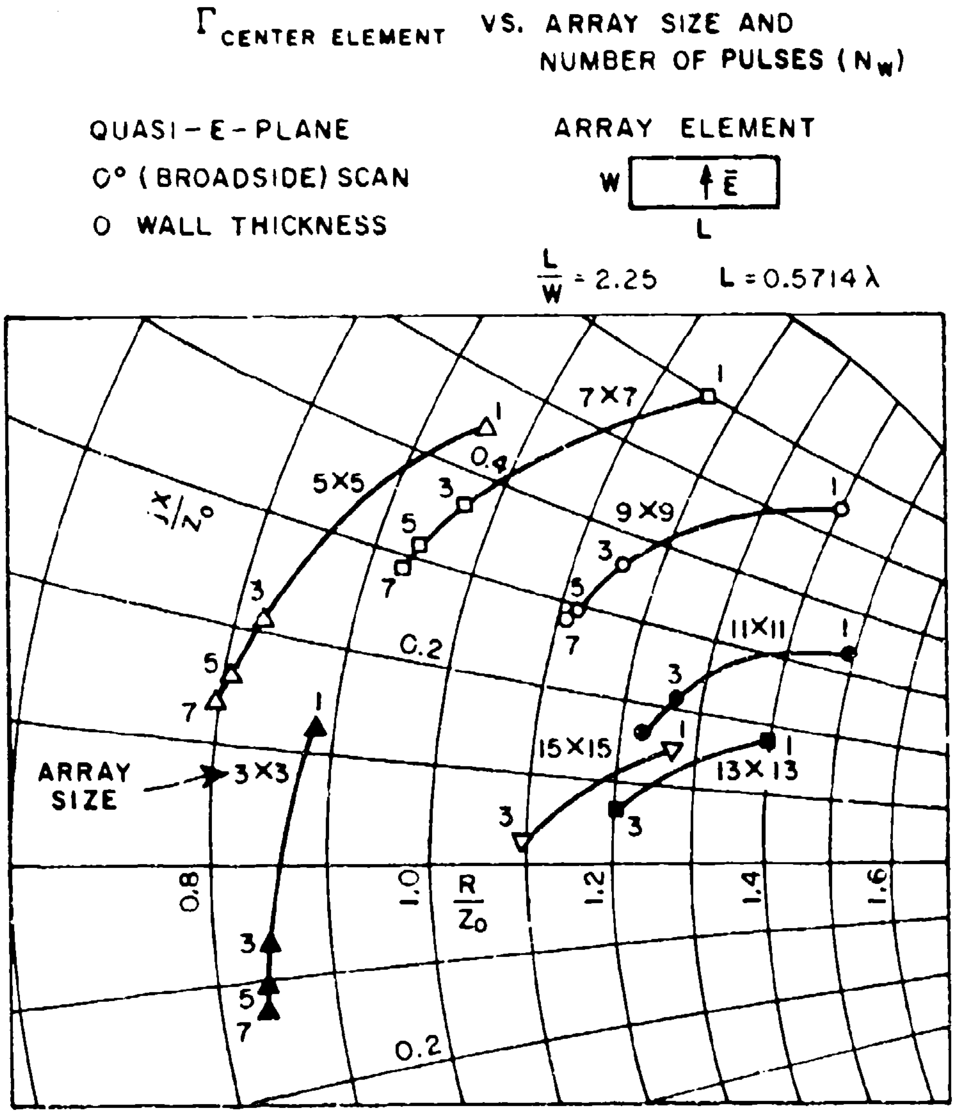

Figure 4-10. Center element reflection coefficient for various sizes of arrays and number of pulses per element array. Array elements are rectangular waveguide-fed apertures. Data points are plotted in the center portion of a Smith chart.

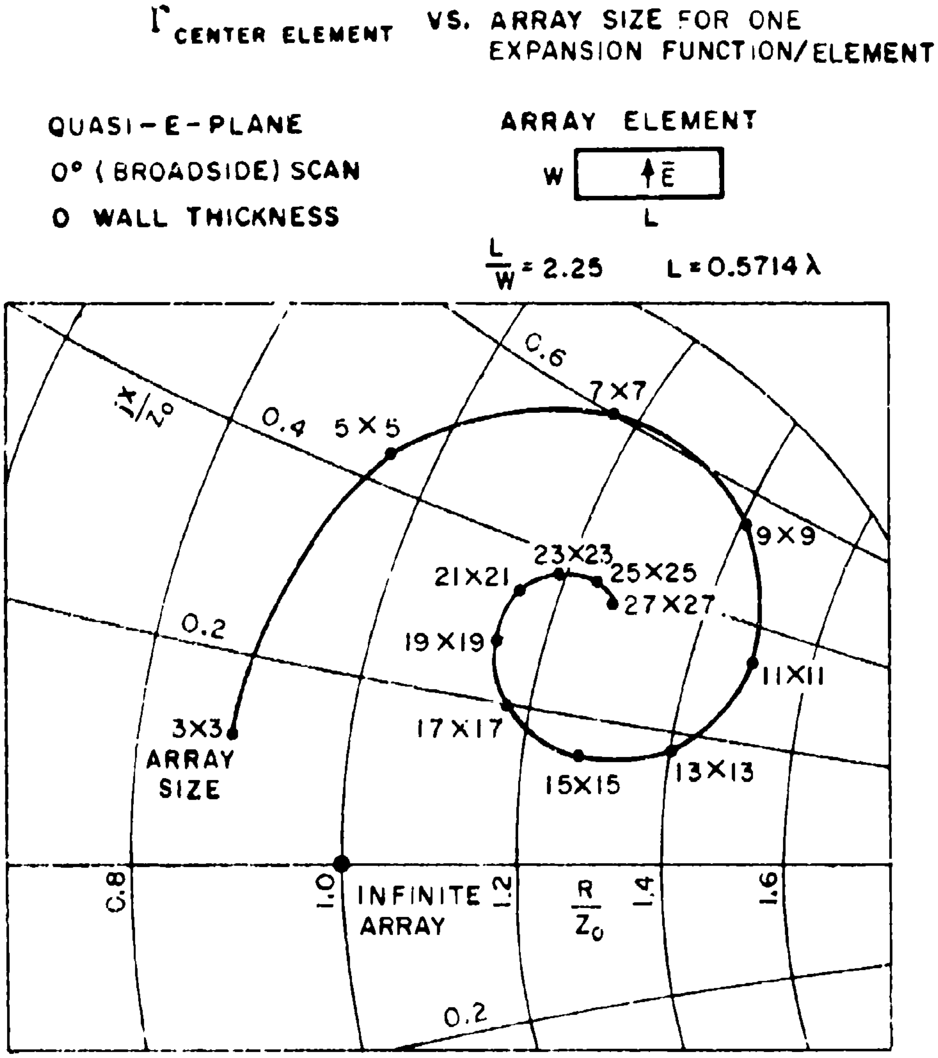

Figure 4-11. Center element reflection coefficient as a function of array size. Array elements are rectangular waveguide-fed apertures. Data points are plotted in the center portion of a Smith chart.

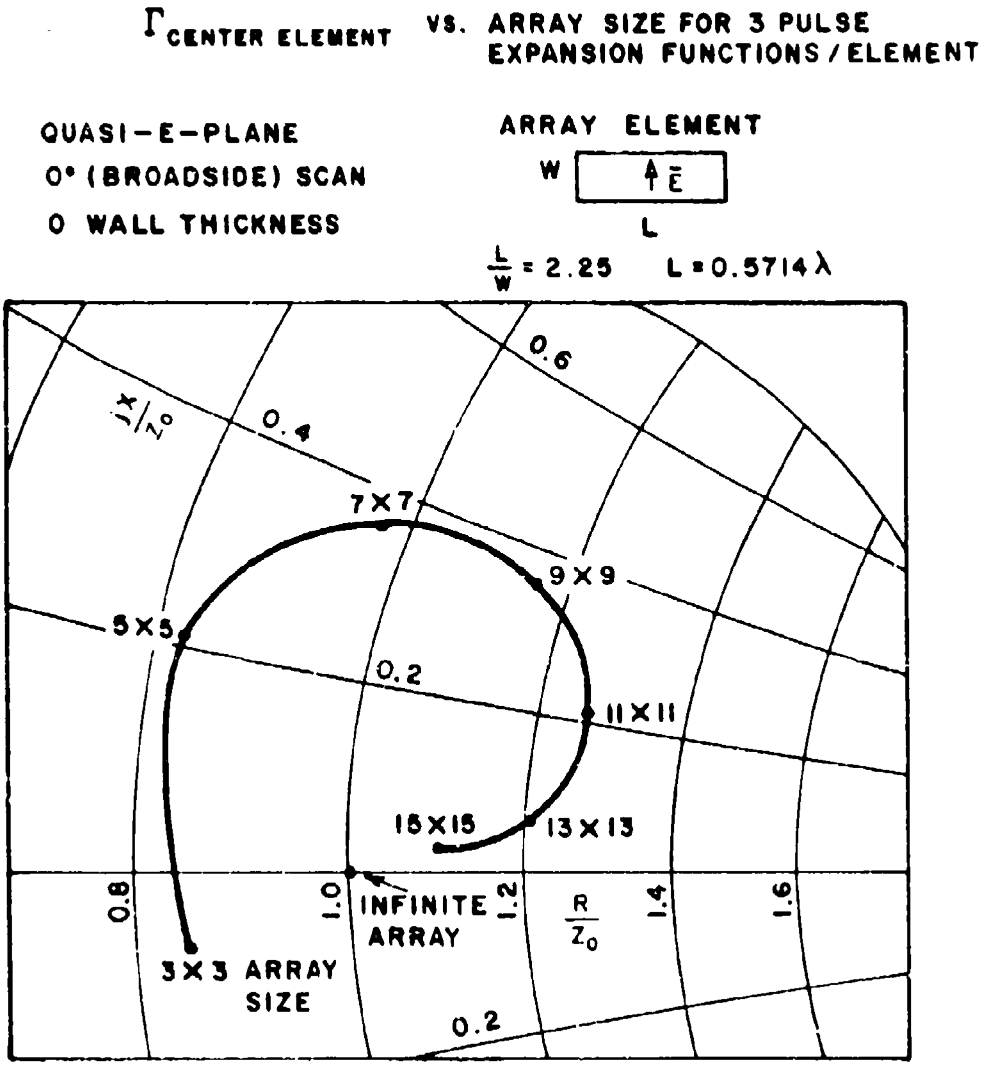

Figure 4-12. Center element reflection coefficient as a function of array size. Array elements are rectangular waveguide-fed apertures. Data points are plotted in the center portion of a Smith chart.

Reflection coefficient data for all the elements of E-plane scanned arrays, in which the elements are square waveguide-fed apertures with zero wall thickness, is given in Appendix K for array sizes 3x3, 5x5, 7x7, 9x9, and 11x11 for various scan angles. The reflection coefficient of the center element of an 11x11 array of square apertures as a function of E-plane scan angles is shown in Figure 4-13. The center element reflection coefficient for H-plane scanning is also shown for comparison. For infinite arrays with interelement spacing equal to 0.5714λ the Wood's anomaly (or blindness effect), for which Γ=1 for all elements, should occur at an E-plane scan angle of 50°. Figure 4-13 seems to indicate the presence of Wood's anomaly at 50° but in a washed out form due to the finiteness of the array. The behavior of the reflection coefficient as a function of scan angle for elements along the center column near the edge of the 11x11 array is examined in Figure 4-14. The three curves represent the reflection coefficients of the edge element, one element removed from the edge, and two elements removed from the edge. The greatest variation is seen to be in going from the edge element to one element removed from the edge. Thereafter, the effects of the edge diminish rapidly. The aperture distributions for the bottom edge element,

11 X 11 ARRAY
CENTER ELEMENT REFLECTION COEFFICIENT
VS. SCAN ANGLE

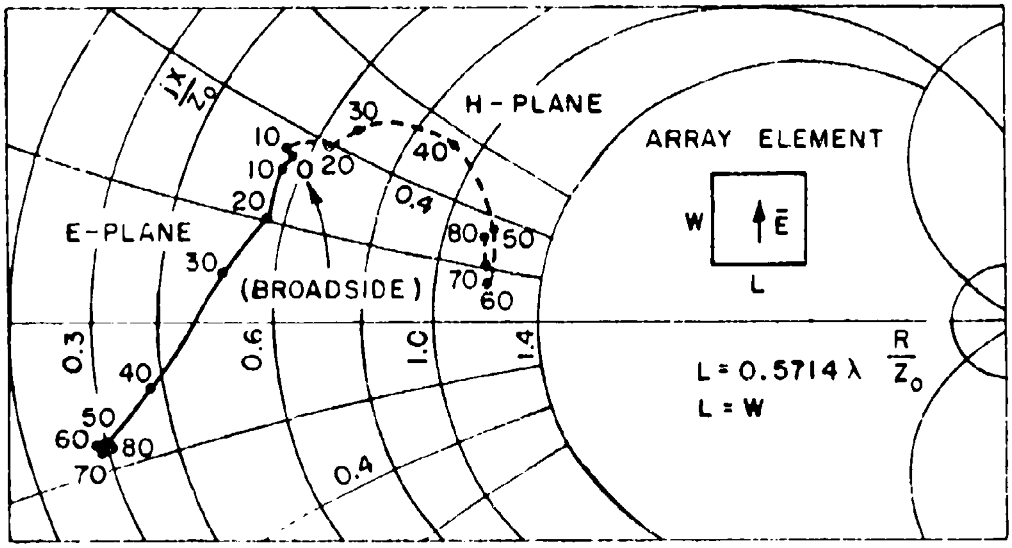

Figure 4-13. Center element reflector coefficient for an 11x11 array of square waveguide-fed apertures as a function of scan angle. Date points are plotted in the center portion of a Smith chart.

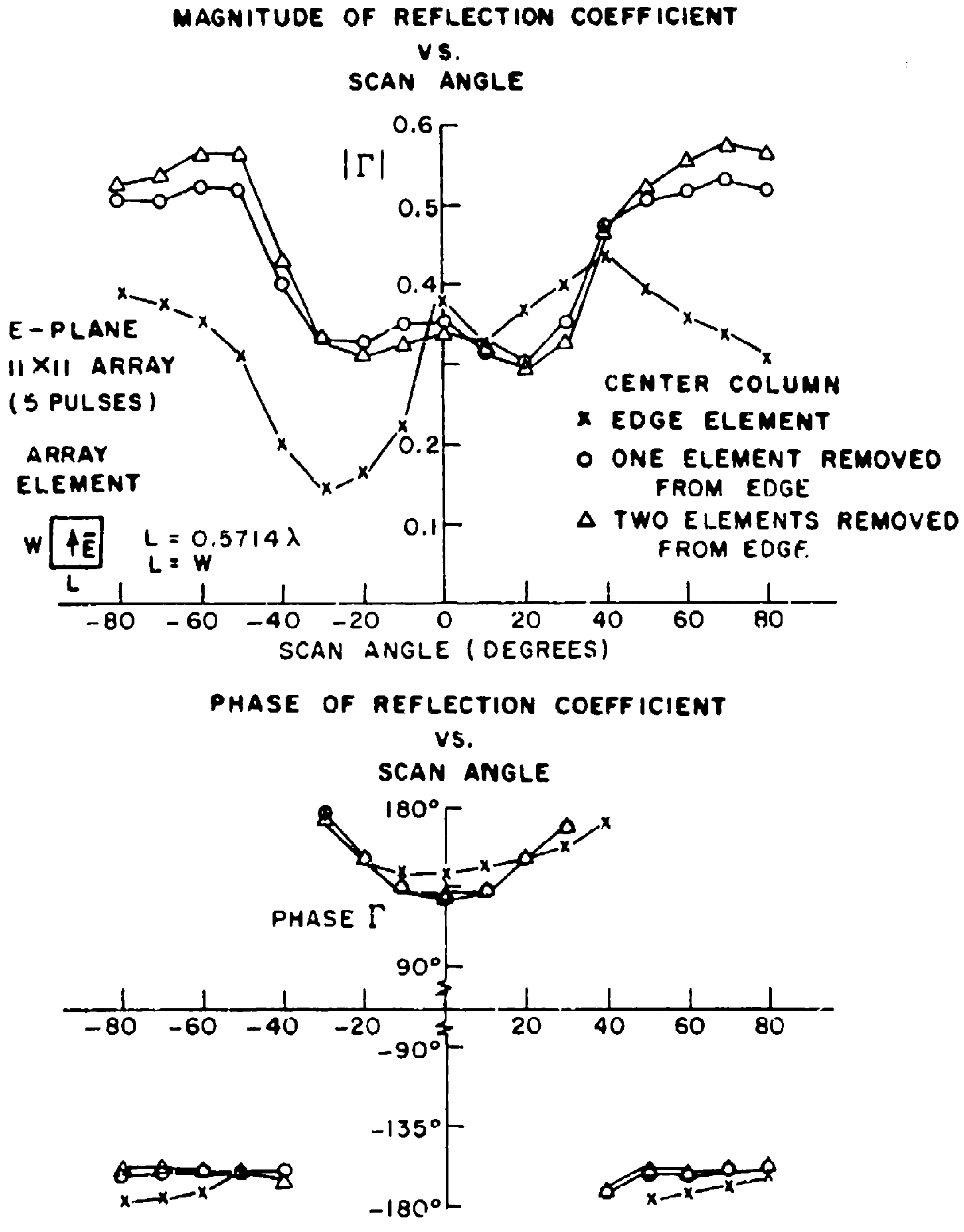

Figure 4-14. Reflection coefficients for elements in the vicinity of the array edge along the center column of an 11x11 array of square waveguide-fed apertures as a function of E-plane scan angle.

one element removed from the edge, and center element along center column of the 11x11 array is shown in Figures 4-15 for an E-plane 0° (broadside) scan and in Figure 4-16 for an E-plane 60° scan. For both scan angles the edge element aperture distribution is highly non-symmetric and differs greatly from the center element. This is to be expected in small finite arrays.

E-plane scanning for arrays of sizes 3x3, 5x5, 7x7, 9x9, and 11x11 in which the elements are rectangular waveguide-fed apertures with length to width ratio 2.25 are considered in Appendix L. The aperture reflection coefficients are shown for all the elements of the arrays for various scan angles. The effect of non-zero wall thickness is also examined in Appendix L for 7x7 and 11x11 arrays. Figure 4-17 shows the results for the center element reflection coefficient, as a function of E-plane scan angle, for an 11x11 array with five rectangular pulse bases per element with zero and 0.02516λ wall thickness. The effect of the 0.02516λ wall thickness is observed to be slight. For the 11x11 array with zero wall thickness the influence of the array finiteness on the reflection coefficients of elements along the center column are shown in Figure 4-18. The greatest variation is again seen to be from the edge element to the edge-adjacent element. The aperture distributions for the bottom edge, edge-adjacent, and center element along the center column of the 11x11 array are shown in Figures 4-19 and 4-20 for 0° and 60° E-plane scan angles, respectively. H-plane scanning will be considered next.

H-plane scanned arrays with square elements (with zero wall thickness) for array sizes 3x3, 5x5, 7x7, 9x9 and 11x11, in which the reflection coefficients of all the elements are given for various scan angles, are presented in Appendix M. The reflection coefficient of the center element of an 11x11 array as a function of H-plane scan angle is shown in Figure 4-21. Results obtained by Amitay, Galindo, and Wu for an infinite array of square apertures (with zero wall thickness), when all elements are excited and when only eleven columns are excited, are shown for comparison. Figure 4-21 shows that as far as the center element is concerned, there is very little difference between an 11x11 array and an infinite array for H-plane scanning. A comparison of the edge element reflection coefficient magnitude for the center row of an 11x11 array and the infinite array with eleven infinite columns of elements excited is shown in Figure 4-22. The agreement between the two curves is excellent. This indicates that using finite excitation in an infinite array environment as done by Amitay, Galindo, and Wu is a good approximation to the behavior of a finite array. The effect of the edge on the reflection coefficients of elements along the center row of the 11x11 H-plane scanned array is shown in Figure 4-23. The behavior of the reflection coefficients near the array edge is the same as that observed for E-plane scanning.

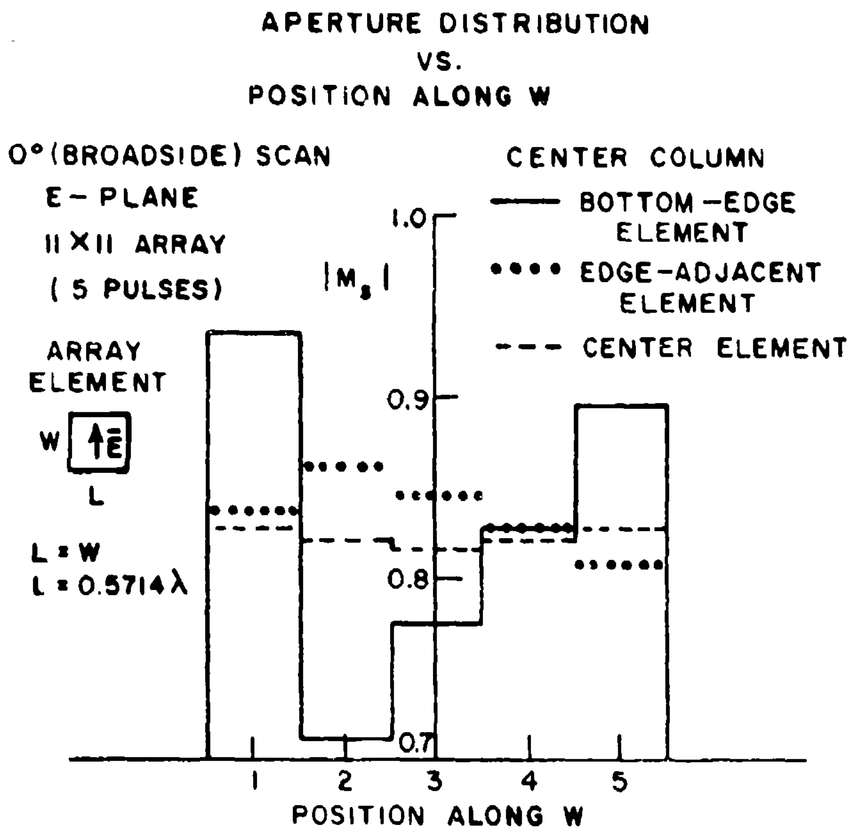

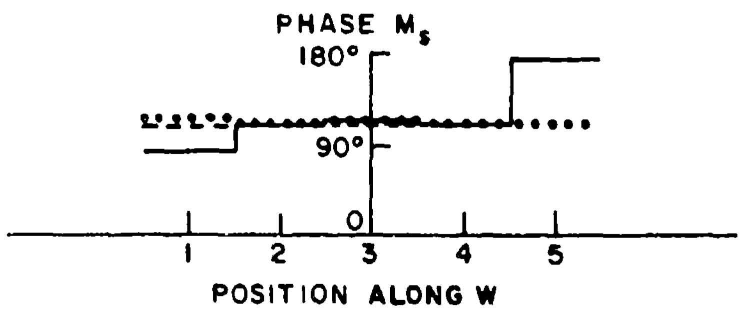

Figure 4-15. Aperture distributions in the vicinity of the array edge along the center column of an 11x11 array of square waveguide-fed elemnts. Position number one refers to the lower edge of each aperture.

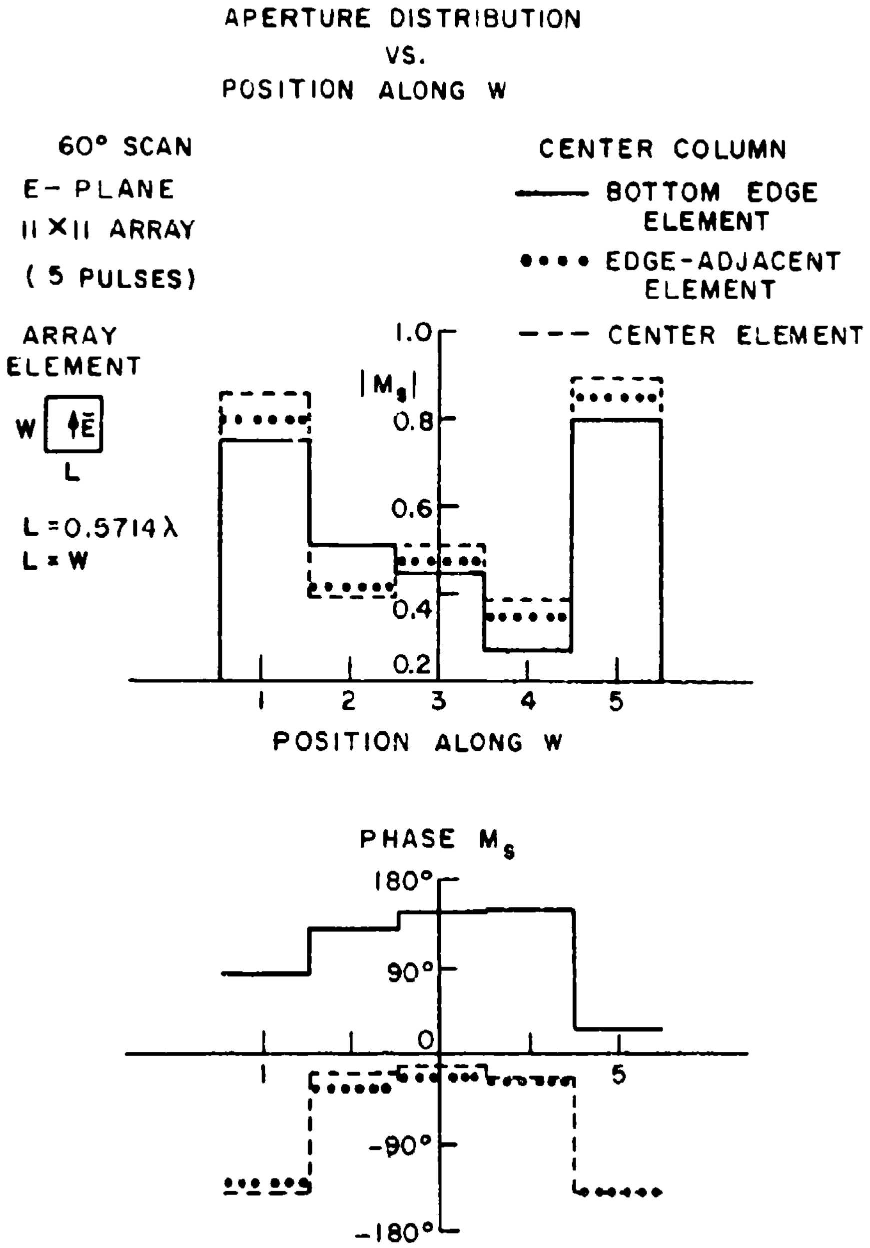

Figure 4-16. Aperture distributions in the vicinity of the array edge along the center column of an 11x11 array of square waveguide-fed elements. Position number one refers to the lower edge of each aperture.

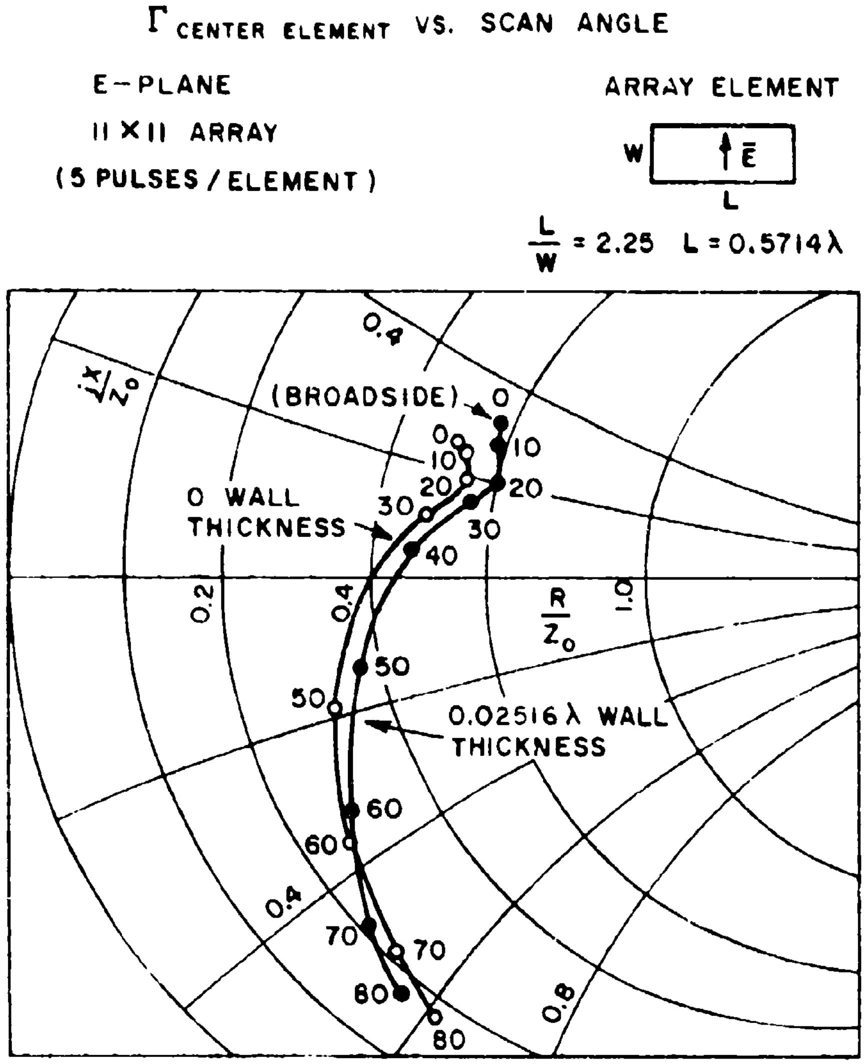

Figure 4-17. The effect of waveguide wall thickness on the center element reflection coefficient of an 11x11 array of rectangular waveguide-fed apertures. Data points are plotted in the center portion of the Smith chart.

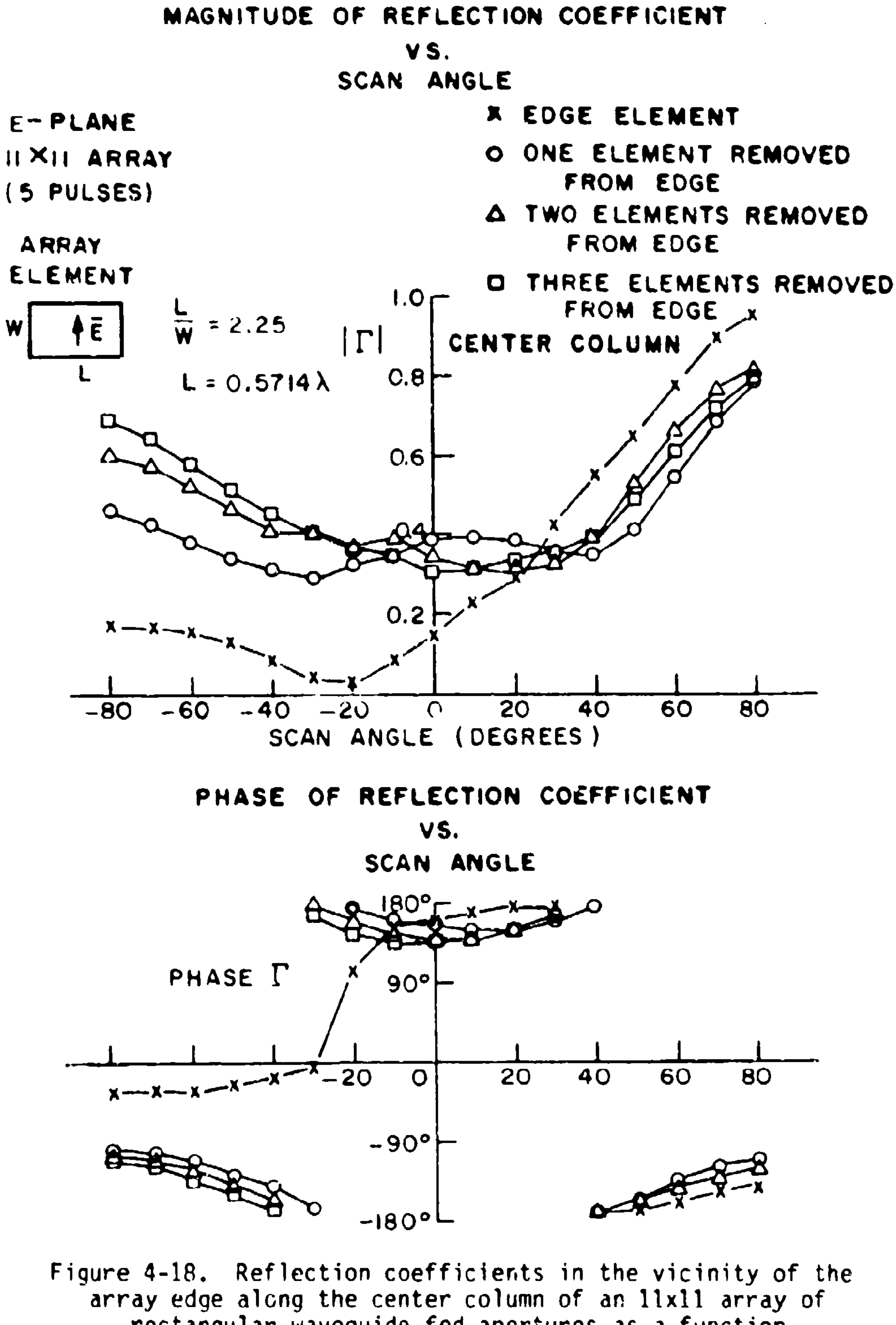

Figure 4-18. Reflection coefficients in the vicinity of the array edge along the center column of an 11x11 array of rectangular waveguide-fed apertures as a function of E-plane scan angle.

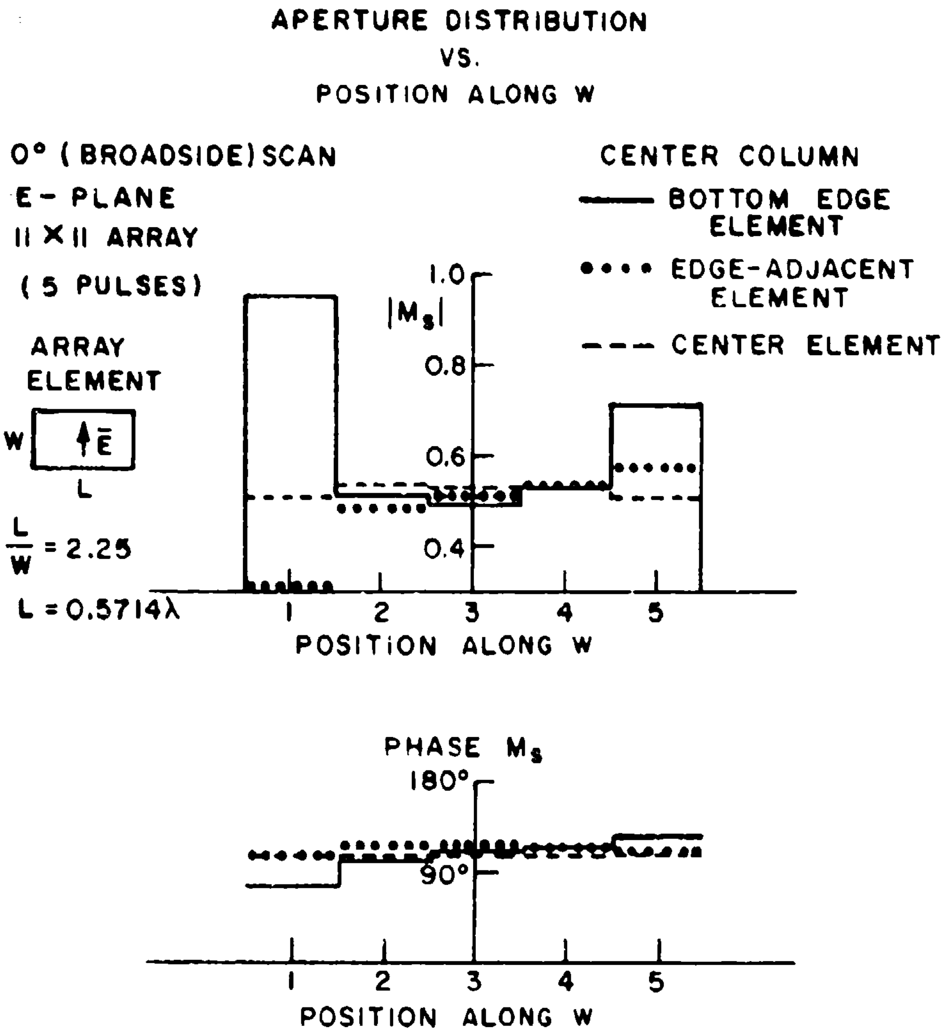

Figure 4-19. Aperture distributions in the vicinity of the array edge along the center column of an 11x11 array of rectangular waveguide-fed apertures. Position number one refers to the lower edge of each aperture.

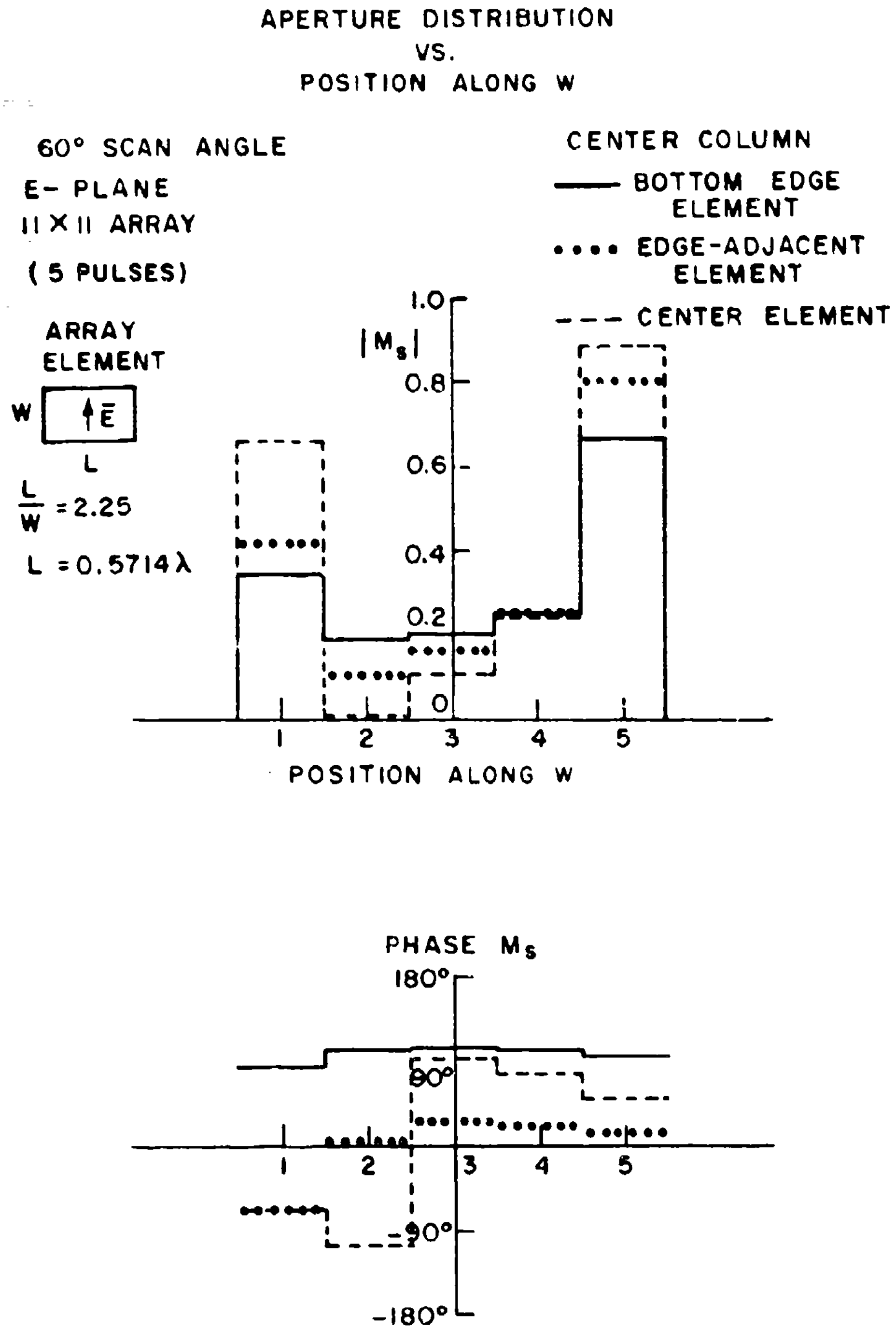

Figure 4-20. Aperture distributions in the vicinity of the array edge along the center column of an 11x11 array of rectangular waveguide-fed apertures. Position number one refers to the lower edge of each aperture.

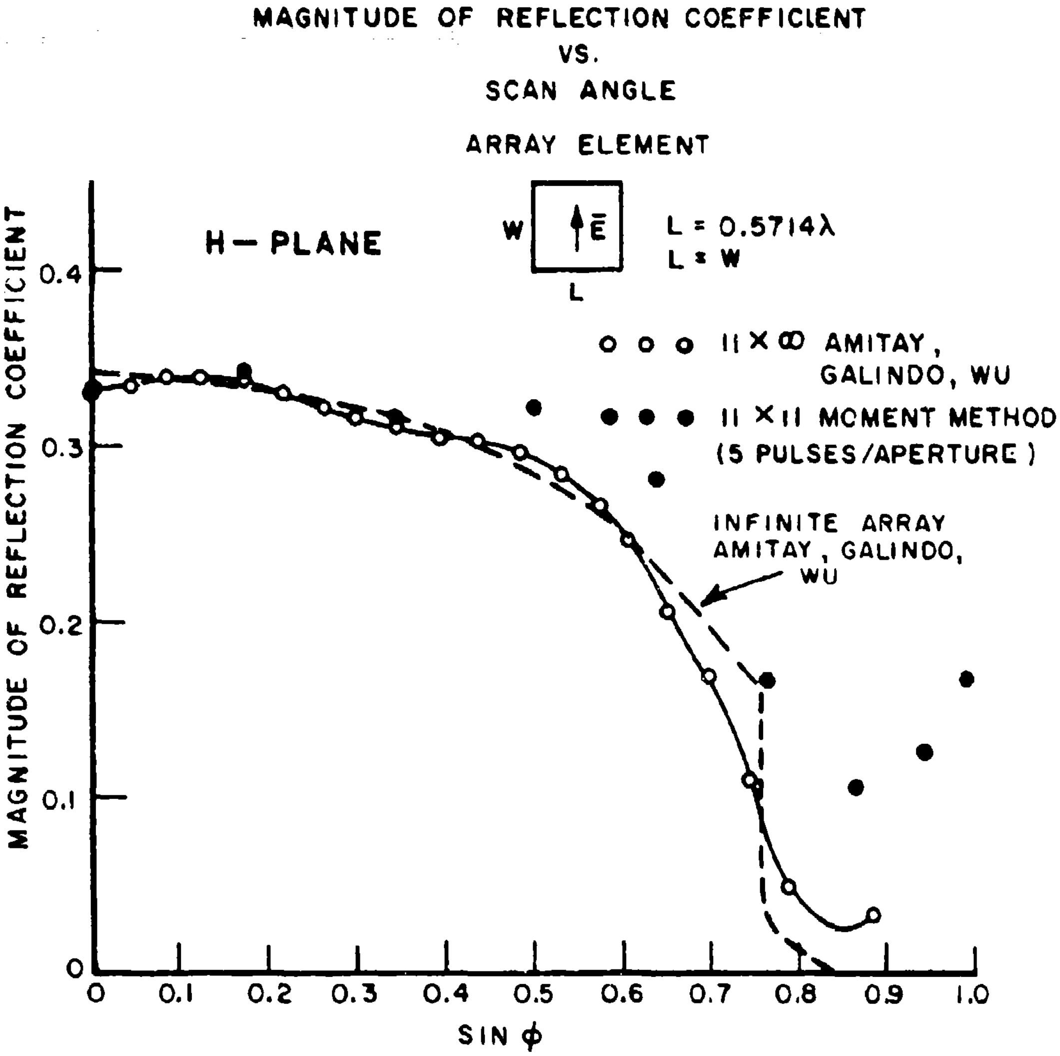

Figure 4-21. Center element reflection coefficient in finite and infinite arrays as a function of H-plane scan angle. Array elements are square waveguide-fed apertures.

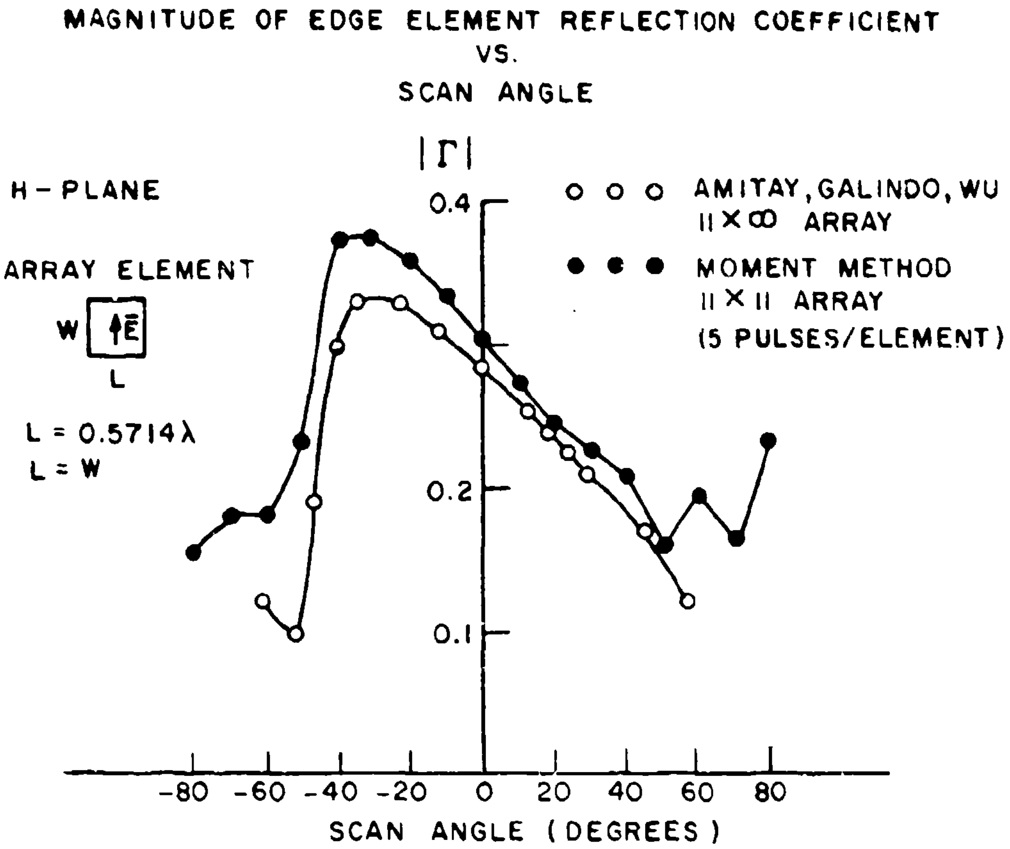

Figure 4-22. Comparison between the magnitude of the edge element reflection coefficient of an 11x11 array and an infinite array with eleven infinite columns of elements excited. Array elements are square waveguide-fed apertures.

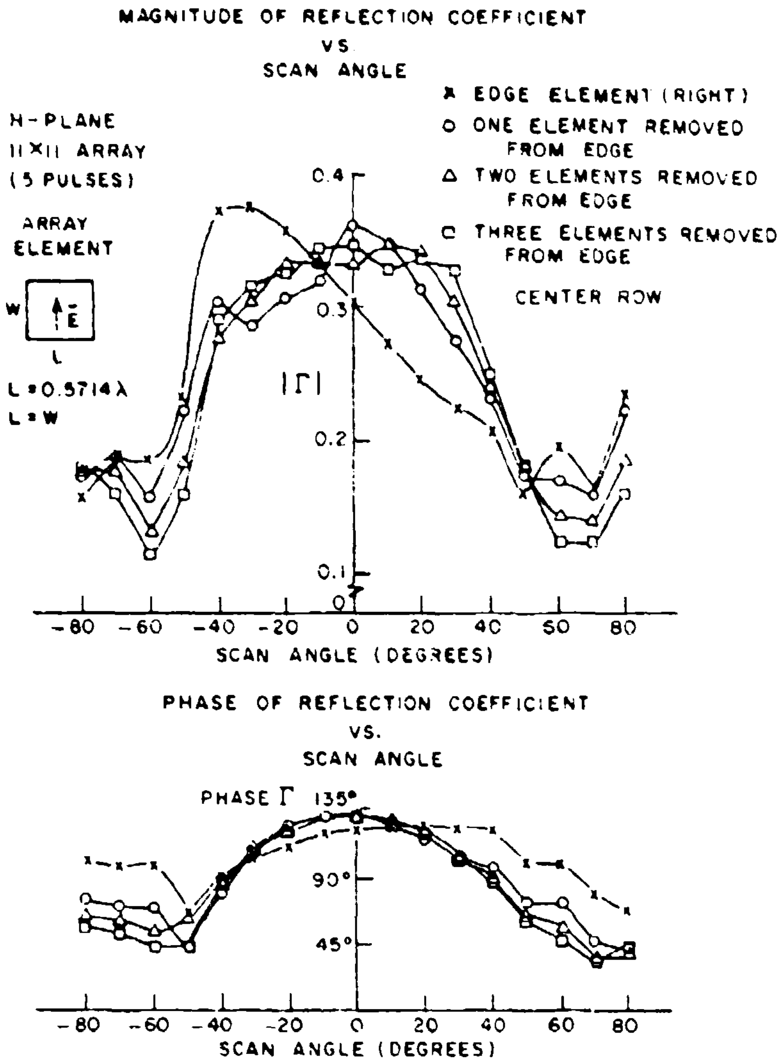

Figure 4-23. Reflection coefficients in the vicinity of the array edge along the center row of an 11x11 array of square waveguide-fed apertures.

The aperture distributions of the right edge element, edge-adjacent element, and cente ... nt along the center row of the 11x11 array are shown in ... 4 for H-plane 0° (broadside) and in Figure 4-25 for H- ... . The aperture distributions are seen to be fairly unif ... . s is due to the center row having five adjacent rows of elements above and below it. Thus, the singularity in the equivalent magnetic current distribution is washed out due to the coupling between adjacent rows.

Finally, consider H-plane scanned arrays in which the array elements are rectangular waveguide-fed apertures with length to width ratio 2.25. Reflection coefficient data for arrays (with zero wall thickness) of sizes 3x3, 5x5, 7x7, 9x9, and 11x11 for various scan angles is presented in Appendix N. The effect of a wall thickness of 0.02516λ is also considered for arrays of sizes 7x7 and 11x11. Figure 4-26 shows the center element reflection coefficient as a function of scan angle for zero and 0.02516λ wall thickness. This difference between the two curves is seen to be slight. The difference is accounted for by the change in the half-space admittance matrix elements for the two cases. The edge effects on the reflection coefficient for elements along the center row of the 11x11 H-plane scanned array are shown in Figure 4-27. Aperture distributions of the edge, edge-adjacent, and center element are shown in Figure 4-28 for a 0° (broadside) H-plane scan and in Figure 4-29 for a 60° H-plane scan. The aperture distributions are fairly uniform, as was the case for square elements.

The ... u time required for solving for the reflection coefficients ... the 11x11 array (zero wall thickness) with five pulse expansion functions for twenty scan angles (E-plane and H-plane in ten degree increments) was about ten minutes. The bulk of the time is spent in the calculation and inversion of the admittance matrix. F... non-zero wall thickness the cpu time increased by about two minutes due to an increase in the number of half-space admittance matrix elements that had to be calculated.

In this section results have been presented for three types of scanning with arrays of either square or rectangular waveguide-fed apertures. Extensive additional results are presented in the appendices. All of the results serve to aid in an understanding of the performance of finite arrays, particularly with regard to the influence of the finite extent of the array upon the reflection coefficients of the various elements.

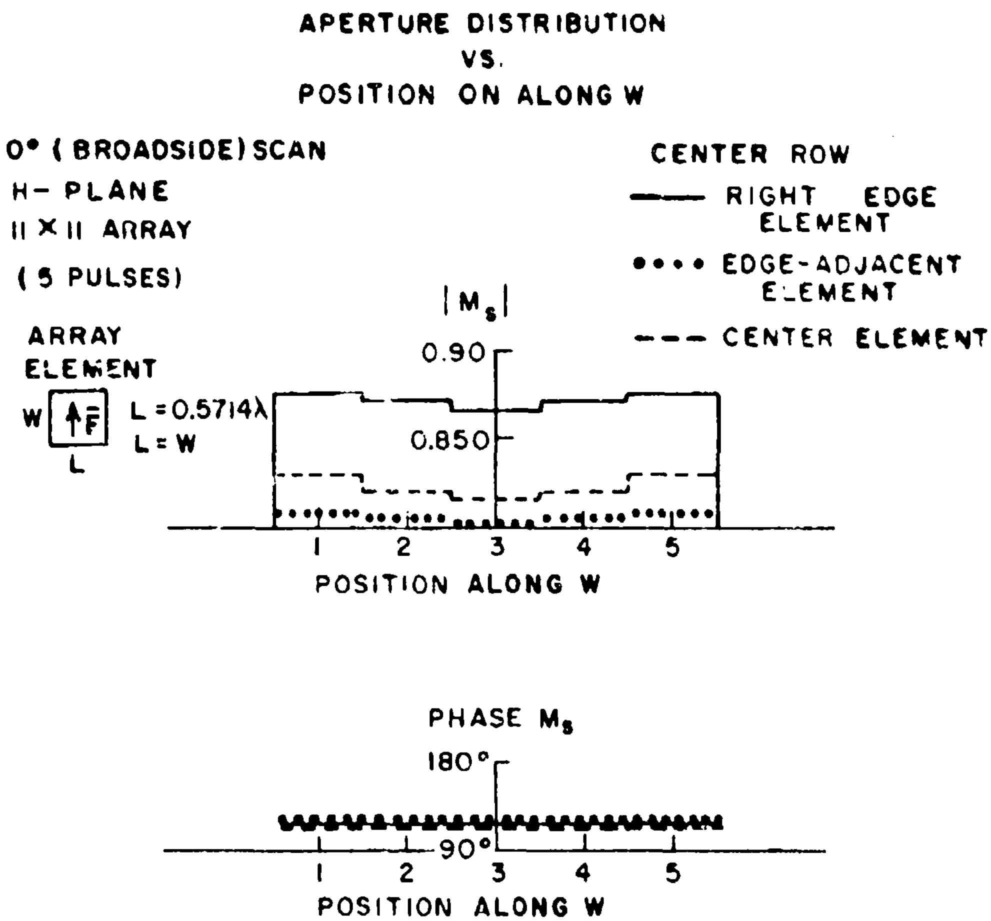

Figure 4-24. Aperture distributions in the vicinity of the array edge along the center row of an 11x11 array of square waveguide-fed apertures. Position number one refers to the lower edge of each aperture.

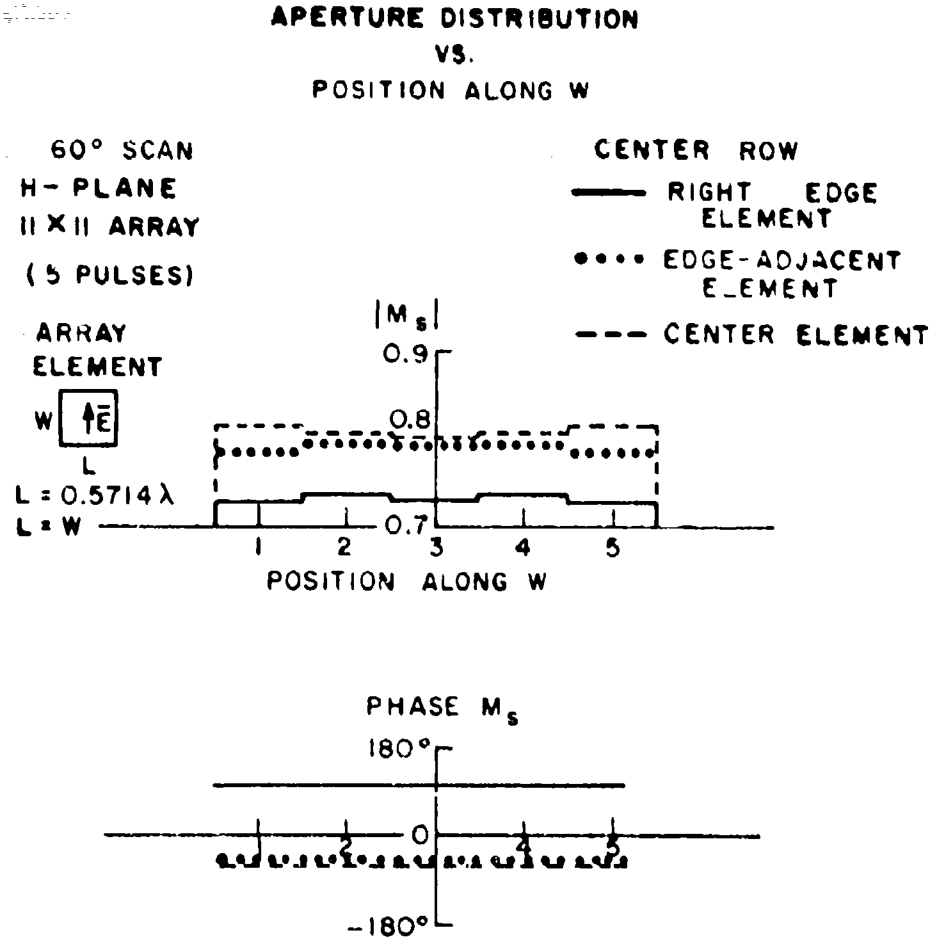

Figure 4-25. Aperture distributions in the vicinity of the array edge along the center row of an 11x11 array of square waveguide-fed apertures. Position number one refers to the lower edge of each aperture.

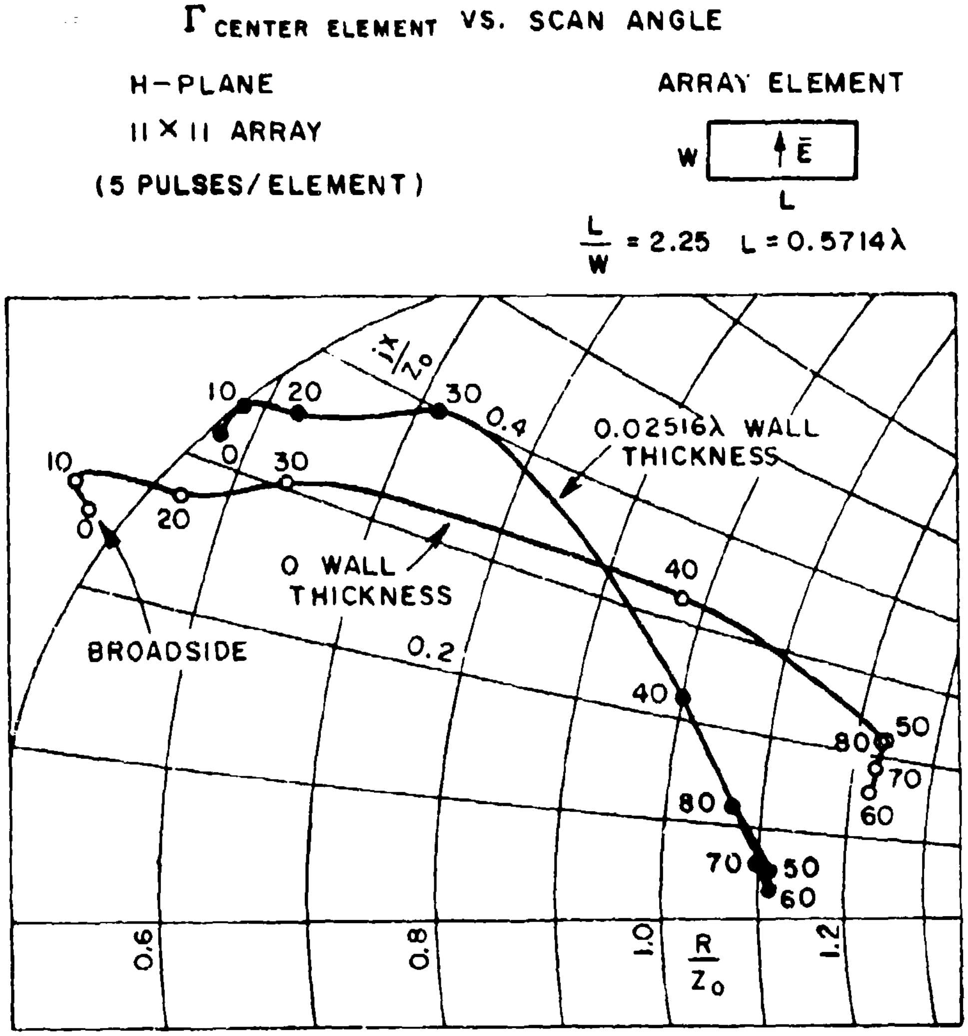

Figure 4-26. The effect of wall thickness on the center element reflection coefficient for an 11x11 array of rectangular waveguide-fed apertures. Data points are plotted in the center portion of a Smith chart.

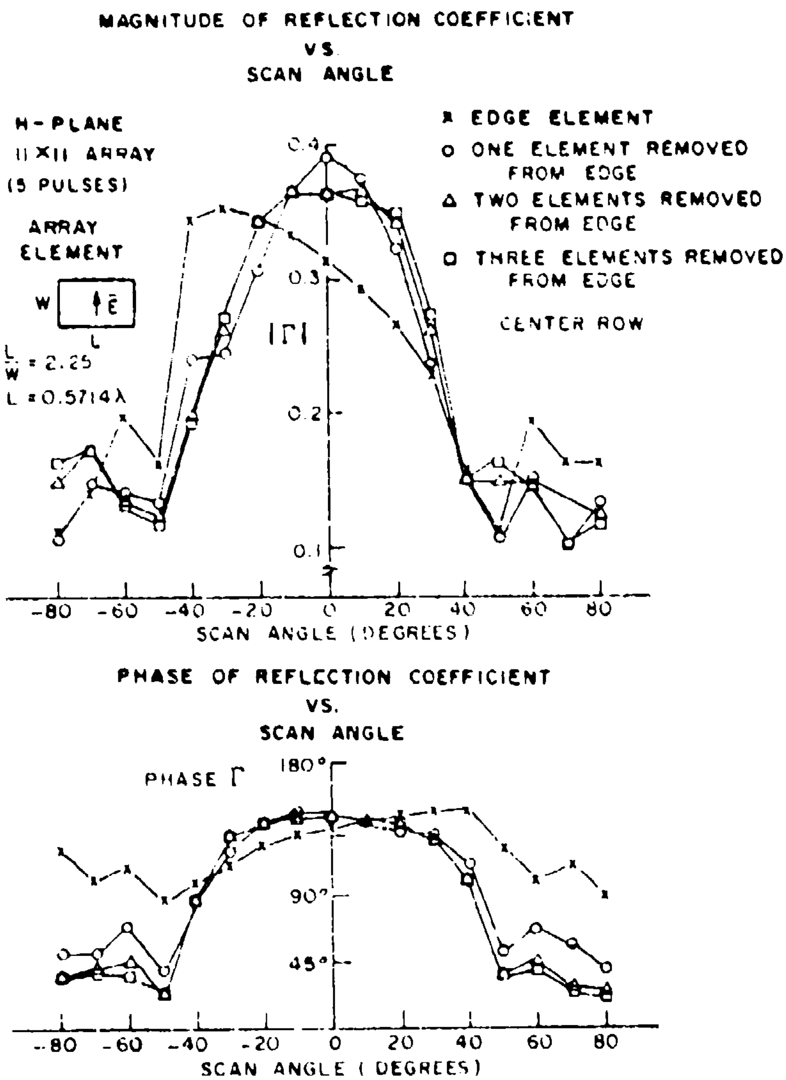

Figure 4-27. Reflection coefficients in the vicinity of the array edge along the center row of an 11x11 array of rectangular waveguide-fed apertures.

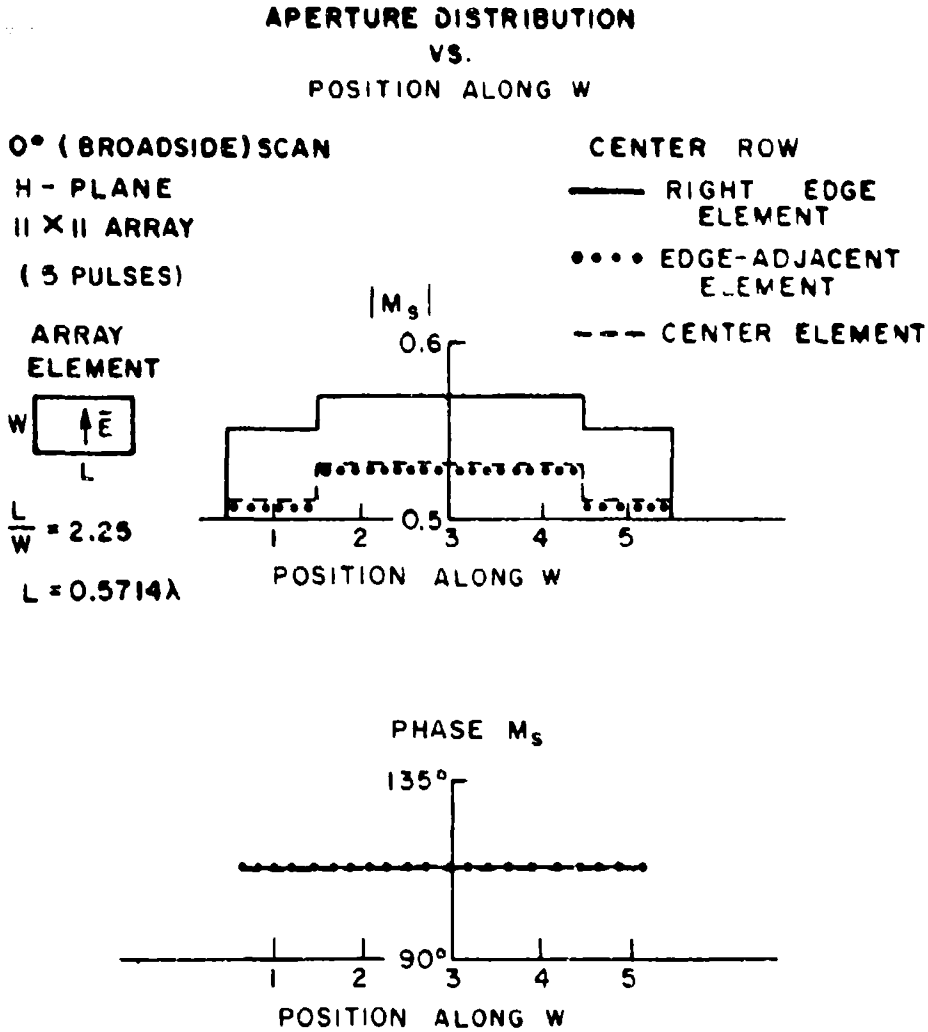

Figure 4-28. Aperture distributions in the vicinity of the array edge along the center row of an 11x11 array of rectangular waveguide-fed apertures. Position number one refers to the lower edge of each aperture.

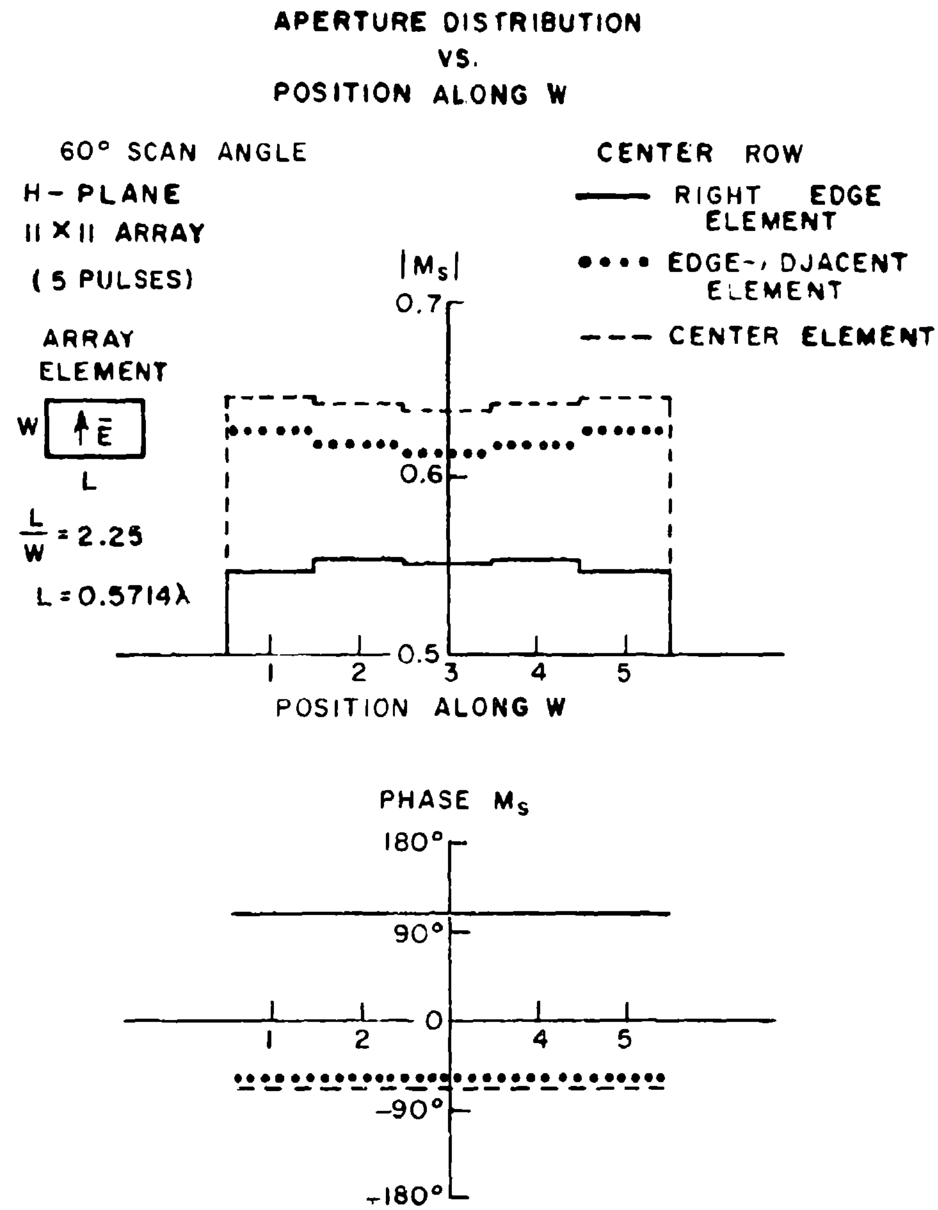

Figure 4-29. Aperture distributions in the vicinity of the array edge along the center row of an 11x11 array of rectangular waveguide-fed apertures. Position number one refers to the lower edge of each aperture.

CHAPTER V
DISCUSSION

The purpose of this study was to analyze finite phased arrays of rectangular and square waveguide-fed apertures. This was done by using the method of moments to find the aperture distribution of each of the array elements, from which element reflection coefficients were obtained. To check the theory, reflection coefficient data for single rectangular and square waveguide-fed apertures was calculated. The results were found to be in excellent agreement with data in the literature. Next, reflection coefficient data was presented for arrays with zero wall thickness, up to size 11x11 using E, H, and quasi-E-plane scanning (the purpose of considering quasi-E-plane scanning was to provide a check on the center element reflection coefficient). For elements of length 0.5714λ, it was found that to be within one to two percent of the converged reflection coefficient value, five pulse expansion functions per aperture along the width (E-plane) were needed. This was true for both rectangular and square elements. The effect of non-zero waveguide wall thickness was also studied and found to modify the reflection coefficients slightly.

The waveguide elements used in this study had a medium inside equal to that of free space, that is, $\mu=\mu_0$ and $\epsilon=\epsilon_0$. The formulation can be directly applied to a completely dielectric filled waveguide by using $\beta=\omega\sqrt{\mu_0\epsilon}$ and $\eta=\sqrt{\mu_0/\epsilon}$, where ϵ is the permittivity of the dielectric, in Equations (D-11) and (E-16). If, however, a short dielectric slab of dimensions equal to the waveguide cross section is used, the formulation must be modified. In this case plane wave reflection coefficients must be introduced when the plane waves from the probe or the aperture reach the edge of the slab. Both Equation (D-11) and Equation (E-16) would need this modification. If the finite array is covered by a dielectric sheet the free space Green's function used in Appendix C no longer applies. In this case the half-space coupling problem would have to be reformulated.

This study considered arrays with elements arranged in a rectangular lattice. Another array configuration that is useful is the triangular grid. An example of the triangular grid is shown in Figure 5-1 where three interlaced rows of elements are used. The triangular grid has the important feature that the array elements can be spaced closer than in a rectangular grid, thus avoiding grating lobes in the array beam pattern.[24] This configuration was not analyzed in the present study because the half-space admittance matrix is no longer block Toeplitz. Due to the elements being interlaced, the half-space admittance matrix will contain

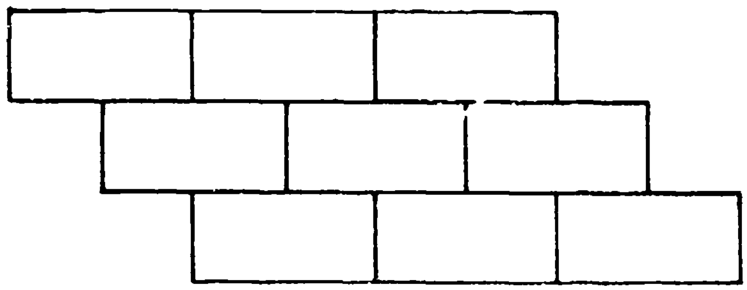

Figure 5-1. Triangular grid array.

some blocks that are not symmetric; hence Sinnot's block Toeplitz computer program cannot be used. As a result ordinary matrix inversion computer programs must be used to solve the system of equations. This results in an increase in cpu time and required storage. A computer program which makes use of the block matrix in the triangular grid case is needed to solve the system of equations more efficiently.

Another problem of interest is a finite array of waveguide-fed apertures in a finite ground plane. A 3x3 array is shown as an example of this in Figure 5-2. This problem can be solved by including contributions due to diffraction from the edges of the ground plane in the half-space admittance matrix. The total admittance matrix is then expressed as

$$\left[Y\right] = \left[Y^{wg}\right] + \left[Y^{hs}\right] + \left[Y^{diffracted}\right] \tag{5-1}$$

This type of solution is referred to as a hybrid technique[25] (method of moments combined with the geometrical theory of diffraction).

Another important addition to the analysis of finite arrays would be the development of a computer program to solve a double-block Toeplitz system of equations. This problem arises when a planar array of dipoles or slots are arranged in a rectangular lattice and more than one expansion function is used per element. While the block Toeplitz computer program can be used to solve the system of equations a double-block Toeplitz subroutine could represent an additional savings in cpu time and storage. Larger finite arrays could then be handled.

Thus, three improvements or refinements discussed above need to be made to the theory and the computer program (the present computer program is listed in Appendix D) in order to handle a larger class of problems. These problems occur often in the analysis of finite phased arrays.

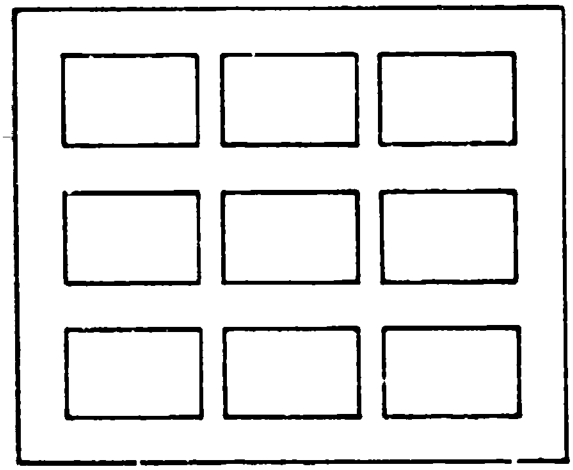

Figure 5-2. 3x3 array of waveguide-fed apertures in a finite ground plane.

APPENDIX A

THE MAGNETIC FIELD RADIATED BY AN INFINITE ARRAY OF RECTANGULAR MAGNETIC SURFACE SOURCES WITH ARBITRARY CURRENT DISTRIBUTION

In this appendix the total magnetic field $\bar{H}_T$, radiated by an infinite planar array of rectangular magnetic surface sources, is derived. The derivation closely follows work done by Munk, Burrell, and Kornbau[26] on periodic surfaces and is included for completeness. This calculation is used in determining $H^{wg}(\bar{M}_x)$ in Equation (3-11) as well as $\bar{H}_a$ in Equation (D-4). The array to be analyzed is shown in Figure A-1 in the rectangular coordinate system. All elements of the array are in the xz-plane and have a magnetic current component that is x-directed. The current distribution of the reference element of the array is arbitrary. All the other elements have the same arbitrary distribution as well as a constant incremental phase shift in both the x and z directions. The entire array is displaced a distance d from the origin along the -y axis. This corresponds to the location of the waveguide-fed aperture in Figure 3-1. The medium in which the array is located has permeability μ and permittivity ε.

Let $\bar{R}$ denote the position vector for the observation point P(x,y,z). In the analysis that follows, first the electric field radiated by an infinite array of Hertzian dipoles with length $d\ell$ is calculated. Next, this field is integrated over the area of each rectangular element of the array to obtain the total electric field $\bar{E}_T$. The expression for $\bar{E}_T$ will be in the form of a plane wave expansion; hence $\bar{H}_T$ can be determined by the plane wave relation

$$\frac{\hat{s} \times \bar{E}_T}{\eta} \tag{A-1}$$

where

$\hat{s} = \hat{x}s_x + \hat{y}s_y + \hat{z}s_z$ is the direction of propagation

η is the impedance of the medium.

The electric field radiated by an infinite array of magnetic Hertzian dipoles can be determined in the following manner: Consider an element of the array in row n and column k, with magnetic current $\hat{p}K_{kn}$ and length $d\ell$ located in the xz-plane as shown in Figure A-2. The unit vector $\hat{p}$ is, in general, completely arbitrary

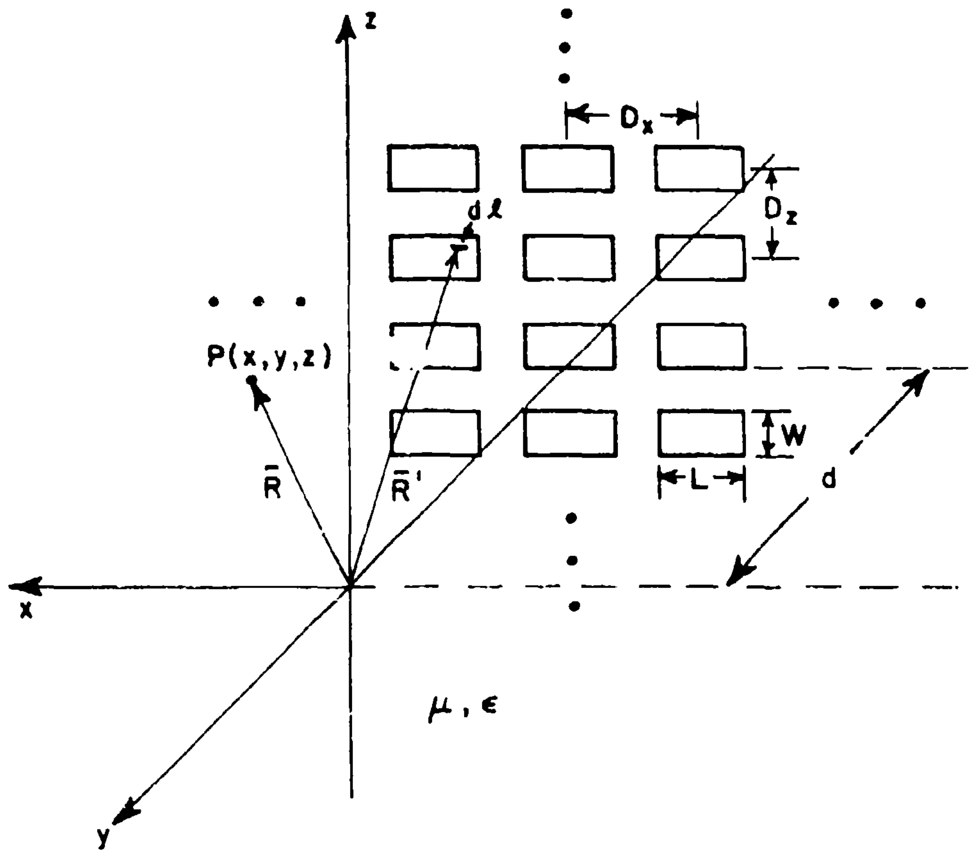

Figure A-1. General view of an infinite array of rectangular surface sources.

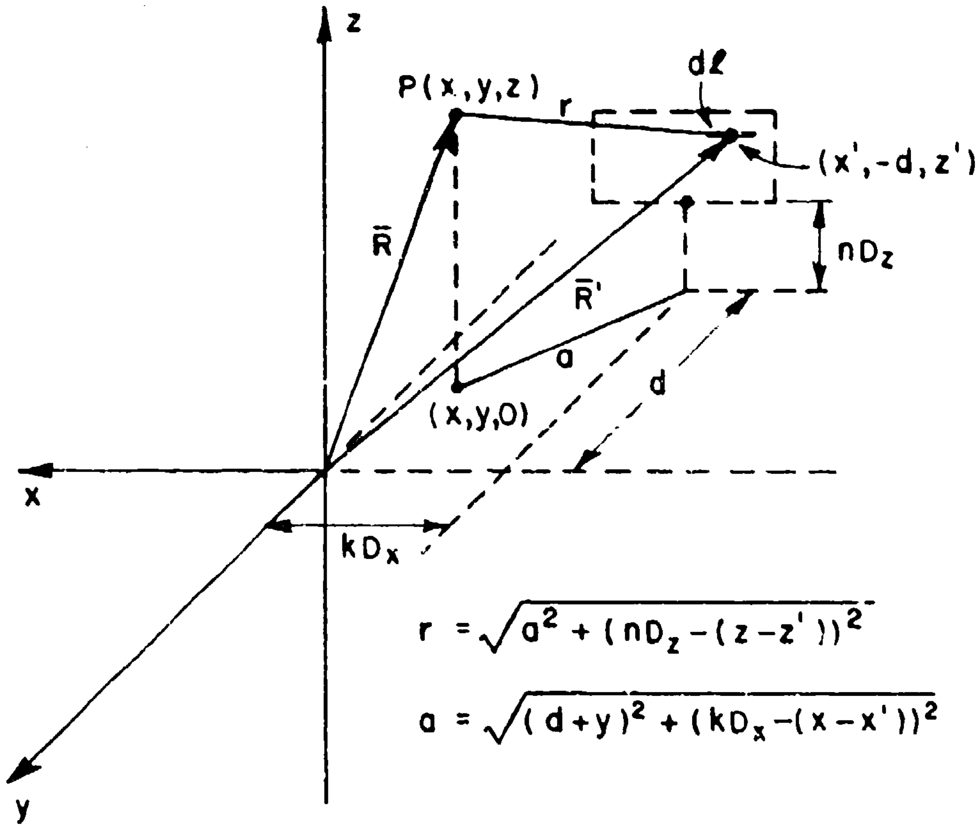

Figure A-2. The geometry involving the observation point P(x,y,z) and the kn'th element of the array.

with components $\hat{x}$, $\hat{y}$, and $\hat{z}$ in the rectangular coordinate system. The reference element of the array is located at the point (x',-d,z'), and the remaining elements are positioned at the points (nD_x+x',-d, kD_z+z') where n and k are integers (positive and negative) and D_x and D_z are the interelement spacings in the x and z directions, respectively. In order to calculate the electric field, first the electric vector potential $\bar{F}$ is calculated, then the equation[27]

$$\bar{E} = -\frac{1}{\epsilon} \nabla \times \bar{F} \tag{A-2}$$

is applied.

The vector potential $\bar{F}_{kn}$ from a single element of the array observed at the point P(x,y,z) is given by

$$\bar{F}_{kn} = \hat{p} \frac{\epsilon K_{kn} \, d\ell}{4\pi r} e^{-j\beta r} \tag{A-3}$$

where $\beta = \frac{2\pi}{\lambda}$ is the propagation constant,

$$r = \sqrt{a^2 + (nD_z-(z-z'))^2} , \tag{A-4}$$

and

$$a = \sqrt{(d+y)^2+(kD_x-(x-x'))^2} . \tag{A-5}$$

By superposition, the total electric vector potential $\bar{F}$ from the entire array is

$$\bar{F} = \sum_{k=-\infty}^{\infty} \sum_{n=-\infty}^{\infty} \bar{F}_{kn}$$

$$= \hat{p} \frac{\epsilon d\ell}{4\pi} \sum_{k=-\infty}^{\infty} \sum_{n=-\infty}^{\infty} K_{kn} \frac{e^{-j\beta r}}{r} . \tag{A-6}$$

For an infinite array scanned in the direction $\hat{s}$ the element currents must be of the Floquet type[28], that is,

$$K_{kn} = K_1 e^{-j\beta kD_z s_z} e^{-j\beta nD_x s_x} \tag{A-7}$$

where K_1 is the terminal current and s_x and s_z are calculated by satisfying boundary conditions for the problem of interest. Substituting Equation (A-7) into (A-6) yields

$$\bar{F} = \hat{p} \quad \frac{\epsilon K_1 d\ell}{4\pi} \sum_{k=-\infty}^{\infty} \sum_{n=-\infty}^{\infty} e^{-j\beta k D_x s_x} .$$

$$\cdot\ e^{-j\beta n D_z s_z} \frac{e^{-j\beta r}}{r}$$

or

$$\bar{F} = \sum_{k=-\infty}^{\infty} \bar{F}_k\, e^{-j\beta k D_x s_x} \qquad \text{(A-8)}$$

where

$$\bar{F}_k = \hat{p} \quad \frac{\epsilon K_1 d\ell}{4\pi} \sum_{n=-\infty}^{\infty} e^{-j\beta n D_z s_z} \frac{e^{-j\beta r}}{r} \qquad \text{(A-9)}$$

represents the vector potential from column k of the array.

$\bar{F}_k$ can be calculated by transforming Equation (A-9) into a faster converging series with use of the Poisson sum formula

$$\sum_{n=-\infty}^{\infty} e^{jn\omega_0 t} F(n\omega_0) = T \sum_{n_1=-\infty}^{\infty} f(t+n_1 T) \qquad \text{(A-10)}$$

where $F(\omega)$ is the Fourier transform of $f(t)$, that is,

$F(\omega) = \mathcal{F}\left[f(t)\right]$, and

$T = \frac{2\pi}{\omega_0}$ is the period.

The required Fourier transform pair[30] for Equation (A-9) is

$$\frac{e^{-j\beta\sqrt{a^2+\omega^2}}}{\sqrt{a^2+\omega^2}} \div \mathcal{F}\left[\ \frac{-j}{2}\, H_0^{(2)}\left(a\sqrt{\beta^2-t^2}\right) p_\beta(t)\right.$$
$$\left. + \frac{1}{\pi}\, K_0\left(a\sqrt{t^2-\beta^2}\right)\left(1-p_\beta(t)\right)\right] \qquad \text{(A-11)}$$

where $H_0^{(2)}$ and K_0 are the Hankle and modified Bessel function, respectively, of zero order and the second kind.

$$p_\beta(t) = \begin{cases} 1 & \text{for } -\beta < t < \beta \\ 0 & \text{otherwise} \end{cases}$$

($p_\beta(t)$ is the pulse function).

By comparison of Equation (A-11) with Equations (A-9) and (A-4) it is evident that the frequency shifting theorem[31]

$$F(\omega-\omega_1) = \mathcal{F}\left[e^{j\omega_1 t} f(t)\right] \tag{A-12}$$

with $\omega_1 = z-z'$, is needed to transform Equation (A-9). Comparing Equations (A-9) through (A-12) it is clear that with

$$\omega_0 = D_z, \quad T = \frac{2\pi}{D_z}, \quad t = -\beta s_z$$

the Poisson sum formula and frequency shifting theorem transform Equation (A-9) to

$$F_k = \hat{p}\,\frac{\varepsilon K_1 d\ell}{4\pi}\,\frac{2\pi}{D_z}\sum_{n_1=-\infty}^{\infty} e^{-j\beta(z-z')\left(s_z + n_1\frac{\lambda}{D_z}\right)}$$

$$\cdot\left[\frac{-j}{2}\,H_0^{(2)}\left(a\sqrt{\beta^2-\left(\beta s_z + n_1\frac{2\pi}{D_z}\right)^2}\right) + \frac{1}{\pi}\,K_0\left(a\sqrt{\left(\beta s_z + n_1\frac{2\pi}{D_z}\right)^2 - \beta^2}\right)\right]. \tag{A-13}$$

Equation (A-13) can be expressed in simpler form as

$$F_k = \hat{p}\,\frac{\varepsilon K_1 d\ell}{2D_z}\sum_{n_1=-\infty}^{\infty} e^{-j\beta(z-z')r_z}$$

$$\cdot\left[\frac{-j}{2}\,H_0^{(2)}(\beta a s_1) + \frac{1}{\pi}\,K_0(\beta a s_2)\right] \tag{A-14}$$

where

$$r_z = s_z + n_1\frac{\lambda}{D_z}, \tag{A-15}$$

$$s_1 = \sqrt{1-(r_z)^2}, \text{ and}$$

$$s_2 = \sqrt{(r_z)^2 - 1}.$$

The summation in Equation (A-14) over n_1 is extended over all values making s_1 and s_2 real. Substituting Equation (A-14) into (A-8) yields

$$\bar{F} = \hat{p} \; \frac{\epsilon K_1 d\ell}{2D_z} \sum_{n_1=-\infty}^{\infty} \sum_{k=-\infty}^{\infty} e^{-j\beta k D_x s_x}$$

$$\cdot \; e^{-j\beta(z-z')r_z} \left[-\frac{j}{2} H_0^{(2)}(\beta a s_1) + \frac{1}{\pi} K_0(\beta a s_2) \right] \; . \tag{A-16}$$

The summation over k in Equation (A-16) will now be transformed into a faster convergent series by use of the Poisson sum formula

$$\sum_{k=-\infty}^{\infty} e^{jk\omega_0 t} F(k\omega_0) = T \sum_{n_2=-\infty}^{\infty} f(t+n_2T) \; . \tag{A-17}$$

The necessary Fourier transform pairs are[32]

$$H_0^{(2)}\left(\beta s_1 \sqrt{(y+d)^2+\omega^2}\right) = \mathcal{F}\left[\frac{e^{-j(y+d)\sqrt{(\beta s_1)^2-t^2}}}{\pi\sqrt{(\beta s_1)^2 - t^2}} \; p_{\beta s_1}(t) \right.$$

$$\left. + \frac{je^{-(y+d)\sqrt{t^2-(\beta s_1)^2}}}{\pi\sqrt{t^2-(\beta s_1)^2}} \left(1-p_{\beta s_1}(t)\right) \right] \tag{A-18}$$

where the pulse function

$$p_{\beta s_1}(t) = \begin{cases} 1 & \text{for } -\beta s_1 < t < \beta s_1 \\ 0 & \text{otherwise} \end{cases}$$

and[33]

$$K_0\left(\beta s_2 \sqrt{(y+d)^2+\omega^2}\right) = \mathcal{F}\left[\frac{e^{-(y+d)\sqrt{(\beta s_2)^2+t^2}}}{2\sqrt{(\beta s_2)^2 + t^2}} \right] . \tag{A-19}$$

By comparison of Equations (A-18) and (A-19) with Equations (A-5) and (A-16) it is clear that the frequency shifting theorem,

given by Equation (A-12) with $\omega_1 = x-x'$, is needed to transform Equation (A-16). From Equation (A-17) choose

$$\omega_0 = D_x, \quad T = \frac{2\pi}{D_x}, \quad t = -\beta s_x$$

then Equation (A-16) becomes

$$\overline{F} = \hat{p} \frac{\epsilon K_1 d\ell}{2D_z} \sum_{n_1=-\infty}^{\infty} \frac{2\pi}{D_x} \sum_{n_2=-\infty}^{\infty} e^{-j\beta(x-x')r_x} \cdot e^{-j\beta(z-z')r_z}$$

$$\cdot \left[\frac{-j}{2} \frac{e^{-j(y+d)\sqrt{(\beta s_1)^2-(\beta s_x+n_2 \frac{2\pi}{D_x})^2}}}{\pi\sqrt{(\beta s_1)^2-(\beta s_x+n_2\frac{2\pi}{D_x})^2}} + \frac{1}{\pi} \frac{e^{-(y+d)\sqrt{(\beta s_2)^2+(\beta s_x+n_2\frac{2\pi}{D_x})^2}}}{2\sqrt{(\beta s_2)^2+(\beta s_x+n_2\frac{2\pi}{D_x})^2}} \right] \tag{A-20}$$

where $\quad r_x = s_x + n_2 \frac{\lambda}{D_x}$.

Substituting s_1 and s_2 into Equation (A-20) yields the compact result

$$\overline{F}(x,y,z) = -\hat{p} \frac{j\epsilon K_1 d\ell}{2\beta D_x D_z} \sum_{n_1=-\infty}^{\infty} \sum_{n_2=-\infty}^{\infty} \frac{e^{-j\beta(\overline{R}-\overline{R}')\cdot\hat{r}_{21}}}{r_y} \tag{A-21}$$

where

$\overline{R} = \hat{x}\, x + \hat{y}\, y + \hat{z}\, z$ is the observation point position vector referred to the origin,

$\overline{R}' = \hat{x}\, x' - \hat{y}\, d + \hat{z}\, z'$ is the source point location,

$\hat{r}_{21} = \hat{x}\, r_x + \hat{y}\, r_y + \hat{z}\, r_z$

denotes the direction of propagation of the bundle of plane waves, and

$$r_y = \pm\sqrt{1-(r_z)^2 - (r_x)^2} \quad . \tag{A-22}$$

In Equation (A-22) the upper sign(+) should be used for $y > -d$, the lower sign (-) for $y < -d$. Furthermore, where the integers n_1, n_2 attain such values making the square root imaginary, the $-j$ value should be used for $y > -d$ and the $+j$ value when $y < -d$. These choices will ensure waves propagating from the array and attenuated as well.

Now that the electric vector potential at an arbitrary point has been found, the total electric field can be determined by Equation (A-2). Applying Equation (A-2) to Equation (A-21) yields

$$\overline{E} = \frac{jK_1 d\ell}{2\beta D_x D_z} \sum_{n_2=-\infty}^{\infty} \sum_{n_1=-\infty}^{\infty} \nabla \times \left(\hat{p}\, \frac{e^{-j\beta(\overline{R}-\overline{R}')\cdot \hat{r}_{21}}}{r_y} \right) . \tag{A-23}$$

Next, apply the vector identity[34]

$$\nabla \times (\phi\overline{A}) = \phi\nabla \times \overline{A} - \overline{A} \times \nabla\phi \tag{A-24}$$

to Equation (A-23) and obtain

$$\overline{E}(x,y,z) = \frac{K_1 d\ell}{2D_x D_z} \sum_{n_2=-\infty}^{\infty} \sum_{n_1=-\infty}^{\infty} \hat{p} \times \hat{R}_{21}\, \frac{e^{-j\beta(\overline{R}-\overline{R}')\cdot\hat{r}_{21}}}{r_y} . \tag{A-25}$$

Equation (A-25) is the electric field from an array of Hertzian dipoles. To obtain the total field radiated by the infinite array of rectangular surface sources it is necessary to integrate Equation (A-25) over the surface of the reference rectangular source. To perform the surface integration the terminal current K_1 in Equation (A-25) must be replaced by a current density $M(x',z')$. Let $d\ell = dx'$ and $p = x$ then,

$$\bar{E}_T(x,y,z) = \frac{-1}{2D_xD_z} \sum_{n_2=-\infty}^{\infty} \sum_{n_1=-\infty}^{\infty} \hat{x} \times \hat{r}_{21}$$

$$\cdot P(\beta,n_1,n_2) \frac{e^{-j\beta\bar{R}\cdot\hat{r}_{21}}}{r_y} \qquad \text{(A-26)}$$

where,

$$P(\beta,n_1,n_2) = \int_0^W \int_{-\frac{L}{2}}^{\frac{L}{2}} M_x(x',z') e^{j\beta\bar{R}'\cdot\hat{r}_{21}} dx'dz' \qquad \text{(A-27)}$$

is the pattern function for a single element of the array. As detailed in Appendix B the magnetic surface current density M_x is arbitrary but is assumed to be known over discrete regions covering the surface $[-L/2 < x' < L/2,\ 0 < z' < W]$. M_x can then be approximated by the superposition of piecewise sinusoidal-uniform surface dipoles modes M_i where,

$$M_i(x',z') = A_i \frac{\sin\beta(\ell-|x''|)}{\sin\beta\ell} \qquad \begin{array}{l} -\ell < x'' < \ell \\ 0 < z'' < W \end{array}$$

where $\quad \ell = \dfrac{L}{N_\ell}$

and the A_i's are the complex coefficients associated with mode i. Since there are N_w and $N_\ell-1$ expansions along the width and length of the rectangular surface, respectively, then

$$M_x = \sum_{m=1}^{N_w} \sum_{n=1}^{N_\ell-1} A_i \frac{\sin\beta(\ell-|x''|)}{\sin\beta\ell}$$

where

$$i = m + (n-1)N_w \quad .$$

The pattern function is then given by (see Equation (B-10))

$$P(\beta,n_1,n_2) = \frac{4}{\beta^2 \sin \beta\ell} e^{j\beta \frac{w}{2} r_z} e^{-j\beta d r_y}$$

$$\cdot \frac{\sin\left(\beta \frac{w}{2} r_z\right)}{r_z} \frac{[\cos(\beta\ell r_x)-\cos\beta\ell]}{(1-(r_x)^2)}$$

$$\cdot \sum_{m=1}^{N_w} \sum_{n=1}^{N_\ell -1} A_i e^{j\beta x_n r_x} e^{j\beta z_m r_z}$$

(A-28)

where $x_n = -\frac{L}{2} + n\ell$,

$z_m = (m-1)\, w$, and

$w = \frac{W}{N_w}$.

Equation (A-26) is a plane wave expansion for $\overline{E}_T$, so $\overline{H}_T$ can be determined by using Equation (A-1), with $s = \hat{r}_{21}$ as

$$\overline{H}_T(x,y,z) = -\frac{1}{2\eta D_x D_z} \sum_{n_2=-\infty}^{\infty} \sum_{n_1=-\infty}^{\infty} \hat{r}_{21} \times (\hat{x} \times \hat{r}_{21})$$

$$\cdot P(\beta,n_1,n_2) \frac{e^{-j\beta \overline{R}\cdot \hat{r}_{21}}}{r_y} . \qquad \text{(A-29)}$$

Using the vector identity[35]

$$A \times (B \times C) = (A \cdot C)\, B - (A \cdot B) C \qquad \text{(A-30)}$$

it follows that

$$\hat{r}_{21} \times (\hat{x} \times \hat{r}_{21}) = \hat{x} - (\hat{r}_{21} \cdot \hat{x})\hat{r}_{21}$$

$$= \hat{x}(1-(r_x)^2) - \hat{y}\, r_x r_y + \hat{z} r_x\, r_z . \qquad \text{(A-31)}$$

Next, let

$$P_2(n_1,n_2) = \frac{4}{\sin\beta\ell} e^{j\beta \frac{w}{2} r_z} \frac{\sin\left(\beta \frac{w}{2} r_z\right)}{r_z}$$

$$\cdot \frac{\left[\cos(\beta\ell\, r_x) - \cos\beta\ell\right]}{(1-(r_x)^2)} \qquad \text{(A-32)}$$

be the element pattern function. (Note that $P_2(n_1,n_2)$ is dimensionless.) Substituting Equations (A-28), (A-31), and (A-32) into Equation (A-29) yields the desired result for the magnetic field

$$\bar{H}_T(x,y,z) = \frac{-1}{2\eta\beta^2 D_x D_z} \sum_{n_2=-\infty}^{\infty} \sum_{n_1=-\infty}^{\infty} \left[\hat{x}(1-(r_x)^2)\right.$$

$$\left. - \hat{y}\, r_x r_y + \hat{z}\, r_x\, r_z \right]$$

$$\cdot\ P_2(n_1,n_1) e^{j\beta x r_x} \frac{e^{-j\beta(y+d) r_y}}{r_y} e^{j\beta z r_z}$$

$$\cdot \sum_{m=1}^{N_w} \sum_{n=1}^{N_\ell - 1} A_i\, e^{j\beta x_n r_x} e^{j\beta z_m r_z}\ . \qquad \text{(A-33)}$$

Note that in Equation (A-33) the coefficient A_i has units of [volts/meter]. Thus, $\bar{H}_T$ has units of [amperes/meter] as it should.

APPENDIX B

THE PATTERN FUNCTION FOR A RECTANGULAR SURFACE DIPOLE WITH ARBITRARY MAGNETIC CURRENT DISTRIBUTION

Consider a rectangular surface dipole with arbitrary magnetic current distribution $M_{x'}(x',z')$, as shown in Figure B-1. Assume that $M_x(x',z')$ is a continuous function but that its values are known for discrete intervals over the surface $[-L/2 < x' < L/2; 0 < z' > W]$. For example, $M_{x'}$ could be known over discrete intervals corresponding to the expansions used in a moment method solution. The pattern function for the rectangular surface source in Figure B-1 is given by (see Equation A-27)

$$P = \int_0^W \int_{-\frac{L}{2}}^{\frac{L}{2}} M_{x'}(x',z') e^{j\beta \bar{R}' \cdot \hat{r}_{21}} dx' dz' \qquad \text{(B-1)}$$

where $\bar{R}' = \hat{x}\, x' - \hat{y}\, d + \hat{z}\, z'$ is the source point position vector,

$\hat{r}_{21} = \hat{x} r_x + \hat{y}\, r_y + \hat{z} r_z$

denotes the direction of propagation.

The rectangular region $[-L/2 < x' < L/2; 0 < z' < W]$ is divided up into N_W expansions along the width and $N_\ell - 1$ overlapping expansions along the length. The particular case where $N_W = 3$ and $N_\ell - 1 = 5$ is shown in Figure B-2. If expansion i is known to have a piecewise-sinusoidal current distribution along the length and is uniform along the width, with complex coefficient A_i, then $M_{x'}$ can be represented as

$$M_{x'}(x',z') = \sum_{m=1}^{N_W} \sum_{n=1}^{N_\ell - 1} M_i \qquad \text{(B-2)}$$

where, $i = m + (n-1)N_W$

Substituting Equation (B-2) into Equation (B-1) yields

$$P = \int_0^W \int_{-\frac{L}{2}}^{\frac{L}{2}} \sum_{m=1}^{N_W} \sum_{n=1}^{N_\ell - 1} M_i \, e^{j\beta \bar{R}' \cdot \hat{r}_{21}} dx' \, dz' \, .$$

(B-3)

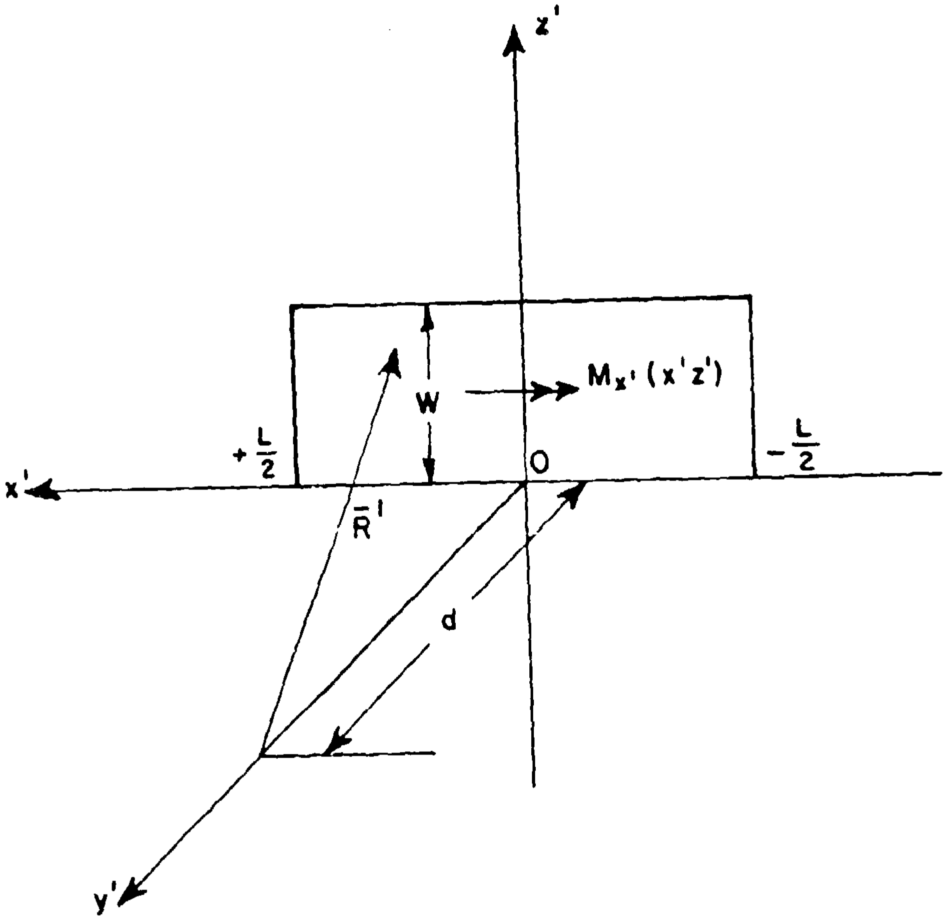

Figure B-1. A rectangular magnetic surface source with arbitrary current distribution.

To simplify the above integration a reference surface dipole M_r is located at the origin as shown in Figure B-3. The vector shift from the origin to expansion function i is $\overline{R}_s = \hat{x}\, x_i' + \hat{z}\, z_i'$. The pattern function can now be expressed equivalently as

$$P = \sum_{m=1}^{N_w} \sum_{n=1}^{N_\ell - 1} e^{j\beta(\hat{x}\, x'_n + \hat{z}\, z'_n) \cdot \hat{r}_{21}}$$

$$\cdot \int_0^w \int_{-\ell}^{\ell} M_r(x'', z'') e^{j\beta \overline{R}'' \cdot \hat{r}_{21}}\, dx''\, dz'' \tag{B-4}$$

where

$$\overline{R}'' = \hat{x}\, x'' - \hat{y}d + \hat{z}\, z'' \quad ,$$

$$M_r(x'', z'') = A_i \frac{\sin \beta(\ell - |x''|)}{\sin \beta\ell} \quad ,$$

$$w = \frac{W}{N_w} \quad ,$$

$$\ell = \frac{L}{N_\ell} ,$$

$$x'_n = \frac{L}{2} - n\ell \text{ , and}$$

$$z'_m = (m-1)\, w \quad .$$

Let

$$P_1(\beta, n_1, n_2) = \int_0^w \int_{-\ell}^{\ell} \frac{\sin \beta(\ell - |x''|)}{\sin \beta\ell}\, e^{j\beta x'' r_x}$$

$$\cdot\, e^{j\beta z'' r_z}\, dx''\, dz'' \tag{B-5}$$

then

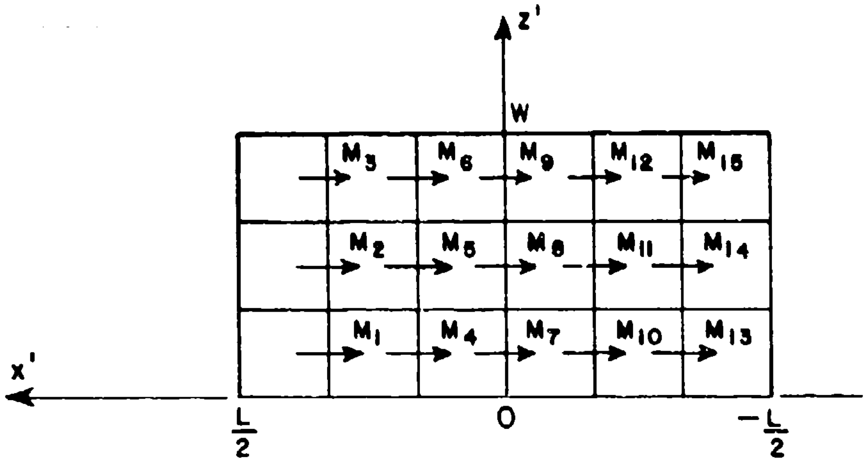

Figure B-2. An example of the expansion used to approximate $M_{x'}(x',z')$.

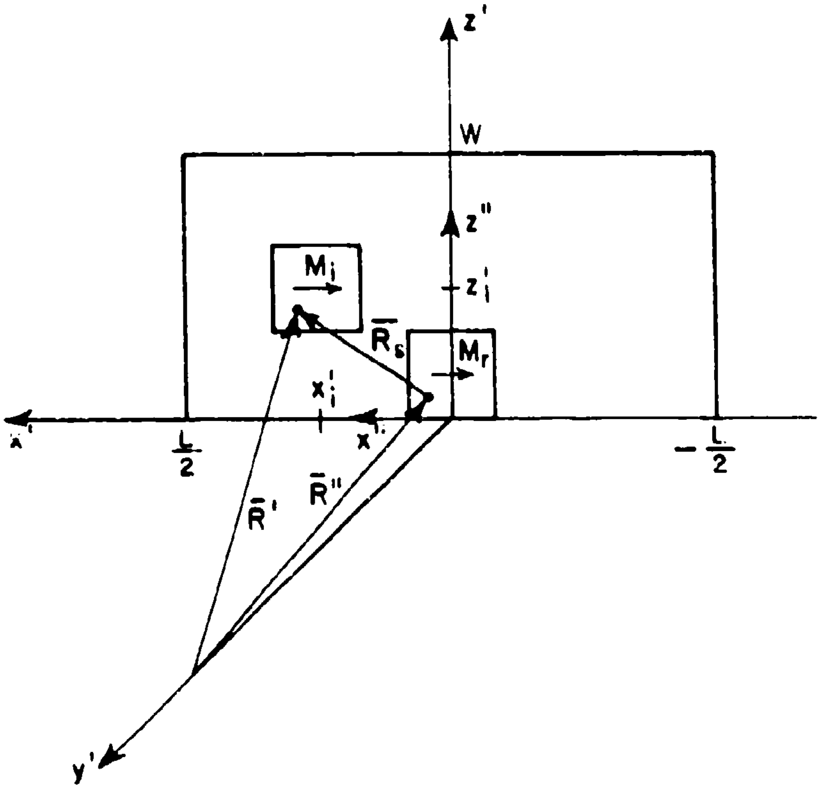

Figure B-3. Introducing a reference dipole at the position x'=0, z'=0.

$$P = P_1(\beta, n_1, n_2)\, e^{-j\beta d r_y} \sum_{m=1}^{N_w} \sum_{n=1}^{N_\ell - 1} A_i\, e^{j\beta x'_n r_x}$$

$$\cdot\, e^{j\beta z'_m r_z} \tag{B-6}$$

The double integral in Equation (B-5) is carried out as follows:

$$\int_0^w e^{j\beta z'' r_z}\, dz''$$

$$= 2e^{j\beta \frac{w}{2} r_z} \frac{\sin \beta \frac{w}{2} r_z}{\beta r_z} \tag{B-7}$$

and from integral tables[36]

$$\int_{-\ell}^{\ell} \sin \beta(\ell - |x''|) e^{j\beta x'' r_x}\, dx''$$

$$= \frac{2}{\ } \frac{[\cos(\beta \ell r_x) - \cos \beta \ell]}{\beta(1 - (r_x)^2)} \tag{B-8}$$

Now let $P_2(n_1, n_2) = \beta^2 P_1(\beta, n_1, n_2)$, then using Equations (B-5), (B-7), and (B-8)

$$P_2(n_1, n_2) = \frac{4e^{j\beta \frac{w}{2} r_z}}{\sin \beta \ell} \quad \frac{\sin\left(\beta \frac{w}{2} r_z\right)}{r_z}$$

$$\cdot\, \frac{[\cos(\beta \ell\, r_x) - \cos \beta \ell]}{(1 - (r_x)^2)} \tag{B-9}$$

Substituting Equation (B-9) into Equation (B-6) yields the desired pattern function

$$P(\beta, n_1, n_1; A_1, \ldots, A_{N_w(N_\ell - 1)}) = \frac{4}{\beta^2 \sin \beta\ell} e^{j\beta \frac{w}{2} r_z} e^{-j\beta d r_y}$$

$$\cdot \frac{\sin\left(\beta \frac{w}{2} r_z\right)}{r_z} \frac{\left[\cos(\beta\ell r_x) - \cos \beta\ell\right]}{(1-(r_x)^2)}$$

$$\cdot \sum_{m=1}^{N_w} \sum_{n=1}^{N_\ell - 1} A_i \, e^{j\beta x_n' r_x} e^{j\beta z_m' r_z} \quad . \qquad \text{(B-10)}$$

APPENDIX C

THE MUTUAL IMPEDANCE BETWEEN TWO RECTANGULAR ELECTRIC SURFACE DIPOLES IN FREE SPACE

In this appendix an expression for determining the mutual impedance between two rectangular electric surface dipoles with arbitrary current distribution is derived.[37] The usefulness of this calculation, in the present report, is for evaluating the free space mutual impedance between two piecewise sinusoidal-uniform surface sources in Equation (3-7).

Consider the two electric surface dipoles m and n in free space shown in Figure C-1. The current distributions of dipoles m and n are given by

$$\bar{J}_m(y,z) = \hat{z}\, I_m\, f_m(z)\, g_m(y) \qquad \begin{array}{c} -\frac{a}{2} < z < \frac{a}{2} \\ -\frac{b}{2} < y < \frac{b}{2} \end{array} \tag{C-1}$$

$$\bar{J}_n(y',z') = \hat{z}\, I_n\, f_n(z')\, g_n(y') \qquad \begin{array}{c} S_z - \frac{a}{2} < z' < S_z + \frac{a}{2} \\ S_y - \frac{b}{2} < y' < S_y + \frac{b}{2} \end{array} \tag{C-2}$$

where f is the arbitrary distribution along the length of the dipole and g is the arbitrary distribution along the width.[38] The induced voltage on dipole m due to dipole n is given by

$$V_{mn} = \frac{1}{I^{(m)t}} \iint_m \bar{E}_n(y,z) \cdot \bar{J}_m^t(y,z)\,dy\,dz \tag{C-3}$$

where

$\bar{E}_n$ is the free-space electric field due to $\bar{J}_n$,

$\bar{J}_m^t$ is the current distribution of dipole m under transmitting conditions, and

$I^{(m)t}$ is the terminal current of dipole m under transmitting conditions. It is defined by the integral of J_m^t at it's terminals and over it's width.

The mutual impedance between dipoles m and n is determined by the relation[39]

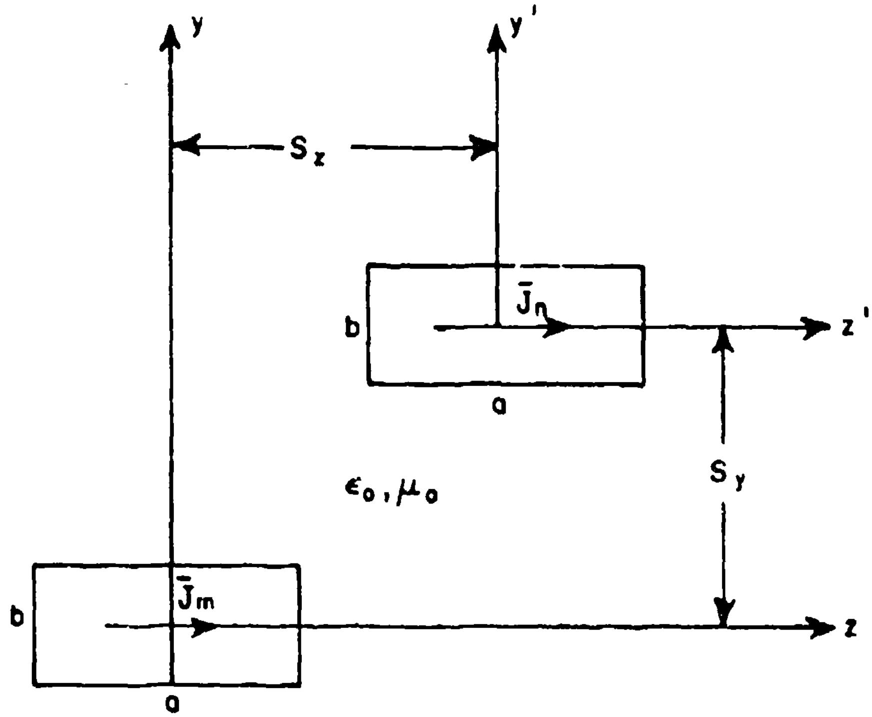

Figure C-1. The geometry involving two electric surface dipoles in free space.

$$Z_{mn} = -\frac{V_{mn}}{I^{(n)}} \tag{C-4}$$

where $I^{(n)}$ is the terminal current of surface dipole n. Combining Equations (C-3) and (C-4) yields

$$Z_{mn} = -\frac{1}{I^{(m)t}I^{(n)}} \iint_m \bar{J}_m^t(y,z) \cdot \bar{E}_n(y,z)\,dy\,dz \tag{C-5}$$

The electric field radiated by source $\bar{J}_n$ can be expressed in terms of the magnetic vector potential as[40]

$$\bar{E}_n(y,z) = -j\omega\bar{A}_n(y,z) + \frac{\nabla\nabla\cdot\bar{A}_n(y,z)}{j\omega\epsilon\mu}$$

or

$$\bar{E}_n(y,z) = \left(-j\omega + \frac{\nabla\nabla\cdot}{j\omega\epsilon\mu}\right)\bar{A}_n(y,z) \qquad (C-6)$$

where[41]

$$\bar{A}_n(y,z) = \mu \iint_n \bar{J}_n(y',z') \cdot \bar{\bar{G}}_o(y,y';z,z')dy'\,dz' \qquad (C-7)$$

is the magnetic vector potential due to source $\bar{J}_n$.

In Equation (C-7) $\bar{\bar{G}}_o$ is the free-space dyadic Green's function and is given by[42]

$$\bar{\bar{G}}_o(y,y';z,z') = [\hat{x}\,\hat{x} + \hat{y}\,\hat{y} + \hat{z}\,\hat{z}]\,\frac{e^{-j\beta\sqrt{(y-y')^2+(z-z')^2}}}{4\pi\sqrt{(y-y')^2+(z-z')^2}} \qquad (C-8)$$

Substituting Equation (C-7) into (C-6) yields

$$\bar{E}_n(y,z) = \left(-j\omega\mu + \frac{\nabla\nabla\cdot}{j\omega\epsilon}\right)\iint_n \bar{J}_n(y',z') \cdot \bar{\bar{G}}_o(y,y';z,z')dy'\,dz' \qquad (C-9)$$

Next, substitute Equations (C-2) and (C-8) into Equation (C-9) with the result

$$\bar{E}_n(y,z) = I_n\left(-j\omega\mu + \frac{\nabla\nabla\cdot}{j\omega\epsilon}\right)\int_{S_z-\frac{a}{2}}^{S_z+\frac{a}{2}}\int_{S_y-\frac{b}{2}}^{S_y+\frac{b}{2}} \hat{z}\, f_n(z')g_n(y')$$

$$G_o(y,y';z,z')dy'\,dz' \qquad (C-10)$$

where

$$G_o = \frac{e^{-j\beta\sqrt{(y-y')^2+(z-z')^2}}}{4\pi\sqrt{(y-y')^2 + (z-z')^2}}$$

is the free-space scalar Green's function. Equation (C-10) can also be expressed as

$$\overline{E}_n(y,z) = I_n \int_{S_y-\frac{b}{2}}^{S_y+\frac{b}{2}} g_n(y')\left[\left(-j\omega\mu + \frac{\nabla\nabla\cdot}{j\omega\epsilon}\right)\int_{S_z-\frac{a}{2}}^{S_z+\frac{a}{2}} \hat{z} f_n(z')\right.$$

$$\left. G_o(y,y';z,z')dz'\right]dy \qquad \text{(C-11)}$$

where the bracketed quantity in Equation (C-11) represents the electric field radiated by a line source with current distribution $\hat{z}\, f_n(z')$. This quantity will be denoted by $\overline{e}_n(y,y';z)$. Thus, Equation (C-11) becomes

$$\overline{E}_n(y,z) = I_n \int_{S_y-\frac{b}{2}}^{S_y+\frac{b}{2}} g_n(y')\ \overline{e}_n(y,y';z)dy' \qquad \text{(C-12)}$$

Substituting Equations (C-1) and (C-12) into Equation (C-5) yields

$$Z_{mn} = -\frac{I_m I_n}{I^{(m)} I^{(n)}} \int_{-\frac{b}{2}}^{\frac{b}{2}} \int_{-\frac{a}{2}}^{\frac{a}{2}} f_m(z) g_m(y)$$

$$\left[\int_{S_y-\frac{b}{2}}^{S_y+\frac{b}{2}} g_n(y')\hat{z}\cdot\overline{e}_n(y,y';z)dy'\right] dz\ dy \qquad \text{(C-13)}$$

Interchanging the order of integration on z and y' in Equation (C-13) gives the result

$$Z_{mn} = -\frac{I_m I_n}{I^{(m)} I^{(n)}} \int_{S_y-\frac{b}{2}}^{S_y+\frac{b}{2}} \int_{-\frac{b}{2}}^{\frac{b}{2}} g_m(y)\, g_n(y')$$

$$\left[\int_{-\frac{a}{2}}^{\frac{a}{2}} f_m(z)\hat{z}\cdot\overline{e}_n(y,y',z)dz\right] dy'\ dy \ . \qquad \text{(C-14)}$$

The bracketed quantity in Equation (C-14) represents the mutual impedance between two line sources with current distributions $f_m(z)$ and $f_n(z')$. This quantity will be denoted by $z_{m,n}(|y-y'|;\ S_z)$. Thus, Equation (C-14) becomes

$$Z_{nm} = -\frac{I_m I_n}{I^{(m)^t} I^{(n)}} \int_{S_y-\frac{b}{2}}^{S_y+\frac{b}{2}} \int_{-\frac{b}{2}}^{\frac{b}{2}} g_m(y) g_n(y') z_{m,n}(|y-y'|\ ;S_z) dy\, dy' \qquad \text{(C-15)}$$

In general, Equation (C-15) is evaluated by a four-fold numerical integration which involves a great deal of computation.

For the case when $f_m(z)$ and $f_n(z)$ have piecewise-sinusoidal distributions, that is,

$$f_m(z) = \frac{\sin\beta\left(\frac{a}{2} - |z|\right)}{\sin\beta\frac{a}{2}} \quad -\frac{a}{2} < z < \frac{a}{2} \qquad \text{(C-16)}$$

$$f_n(z') = \frac{\sin\beta\left(\frac{a}{2} - |z'|\right)}{\sin\beta\frac{a}{2}} \quad -\frac{a}{2} < z' < \frac{a}{2} \qquad \text{(C-17)}$$

the mutual impedance $z_{m,n}(|y-y'|;S_z)$ can be evaluated in closed form in terms of sine and cosine integrals. A computer program which does this is given in a report by Costello and Munk[43]. A similar formula for $z_{m,n}(|y-y'|;S_z)$ has been derived and programmed by Richmond[44]. The terminal currents in Equation (C-15) are found by integrating the currents given by Equations (C-1) and (C-2) at the terminals and over their widths, that is,

$$I^{(m)^t} = \int_{-\frac{b}{2}}^{\frac{b}{2}} I_m\, f_m(0) g_m(z) dy \qquad \text{(C-18)}$$

$$I^{(n)} = \int_{S_y - \frac{b}{2}}^{S_y + \frac{b}{2}} I_n f_n(0) g_n(y') dy' \quad . \tag{C-19}$$

For the piecewise sinusoidal-uniform surface current distribution used in Chapter III let $g_m(y) = g_n(y') = 1$, then from Equations (C-18) and (C-19)

$$I^{(m)^t} = I_m b \tag{C-20}$$

$$I^{(n)} = I_n b \quad . \tag{C-21}$$

Substituting Equations (C-20) and (C-21) into Equation (C-19) yields

$$Z_{mn} = \frac{1}{b^2} \int_{S_y - b/2}^{S_y + b/2} \int_{-b/2}^{b/2} Z_{m,n}(|y-y'|; S_z) dy \, dy' \quad . \tag{C-22}$$

The double integral in Equation (C-22) involves a lengthy computation,[45] but can be reduced to a single integral in the following manner:

Consider the y,y' axes redrawn in Figure C-2. The square PQRS is the range of the double integration. Next, consider the line $y' = y + c$ or $|y' - y| = |c|$ = constant. The mutual impedance $Z_{m,n}(|y - y'|; S_z)$ is thus a constant along the line $y' = y + c$. This observation suggests the following transformation: Let

$$u = \sqrt{2}(y+y') \qquad y = \frac{1}{\sqrt{2}}(u-v)$$

$$v = \sqrt{2}(-y+y') \qquad y' = \frac{1}{\sqrt{2}}(u+v) \tag{C-23}$$

then $|y-y'| = \sqrt{2}|v|$.

This transformation represents a rotation of forty-five degrees for the y,y' axes (relabeled as u,v) as shown in Figure C-3. Next, the differential area dy dy' is transformed according to the following relation:[46]

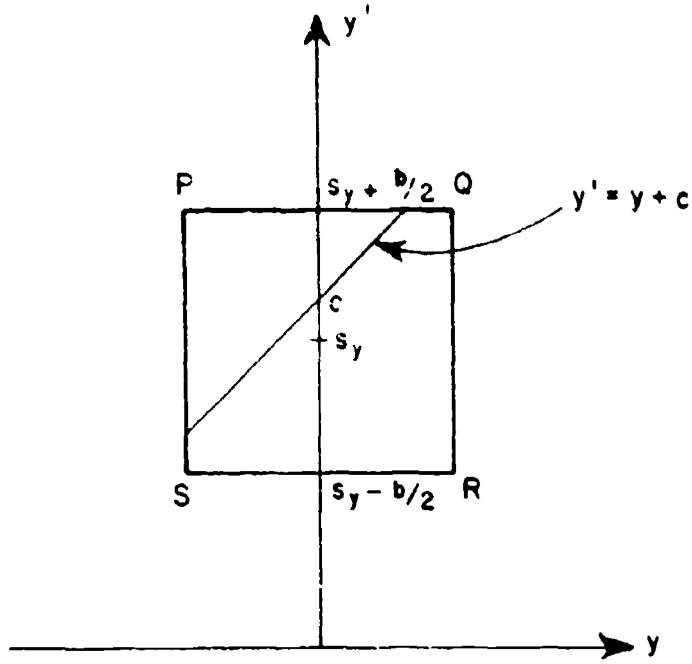

Figure C-2. In the yy' plane the square PQRS represents the range of integration in Equation (C-22).

$$dy\,dy' = \left| J\left(\frac{y,y'}{u,v}\right) \right| \quad du\,dv \tag{C-24}$$

where

$$J\left(\frac{y,y'}{u,v}\right) = \begin{vmatrix} \frac{\partial y}{\partial u} & \frac{\partial y}{\partial v} \\ \frac{\partial y'}{\partial u} & \frac{\partial y'}{\partial v} \end{vmatrix} \tag{C-25}$$

is the Jacobian of the transformation.

From Equations (C-23) and (C-25) it follows that

$$J\left(\frac{y,y'}{u,v}\right) = \begin{vmatrix} \frac{1}{\sqrt{2}} & -\frac{1}{\sqrt{2}} \\ \frac{1}{\sqrt{2}} & \frac{1}{\sqrt{2}} \end{vmatrix} = 1 \quad .$$

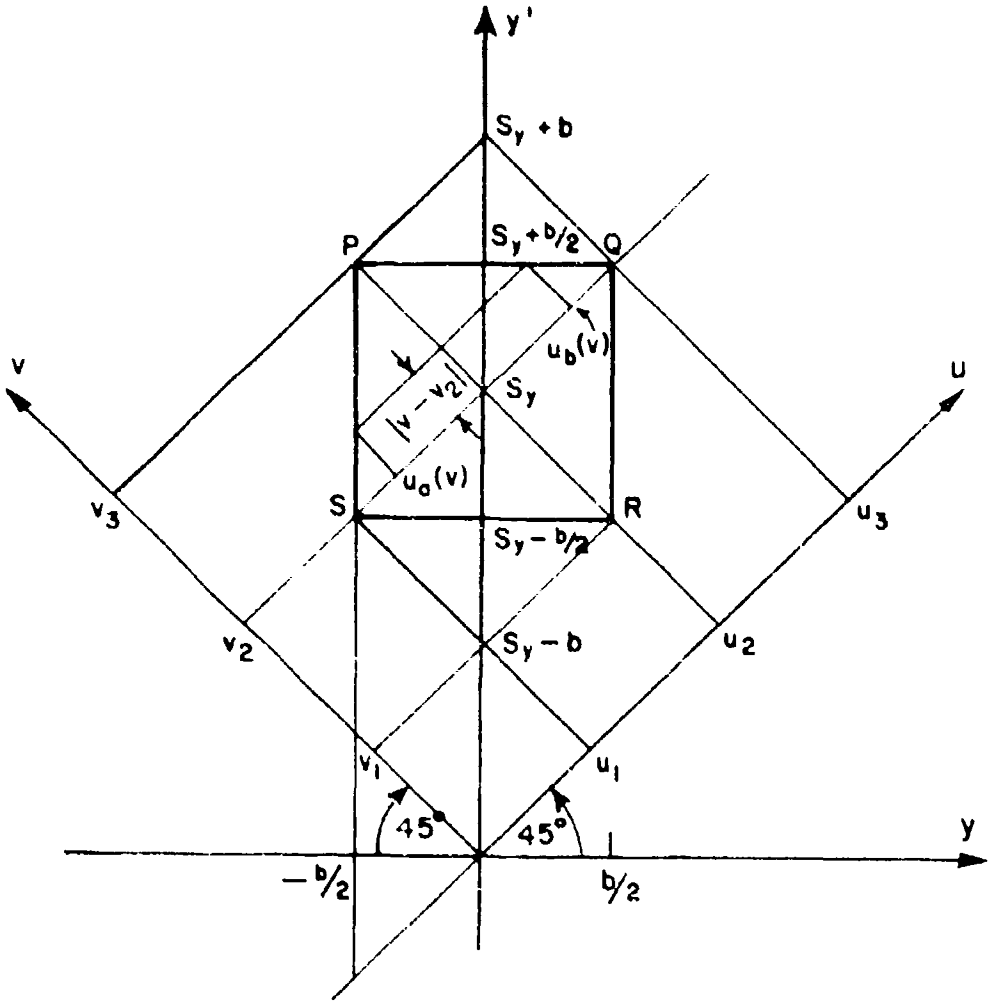

Figure C-3. A forty-five degree rotation of the y,y' axes results in the u,v axes that are used in reducing Equation (C-22) to a single integral.

Equation (C-25) can now be written as

$$Z_{mn} = \frac{1}{b^2} \int_{v_1}^{v_3} \int_{u_a(v)}^{u_b(v)} z_{m,n}(\sqrt{2}\,|v|\,, S_z)\,du\,dv \qquad \text{(C-26)}$$

where, from Figure C-3

$$u_1 = \frac{S_y - b}{\sqrt{2}} \qquad u_2 = \frac{S_y}{\sqrt{2}} \qquad u_3 = \frac{S_y + b}{\sqrt{2}}$$

$$v_1 = \frac{S_y - b}{\sqrt{2}} \qquad v_2 = \frac{S_y}{\sqrt{2}} \qquad v_3 = \frac{S_y + b}{\sqrt{2}}$$

$$u_a(v) = u_1 + |v - v_2|\,, \qquad u_b(v) = u_3 - |v - v_2|\,.$$

Since the integrand in Equation (C-26) is independent of u it is clear that it is only necessary to integrate over half the range and multiply the result by two, thus

$$Z_{mn} = \frac{2}{b^2} \int_{v_1}^{v_3} \int_{u_2}^{u_b(v)} z_{m,n}(\sqrt{2}\,|v|\,; S_z)\,du\,dv$$

$$= \frac{2}{b^2} \int_{\frac{S_y - b}{\sqrt{2}}}^{\frac{S_y + b}{\sqrt{2}}} z_{m,n}(\sqrt{2}\,|v|\,; S_z) \left[\int_{\frac{S_y}{\sqrt{2}}}^{\frac{S_y + b}{\sqrt{2}} - \left|v - \frac{S_y}{\sqrt{2}}\right|} du \right] dv$$

$$= \frac{2}{b^2} \int_{\frac{S_y - b}{\sqrt{2}}}^{\frac{S_y + b}{\sqrt{2}}} \left(\frac{b}{\sqrt{2}} - \left|v - \frac{S_y}{\sqrt{2}}\right| \right) z_{m,n}(\sqrt{2}\,|v|\,; S_z)\,dv\,. \qquad \text{(C-27)}$$

The integrand in Equation (C-27) is an even function about $v = \frac{S_y}{\sqrt{2}}$ so

$$Z_{mn} = \frac{4}{b^2} \int_{\frac{S_y}{\sqrt{2}}}^{\frac{S_y+b}{\sqrt{2}}} \left(\frac{b}{\sqrt{2}} - \left| v - \frac{S_y}{\sqrt{2}} \right| \right) z_{m,n}(\sqrt{2}\ |v|\ ;S_z)dv. \tag{C-28}$$

By Simpson's rule[47] Equation (C-28) becomes

$$Z_{mn} = \frac{4}{b^2} \quad \frac{\Delta v}{3} \sum_{k=1}^{NMAX} \left(\frac{b}{\sqrt{2}} - \left| v_k - \frac{S_y}{\sqrt{2}} \right| \right) z_{m,n}(\sqrt{2}\ |v_k|;S_z) \tag{C-29}$$

where

$\Delta v = \frac{b/\sqrt{2}}{NMAX-1}$,

$v_k = S_y/\sqrt{2} + \Delta v(k-1)$,

NMAX is the number of sample points.

Equation (C-29) is the desired expression for determining the mutual impedance $Z_{mn}^{\text{free space}}$ in Equation (3-7).

APPENDIX D
THE MUTUAL ADMITTANCE BETWEEN A MAGNETIC SURFACE DIPOLE AND AN INFINITE PLANAR ARRAY OF MAGNETIC SURFACE DIPOLES

This appendix considers the calculation of the mutual admittance between an exterior rectangular magnetic surface dipole and an infinite array of rectangular magnetic surface dipoles. This calculation is used in evaluating the waveguide mutual admittances in Chapter III, see Equations (3-8), (3-9), and (3-10). The array configuration is shown in Figure D-1. The expression for mutual admittance will be obtained by using the dual of the definition of mutual impedance.

The mutual impedance between an infinite array of electric surface dipoles and an exterior electric surface dipole can be found in the following manner:[48] Let $\overline{E}_a$ represent the electric field radiated by the infinite array and $\overline{J}_a(x,z)$ be the electric current density function of the reference element of the array under transmitting conditions. Next, let $\overline{J}_e(x,z)$ be the electric current density function of the exterior element under transmitting conditions. The voltage induced across the terminals of the exterior element when the field from the array is incident is given by (see Equation (C-3))

$$V_{ea} = \frac{1}{I^{(a)}} \iint_e \overline{E}_a(x,-d,z) \cdot \overline{J}_e(x,z)\, dx\, dz \qquad \text{(D-1)}$$

where

$I^{(a)}$ is the terminal current for $\overline{J}_a$.

The mutual impedance between the exterior element and the array is then given by (see Equation (C-4))

$$Z_{ea} = -\frac{V_{ea}}{I^{(e)}} \qquad \text{(D-2)}$$

where $I^{(e)}$ is the terminal current for $\overline{J}_e$.

Substituting Equation (D-1) into (D-2) yields

$$Z_{ea} = -\frac{1}{I^{(a)} I^{(e)}} \iint_e \overline{E}_a(x,-d,z) \cdot \overline{J}_e(x,z)\, dx\, dz \ . \qquad \text{(D-3)}$$

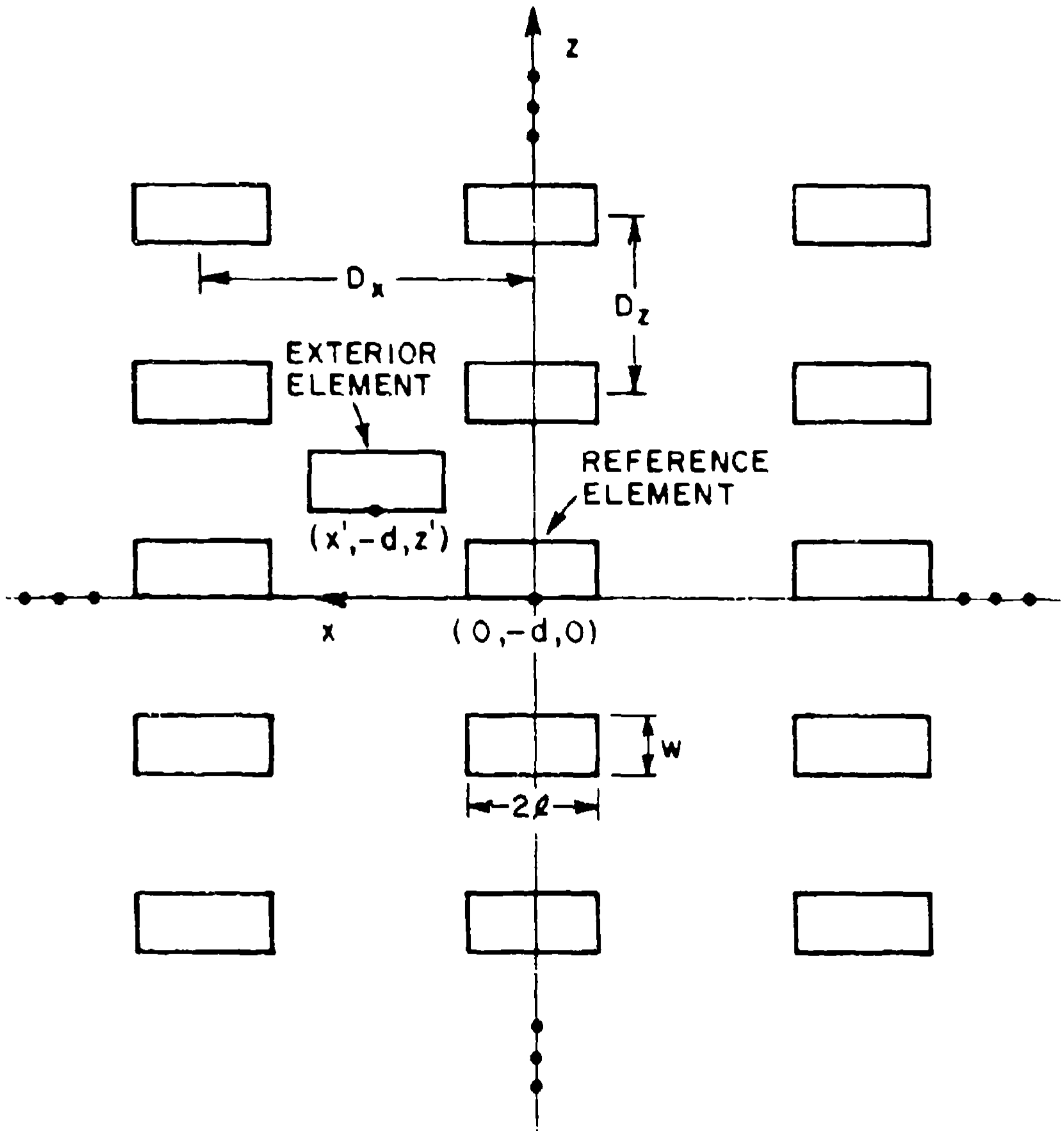

Figure D-1. Infinite array of rectangular surface sources and an exterior element in the xz plane.

By taking the dual of Equation (D-3) the mutual admittance is found to be

$$Y_{ea} = -\frac{1}{K^{(a)}K^{(e)}} \iint_e \bar{H}_a(x,-d,z) \cdot \bar{M}_e(x,z)dx\,dz \tag{D-4}$$

where $\bar{H}_a(x,-d,z)$ is the magnetic field radiated by an infinite array of magnetic surface sources,

$K^{(a)}$ and $K^{(e)}$ are the terminal currents of the magnetic current densities $\bar{M}_a$ and $\bar{M}_e$.

The magnetic current densities that will be considered here are rectangular piecewise sinusoidal-uniform surface sources (with half-length $\ell = L/N$ and width $w = W/N_W$), that is,

$$\bar{M}_a(x,z) = \hat{x}\, K_a \frac{\sin\beta(\ell - |x|)}{\sin\beta\ell} \qquad -\ell \le x \le \ell, \quad 0 < z \le w \tag{D-5}$$

$$\bar{M}_e(x,z) = \hat{x}\, K_e \frac{\sin\beta(\ell - |x-x'|)}{\sin\beta\ell} \qquad -\ell + x' \le x \le \ell + x'; \quad z' \le z \le w + z' \tag{D-6}$$

where, from Chapter III,

L is the length of the waveguide (see Figure 3-1) and W is the width,

$N_\ell - 1$ is the number of bases along the length, and

N_W is the number of bases along the width.

From Appendix A, Equation (A-33), the x-component of the magnetic field radiated by an infinite array of rectangular surface sources with piecewise sinusoidal-uniform current distribution is given by

$$H_{a_x}(x,-d,z) = -\frac{1}{2\eta\beta^2 D_x D_z} \sum_{n_2=-\infty}^{\infty} \sum_{n_1=-\infty}^{\infty} (1-(r_x)^2) \cdot P_2(n_1,n_2) e^{-j\beta x r_x} \frac{1}{r_y} e^{-j\beta z r_z} \tag{D-7}$$

where $P_2(n_1,n_2)$ is the pattern function for the current distribution in Equation (D-5) given by Equation (A-32),

$$r_x = s_x + n_2 \frac{\lambda}{D_x} ,$$

$$r_z = s_z + n_1 \frac{\lambda}{D_z} , \text{ and}$$

$$r_y = \sqrt{1 - (r_z)^2 - (r_x)^2} .$$

To simplify the mutual admittance calculation the exterior element is shifted from (x',z') to $(0,0)$ and the reference element of the infinite array is shifted to the location $(-x',-z')$. From Equations (D-5) and (D-6) the terminal currents are

$$K^{(a)} = \int_0^w M_a(0,z)dz = w\, K_a \tag{D-8}$$

$$K^{(a)} = \int_0^w M_e(0,z)dz = w\, K_e . \tag{D-9}$$

Substituting the above information into Equation (D-4) yields

$$Y_{ea} = \frac{1}{2\eta\beta^2 D_x D_z w^2} \sum_{n_2=-\infty}^{\infty} \sum_{n_1=-\infty}^{\infty} \frac{(1 - (r_x)^2)}{r_y}$$

$$\cdot\, P_2(n_1,n_2) \int_0^w \int_{-\ell}^{\ell} \frac{\sin \beta(\ell - |x|)}{\sin \beta\ell}\, e^{-j\beta(x-x')\, r_x}$$

$$\cdot\, e^{-j\beta(z-z')\, r_z}\, dx\, dz . \tag{D-10}$$

The double integral in Equation (D-10) is simply $\frac{P_2^t(n_1,n_2)}{\beta^2}$, that is, the pattern function under transmitting conditions (note $P_2^t(n_1,n_2) = P_2^*(n_1,n_2)$ where * means conjugate). Thus, Equation (D-10) simplifies to the desired result

$$Y_{ea} = \frac{1}{2\pi\beta^4 D_x D_z w^2} \sum_{n_2=-\infty}^{\infty} \sum_{n_1=-\infty}^{\infty} \frac{(1 - (r_x)^2)}{r_y}$$

$$\cdot\ P_2(n_1,n_2) P_2^t(n_1,n_2)\, e^{j\beta x' r_x}\, e^{j\beta z' r_z} . \qquad \text{(D-11)}$$

APPENDIX E
THE EXCITATION CURRENT MATRIX ELEMENT CALCULATION

In this appendix an expression is obtained for evaluating an element of the current excitation matrix in Equation (3-4) for the aperture region of the probe-fed cavity-backed slot antenna shown in Figure 3-2. In Chapter III the excitation current was defined as

$$I_m = \frac{\langle \bar{M}_m, \bar{H}_x^i \rangle}{K^{(m)}} \tag{E-1}$$

where $\bar{M}_m$ is an expansion function,

$K^{(m)}$ is the terminal current for $\bar{M}_m$, and

$\bar{H}_x^i$ is the magnetic field incident upon the aperture due to the probe source in the waveguide.

The incident magnetic field is obtained by first using the method of images to replace the probe and the cavity-backed waveguide by two infinite arrays of dipoles. Infinite array techniques are then used to obtain a plane wave expansion for H_x^i. Using the inner product defined by Equation (3-5) the excitation current can be expressed as

$$I_m = \frac{1}{K^{(m)}} \iint_m \bar{M}_m \cdot \bar{H}_x^i \, dx \, dz \ . \tag{E-2}$$

In Equation (E-2) an assumption is that some propagating mode is incident on the aperture due to the probe source in the waveguide. Furthermore, Equation (E-2) is valid for a perfect electric conductor covering the aperture. For convenience the perfect conductor can be removed and the magnetic current $\bar{M}_m$ doubled by image theory. Equation (E-2) then becomes

$$I_m = \frac{2}{K^{(m)}} \iint_m \bar{M}_m \cdot \bar{H}_x^i \, dx \, dz \tag{E-3}$$

where $\bar{H}_x^i$ is the x component of the magnetic field radiated by the probe source in the cavity-backed waveguide.

The above expression can also be obtained from basic antenna principles as follows: An x-directed linear dipole mode m is shown in Figure E-1. Let an electric field $\bar{E}^i$ be incident upon it. The voltage induced across its terminals is given by[49]

$$V_{m_{dipole}} = \frac{1}{I^{(m)}} \int_{-\ell}^{\ell} \bar{E}^i \cdot \hat{x} \; I_m(x) dx \qquad \text{(E-4)}$$

where $I_m(x)$ is the current distribution of dipole m under transmitting conditions,

$I^{(m)}$ is the terminal current.

Next, let the same electric field be incident on the strip dipole mode m shown in Figure E-1. The induced voltage across the terminals of this mode is

$$V_{m_{\substack{strip\\dipole}}} = \frac{1}{J^{(m)} dz} \int_{-\ell}^{\ell} \bar{E}^i \cdot \hat{x} \; J_m(x) dx \; dz$$

$$= \frac{1}{J^{(m)}} \int_{-\ell}^{\ell} \bar{E}^i \cdot \hat{x} \; J_m(x) \; dx \qquad \text{(E-5)}$$

where, $J_m(x)$ is the current density of strip dipole m under transmitting conditions

$J^{(m)}$ is the terminal current density.

Finally, let the incident electric field illuminate a rectangular dipole mode of width w and length 2ℓ shown in Figure E-1. The induced voltage across the terminals can be found by integrating the strip dipole of width dz over the width of the rectangular dipole, so

$$V_{m_{\substack{rectangular\\dipole}}} = \int_0^w \frac{1}{J^{(m)}(0,z)} \int_{-\ell}^{\ell} \bar{E}^i \cdot \hat{x} \; J_m(x,z) dx \; dz \; . \qquad \text{(E-6)}$$

For the particular case where the current density is not a function of z, Equation (E-6) simplifies to

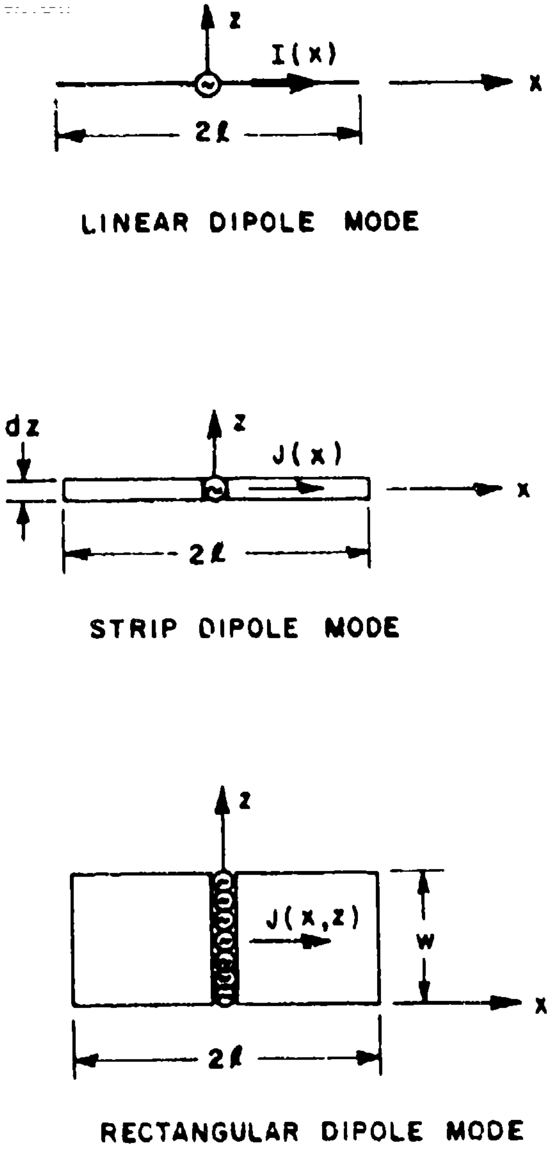

Figure E-1. Linear, strip, and rectangular dipole modes.

$$V_{m_{\substack{\text{rectangular}\\ \text{dipole}}}} = \frac{1}{J^{(m)}} \int_0^w \int_{-\ell}^{\ell} \mathbf{E}^i \cdot \hat{x}\, J_m(x)\,dx\,dz \quad . \tag{E-7}$$

The above quantity has units of volt-meters. To obtain volts it is necessary to divide by the width w of the dipole, with the result

$$V_{m_{\substack{\text{rectangular}\\ \text{dipole}}}} = \frac{1}{J^{(m)}w} \int_0^w \int_{-\ell}^{\ell} \mathbf{E}^i \cdot \hat{x}\, J_m(x)\,dx\,dz\ , \tag{E-8}$$

but $I^{(m)} = J^{(m)}w$ so

$$V_{m_{\substack{\text{rectangular}\\ \text{dipole}}}} = \frac{1}{I^{(m)}} \int_0^w \int_{-\ell}^{\ell} \mathbf{E}^i \cdot \hat{x}\, J_m(x)\,dx\,dz. \tag{E-9}$$

An expression for the induced current on a rectangular magnetic dipole can now be obtained by taking the dual[50] of Equation (E-9), with the result[48]

$$I_{m_{\substack{\text{rectangular}\\ \text{dipole}}}} = \frac{1}{K^{(m)}} \int_0^w \int_{-\ell}^{\ell} \mathbf{H}^i \cdot \hat{x}\, M_m(x)\,dx\,dz. \tag{E-10}$$

Equation (E-10) is seen to be equal to Equation (E-2).

Using Equation (E-10), with the incident magnetic field H_x^i due to the probe source in the rectangular cavity-backed waveguide, the excitation current matrix element I_m (see Figure E-2) is found as follows: The x-component of the magnetic field radiated by a linear monopole of length h, with assumed sinusoidal distribution, in a rectangular cavity-backed waveguide has been derived in detail in a previous paper[51]. This was done by first using image theory to replace the probe and the cavity-backed waveguide with equivalent sources. The equivalent sources for this problem are two infinite arrays of dipoles as shown in Figure E-3. Infinite array techniques were then used to obtain the magnetic field in terms of the following plane wave expansion, which represents all possible modes (propagating and evanescent) in the waveguide,

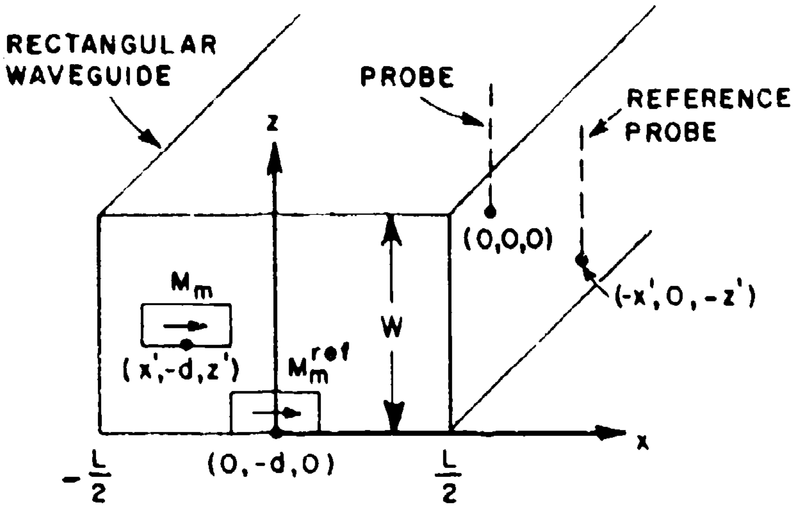

Figure E-2. Introducing a reference dipole and probe.

$$H_x^i(x,-d,z) = \frac{I_0}{4\beta LW} \sum_{m=0}^{1} \sum_{n_2=-\infty}^{\infty} \sum_{n_1=-\infty}^{\infty} (-1)^m \, p_1(n_1)$$

$$\cdot \; e^{-j\beta x r_x^i} \; e^{-j\beta(m2c+d) r_y^i} \; e^{-j\beta z r_z^i} \qquad \text{(E-11)}$$

where,

I_o is the terminal current of the probe and is assumed to be one ampere,

$$r_x^i = (n_2 + \tfrac{1}{2}) \frac{\lambda}{L}$$

$$r_z^i = n_1 \frac{\lambda}{2W}$$

$$r_y^i = \sqrt{1-(r_z^i)^2 - (r_x^i)^2}$$

$$p_1(n_1) = \frac{2\left[\cos(\beta h r_z^i) - \cos\beta h\right]}{(1 - (r_z^i)^2)} \qquad \text{(E-12)}$$

is the pattern function of a single element of the array,

m=0,1 corresponds to the two infinite dipole arrays.

The propagating modes in the waveguide correspond to r_y^i real. Evanescent modes are accounted for when r_y^i becomes imaginary. There are other equivalent methods for obtaining H_x^i, for example by mode matching[52] and by employing a waveguide Green's function[53].

In order to simplify the calculation of I_m the expansion function $\bar{M}_m$ is shifted to the location (0,-d,0), see Figure E-2 and the two infinite arrays of dipoles are shifted by the amount (-x',0,-z'). Note that in Figure E-3 the magnetic current is doubled at the aperture due to the perfect electric conductor, thus $2\bar{M}_m$ should be used in Equation (E-10). For rectangular piecewise sinusoidal-uniform surface expansion functions with half length ℓ and width w

$$M = -\hat{x}\, K_x \frac{\sin \beta(\ell - |x|)}{\sin \beta\ell} \qquad \begin{matrix} -\ell \le x \le \ell \\ 0 \le z \le w \end{matrix} \tag{E-13}$$

where $\ell = \dfrac{L_i}{N_\ell}$

$w = \dfrac{W_i}{N_w}$

$N_\ell - 1$ is the number of expansion functions along the length of the aperture, and N_w is the number of expansion functions along the width.

By integrating $\bar{M}_m$ over it's width and at it's terminals the terminal current in Equation (E-1) is found to be

$$K^{(m)} = \int_0^w M_m(0)dx = -w\,K_m \tag{E-14}$$

In reference to Equation (E-11) note that

$$\sum_{m=0}^{1} e^{j\pi m}\, e^{-j\beta(m2c+d)r_y^i} = e^{-j\beta d r_y^i}(1 - e^{-j\beta 2c r_y^i}).$$

Substituting the above quantities into Equation (E-10) yields

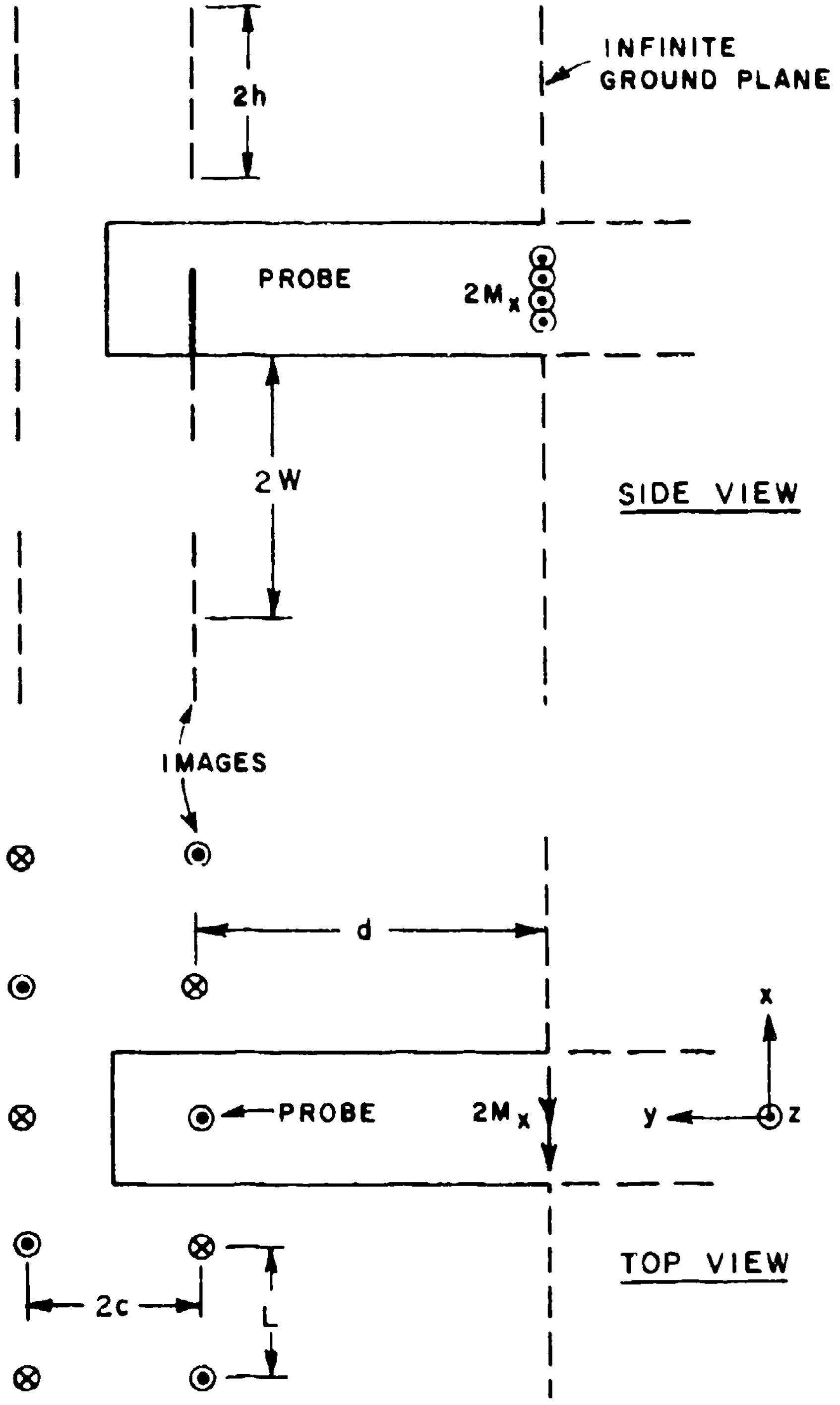

Figure E-3. Method of images model of probe-fed waveguides.

$$I_n = \frac{I_0}{4\beta LW} \sum_{n_2=-\infty}^{\infty} \sum_{n_1=-\infty}^{\infty} p_1(n_1)\, e^{-j\beta d r_y^i}(1-e^{-j\beta 2c r_y^i})$$

$$\cdot \frac{2}{w} \int_0^w \int_{-\ell}^{\ell} e^{-j\beta(x-x')\, r_x^i}\; e^{-j\beta(z-z')\, r_z^i}$$

$$\cdot \frac{\sin \beta(\ell-|x|)}{\sin \beta\ell}\, dx\, dz \qquad \text{(E-15)}$$

Using Equations (B-5) and (B-9), Equation (E-15) can be expressed as

$$I_m = \frac{I_0}{2\beta^3 LWw} \sum_{n_2=-\infty}^{\infty} \sum_{n_1=-\infty}^{\infty} p_1(n_1) P_2^t(n_1,n_2)\, e^{-j\beta d r_y^i}(1-e^{-j\beta 2c r_y^i})$$

$$\cdot\, e^{j\beta x'\, r_x^i}\; e^{j\beta z'\, r_z^i} \qquad \text{(E-16)}$$

where $P_2(n_1,n_2)$ is given by Equation (B-9)

Equation (E-16) is the desired expression for computing values of I_m.

APPENDIX F
THE METHOD OF WEIGHTED RESIDUALS

In this appendix the method of weighted residuals[54] (commonly referred to as the method of moments) is presented. This method is used to obtain an approximate solution for operator equations of the form

$$L_{op}\,\phi(x) = f(x) \qquad \text{(F-1)}$$

where L_{op} is some operator. The approximate solution for the function $\phi(x)$ is found by using the trial function expansion

$$\phi_a(x) = \sum_{i=1}^{N} C_i\,\phi_i(x) \qquad \text{(F-2)}$$

where N is the number of unknowns and C_i is the unknown coefficient associated with the trial function $\phi_i(x)$. The residual is defined over some interval $[\alpha,\beta]$ as

$$R(x) = \sum_{i=1}^{N} C_i L_{op}\,\phi_i(x) - f(x) \qquad \text{(F-3)}$$

The residual represents the difference between the approximate solution $\phi_a(x)$ and the true solution $\phi(x)$. The N coefficients C_i are determined by the N equations

$$\int_{\alpha}^{\beta} w_j(x)\,R(x)dx = 0, \quad j = 1,2,\ldots,N \qquad \text{(F-4)}$$

where $w_j(x)$ is a weighting function. The integral in Equation (F-4) represents an attempt to minimize the difference between the approximate and true solutions with respect to a given weighting function. The amount of error in the approximate solution depends on how well the trial and weighting functions model a desired problem. For the case when the weighting functions are chosen equal to the trial function (Galerkin's method) the error will be of second order[55]. That is, for a ten percent error in the trial function the approximate solution ϕ_a will have a one percent error with respect to the actual solution ϕ.

To reduce the integral equation in Equation (F-4) to a system of simultaneous equations, substitute Equation (F-3) into Equation (F-4) which yields

$$\int_{\alpha}^{\beta} w_j(x) \left[\sum_{i=1}^{N} C_i L_{op} \phi_i(x) - f(x) \right] dx = 0$$

$$j=1,2,\ldots,N \qquad \text{(F-5)}$$

or

$$\int_{\alpha}^{\beta} w_j(x) \sum_{i=1}^{N} C_i L_{op} \phi_i(x) dx = \int_{\alpha}^{\beta} w_j(x) f(x) dx$$

$$j=1,2,\ldots,N \qquad \text{(F-6)}$$

Next, interchange the order of integration and summation in Equation (F-6) with the result

$$\sum_{i=1}^{N} C_i \int_{\alpha}^{\beta} w_j(x) L_{op} \phi_i(x) dx = \int_{\alpha}^{\beta} w_j(x) f(x) dx$$

$$j=1,2,\ldots,N \qquad \text{(F-7)}$$

Define

$$Y_{ij} = \int_{\alpha}^{\beta} w_j(x) L_{op} \phi_i(x) dx \qquad \text{(F-8)}$$

and

$$I_j = \int_{\alpha}^{\beta} w_j(x) f(x) dx \qquad \text{(F-9)}$$

Substituting Equations (F-8) and (F-9) into Equation (F-7) yields the compact form

$$\sum_{i=1}^{N} C_i Y_{ij} = I_j \qquad j=1,2,\ldots,N \ . \qquad \text{(F-10)}$$

In matrix notation the solution for the coefficients C_i can be expressed by matrix inversion as

$$(C) = [Y]^{-1}(I) \qquad \text{(F-11)}$$

If Galerkin's method is used set $w_j(x) = \phi_j(x)$ in Equations (F-8) and (F-9). That is, the weight function and the trial function are the same in Galerkin's method.

APPENDIX G
INFINITE WAVEGUIDE: TEST CASE

In this appendix the theory introduced in Chapters II and III and Appendices A through F will be applied to the infinitely long rectangular waveguide shown in Figure G-1. The probe source is assumed to be operating such that the TE_{10} mode is generated. Since the waveguide extends to infinity (with no discontinuities) the dominant mode will continue to propagate in the -y direction with transmission coefficient equal to one. The above mentioned theory will be used to verify that this is true at y=-d.

The first step in the solution is to place a perfect electric conductor in the waveguide at y=-d. Next, magnetic current sheets $\overline{M}_s$ and $-\overline{M}_s$ are placed on the left and right sides of the conductor. This results in the equivalent situations for regions wg_1 and wg_2 shown in Figure G-2. Only one piecewise sinusoidal-uniform expansion function will be used to approximate $\overline{M}_s$ for convenience. Thus, the magnetic current can be expressed as

$$\overline{M}_s = \frac{V_1}{K^{(1)}} \overline{M}_1 \qquad \text{(G-1)}$$

where $\overline{M}_1$ is given by Equation (3-3),

$K^{(1)} = W K_1$ is the terminal current found by integrating over the width of M_1, and

V_1 is the unknown constant to be determined.

Using Equation (2-10) the unknown voltage response can be expressed as

$$V_1 = \frac{I_1}{Y^{wg_1}_{1,1} + Y^{wg_2}_{1,1}} \qquad \text{(G-2)}$$

By symmetry $Y^{wg_1}_{1,1} = Y^{wg_2}_{1,1}$ so

$$V_1 = \frac{I_1}{2Y^{wg_1}_{1,1}} \quad . \qquad \text{(G-3)}$$

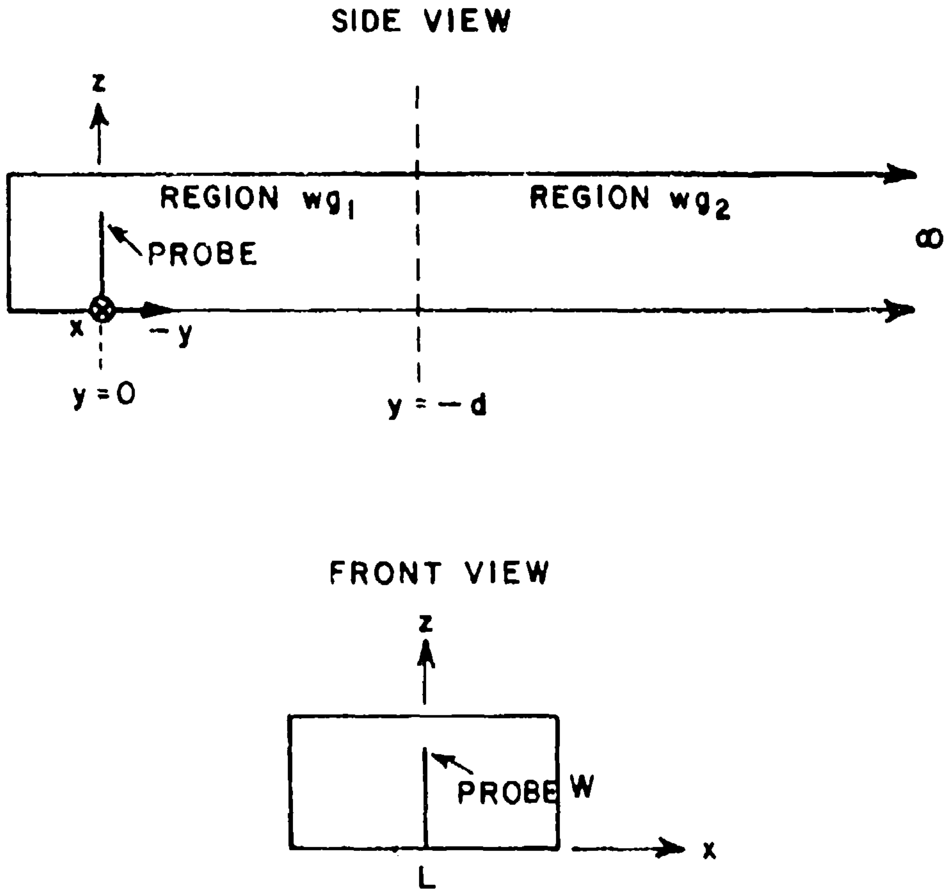

Figure G-1. A probe-fed rectangular waveguide extends to infinity.

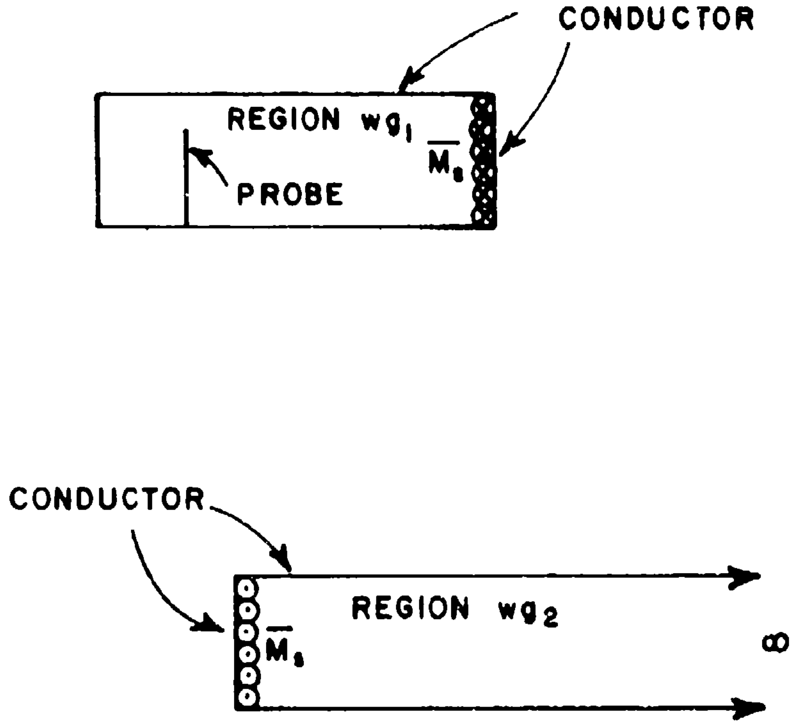

Figure G-2. Equivalent situations for regions wg_1 and wg_2.

The excitation current I_1 for the TE_{10} mode can be determined from Equation (E-16) using $n_1=0$ and $n_2=0,-1$. Expressing I_1 in terms of the incident magnetic field yields

$$I_1 = \frac{4}{\beta^2 W} H_x^i P_2^t(0,0) \tag{G-4}$$

where $P_2(0,0)$ is given by Equation (B-9) with $s_z=0$, $s_x=\lambda/2D_x$. The factor of four in Equation (G-4) arises from a factor of two because of the perfect conductor and a factor of two from the two terms $n_2=0,-1$. The waveguide self admittance is found from Equation (D-11) using $x'=0$, $y'=0$, and $n_1=0$, $n_2=0,-1$ with the result

$$Y_{1,1}^{wg_1} = \frac{2}{\eta\beta^4 D_x D_z W^2} \sqrt{1-\left(\frac{\lambda}{2D_x}\right)^2}\,|P_2(0,0)|^2 \tag{G-5}$$

where a factor of two was used to include the effect of the perfect conductor. Next define the TE_{10} transmission coefficient as the ratio of the x component of the magnetic field radiated by $-M_s$ (at $y=-d$) to the incident magnetic field (at $y=-d$), that is,

$$T = \left.\frac{H_x^{wg_1}(-M_s)}{H_x^i}\right|_{y=-d} . \tag{G-6}$$

For convenience the transmission coefficient will be calculated at the midpoint of the aperture ($x = 0$, $z = W/2$). From Equation (3-12) with $n_1=0, n_2=0,-1$ and $x=0$ the scattered TE_{10} magnetic field due to $-M_s$ at $y=-d$ is

$$H_x^{wg_1}(-M_s) = \frac{1}{\eta\beta^2 D_x D_z} \sqrt{1-\left(\frac{\lambda}{2D_x}\right)^2}\;\frac{V_1}{W} P_2(0,0). \tag{G-7}$$

Substituting Equations (G-3), (G-4), and (G-5) into (G-7) yields

$$H_x^{wg_1}(-M_s) = \frac{\frac{1}{\eta\beta^2 D_x D_z}\sqrt{1-\left(\frac{\lambda}{2D_x}\right)^2}\;\frac{4}{\beta^2 W^2} H_x^i P_2^t(0,0)P_2(0,0)}{\frac{4}{\eta\beta^4 D_x D_z W^2}\sqrt{1-\left(\frac{\lambda}{2D_x}\right)^2}\,|P_2(0,0)|^2} \tag{G-8}$$

which reduces to

$$H_x^{wg_1}(-\bar{M}_s) = H_x^i \, . \qquad \text{(G-9)}$$

Substituting Equation (G-9) into (G-6) yields T = 1 as desired.

APPENDIX H

5 x 5 ARRAY OF SQUARE APERTURES: CONVERGENCE TEST FOR REQUIRED NUMBER OF OVERLAPPING PIECEWISE SINUSOIDAL EXPANSION FUNCTIONS PER APERTURE

This appendix addresses the problem of determining the required number of overlapping piecewise sinusoidal expansion functions per aperture in a finite array such that the aperture reflection coefficients have converged. Square array elements with aperture lengths L=0.5714 are assumed. It is assumed that to obtain a reflection coefficient that has converged (but not necessarily to the correct value) the required number of overlapping piecewise-sinusoidal expansion functions will be independent of the number of pulse expansion functions used in the transverse direction. Thus, one pulse expansion function is used along the aperture width (E-plane) for convenience. An additional assumption is that the convergence in either expansion direction will be about the same for each of the finite arrays of sizes 3x3, 5x5, 7x7, 9x9, and 11x11 with either square or rectangular elements (L=0.5714λ).

A 5x5 array of square elements was chosen as a test case. Reflection coefficients for one and three piecewise sinusoidal expansion functions were computed for E, H, and quasi-E-plane scan angles of 0^o (broadside), 30^o, and 60^o. The results are presented in Figures H-1 through H-8. Generally, the data shows that the magnitudes of the reflection coefficients for one and three piecewise sinusoids are within a few percent of each other and the phases of the reflection coefficients within a few degrees. Thus, one piecewise sinusoidal expansion function should provide good reflection coefficient data for small finite arrays if L ≈ 0.57λ. This approximation is used in the finite arrays dealt with in Chapter IV.

5x5 Array

1 piecewise sinusoidal expansion function

CENTER COLUMN ↓

↑	↑	↑
↑	↑	↑ $\bar{E}$
.07 -56°	.11 -132°	.09 -119°
.20 -61°	.24 -83°	.25 -96°
.10 -142°	.18 -161°	.19 -154°

3 piecewise sinusoidal expansion functions

CENTER COLUMN ↓

↑	↑	↑
↑	↑	↑ $\bar{E}$
.07 -54°	.11 -136°	.10 -129°
.19 -60°	.23 -85°	.26 -99°
.10 -141°	.18 -163°	.20 -158°

E-plane
0°
(Broadside)

Figure H-1. 5x5 array: reflection coefficient convergence test.

5x5 Array

1 piecewise sinusoidal expansion function

		CENTER COLUMN
.20 152°	.24 146°	.29 164°
.27 -156°	.33 -161°	.41 -160°
.23 -138°	.27 -142°	.38 -144°
.22 -146°	.26 -156°	.34 -147°
.35 -130°	.43 -142°	.46 -137°

3 piecewise sinusoidal expansion functions

		CENTER COLUMN
.20 150°	.24 144°	.30 163°
.26 -157°	.34 -164°	.42 -161°
.23 -139°	.27 -144°	.38 -146°
.22 -146°	.26 -158°	.34 -150°
.35 -130°	.43 -144°	.46 -140°

E-plane
30°

Figure H-2. 5x5 array: Reflection coefficient convergence test.

5x5 Array

1 piecewise sinusoidal
expansion function

CENTER COLUMN

.44 160°	.60 154°	.50 154°
.57 168°	.74 161°	.63 164°
.60 169°	.79 162°	.67 166°
.58 169°	.75 162°	.65 165°
.46 163°	.62 157°	.53 157°

3 piecewise sinusoidal
expansion functions

CENTER COLUMN

.44 160°	.61 154°	.52 153°
.57 168°	.74 160°	.63 163°
.60 169°	.79 161°	.69 164°
.58 169°	.76 161°	.67 163°
.46 163°	.63 157°	.56 155°

E-plane
60°

Figure H-3. 5x5 array: reflection coefficient convergence test.

5x5 Array
H-plane 30°

1 piecewise sinusoidal
expansion function

.16 38°	.17 -8°	.14 -10°	.15 -12°	.20 -44°	← CENTER ROW
.17 19°	.30 0°	.32 -4°	.33 -4°	.41 -27°	
.10 80°	.07 -7°	.05 -20°	.06 -26°	.15 -71°	

3 piecewise sinusoidal
expansion functions

.18 33°	.19 -9°	.16 -11°	.17 -14°	.21 -44°	← CENTER ROW
.20 15°	.31 -3°	.34 -4°	.34 -4°	.42 -25°	
.10 65°	.08 -15°	.07 -21°	.08 -28°	.16 -68°	

Figure H-4. 5x5 array: reflection coefficient
convergence test.

5x5 Array
H-plane 60°

1 piecewise sinusoidal
expansion function

.25 0°	.38 0°	.40 -2°	.38 0°	.26 -2°	← CENTER ROW
.25 -7°	.38 14°	.39 17°	.38 15°	.25 -5°	
.13 -37°	.24 -21°	.25 -22°	.23 -21°	.13 -40°	

3 piecewise sinusoidal
expansion functions

.25 -1°	.37 -1°	.39 -3°	.37 -1°	.26 -2°	← CENTER ROW
.25 -9°	.37 10°	.36 13°	.37 11°	.25 -8°	
.13 -40°	.23 -23°	.24 -24°	.22 -23°	.13 -41°	

Figure H-5. 5x5 array: reflection coefficient convergence test.

5x5 Array

1 piecewise sinusoidal expansion function

CENTER COLUMN

↑	↑	↑
↑	↑	↑ $\overline{E}$
.26 -1°	.38 0°	.40 -2°
.25 -6°	.38 15°	.39 17°
.13 -39°	.23 -21°	.25 -22°

3 piecewise sinusoidal expansion functions

CENTER COLUMN

↑	↑	↑
↑	↑	↑ $\overline{E}$
.26 -2°	.37 -1°	.39 -3°
.25 -9°	.37 11°	.36 13°
.13 -41°	.23 -23°	.24 -24°

Quasi-E-plane
0°
(Broadside)

Figure H-6. 5x5 array: reflection coefficient convergence test.

5x5 Array

1 piecewise sinusoidal expansion function

		CENTER COLUMN
.18 -178°	.10 168°	.08 150°
.20 -128°	.11 -85°	.08 -80°
.17 -122°	.08 -81°	.06 -87°
.19 -113°	.14 -86°	.13 90°
.30 -83°	.35 -58°	.35 -59°

3 piecewise sinusoidal expansion functions

		CENTER COLUMN
.18 -175°	.10 174°	.09 159°
.20 -127°	.12 -89°	.09 -94°
.17 -121°	.08 -86°	.07 -101°
.19 -113°	.14 -88°	.14 -95°
.30 -84°	.34 -61°	.34 -63°

Quasi-E-plane
30°

Figure H-7. 5x5 array: reflection coefficient convergence test.

5x5 Array

1 piecewise sinusoidal expansion function

		CENTER COLUMN
.21 -131°	.41 -104°	.47 -98°
.39 -140°	.54 -117°	.58 -113°
.43 -139°	.57 -116°	.60 -113°
.39 141°	.53 -116°	.57 -112°
.22 -132°	.41 -100°	.47 -94°

3 piecewise sinusoidal expansion functions

		CENTER COLUMN
.20 -135°	.36 -104°	.42 -97°
.37 -143°	.49 -118°	.51 -114°
.41 -141°	.52 -117°	.54 -114°
.38 -144°	.49 -117°	.51 -112°
.21 -138°	.36 -101°	.42 -93°

Quasi-E-plane
60°

Figure H-8. 5x5 array: reflection coefficient convergence test.

APPENDIX I

REFLECTION COEFFICIENT TABULATION: QUASI-E-PLANE SCANNING WITH SQUARE WAVEGUIDE-FED APERTURES, L=0.5714λ.

3x3 array 7 pulses/aperture

Quasi-E-plane

.06 70^{o}	.11 20^{o}	.06 70^{o}	
.23 105^{o}	.25 90^{o}	.23 105^{o}	0^{o} (Broadside)
.06 70^{o}	.11 20^{o}	.06 70^{o}	

.33 -84^{o}	.42 -73^{o}	.33 -84^{o}	
.54 -92^{o}	.64 -83^{o}	.54 -92^{o}	60^{o}
.33 -81^{o}	.43 -70^{o}	.33 -81^{o}	

Figure I-1, Reflection coefficients for elements in a 3x3 phased array.

5x5 array 7 pulses/aperture

CENTER COLUMN

↑	↓	↑	
↑	↓	↑ E	
.17 93°	.17 53°	.18 43°	0° (Broadside)
.17 108°	.16 80°	.16 75°	
.02 67°	.12 -10°	.14 -14°	

Quasi-E-plane

CENTER COLUMN

.34 -77°	.54 -63°	.60 -60°	
.61 -80°	.86 -70°	.93 -68°	
.66 -77°	.93 -68°	1.0 -67°	60°
.60 -80°	.85 -70°	.91 .67°	
.34 -75°	.54 -60°	.60 -57°	

Figure I-2. Reflection coefficients for elements in a 5x5 phased array.

7x7 array 7 pulses/aperture

CENTER COLUMN

↓	↑	↓	↑
↓	↑	↓	↑
↓	↑	↓	↑ E
.14 99°	.12 60°	.11 45°	.10 39°
.17 103°	.15 62°	.15 44°	.15 40°
.18 116°	.14 87°	.11 76°	.10 73°
.01 106°	.10 -22°	.14 -29°	.15 -31°

Quasi-E-plane
0° (Broadside)

Figure I-3. Reflection coefficients for elements in a 7x7 phased array.

7x7 array 7 pulses/aperture

			CENTER COLUMN
.33 -80°	.53 -62°	.62 -56°	.64 -54°
.58 -81°	.84 -68°	.96 .62°	.99 -60°
.60 -74°	.93 -63°	1.07 -57°	1.11 -56°
.59 -73°	.93 -61°	1.08 -56°	1.12 -54°
.60 -75°	.92 -63°	1.05 -57°	1.09 -55°
.58 -82°	.83 -67°	.93 -61°	.96 -59°
.33 -79°	.52 -60°	.60 -54°	.62 -51°

Quasi-E-plane
60°

Figure I-4. Reflection coefficients for elements in a 7x7 phased array.

9x9 array 7 pulses/aperture

CENTER COLUMN

↑	↓	↑	↓	↑
↑	↓	↑	↓	↑
↑	↓	↑	↓	↑
↑	↓	↑	↓	↑ E
.16 113°	.12 74°	.11 56°	.11 48°	.10 46°
.15 103°	.13 66°	.10 48°	.09 33°	.09 27°
.18 103°	.15 67°	.13 50°	.13 41°	.12 39°
.19 120°	.14 96°	.11 89°	.09 86°	.08 84°
.02 120°	.09 -24°	.14 -35°	.15 -40°	.16 -42°

Quasi-E-plane
0° (Broadside)

Figure I-5. Reflection coefficients for elements in a 9x9 phased array.

9x9 array 7 pulses/aperture

CENTER COLUMN

.34 -80°	.53 -64°	.61 -58°	.62 -54°	.61 -53°
.59 -82°	.85 -69°	.95 -62°	.96 -58°	.96 -57°
.61 -76°	.91 -64°	1.04 -56°	1.07 -52°	1.07 -51°
.56 -76°	.89 -61°	1.03 -53°	1.08 -48°	1.08 -47°
.54 -77°	.88 -61°	1.02 -53°	1.07 -48°	1.08 -46°
.57 -76°	.89 -62°	1.03 -54°	1.07 -49°	1.07 -47°
.61 -77°	.92 -64°	1.03 -57°	1.05 -53°	1.05 -52°
.60 -82°	.85 -69°	.93 -62°	.94 -59°	.93 -58°
.34 -78°	.53 -62°	.60 -56°	.60 -53°	.60 -52°

Quasi-E-plane
60°

Figure I-6. Reflection coefficients for elements in a 9x9 phased array.

11x11 array 5 pulses/aperture

CENTER COLUMN

↓	↑	↓	↑	↓	↓
↓	↑	↓	↑	↓	↑
↓	↑	↓	↑	↓	↑
↓	↑	↓	↑	↓	↑
↓	↑	↓	↑	↓	↑ $\bar{E}$
.19 100°	.16 70°	.14 56°	.12 44°	.11 36°	.11 33°
.17 100°	.15 69°	.13 56°	.10 50°	.10 48°	.09 47°
.17 94°	.15 65°	.13 52°	.10 42°	.09 35°	.09 32°
.21 96°	.18 67°	.16 53°	.15 46°	.13 42°	.13 41°
.21 111°	.17 91°	.13 88°	.10 89°	.09 92°	.08 93°
.04 91°	.09 -12°	.13 -29°	.15 -37°	.15 -42°	.16 -43°

Quasi-E-plane
0° (Broadside)

Figure I-7. Reflection coefficients for elements in a 11x11 phased array.

11x11 array 5 pulses/aperture

					CENTER COLUMN
.31 -82°	.52 -66°	.61 -59°	.62 -57°	.61 -57°	-60 -57°
.55 -84°	.84 -72°	.95 -65°	.97 -62°	.95 -61°	.94 -61°
.57 -78°	.91 -66°	1.04 -60°	1.06 -56°	1.05 -54°	1.04 -53°
.52 -79°	.87 -65°	1.02 -57°	1.04 -52°	1.03 -49°	1.01 -49°
.51 -84°	.86 -67°	.99 -57°	1.01 -51°	.99 -48°	.98 -47°
.52 -85°	.86 -68°	.99 -57°	1.01 -51°	.98 -47°	.97 -46°
.51 -83°	.86 -66°	1.00 -57°	1.02 -51°	1.00 -48°	.99 -48°
.53 -78°	.88 -65°	1.02 -57°	1.05 -52°	1.03 -51°	1.02 -50°
.57 -78°	.91 -66°	1.04 -60°	1.06 -56°	1.04 -55°	1.03 -55°
.55 -85°	.83 -71°	.93 -65°	.95 -62°	.93 -61°	.93 -61°
.30 -81°	.51 -63°	.59 -57°	.60 -55°	.59 -55°	.59 -56°

Quasi-E-plane
60°

Figure I-8. Reflection coefficients for elements in a 11x11 phased array.

APPENDIX J

REFLECTION COEFFICIENT TABULATION: QUASI-E-PLANE SCANNING WITH RECTANGULAR WAVEGUIDE-FED APERTURES FOR L/W = 2.25, L=0.5714 λ

3x3 array 7 pulses/aperture

.07 -2^{0}	.14 -2^{0}	.07 -2^{0}
.17 -167^{0}	.11 -139^{0}	.17 -167^{0}
.07 -2^{0}	.14 -2^{0}	.07 -2^{0}

Quasi-E-plane
0^{0} (Broadside)

Figure J-1. Reflection coefficients for elements in a 3x3 phased array.

5x5 array 7 pulses/aperture

CENTER COLUMN

↑	↓	↑
↑	↓	↑
.21 141°	.15 138°	.14 142°
.12 161°	.03 148°	.01 158°
.12 -20°	.26 -14°	.28 -14°

Quasi-E-plane
0° (Broadside)

Figure J-2. Reflection coefficients for elements in a 5x5 phased array.

7x7 array 7 pulses/aperture

CENTER COLUMN

↓	↑	↓	↑
↓	↑	↓	↑
↓	↑	↓	↑ E
.19 122°	.18 98°	.16 95°	.15 95°
.18 135°	.11 111°	.08 101°	.07 99°
.12 160°	.05 -99°	.09 -68°	.10 -65°
.13 -23°	.24 -24°	.28 -29°	.29 -31°

Quasi-E-plane
0° (Broadside)

Figure J-3. Reflection coefficients for elements in a 7x7 phased array.

9x9 array 7 pulses/aperture

CENTER COLUMN

↑	↓	↑	↓	↑
↑	↓	↑	↓	↑
↑	↓	↑	↓	↑
↑	↓	↑	↓	↑ E
.18 119°	.16 77°	.15 65°	.15 61°	.14 60°
.19 120°	.14 90°	.12 77°	.10 71°	.09 70°
.18 131°	.10 127°	.05 148°	.04 -172°	.04 -156°
.11 175°	.06 -121°	.10 -96°	.13 -93°	.14 -92°
.11 -35°	.22 -25°	.25 -29°	.26 -32°	.26 -33°

Quasi-E-plane
0° (Broadside)

Figure J-4. Reflection coefficients for elements in a 9x9 phased array.

9x9 array 7 pulses/aperture

CENTER COLUMN

.53 -127°	.54 -118°	.58 -118°	.61 -118°	.62 -119°
.31 -138°	.35 -131°	.40 -129°	.44 -127°	.46 -126°
.30 -121°	.33 -111°	.39 -110°	.43 -109°	.44 -108°
.31 -126°	.40 -113°	.47 -108°	.51 -106°	.52 -106°
.30 -127°	.37 -113°	.44 -108°	.48 -106°	.49 -105°
.29 -125°	.36 -102°	.41 -96°	.43 -94°	.44 -94°
.26 -112°	.35 -87°	.41 -81°	.44 -80°	.45 -79°
.25 -80°	.34 -61°	.39 -60°	.41 -61°	.42 -61°
.30 -1[illegible]°	.41 -17°	.44 -19°	.44 -21°	.44 -21°

Quasi-E-plane
30°

Figure J-5. Reflection coefficients for elements in a 9x9 phased array.

9x9 array 7 pulses/aperture

CENTER COLUMN

.74 -92°	1.03 -75°	1.14 -68°	1.18 -64°	1.18 -64°
.57 -67°	.82 -54°	.91 -48°	.94 -46°	.95 -45°
.72 -74°	1.01 -60°	1.11 -55°	1.15 -53°	1.16 -52°
.68 -75°	.88 -63°	.96 -59°	.98 -58°	.99 -57°
.68 -74°	.89 -60°	.96 -56°	.98 54	.98 -53°
.68 -73°	.84 -63°	.90 -60°	.93 -59°	.94 -59°
.61 -74°	.73 -60°	.76 -57°	.77 -56°	.77 -56°
.[illegible]8 [illegible]	.60 -50°	.66 -49°	.67 -48°	.67 -48°
.41 -20°	.52 -19°	.53 -21°	.52 -22°	.52 -23°

Quasi-E-plane

Figure J-6. Reflection coefficients for elements in a 9x9 phased array.

11x11 array 7 pulses/aperture

CENTER COLUMN

↓	↑	↓	↑	↓	↑
↓	↑	↓	↑	↓	↑
↓	↑	↓	↑	↓	↑
↓	↑	↓	↑	↓	↑
↓	↑	↓	↑	↓	↑ E
.20 108°	.15 68°	.14 46°	.13 37°	.13 33°	.12 32°
.18 107°	.15 74°	.13 59°	.11 51°	.10 47°	.10 46°
.17 113°	.15 91°	.11 92°	.08 98°	.07 106°	.06 110°
.18 135°	.11 125°	.08 140°	.07 164°	.08 179°	.08 -176°
.14 169°	.05 -136°	.08 -101°	.10 -93°	.11 -99°	.17 -100°
.10 -22°	.21 -21°	.25 -26°	.26 -128°	.26 -30°	.27 -30°

Quasi-E-plane
0° (Broadside)

Figure J-7. Reflection coefficients for elements in a 11x11 phased array.

APPENDIX K

REFLECTION COEFFICIENT TABULATION: E-PLANE SCANNING WITH SQUARE WAVEGUIDE-FED APERTURES, L=0.5714λ

3x3 array 7 pulses/aperture

.21 144^{o}	.33 148^{o}	.21 144^{o}	
.32 128^{o}	.40 132^{o}	.32 128^{o}	0^{o} (Broadside)
.21 144^{o}	.33 148^{o}	.21 144^{o}	

E-plane

.35 178^{o}	.47 163^{o}	.35 178^{o}	
.28 158^{o}	.41 -178^{o}	.28 158	30^{o}
.07 -140^{o}	.18 179	.07 -140^{o}	

Figure K-1. Reflection coefficients for elements in a 3x3 phased array.

3x3 array 7 pulses/aperture

.32 -154°	.46 -177°	.32 -154°	
.43 -134°	.54 -159°	.43 -134°	50°
.22 -133°	.33 -163°	.22 -133°	

E-plane

.22 -133°	.33 -162°	.22 -133°	
.43 -134°	.53 -159°	.43 -134°	80°
.33 -154°	.46 -177°	.33 -154°	

Figure K-2. Reflection coefficients for elements in a 3x3 phased array.

5x5 array 7 pulses/aperture

E-plane

		CENTER COLUMN	
↑	↑	↑	
↑	↑	↑	
.30 130°	.37 138°	.33 139°	0° (Broadside)
.31 .128°	.38 133°	.33 138°	
.22 143°	.31 146°	.27 152°	

		CENTER COLUMN	
.36 177°	.44 164°	.41 178°	
.30 -166°	.38 177°	.35 -167°	
.28 -167	.37 177°	.34 -169°	30°
.27 -161°	.36 -177°	.32 -165°	
.06 -150°	.15 178°	.13 -165°	

Figure K-3. Reflection coefficients for elements in a 5x5 phased array.

5x5 array 7 pulses/aperture

CENTER COLUMN

.33 -158°	.45 -175°	.35 -166°	
.48 -138°	.58 -158°	.47 -146°	
.49 -134°	.60 -153°	.49 -144°	50°
.47 -133°	.55 -150°	.48 -144°	
.24 -135°	.32 -156°	.29 -152°	

E-plane

CENTER COLUMN

.24 -135°	.31 -156°	.29 -152°	
.46 -133°	.55 -150°	.48 -144°	
.49 -134°	.60 -153°	.49 -144°	80°
.47 -138°	.58 -158°	.47 -146°	
.33 -158°	.45 -175°	.35 -166°	

Figure K-4. Reflection coefficients for elements in a 5x5 phased array.

7x7 array 7 pulses/aperture

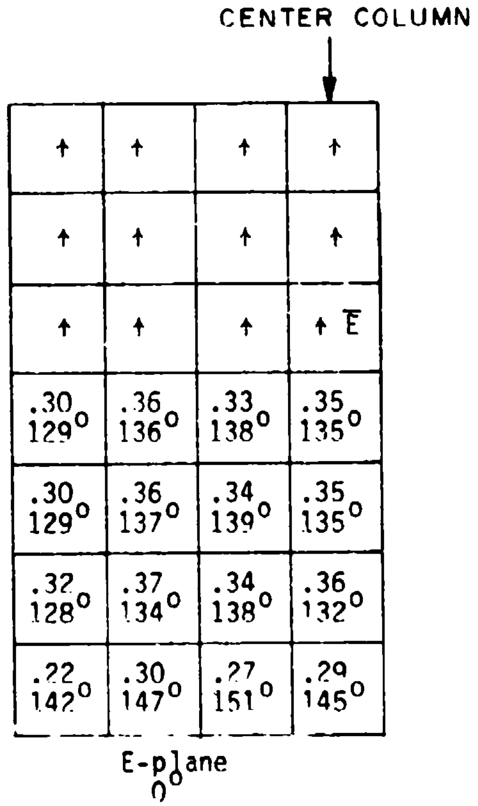

Figure K-5. Reflection coefficients for elements
in a 7x7 phased array.

7x7 array 7 pulses/aperture

			CENTER COLUMN
.36 176°	.43 165°	.41 176°	.42 165°
.30 -167°	.38 178°	.37 -170°	.36 178°
.28 -168°	.35 179°	.35 -168°	.34 178°
.28 -168°	.35 177°	.33 -168°	.34 177°
.28 -169°	.36 177°	.33 -172°	.35 178°
.27 -163°	.35 -177°	.33 -168°	.33 -175°
.06 -156°	.15 179°	.14 -170°	.13 180°

E-plane
30°

Figure K-6. Reflection coefficients for elements in a 7x7 phased array.

7x7 array 7 pulses/aperture

			CENTER COLUMN
.33 158°	.43 -174°	.36 -168°	.42 -170°
.48 -138°	.56 -158°	.47 -149°	.56 -153°
.49 -135°	.59 -154°	.49 -148°	.58 -150°
.51 -135°	.60 -153°	.51 -148°	.58 -149°
.51 -134°	.59 -152°	.53 -146°	.57 -148°
.47 -133°	.55 -150°	.51 -145°	.52 -147°
.24 -136°	.32 -156°	.30 -152°	.29 -154°

E-plane
50°

Figure K-7. Reflection coefficients for elements in a 7x7 phased array.

7x7 array 7 pulses/aperture

CENTER COLUMN

.24 -136°	.32 -156°	.30 -151°	.29 -154°
.47 -133°	.55 -150°	.51 -145°	.52 -147°
.51 -134°	.60 -152°	.53 -146°	.57 -148°
.50 -135°	.60 -153°	.51 -148°	.58 -149°
.49 -135°	.59 -154°	.49 -148°	.58 -150°
.47 -139°	.56 -158°	.47 -149°	.56 -153°
.33 -158°	.43 -174°	.36 -168°	.42 -170°

E-plane
80°

Figure K-8. Reflection coefficients for elements in a 7x7 phased array.

9x9 array 7 pulses/aperture

CENTER COLUMN

↑	↑	↑	↑	↑
↑	↑	↑	↑	↑
↑	↑	↑	↑	↑
↑	↑	↑	↑	↑ $\bar{E}$
.30 128°	.37 137°	.34 138°	.35 134°	.35 139°
.30 129°	.36 137°	.33 138°	.35 135°	.34 138°
.30 128°	.36 138°	.34 138°	.34 135°	.35 139°
.32 127°	.37 134°	.35 137°	.36 133°	.36 137°
.22 142°	.30 147°	.28 150°	.28 146°	.28 150°

E-plane
0°

Figure K-9. Reflection coefficients for elements in a 9x9 phased array.

9x9 array 7 pulses/aperture

CENTER COLUMN

				CENTER COLUMN
.37 175°	.43 165°	.42 175°	.41 166°	.42 175°
.30 -167°	.38 179°	.37 -170°	.36 179°	.37 -171°
.28 -169°	.35 179°	.35 -170°	.33 179°	.35 -170°
.28 -169°	.35 178°	.34 -170°	.33 177°	.34 -170°
.28 -169°	.34 178°	.34 -170°	.33 178°	.34 -171°
.27 -170°	.34 177°	.33 -171°	.33 178°	.33 -172°
.28 -171°	.36 177°	.33 -173°	.34 179°	.34 -174°
.27 -164°	.35 -176°	.33 -169°	.33 -174°	.34 -170°
.06 -155°	.16 180°	.14 -171°	.14 -177°	.15 -173°

E-plane
30°

Figure K-10. Reflection coefficients for elements in a 9x9 phased array.

9x9 array 7 pulses/aperture

CENTER COLUMN

.34 -157°	.43 -174°	.37 -168°	.41 -168°	.38 -171°
.48 -138°	.56 -158°	.48 -149°	.55 -151°	.49 -153°
.50 -134°	.58 -154°	.49 -147°	.57 -148°	.50 -151°
.50 -135°	.59 -153°	.50 -148°	.57 -147°	.52 -150°
.51 -135°	.60 -153°	.52 -148°	.57 -148°	.54 -150°
.51 -135°	.61 -153°	.53 -147°	.57 -149°	.55 -148°
.51 -135°	.60 -151°	.54 -146°	.57 -149°	.55 -147°
.48 -134°	.56 -149°	.52 -145°	.53 -148°	.53 -145°
.29 -136°	.32 -155°	.31 -152°	.30 -154°	.31 -153°

E-plane
50°

Figure K-11. Reflection coefficients for elements in a 9x9 phased array.

9x9 array 7 pulses/aperture

CENTER COLUMN

.24 -136°	.32 -155°	.31 -152°	.30 -154°	.31 -152°
.48 -134°	.55 -149°	.52 -145°	.53 -148°	.52 -145°
.51 -135°	.60 -151°	.54 -146°	.57 -149°	.55 -147°
.51 -135°	.61 -153°	.53 -147°	.57 -149°	.55 -148°
.51 -135°	.60 -153°	.52 -148°	.57 -149°	.54 -150°
.50 -135°	.59 -153°	.50 -148°	.57 -147°	.52 -150°
.50 -135°	.58 -154°	.49 -147°	.57 -148°	.50 -151°
.48 -139°	.55 -158°	.48 -149°	.55 -151°	.49 -153°
.34 -157°	.43 -175°	.37 -168°	.41 -169°	.38 -171°

E-plane
80°

Figure K-12. Reflection coefficients for elements in a 9x9 phased array.

11x11 array 5 pulses/aperture

					CENTER COLUMN
↑	↑	↑	↑	↑	↑
↑	↑	↑	↑	↑	↑
↑	↑	↑	↑	↑	↑
↑	↑	↑	↑	↑	↑
↑	↑	↑	↑	↑	↑
.30 122°	.36 131°	.33 132°	.34 130°	.35 132°	.34 130°
.31 122°	.37 131°	.34 131°	.35 129°	.35 132°	.34 129°
.30 122°	.36 131°	.33 132°	.35 130°	.34 132°	.34 130°
.30 122°	.36 132°	.34 132°	.34 130°	.35 132°	.34 130°
.32 121°	.37 129°	.34 130°	.36 127°	.36 131°	.35 127°
.22 136°	.31 143°	.27 145°	.28 142°	.28 145°	.28 142°

E-plane
0°

Figure K-13. Reflection coefficients for elements in an 11x11 phased array.

11x11 array 5 pulses/aperture

CENTER COLUMN

.36 167°	.42 158°	.40 168°	.41 159°	.41 167°	.40 159°
.28 -179°	.38 169°	.35 180°	.35 169°	.36 179°	.35 170°
.28 -180°	.35 169°	.34 -180°	.33 169°	.35 179°	.33 170°
.27 -180°	.34 168°	.33 -180°	.33 169°	.34 180°	.32 169°
.27 179°	.34 168°	.32 179°	.33 168°	.33 178°	.32 168°
.27 178°	.35 168°	.33 178°	.33 167°	.33 178°	.33 167°
.27 178°	.35 168°	.33 179°	.33 168°	.33 178°	.33 169°
.27 178°	.35 168°	.33 178°	.33 169°	.33 176°	.33 170°
.28 178°	.36 168°	.33 177°	.34 170°	.34 175°	.34 170°
.27 -174°	.36 175°	.33 -179°	.34 177°	.34 180°	.33 177°
.06 -168°	.17 174°	.14 -178°	.14 177°	.15 179°	.14 178°

E-plane
30°

Figure K-14. Reflection coefficients for elements in an 11x11 phased array.

11x11 array 5 pulses/aperture

					CENTER COLUMN
.33 -166°	.44 177°	.37 -176°	.41 -178°	.40 -180°	.39 -177°
.46 -148°	.55 -169°	.47 -160°	.53 -163°	.49 -164°	.51 -161°
.47 -145°	.58 -166°	.48 -158°	.55 -159°	.51 -162°	.53 -158°
.48 -145°	.58 -164°	.49 -158°	.55 -158°	.52 -162°	.53 -157°
.48 -145°	.59 -164°	.50 -159°	.55 -159°	.53 -161°	.53 -158°
.48 -146°	.59 -164°	.50 -159°	.56 -160°	.53 -161°	.54 -159°
.48 -147°	.60 -164°	.51 -160°	.56 -160°	.53 -161°	.56 -160°
.49 -147°	.60 -164°	.52 -159°	.57 -161°	.54 -160°	.56 -160°
.49 -146°	.60 -162°	.54 -158°	.56 -160°	.55 -159°	.56 -160°
.46 -145°	.55 -160°	.51 -156°	.52 -158°	.52 -157°	.52 -158°
.24 -146°	.34 -164°	.31 -161°	.31 -163°	.32 -162°	.31 -162°

E-plane
50°

Figure K-15. Reflection coefficients for elements in an 11x11 phased array.

APPENDIX L

REFLECTION COEFFICIENT TABULATION: E-PLANE SCANNING WITH RECTANGULAR WAVEGUIDE-FED APERTURES FOR L /W=2.25, L=0.5714 λ

3x3 array 7 pulses/aperture

E-plane

.11 147°	.22 147°	.11 147°	
.36 167°	.50 161°	.36 167°	0° (Broadside)
.11 147°	.22 147°	.11 147°	

.44 -157°	.55 -173°	.44 -157°	
.21 -159°	.31 -176°	.21 -159°	30°
.14 -17°	.02 -31°	.14 -17°	

.66 -127°	.76 -143°	.66 -127°	
.35 -77°	.34 -97°	.35 -77°	60°
.20 -30°	.07 -46°	.20 -30°	

Figure L-1. Reflection coefficients for elements in a 3x3 phased array.

5x5 array 7 pulses/aperture

CENTER COLUMN

↑	↑	↑	
↑	↑	↑ E	
.37 134°	.44 134°	.38 141°	0° (Broadside)
.31 151°	.39 150°	.35 157°	
.09 169°	.18 167°	.16 176°	

E-plane

CENTER COLUMN

.40 -170°	.47 177°	.44 -171°	
.35 171°	.44 163°	.38 171°	
.32 -164°	.41 -175°	.37 -167°	30°
.25 -149°	.34 -166°	.31 -156°	
.12 -3°	.05 26°	.06 -21°	

Figure L-2. Reflection coefficients for elements in a 5x5 phased array.

5x5 array 7 pulses/aperture

		CENTER COLUMN
.76 -135°	.85 -148°	.77 -142°
.50 -104°	.54 -119°	.52 -113°
.55 -111°	.59 -127°	.56 -120°
.37 -90°	.37 -107°	.39 -102°
.21 -23°	.13 -31°	.15 -34°

E-plane
60°

Figure L-3. Reflection coefficients for elements in a 5x5 phased array.

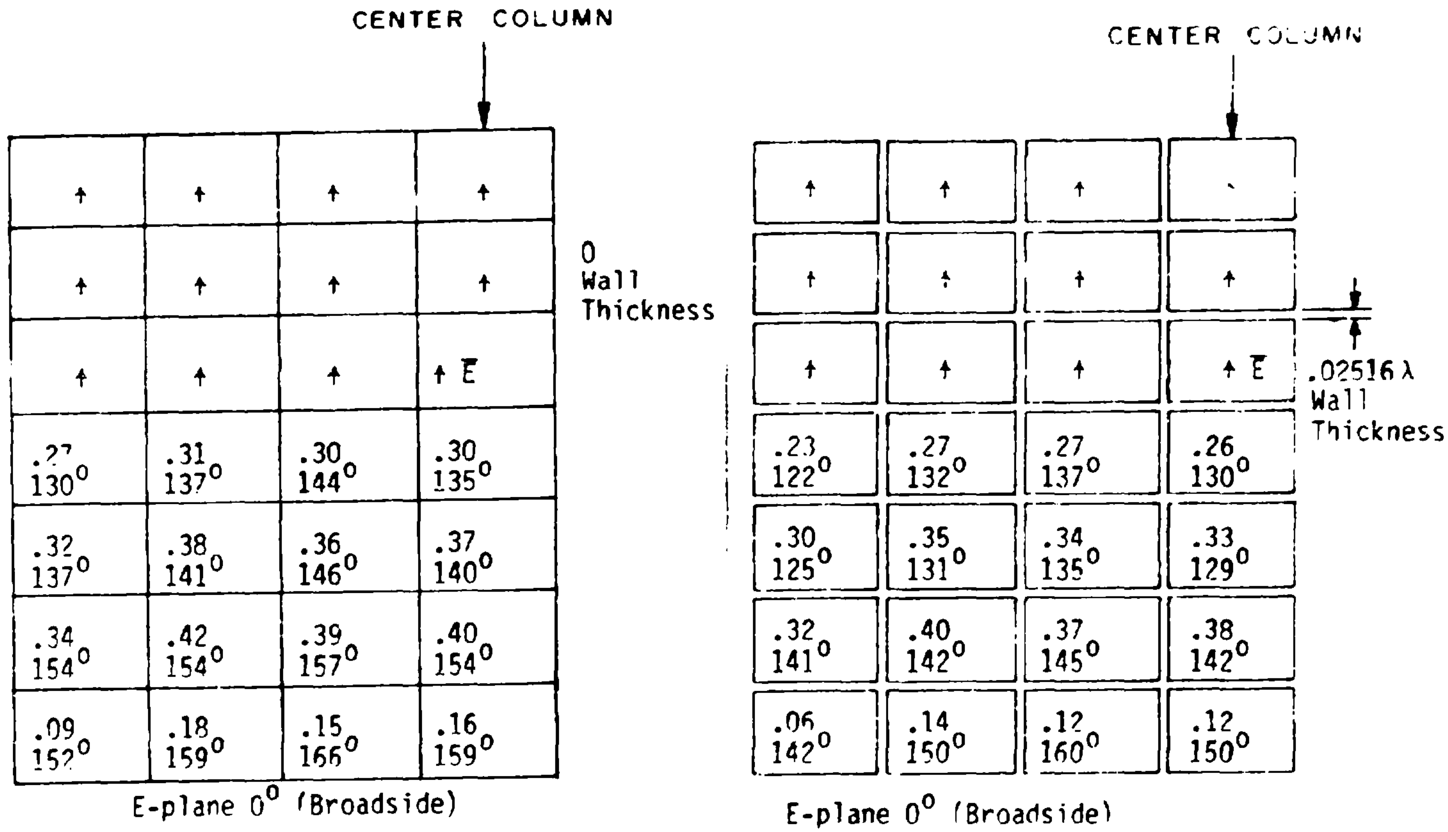

Figure L-4. Reflection coefficients for elements in a 7x7 phased array with zero and non-zero wall thickness.

CENTER COLUMN

0 Wall Thickness

.38 -166°	.42 -179°	.43 -167°	.42 -178°
.32 163°	.38 155°	.34 166°	.37 156°
.30 178°	.38 169°	.34 178°	.37 170°
.36 180°	.45 170°	.41 177°	.43 172°
.32 -169°	.41 -179°	.38 -172°	.39 -178°
.24 -147°	.32 -161°	.31 -155°	.30 -160°
.11 0°	.03 36°	.04 -4°	.05 16°

E-plane 30°

CENTER COLUMN

0.02516λ Wall Thickness

.33 -170°	.35 178°	.39 -171°	.35 178°
.26 154°	.31 145°	.29 158°	.30 146°
.26 170°	.33 159°	.31 170°	.32 160°
.32 168°	.39 158°	.36 166°	.37 159°
.30 -177°	.37 173°	.36 180°	.35 174°
.23 -155°	.30 -170°	.29 165°	.28 -158°
.14 -10°	.06 7°	.07 -14°	.07 -3°

E-plane 30°

Figure L-5. Reflection coefficients for elements in a 7x7 phased array with zero and non-zero wall thickness.

CENTER COLUMN (left grid, right-hand column) — 0 Wall Thickness

.77 -138°	.88 -152°	.79 -148°	.85 -149°
.53 -112°	.59 -128°	.54 -123°	.57 -125°
.63 -120°	.70 -135°	.64 -130°	.68 -133°
.54 -112°	.58 -126°	.57 -121°	.57 -124°
.52 -100°	.56 -123°	.54 -119°	.55 -121°
.37 -93°	.38 -110°	.39 -104°	.38 -108°
.22 -21°	.14 -28°	.15 -33°	.15 -26°

E-plane 60°

CENTER COLUMN (right grid, right-hand column) — 0.02516λ Wall Thickness

.70 -143°	.78 -158°	.71 -153°	.76 -155°
.54 -116°	.60 -133°	.55 -127°	.58 -130°
.58 -126°	.62 -142°	.58 -136°	.61 -139°
.55 -115°	.58 -130°	.57 -125°	.57 -127°
.50 -113°	.51 -128°	.51 -122°	.51 -125°
.40 -96°	.39 -111°	.41 -108°	.39 -100°
.24 -24°	.16 -26°	.17 -30°	.18 -28°

E-plane 60°

Figure L-6. Reflection coefficients for elements in a 7x7 phased array with zero and non-zero wall thickness.

9x9 array 7 pulses/aperture

CENTER COLUMN

↑	↑	↑	↑	↑
↑	↑	↑	↑	↑
↑	↑	↑	↑	↑
↑	↑	↑	↑	↑ $\bar{E}$
.28 141°	.34 151°	.33 152°	.32 148°	.34 152°
.29 135°	.35 143°	.33 145°	.33 141°	.34 145°
.34 134°	.40 138°	.37 141°	.38 138°	.38 141°
.32 152°	.40 154°	.37 157°	.38 154°	.38 157°
.09 160°	.18 164°	.16 171°	.16 164°	.17 170°

E-plane 0° (Broadside)

Figure L-7. Reflection coefficients for elements in a 9x9 phased array.

9x9 array 7 pulses/aperture

				CENTER COLUMN
.40 -165°	.44 -175°	.46 -166°	.43 -175°	.46 -166°
.30 167°	.35 160°	.33 171°	.35 161°	.34 170°
.26 180°	.33 171°	.31 -177°	.32 172°	.31 -179°
.32 173°	.39 164°	.35 174°	.37 166°	.36 173°
.32 173°	.39 164°	.35 173°	.37 166°	.36 172°
.35 -179°	.43 173°	.40 179°	.41 174°	.41 178°
.33 -170°	.42 -179°	.39 -174°	.40 -177°	.40 -175°
.23 -147°	.31 -162°	.30 -155°	.29 -159°	.30 -157°
.11 -3°	.03 28°	.03 -13°	.04 8°	.03 -8°

E-plane 30°

Figure L-8. Reflection coefficients for elements in a 9x9 phased array.

9x9 array 7 pulses/aperture

CENTER COLUMN

.76 -141°	.88 -154°	.78 -151°	.84 -150°	.80 -151°
.52 -116°	.60 -132°	.53 -128°	.57 -128°	.54 -129°
.64 -124°	.73 -140°	.65 -135°	.70 -137°	.66 -136°
.58 -119°	.64 -134°	.59 -129°	.62 -131°	.60 -130°
.61 -118°	.67 -133°	.62 -128°	.65 -130°	.63 -129°
.56 -113°	.60 -128°	.58 -122°	.58 -125°	.58 -123°
.52 -108°	.55 -122°	.54 -118°	.54 -120°	.55 -119°
.37 -94°	.39 -110°	.39 -106°	.39 -107°	.39 -107°
.22 -20°	.14 -27°	.16 -31°	.15 -26°	.15 -31°

E-plane 60°

Figure L-9. Reflection coefficients for elements in a 9x9 phased array.

11x11 array 5 pulses/aperture

CENTER COLUMN

↑	↑	↑	↑	↑	↑
↑	↑	↑	↑	↑	↑
↑	↑	↑	↑	↑	↑
↑	↑	↑	↑	↑	↑
↑	↑	↑	↑	↑	↑ E
.31 136°	.39 145°	.36 143°	.36 143°	.38 144°	.36 143°
.29 135°	.36 144°	.33 144°	.33 143°	.35 144°	.33 143°
.28 130°	.33 136°	.31 141°	.32 138°	.32 141°	.31 138°
.34 133°	.33 139°	.37 140°	.38 137°	.37 140°	.37 137°
.33 150°	.42 152°	.39 154°	.40 151°	.40 154°	.39 151°
.08 149°	.18 159°	.15 164°	.15 159°	.16 163°	.15 160°

E-plane 0° (Broadside)

Figure E-10. Reflection coefficients for elements in an 11x11 phased array.

11x11 array 5 pulses/aperture

CENTER COLUMN

					CENTER COLUMN
.39 -171°	.44 180°	.45 -173°	.42 180°	.45 -172°	.42 180°
.32 164°	.38 159°	.36 168°	.37 159°	.36 167°	.37 159°
.28 179°	.34 171°	.33 -179°	.33 171°	.33 -180°	.33 172°
.30 174°	.37 165°	.35 175°	.36 166°	.35 174°	.35 167°
.28 169°	.34 161°	.31 173°	.33 163°	.32 170°	.32 164°
.30 169°	.37 162°	.34 171°	.35 164°	.35 169°	.35 164°
.33 168°	.41 161°	.37 167°	.39 162°	.38 166°	.38 163°
.34 175°	.43 167°	.39 173°	.41 169°	.40 172°	.40 169°
.34 -174°	.43 178°	.40 -178°	.41 170°	.41 -170°	.40 170°
.23 -153°	.32 -167°	.30 -162°	.30 -164°	.31 -153°	.30 -164°
.11 -5°	.02 21°	.04 -20°	.04 -2°	.03 -9°	.04 -8°

E-plane 30°

Figure L-11. Reflection coefficients for elements in an 11x11 phased array.

11x11 array 5 pulses/aperture

CENTER COLUMN ↓ (last column)

.72 -145°	.85 -159°	.74 -157°	.79 -156°	.78 -157°	.78 -156°
.50 -124°	.59 -141°	.51 -138°	.55 -137°	.54 -139°	.54 -137°
.62 -132°	.72 -148°	.62 -145°	.68 -144°	.65 -146°	.67 -144°
.56 -128°	.64 -144°	.57 -140°	.61 -140°	.59 -141°	.61 -140°
.60 -128°	.69 -144°	.61 -140°	.66 -140°	.63 -141°	.65 -140°
.58 -125°	.65 -141°	.59 -136°	.62 -138°	.60 -137°	.62 -137°
.59 -122°	.65 -138°	.61 -133°	.63 -135°	.62 -134°	.62 -135°
.55 -118°	.60 -134°	.57 -120°	.58 -131°	.57 -130°	.58 -130°
.50 -112°	.54 -127°	.53 -123°	.53 -125°	.53 -123°	.53 -125°
.37 -98°	.39 -116°	.39 -111°	.38 -113°	.39 -112°	.38 -112°
.22 -21°	.14 -29°	.15 -33°	.15 -30°	.15 -31°	.15 -31°

E-plane 60°

Figure L-12. Reflection coefficients for elements in an 11x11 phased array.

11x11 array 5 pulses/aperture

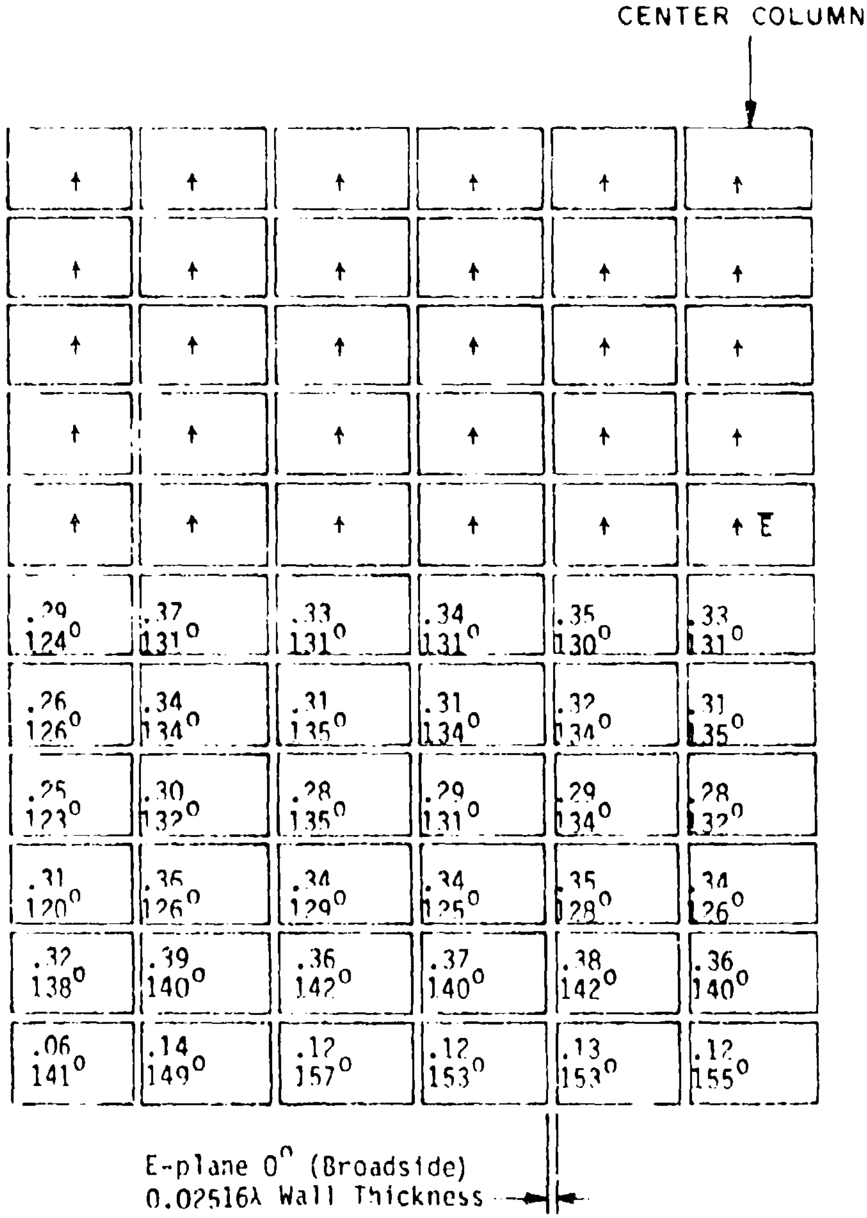

Figure L-13. Reflection coefficients for elements in an 11x11 phased array with non-zero wall thickness.

11x11 array 5 pulses/aperture

CENTER COLUMN

.33 -177°	.38 174°	.39 -180°	.35 175°	.40 180°	.35 175°
.28 154°	.33 150°	.33 158°	.31 149°	.33 158°	.31 150°
.25 172°	.31 165°	.32 174°	.29 165°	.32 173°	.29 166°
.26 165°	.32 156°	.32 167°	.30 158°	.32 165°	.30 159°
.23 165°	.29 156°	.28 168°	.27 158°	.29 166°	.27 160°
.25 160°	.32 152°	.30 162°	.30 155°	.31 160°	.30 156°
.27 158°	.34 150°	.31 159°	.32 153°	.32 157°	.32 154°
.30 165°	.39 157°	.36 164°	.36 159°	.37 162°	.36 160°
.30 177°	.39 168°	.36 173°	.36 170°	.37 171°	.36 171°
.22 -157°	.29 -173°	.28 -167°	.28 -170°	.28 -169°	.28 -168°
.13 -10°	.05 14°	.06 -10°	.06 -2°	.06 -2°	.06 -5°

E-plane 30°
0.02516λ Wall Thickness

Figure L-14. Reflection coefficients for elements in an 11x11 phased array with non-zero wall thickness.

11x11 array 5 pulses/aperture

CENTER COLUMN

.65 -150°	.75 -165°	.66 -161°	.71 -160°	.69 -162°	.69 -160°
.49 -127°	.58 -145°	.50 -141°	.54 -140°	.52 -142°	.53 -140°
.55 -138°	.64 -155°	.56 -150°	.61 -151°	.58 -152°	.60 -150°
.55 -130°	.62 -147°	.55 -143°	.59 -144°	.57 -144°	.59 -143°
.56° -132°	.63° -150°	.56° -144°	.60 -146°	.58 -146°	.60 -146°
.56 -128°	.62 -144°	.58 -139°	.60 -141°	.59 -140°	.59 -141°
.55 -127°	.60 -143°	.56 -137°	.58 -140°	.57 -139°	.58 -139°
.54 -121°	.58 -136°	.56 -132°	.56 -134°	.57 -132°	.56 -134°
.48 -115°	.51 -130°	.50 -126°	.50 -127°	.50 -127°	.50 -127°
.38 -100°	.38 -116°	.39 -113°	.38 -114°	.39 -113°	.39 -113°
.24 -26°	.16 -28°	.17 -33°	.17 -30°	.17 -31°	.17 -31°

E-plane 60°

0.02516λ Wall Thickness

Figure L-15. Reflection coefficients for elements in an 11x11 phased array with non-zero wall thickness.

APPENDIX M

REFLECTION COEFFICIENT TABULATION: H-PLANE SCANNING WITH SQUARE WAVEGUIDE-FED APERTURES, $L=0.5714\lambda$

3x3 array 7 pulses/aperture

30°

.24 103°	.10 118°	.15 169°
.39 106°	.29 111°	.28 125°
.24 103°	.10 118°	.15 169°

50°

.12 72°	.09 26°	.03 157°
.27 98°	.25 92°	.23 116°
.12 72°	.09 26°	.03 157°

80°

.03 157°	.09 26°	.12 72°
.23 116°	.25 92°	.27 98°
.03 157°	.09 26°	.12 72°

H-plane

Figure M-1. Reflection coefficients for elements in a 3x3 phased array.

5x5 array 7 pulses/aperture

.37 107°	.26 108°	.26 114°	.24 112°	.19 135°	← CENTER ROW
.40 109°	.32 110°	.33 111°	.31 109°	.24 122°	30°
.26 109°	.16 116°	.17 122°	.15 122°	.13 161°	

H-plane

.23 84°	.21 57°	.17 54°	.15 68°	.16 108°	← CENTER ROW
.23 86°	.20 71°	.17 83°	.18 101°	.22 126°	50°
.12 58°	.14 11°	.11 -6°	.05 -12°	.07 171°	

Figure M-2. Reflection coefficients for elements in a 5x5 phased array.

5x5 array 7 pulses/aperture

.16 108°	.15 68°	.18 54°	.21 57°	.23 84°	← CENTER ROW
.22 126°	.19 101°	.17 83°	.20 71°	.23 86°	
.07 171°	.05 -11°	.11 -6°	.14 11°	.12 58°	

H-plane
80°

Figure M-3. Reflection coefficients for elements in a 5x5 phased array.

7x7 array 7 pulses/aperture

.36 109°	.28 113°	.32 117°	.33 111°	.31 107°	.27 110°	.22 126°	CENTER ROW
.36 110°	.27 113°	.30 116°	.29 111°	.27 111°	.24 115°	.21 132°	
.38 111°	.31 114°	.35 115°	.35 109°	.31 107°	.28 111°	.25 124°	
.25 110°	.16 123°	.20 128°	.20 119°	.17 115°	.14 125°	.15 161°	

H-plane
30°

Figure M-4. Reflection coefficients for elements in a 7x7 phased array.

7x7 array 7 pulses/aperture

.23 79°	.20 56°	.16 54°	.13 66°	.13 85°	.15 99°	.17 127°	← CENTER ROW
.22 80°	.20 52°	.17 48°	.16 55°	.17 66°	.17 79°	.18 109°	
.22 82°	.19 62°	.16 67°	.15 83°	.18 96°	.21 102°	.23 119°	
.12 51°	.15 5°	.14 -11°	.11 -16°	.07 -12°	.03 12°	.07 162°	

H-plane
50°

Figure M-5. Reflection coefficients for elements in a 7x7 phased array.

7x7 array 7 pulses/aperture

.17 127°	.15 99°	.13 85°	.13 67°	.16 54°	.21 56°	.23 79°	← CENTER ROW
.18 109°	.17 79°	.17 66°	.16 56°	.17 48°	.20 63°	.22 80°	
.23 119°	.22 102°	.18 96°	.15 83°	.16 67°	.19 62°	.22 81°	
.07 162°	.03 14°	.07 -11°	.11 -16°	.14 -10°	.15 3°	.13 51°	

H-plane
80°

Figure M-6. Reflection coefficients for elements in a 7x7 phased array.

9x9 array 7 pulses/aperture

.36 108°	.27 112°	.29 118°	.31 115°	.30 113°	.29 113°	.28 112°	.26 113°	.21 130°	← CENTER ROW
.36 108°	.27 113°	.31 119°	.32 114°	.32 112°	.32 111°	.30 108°	.26 109°	.21 128°	
.35 108°	.26 [illegible]	.29 119°	.30 115°	.29 114°	.29 114°	.28 111°	.24 112°	.20 133°	
.38 109°	.30 113°	.33 117°	.35 113°	.34 111°	.33 111°	.32 109°	.29 109°	.24 124°	
.24 108°	.15 123°	.19 131°	.20 124°	.19 122°	.19 121°	.18 118°	.14 122°	.14 162°	

H-plane
30°

Figure M-7. Reflection coefficients for elements in a 9x9 phased array.

9x9 array 7 pulses/aperture

.23 75°	.21 43°	.17 43°	.15 51°	.16 63°	.18 71°	.19 77°	.20 87°	.21 112°	← CENTER ROW
.22 77°	.20 51°	.16 48°	.13 54°	.13 64°	.14 72°	.15 80°	.15 89°	.16 120°	
.21 78°	.19 48°	.16 42°	.15 48°	.16 56°	.17 62°	.18 65°	.17 74°	.16 109°	
.21 78°	.19 56°	.15 59°	.14 72°	.16 84°	.18 89°	.21 92°	.23 97°	.23 115°	
.13 46°	.16 2°	.16 -13°	.13 -19°	.11 -17°	.09 -9°	.07 0°	.04 17°	.06 161°	

H-plane
50°

Figure M-8. Reflection coefficients for elements in a 9x9 phased array.

9x9 array 7 pulses/aperture

.21 112°	.20 96°	.19 77°	.18 71°	.16 63°	.15 52°	.17 44°	.21 49°	.22 75°	← CENTER ROW
.16 120°	.16 90°	.15 80°	.14 72°	.13 66°	.14 55°	.16 49°	.20 51°	.22 77°	
.16 108°	.17 74°	.18 65°	.17 62°	.16 57°	.15 49°	.16 49°	.19 49°	.21 78°	
.23 116°	.23 97°	.21 92°	.18 80°	.16 84°	.14 72°	.15 59°	.19 57°	.21 79°	
.06 152°	.04 12°	.07 [illegible]°	.08 -8°	.11 -15°	.12 -19°	.15 -13°	.17 3°	.19 47°	

H-plane
30°

Figure M-9. Reflection coefficients for elements in a 9x9 phased array.

11x11 array 5 pulses/aperture

.32 104°	.29 105°	.31 111°	.32 109°	.31 109°	.32 110°	.32 108°	.33 104°	.30 103°	.27 105°	.22 120°	← CENTER ROW
.32 103°	.28 106°	.30 111°	.31 108°	.30 109°	.30 112°	.32 110°	.32 107°	.29 105°	.27 107°	.22 122°	
.37 103°	.28 106°	.31 112°	.33 109°	.32 108°	.32 109°	.33 105°	.33 105°	.31 103°	.28 104°	.22 119°	
.37 103°	.28 105°	.29 112°	.30 110°	.29 111°	.31 112°	.31 109°	.30 106°	.29 106°	.26 109°	.21 122°	
.40 104°	.32 106°	.34 110°	.35 106°	.33 107°	.34 110°	.36 [illegible]	.35 102°	.33 102°	.30 105°	.25 116°	
.26 104°	.16 114°	.19 122°	.20 119°	.19 110°	.20 [illegible]	.21 113°	.20 112°	.18 [illegible]	.15 117°	.14 152°	

H-plane
30°

Figure X-10. Reflection coefficients for elements in an 11x11 phased array.

11x11 array 5 pulses/aperture

.22 57°	.22 43°	.18 38°	.16 43°	.16 51°	.17 55°	.18 57°	.18 58°	.19 62°	.17 72°	.16 103°	← CENTER ROW
.24 70°	.22 46°	.19 49°	.17 45°	.17 54°	.18 60°	.20 64°	.20 67°	.20 71°	.20 82°	.20 109°	
.22 72°	.22 40°	.18 45°	.16 50°	.15 57°	.16 61°	.17 63°	.17 66°	.17 74°	.17 86°	.18 114°	
.22 [illegible]	.21 43°	.18 36°	.17 40°	.17 47°	.19 51°	.20 53°	.20 54°	.19 56°	.18 67°	.16 100°	
.23 70°	.21 50°	.17 51°	.16 61°	.17 72°	.19 77°	.21 78°	.22 80°	.23 83°	.23 91°	.23 111°	
.14 43°	.18 4°	.17 -11°	.15 -16°	.13 -13°	.12 - 7°	.11 - 2°	.11 1°	.09 4°	.06 17°	.06 150°	

H-plane
50°

Figure M-11. Reflection coefficients for elements in an 11x11 phased array.

APPENDIX N

REFLECTION COEFFICIENT TABULATION: H-PLANE SCANNING WITH RECTANGULAR WAVEGUIDE-FED APERTURES FOR L/W=2.25, L=0.5714λ

3x3 array 7 pulses/aperture

.17 82°	.05 71°	.07 -180°
.29 140°	.26 176°	.37 -175°
.17 82°	.03 71°	.07 -180°

30°

H-plane

.07 0°	.14 -2°	.07 -5°
.16 -169°	.11 -139°	.17 -166°
.07 0°	.14 -2°	.07 -5°

60°

Figure N-1. Reflection coefficients for elements in a 3x3 phased array.

5x5 array 7 pulses/aperture

.42 118°	.37 122°	.39 123°	.37 123°	.33 132°	← CENTER ROW
.33 125°	.25 133°	.27 135°	.24 135°	.23 158°	30°
.15 81°	.07 33°	.05 39°	.06 9°	.10 -91°	

H-plane

.20 139°	.15 136°	.14 142°	.16 140°	.22 142°	← CENTER ROW
.12 158°	.03 141°	.01 157°	.03 153°	.13 163°	60°
.13 -18°	.26 -14°	.28 -14°	.25 -14°	.12 -22°	

Figure N-2. Reflection coefficients for elements in a 5x5 phased array.

7x7 array 7 pulses/aperture

.35 111°	.33 111°	.33 109°	.32 10[illegible]°	.28 106°	.26 107°	.2[illegible] 116°	← CENTER ROW
.36 118°	.30 123°	.33 12[illegible]°	.32 1[illegible]7°	.28 117°	.26 124°	.25 138°	
.32 131°	.25 147°	.29 149°	.28 144°	.26 145°	.24 153°	.28 170°	
.15 84°	.05 68°	.06 103°	.08 91°	.07 76°	.04 63°	.05 -124°	

H-plane
30°

Figure N-3. Reflection coefficients for elements in a 7x7 phased array.

7x7 array 7 pulses/aperture

.18 121°	.17 95°	.15 93°	.15 95°	.16 96°	.18 100°	.20 123°	← CENTER ROW
.18 133°	.11 108°	.08 99°	.07 99°	.09 103°	.12 113°	.19 135°	
.11 167°	.05 -92°	.09 -66°	.10 -65°	.09 -70°	.05 -106°	.13 170°	
.13 -21°	.24 -23°	.28 -29°	.23 -31°	.27 -29°	.23 -25°	.12 -26°	

H-plane
60°

Figure N-4. Reflection coefficients for elements in a 7x7 phased array.

7x7 array 7 pulses/aperture

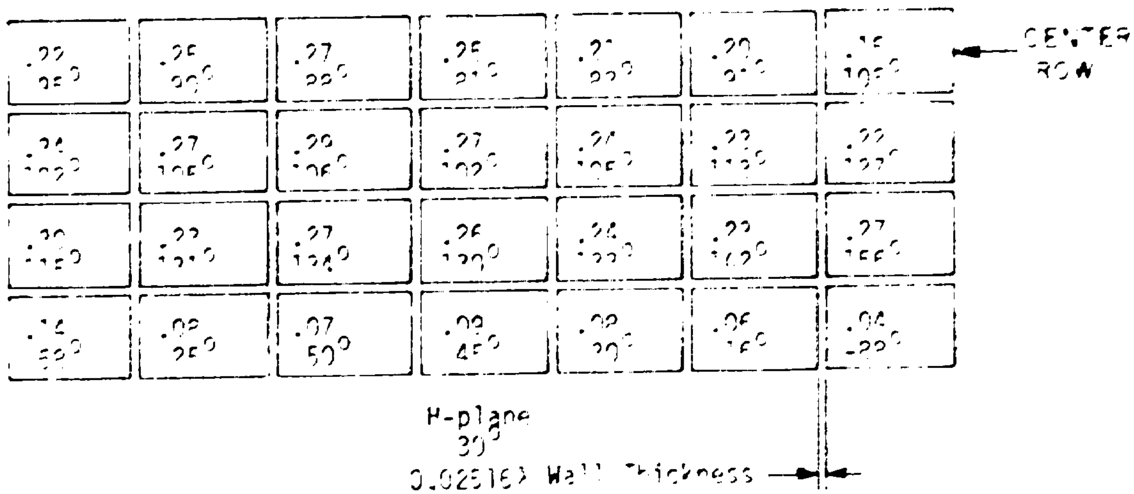

Figure N-5. Reflection coefficients for elements in a 7x7 phased array.

7x7 array 7 pulses/aperture

.20 104°	.19 82°	.16 78°	.14 76°	.13 74°	.14 76°	.16 108°	← CENTER ROW
.20 119°	.13 103°	.09 100°	.07 99°	.07 96°	.10 99°	.17 119°	
.15 158°	.07 -161°	.09 -123°	.10 -112°	.09 -112°	.05 -142°	.12 151°	
.11 -45°	.19 -37°	.22 -43°	.23 -45°	.23 -42°	.22 -35°	.13 -22°	

H-plane
60°
0.02516λ Wall Thickness

Figure N-5. Reflection coefficients for elements in a 7x7 phased array.

9x9 array 7 pulses/aperture

CENTER ROW

.21 114°	.21 118°	.24 122°	.24 117°	.22 116°	.22 117°	.22 115°	.12 114°	.14 151°
.24 113°	.25 118°	.29 122°	.30 117°	.28 116°	.28 116°	.27 114°	.24 115°	.19 136°
.37 116°	.31 126°	.36 129°	.37 124°	.36 123°	.36 122°	.35 120°	.31 124°	.29 136°
.31 128°	.25 145°	.30 146°	.30 140°	.29 139°	.29 138°	.27 135°	.24 143°	.26 165°
.14 83°	.05 52°	.05 89°	.07 78°	.07 69°	.07 64°	.06 52°	.05 23°	.07 -101°

H-plane
30°

Figure N-7. Reflection coefficients for elements in a 9x9 phased array.

9x9 array 7 pulses/aperture

CENTER ROW

.17 121°	.15 75°	.15 63°	.14 60°	.14 60°	.15 62°	.16 66°	.17 77°	.19 118°
.18 120°	.14 88°	.11 75°	.10 70°	.09 70°	.10 73°	.12 79°	.15 91°	.19 119°
.18 130°	.10 124°	.04 148°	.03 -169°	.04 -157°	.04 -176°	.06 148°	.11 128°	.19 132°
.11 173°	.05 -114°	.10 -93°	.13 -91°	.14 -92°	.13 -94°	.10 -100°	.06 -129°	.12 176°
.12 -32°	.23 -25°	.26 -29°	.26 -32°	.26 -33°	.25 -32°	.24 -29°	.22 -25°	.11 -37°

H-plane
60°

Figure N-8. Reflection coefficients of elements in a 9x9 phased array.

11x11 array 5 pulses/aperture

CENTER ROW

.25 114°	.24 121°	.26 120°	.27 120°	.28 131°	.29 130°	.29 126°	.27 125°	.26 126°	.24 122°	.22 148°
.25 112°	.25 115°	.27 122°	.27 121°	.27 122°	.29 122°	.29 118°	.27 116°	.26 116°	.24 110°	.29 132°
.25 100°	.28 110°	.31 114°	.31 110°	.30 100°	.31 111°	.32 100°	.31 106°	.29 105°	.27 108°	.29 110°
.22 115°	.31 120°	.35 123°	.35 118°	.33 118°	.34 121°	.35 119°	.35 116°	.32 115°	.29 110°	.27 122°
.23 125°	.25 142°	.29 145°	.29 141°	.27 142°	.29 144°	.30 141°	.29 138°	.26 139°	.24 156°	.30 155°
.15 81°	.06 55°	.06 88°	.07 82°	.06 84°	.06 95°	.08 90°	.08 73°	.07 66°	.05 49°	.05 -111°

H-plane
30°

Figure N-3. Reflection coefficients for elements in an 11x11 phased array.

11x11 array 5 pulses/aperture

CENTER ROW

.20 110°	.14 70°	.13 46°	.13 36°	.12 32°	.12 32°	.13 34°	.14 38°	.15 45°	.15 66°	.19 106°
.18 108°	.15 74°	.12 59°	.11 50°	.10 46°	.10 46°	.10 48°	.12 52°	.14 60°	.16 73°	.18 106°
.17 112°	.15 89°	.11 90°	.08 97°	.06 105°	.06 109°	.07 106°	.09 99°	.12 93°	.16 92°	.17 113°
.17 133°	.10 122°	.07 140°	.07 167°	.08 -179°	.08 -177°	.08 176°	.08 160°	.09 130°	.12 126°	.10 136°
.13 160°	.05 -125°	.08 -95°	.10 -95°	.11 -98°	.12 -100°	.11 -101°	.09 -106°	.07 -106°	.06 145°	.15 160°
.11 -22°	.22 -22°	.25 -27°	.26 -29°	.27 -30°	.27 -30°	.26 -29°	.26 -27°	.24 -25°	.21 -20°	.10 -21°

H-plane
60°

Figure N-10. Reflection coefficients for elements in an 11x11 phased array.

11x11 array 5 pulses/aperture

CENTER ROW

.32 10°	.24 111°	.27 118°	.28 115°	.28 114°	.28 112°	.27 110°	.26 111°	.25 113°	.22 117°	.22 124°
.30 100°	.22 105°	.25 110°	.26 106°	.25 105°	.25 104°	.25 102°	.23 101°	.22 104°	.21 107°	.18 129°
.31 96°	.23 96°	.25 98°	.27 93°	.26 92°	.26 93°	.26 90°	.25 87°	.23 80°	.21 92°	.15 111°
.35 100°	.28 105°	.32 108°	.32 103°	.30 103°	.31 105°	.32 102°	.30 100°	.27 101°	.26 107°	.24 121°
.30 112°	.28 128°	.27 131°	.27 127°	.27 128°	.28 128°	.27 126°	.26 124°	.24 127°	.23 135°	.26 152°
.14 59°	.08 20°	.36 47°	.08 49°	.08 46°	.08 48°	.09 44°	.09 36°	.08 27°	.03 14°	.05 -88°

H-plane
30°
0.02516λ wall thickness

Figure N-11. Reflection coefficients for elements in an 11x11 phased array with non-zero waveguide wall thickness.

11x11 array 5 pulses/aperture

CENTER ROW

.12 94^0	.09 46^0	.09 20^0	.08 14^0	.07 14^0	.06 16^0	.05 19^0	.06 25^0	.08 39^0	.11 62^0	.18 93^0
.13 97^0	.12 56^0	.10 45^0	.09 43^0	.07 47^0	.06 53^0	.06 54^0	.07 52^0	.09 52^0	.12 62^0	.16 94^0
.16 106^0	.15 78^0	.15 78^0	.13 85^0	.11 94^0	.10 100^0	.10 100^0	.10 91^0	.11 78^0	.13 74^0	.15 102^0
.21 120^0	.16 109^0	.14 111^0	.12 119^0	.12 130^0	.11 138^0	.11 141^0	.10 136^0	.09 122^0	.11 109^0	.18 119^0
.16 148^0	.07 162^0	.05 -159^0	.07 -143^0	.08 -139^0	.10 -138^0	.10 -135^0	.10 -132^0	.09 -135^0	.06 -169^0	.14 149^0
.11 -29^0	.20 -27^0	.22 -34^0	.23 -38^0	.23 -42^0	.23 -44^0	.23 -45^0	.23 -43^0	.22 -39^0	.20 -31^0	.11 -25^0

H-plane
60^0
0.02516 λ Wall Thickness

Figure N-12. Reflection coefficients for elements in an 11x11 phased array with non-zero waveguide wall thickness.

APPENDIX O

COMPUTER PROGRAM

A listing of the fortran computer program used to calculate reflection coefficients for waveguide-fed apertures in a finite phased array is given in this appendix. The input parameters are discussed within the program. The program is set up to analyze a finite array of arbitrary size. The dimensions of the matrices VT, YWG, YHS, PS, CZ, PHAZF, R, T, and YR must be specified for a particular array size. The output consists of the first row of the half-space admittance matrix, the upper right triangle of the self-block $[Y^{wg}]_{1,1}$ of the waveguide admittance matrix, the first row of the total admittance matrix, and the excitation current matrix. The system of equations is then solved and the voltage response (in volts) is printed out in normalized amplitude, amplitude, and phase. Next, the aperture reflection and transmission coefficients are printed out in amplitude and phase. The corresponding incident and reflected fields are also printed out. Also printed out are the aperture admittances.

Sample output is given for a 3x3 phased array of rectangular waveguide-fed apertures with seven pulse bases per aperture (N_y=7) for an E-plane 0° (broadside) scan angle. The reflection coefficient data corresponds to Figure L-1.

```
C***THIS PROGRAM ANALYZES M X N PHASED ARRAYS OF RECTANGULAR WAVEGUIDE
C    -FED APERTURES
C*****DOES E,H, AND QUASI-E-PLANE SCANS
C*****PROGRAM SOLVES FOR THE APERTURE DISTRIBUTION OF PROBE-
C*****FED CAVITY-BACKED SLOT ANTENNAS VIA THE METHOD OF MOMENTS.
C
C*****PROGRAM ALSO CALCULATES REFLECTION COEFFICIENTS FOR RECTANGULAR
C*****WAVEGUIDE-FED APERTURES WITH KNOWN APERTURE DISTRIBUTION.
C
C*****USES PIECEWISE-SINUSOIDAL BASES ALONG THE LENGTH (H-PLANE)
C*****AND UNIFORM BASES ALONG THE WIDTH (E-PLANE) OF APERTURE
C
C*****SUBROUTINES CALLED
C
C       1       SIMPC
C       2       COMPLEX FUNCTION ZMN
C       3       SICI
C       4       ZAPCAL
C       5       ZMNPSD
C       6       CROUT
C       7       VPLIS2
C       8       REFLE2
C       9       ATOEPL
C      10       RRTOPL
C      11       PLTSCL
C
C*****INPUT PARAMETERS
C
C        FREQ     =OPERATING FREQUENCY OF PROBE
C        ZLEN     =APERTURE LENGTH (H-PLANE)
C        YHT      =APERTURE WIDTH (E-PLANE)
C        RLM      =LENGTH OF PROBE
C        D        =DISTANCE FROM PROBE TO APERTURE
C        CB       =DISTANCE FROM PROBE TO BACK WALL
C        ABFACT   =LENGTH TO WIDTH RATIO OF APERTURE
C        MMAX     =# OF SAMPLE POINTS FOR YMN HALF-SPACE CALCULATION
C        NZ       =NUMBER OF CELLS ALONG THE LENGTH (H-PLANE) OF THE APERTURE
C                  (NZ-1 IS THE # OF OVERLAPPING PIECEWISE-SINUSOIDS)
C        NW       =# OF PULSE BASES ALONG THE WIDTH (E-PLANE) OF THE APERTURE
C        KWCA     =# OF WEAK-COUPLED (H-PLANE) APERTURES
C        KSCA     =# OF STRONG-COUPLED (E-PLANE) APERTURES
C          (ARRAY IS OF SIZE KWCA X KSCA)
C        DWCA     =WALL THICKNESS BETWEEN WEAK-COUPLED APERTURES IN CM.
C        DSCA     =WALL THICKNESS BETWEEN STRONG-COUPLED APERTURES IN CM.
C        TESCAN,THSCAN,TEQSCA ARE FOR E,H,AND QUASI-E-PLANE SCANS
C                                =1 IF DESIRED, =0 IF NOT.
C        THETAO    =INITIAL SCAN ANGLE (E,H,OR Q.E.) W.R.T. ARRAY NORMAL
C        THETAF    =FINAL SCAN ANGLE W.R.T. ARRAY NORMAL
C        NSCANS    =NUMBER OF SCAN ANGLES (E,H,OR Q.E.)
C
         OPTIONS 32K,FP
         COMMON /LAB/YWG,YHS,PS,CZ
         COMMON PI,DY,CY,DZ,RLM,D,YHT,ZLEN
         DIMENSION C(71)
         COMPLEX VT(63),YWG(7,7),YHS(21,63),PS(5087),CZ(2107)
```

```
      COMPLEX FRAZE(65),R(9),T(9),YR(9)
      COMPLEX VV
      COMPLEX VA,VB,VC,VD,VTA,VTB,VPA,VPB,EQUALFN
      COMPLEX JCOM,Z0,YC
      CALL LABEL(5)
      CALL ASSIGN(EHALVU02,0,0,6)
      CALL DEASSG
      IREAD=0
      K1=1
      ABFACT=2.25
C****YHT,ZLEN,RLM,DX,DY,DZ,CH,ETC ALL IN CENTIMETERS****
      DO 116 ITE=1,NT
      IREAD=IREAD+1
      ZLEN=7.21
      YHT=ZLEN/ABFACT
      RLM=2.50
      CH=1.587
      DX=ZLEN
      DY=2*CH
      DZ=2.*YHT
      E=10.78
      PI=3.1415926
      TP=2.*PI
      JCOM=(0.,1.)
      FREQ=2.376E9
      KMAX=71
      NW=7
      NZ=2
      ETA=376.73
      RLAMDA=2.997925E+10/FREQ
      YL=YHT/RLAMDA
      ZL=ZLEN/RLAMDA
      IF(IREAD.GT.1) GO TO 444
      KWCA=3
      KSCA=3
      NUMAPE=KWCA*KSCA
      DWCA=0.0
      DSCA=0.0
      DWCA=DWCA/RLAMDA
      DSCA=DSCA/RLAMDA
      IESCAN=1
      IHSCAN=0
      IEHSCA=0
      THETAU=0.
      THETAE=0.
      NSCANS=1
333   CONTINUE
444   CONTINUE
      NZS=NZ-1
      MODES=NW*(NZ-1)
      KAW=KWCA-1
      KAS=KSCA-1
      MODESS=MODES*NUMAPE
C*****CALCULATE FIRST ROW OF Y MATRIX
      MODI=MODES*KWCA
```

```
      CALL ZAPCAL(KWCA,KSCA,MODT,MODESS,DWCA,DSCA,YL,ZL,NW,NZ,NMAX
     &,YHS)
C
C*****FILL THE HALF-SPACE ADMITTANCE MATRIX
C
      IDMB=KSCA*NW
      NSIZE=KWCA*IDMB
      IBLT=0
      IF(KWCA.GT.1)IBLT=1
      IF(IBLT.EQ.1)GO TO 7595
C*****FILL IN THE FIRST BLOCK (Y11) OF Y MATRIX
      DO 1 I=2,MODESS
      DO 1 J=I,MODESS
      K=1+J-I
      YHS(I,J)=YHS(1,K)
1     CONTINUE
C
7595  IF(DSCA.EQ.0.AND.KWCA.GT.1)CALL ATOEPL(IBLT,KWCA,IDMB,NSIZE,YHS)
      IF(DSCA.NE.0.)CALL HPTCPL(DSCA,NW,IDMB,KWCA,NSIZE,YHS)
9903  CONTINUE
      KCUR=(NZ-1)*NW
      IF(KWCA.GT.1) CCSPAZ=DWCA*ZL
      IF(KSCA.GT.1) CCSPAY=DSCA*YL
      IF(KSCA.GT.1) WRITE(6,9449)CCSPAY
9449  FORMAT(' CENT TO CENT E-PLANE SPACING=',F10.4,2X,'WAVLGTHS')
      IF(KWCA.GT.1) WRITE(6,9389)CCSPAZ
9389  FORMAT(' CENT TO CENT H-PLANE SPACING=',F10.4,2X,'WAVLGTHS')
      WRITE(6,1001)
1001  FORMAT(/,' ***PIECEWISE SINUSOIDAL-UNIFORM EXPANSIONS ***')
      WRITE(6,3422)
 3422 FORMAT(10X,'...PROGRAM FARRAY...BY ALAN FENN...')
      WRITE(6,124) NMAX,FREQ,AHFACT
      WRITE(6,1452) YL,ZL,NW,NZ
      WRITE(6,4511)
4511  FORMAT(' **FIRST ROW OF HALF-SPACE ADMITTANCE MATRIX (MHOS)',/)
      LLM=1
      DO 2239 LLM=1,1
      DO 2239 LL=LLM,MODESS
      WRITE(6,3772) LLM,LL,YHS(LLM,LL)
3772  FORMAT(' YHS(',I1,',',I3,')=',2E12.5)
2239  CONTINUE
      WRITE(6,3975)
3975  FORMAT(/)
      CALL ZAPER2(DX,BLANDA,YHT,ZLEN,MODES,NW,YWG)
      WRITE(6,4512)
4512  FORMAT(' **SELF BLOCK (Y11) OF WAVEGUIDE-ADMITTANCE MATRIX
     2(MHOS)',/)
      DO 21 LLM=1,MODES
      DO 21 LL=LLM,MODES
      WRITE(6,3734) LLM,LL,YWG(LLM,LL)
3734  FORMAT(' YWG(',I1,',',I1,')=',2E12.5)
21    CONTINUE
      WRITE(6,2222)
2222  FORMAT(/)
C*****FILL THE TOTAL ADMITTANCE MATRIX
```

```
      DO 7356 I=1,KSCA
      DO 795 IMJ=1,MODES
      DO 795 JMJ=1,MODES
      IIMJ=(I-1)*MODES+IMJ
      JJMJ=(I-1)*MODES+JMJ
      YHS(IIMJ,JJMJ)=YWG(IMJ,JMJ)+YHS(IIMJ,JJMJ)
795   CONTINUE
7356  CONTINUE
      WRITE(6,4513)
4513  FORMAT(' **FIRST ROW OF TOTAL ADMITTANCE MATRIX (MHOS)',/)
      I=1
      DO 7395 I=1,1
      DO 7395 J=1,MODESS
      WRITE(6,2665)I,J,YHS(I,J)
2665  FORMAT(' Y(',I1,',',I3,')=',2E12.5)
7395  CONTINUE
      DO 57 I=1,IDMR
      DO 57 J=1,MODESS
      ICO=(J-1)*IDMR+I
      CZ(ICO)=YHS(I,J)
57    CONTINUE
      ICOUNT=0
      DO 9999 IS=1,3
      IF(IS.LT.3) GO TO 9000
9000  DO 6565 NSCA=1,NSCANS
4554  WRITE(6,5555)
5555  FORMAT(/)
      IF(NSCANS.EQ.1) GO TO 7917
      THETAS=((THETAF-THETAO)/(NSCANS-1))*(NSCA-1)+THETAO
7917  IF(NSCANS.EQ.1) THETAS=THETAO
      SIZE=ZLEN/RLAMDA
      NMOD=1
      IF(SIZE.GE.1.5)NMOD=2
      DO 7521 ISS=1,NMOD
      IDOM=1+2*(ISS-1)
      IF(KWLD.LT.1.OR.KSCA.GT.1) WRITE(6,9191) THETAS
9191  FORMAT(' SCAN ANGLE IN DEGREES (W.R.T. ARRAY NORMAL)=',F10.5)
C     WRITE(6,918)
918   FORMAT(/,5X,'ADMITTANCE MATRIX (FIRST ROW)',/)
C     WRITE(6,920)(J,Z(1,J),J=1,MODESS)
920   FORMAT('I=1',3X,'J=',I4,3X,'Z(1,J)=',2E12.5)
C
C*****THIS PART FINDS THE CURRENT EXCITATION MATRIX***
C
      THERAD=THETAS*PI/180.
      PHI=0.0
      WRITE(6,923)IDOM
923   FORMAT(/,' EXCITATION MATRIX (AMPS)',2X,'TE',I1,'0',2X,'MODE',/)
      IF(IESCAN.EQ.0.AND.IS.EQ.1) GO TO 9999
      IF(IS.EQ.3) GO TO 9344
      IF(IS.EQ.2) GO TO 9343
      WRITE(6,9243)
9243  FORMAT('  ******E-PLANE SCAN*******')
      DSEP=DSCA*YL
      CALL VPOIS2(IDOM,RLAMDA,MODES,NW,NZS,VT)
```

```
      PHAZF(1)=(1.,0.)
      NALFP=0
      DO 8775 JK=1,KWCA
      DO 8775 IK=1,KSCA
      NALFP=NALFP+1
      ALPHAN=-2.*PI*(IK-1)*DSEP*SIN(THERAD)
      IF(IK.EQ.2.AND.JK.EQ.1)ALPHDF=ALPHAN/(IK-1)*180./PI
      IF(IK.EQ.2.AND.JK.EQ.1) WRITE(6,9393) ALPHDF
      EJALFN=CEXP(JCOM*ALPHAN)
      PHAZF(NALFP)=EJALFN
      NMOL=1+(IK-1)*MODES+(JK-1)*MODES*KSCA
      NMOU=NMOL+NW-1
      IFCV=0
      DO 7202 IMAT=NMOL,NMOU
      IFCV=IFCV+1
      VT(IMAT)=VT(IFCV)*EJALFN
7202  CONTINUE
8775  CONTINUE
      GO TO 1133
9343  CONTINUE
      IF(IHSCAN.EQ.0) GO TO 9999
      WRITE(6,9244)
9244  FORMAT('  *****H-PLANE SCAN*****')
      DSEP=DWCA+ZL
      CALL VPOIS2(IDOM,KLAMDA,MODES,NW,NZS,VT)
      PHAZF(1)=(1.,0.)
      NALFP=0
      DO 8776 JK=1,KWCA
      DO 8776 IK=1,KSCA
      NALFP=NALFP+1
      ALPHAN=-2.*PI*(JK-1)*DSEP*SIN(THERAD)
      IF(JK.EQ.2.AND.IK.EQ.1)ALPHDF=ALPHAN/(JK-1)*180./PI
      IF(JK.EQ.2.AND.IK.EQ.1)WRITE(6,9393)ALPHDF
4219  EJALFN=CEXP(JCOM*ALPHAN)
      PHAZF(NALFP)=EJALFN
      NMOL=1+(IK-1)*MODES+(JK-1)*MODES*KSCA
      NMOU=NMOL+NW-1
      IFCV=0
      DO 7203 IMAT=NMOL,NMOU
      IFCV=IFCV+1
      VT(IMAT)=VT(IFCV)*EJALFN
7203  CONTINUE
8776  CONTINUE
      GO TO 1133
9344  CONTINUE
      IF(IEQSCA.EQ.0) GO TO 9999
      WRITE(6,9245)
9245  FORMAT('  ****QUASI-E PLANE SCAN****')
      DSEP=DSCA+YL
      CALL VPOIS2(IDOM,KLAMDA,MODES,NW,NZS,VT)
      PHAZF(1)=(1.,0.)
      NALFP=0
      DO 8777 JK=1,KWCA
      DO 8777 IK=1,KSCA
      NALFP=NALFP+1
```

```
      ALPHAN=-2.*PI*(IK-1)*DSEP*SIN(THERAD)
      IF(IK.  .2.AND.UK.EQ.1)ALPHDF=(ALPHAN/(IK-1))*180./PI
      IF(IK.  .2.AND.UK.EQ.1) WRITE(6,9393) ALPHDF
9393  FORMAT(/,  PHASE SHIFT (IN DEGREES) BETWEEN  ELEMENTS=',F10.5,/)
      EQALEG=CEXP(UCOM*(ALPHAN+(UK-1)*PI))
      PHSZE(  ALEE)=EQALEE
      NVEL=1+(IK-1)*MODES+(UK-1)*MODES*KSCA
      NMOD=MODE+K-1
      IFCV=0
      DO 7261 INAI=NMOD, NEL
      IFCV=IFCV+1
      VI(INAI)=VI(IFCV)*EQALEA
7261  CONTINUE
9777  CONTINUE
1155  IF(KSCA.EQ.1.AND.NSCA.EQ.1) GO TO 9771
      ICUR=0
9219  VCMOR=0.0
      DO 4000 IV=1,MODESS
      VVA=CABS(VI(IV))
      IF(VVA.GT.VCMOR)VCMOR=VVA
4000  CONTINUE
      IF(VCMOR.LE.0) VCMOR=1.
      DO 4444 IV=1,MODESS
      VV=VI(IV)
      VVA=CABS(VV)
      VSCOR=VVA/VCMOR
      VPH=0.0
      IF(VVA.GT.0) VPH=57.29578*ATAN2(AIMAG(VV),REAL(VV))
      WRITE(6,2540)IV,VSCOR,VVA,VPH
2540  FORMAT(1X,115,1F10.5,1F15.7,1F10.6)
4444  CONTINUE
      IF(ICUR.EQ.1) GO TO 7971
9771  CONTINUE
      IUM=NUMAPE*EV
      ICC=IUM
      ISYM=0
      IWR=0
      I12=1
      IF(IGO ,EQ.3)I12=2
      IF(NSCA.GT.1) I12=2
      N=MODESS
      IENTRY=4
      ICOUNT=ICOUNT+1
      IF(ICOUNT.GT.1) IENTRY=3
      IF(NUMAPE.EQ.1) GO TO 3589
      IF(KKCA.GE.3)CALL GETSOL(CZ,VI,PS,KKC ,IOMB,IENTY)
3589  IF(NUMAPE.EQ.1) CALL CROUT(YDS,VI,ICC,ISYM,IWR,I12,N)
      NCUR=NW*(I2-1)
      IF(KSCA.GT.1.OR.KKCA.GT.1) NCUR=MODESS
      WRITE(6,1695)
1695  FORMAT(/,' ********************************************')
      WRITE(6,450)IHOM
450   FORMAT(/,' VOLTAGE MATRIX (RESPONSE)',2X,'TE',I1,'0',2X,'MODE')
      IF(NUMAPE.EQ.1) GO TO 7971
      ICUR=1
```

```
      GO TO 9219
7971  CONTINUE
C     GO TO 2000
C
C****THIS PART FILES THE REFLECTION COEFFICIENTS
C
      CALL REFLE2(IS,KWCA,KSCA,IDOM,VT,MODESS,NW,NZS,RLAMDA,NUMAPE,
     2PHAZE,3,1)
C     WRITE(6,449)IDOM
449   FORMAT(/,'REFLECTION COEFFICIENTS',2X,'TE',I1,'0',2X,'MODE',/)
C     DO 448 I=1,NUMAPE
C     WRITE(6,76)I,R(I)
76    FORMAT('APERTURE',2X,I4,3X,'REFLECTION COEFFICIENT=',2E15.6)
448   CONTINUE
C
C****THIS PART FILES THE APERTURE ADMITTANCES
C
      WRITE(6,3037)
3037  FORMAT(/,' APERTURE ADMITTANCES (MHOS)',/)
      CLIGHT=2.997925E+10
      FREQC=CLIGHT/(2.*DX)
      IF(FREQ.GT.FREQC)Z0=CMPLX(ETA/SQRT(1.-(FREQC/FREQ)**2),0.)
      IF(FREQ.LT.FREQC)Z0=CMPLX(0.,ETA/SQRT((FREQC/FREQ)**2-1.))
      Y0=1./Z0
      WRITE(6,7898)Y0
7898  FORMAT(' Y0=',2X,2E12.5)
      DO 2797 IY=1,NUMAPE
      YR(IY)=Y0*(1.-R(IY))/(1.+R(IY))
      WRITE(6,772)IY,YR(IY)
772   FORMAT(' APERTURE',I4,3X,'APERTURE ADMITTANCE=',2E12.5)
2797  CONTINUE
7521  CONTINUE
2000  WRITE(6,124) NMAX,FREQ,ABFACT
124   FORMAT(/,' NMAX=',I4,3X,'FREQUENCY=',E12.5,3X,'(A/B)=',F10.3,/)
      WRITE(6,1432) YL,ZL,NW,NZ
1432  FORMAT(' YL=',F7.4,' WAVLGTHS',3X,'ZL=',F7.4,' WAVLGTHS',3X,
     23X,'NW=',I4,3X,'NZ=',I4,/)
      IF(KAW.EQ.0.AND.KAS.EQ.0) WRITE(6,4278)
4278  FORMAT('ONE APERTURE...NO MUTUAL COUPLING')
      IF(KAW.GT.0) WRITE(6,4279) KWCA,DWCA
4279  FORMAT(' # OF WEAK-COUPLED APERTURES=',I4,3X,
     2'DWCA=',F10.5,' WAVLGHTS')
      IF(KAS.GT.0) WRITE(6,4280) KSCA,DSCA
4280  FORMAT(' # OF STRONG-COUPLED APERTURES=',I4,3X,
     2'DSCA=',F10.5,' WAVLGHTS',/)
      IF(NSCANS.EQ.0) GO TO 112
6565  CONTINUE
6969  CONTINUE
112   CONTINUE
      CLOSE 6
 69   CALL EXIT
      END
      SUBROUTINE ZAPER2(DXR,RLAMDA,YHT,ZLEN,MODES,NW,Z)
      COMPLEX Z(MODES,MODES),ZDIF,ZSUM
      PHI1=ASIN(RLAMDA/(2.*DXR))*180./3.14159265
```

```
      WRITE(6,432)PHI1
432   FORMAT(' PHI1=',F8.4,2X,'DEGREES',/)
      DZR=YHT
      H=YHT/NW
      DO 7 K=1,MODES
      DO 7 L=K,MODES
      ZPDIF=H*(L-K)
      ZPSUM=H*(K+L-1)
      MCENTR=(MODES+1)/2
      ISPACE=1
      IF(L.NE.MCENTR)ISPACE=2
      SPACE=DZR*ISPACE
      CALL ZPOIS2(MODES,NW,ISPACE,SPACE,RLAMDA,ZPDIF,ZDIF)
      IF(ISPACE.EQ.1) GO TO 71
      CALL ZPOIS2(MODES,NW,ISPACE,SPACE,RLAMDA,ZPSUM,ZSUM)
      Z(K,L)=2.*(ZDIF+ZSUM)
71    IF(ISPACE.EQ.1) Z(K,L)=2.*ZDIF
7     CONTINUE
      DO 25 K=1,MODES
      DO 25 L=K,MODES
      Z(L,K)=Z(K,L)
25    CONTINUE
      RETURN
      END
      SUBROUTINE ZPOIS2(MODES,NW,ISPACE,DZR,RLAMDA,ZP,Z)
      COMMON PI,DX,DY,DZ,RLMID,YHT,ZLEN
      COMPLEX J,PZ1,SZ1,XEXP,P,SUM1,SUM2,TERM2,Z
      COMPLEX ZEXP
      J=(0.,1.)
      ETA=376.73
      B=2.*PI/RLAMDA
      DXR=DX
      H=YHT/NW
      RHL=ZLEN/2.
      XP=0.0
      CONST=1./(2.*B**4*ETA*DXR*DZR*(YHT/NW)**2*(SIN(B*RHL)**2))
      Z=(0.,0.)
      SUM1=(0.,0.)
C
C***SEARCH FOR POSSIBLE N1'S****
C
      DO 13 NM=1,11
      N1=NM-1
46    CONTINUE
      ZEXP=CEXP(-J*B*ZP*N1*RLAMDA/DZR)
      PZ1=(4.,0.)
      IF(N1.EQ.0)GO TO 77
      PZ2=SIN(B*H/2.*N1*RLAMDA/DZR)/(N1*RLAMDA/DZR)
77    IF(N1.EQ.0)PZ2=B*H/2.
      SUM2=(0.,0.)
C
C***SEARCH FOR POSSIBLE N2'S****
C
      ITEST2=0
      DO 14 NN=1,201
```

```
      N2=NN-1
 47   CONTINUE
      Q21=1.-(N1*RLAMDA/DZR)**2-((N2+.5)*RLAMDA/DXR)**2
      IF(Q21.GT.0.)S21=CMPLX(SQRT(Q21),0.)
      IF(Q21.LT.0.)S21=-J*SQRT(ABS(Q21))
      PX=(COS(B*RHL*RLAMDA/DXR*(N2+.5))-COS(B*RHL))
      XEXP=CEXP(-J*B*XP*RLAMDA/DXR*(N2+.5))
      P=PZ1*PZ2*PX
      DENOM=1.-(RLAMDA/DXR*(N2+.5))**2
      TERM2=(P**2)/S21*XEXP/DENOM*ZEXP
C     WRITE(6,-)TERM2,N1,N2
      IF(CABS(TERM2).LT.CABS(0.001*SUM2))ITEST2=ITEST2+1
      IF(ITEST2.EQ.12) GO TO 80
      SUM2=SUM2+TERM2
      IF(N2.LE.0) GO TO 14
      N2=-N2
      GO TO 47
 14   CONTINUE
 80   SUM1=SUM1+SUM2
      IF(N1.LE.0) GO TO 13
      N1=-N1
      GO TO 46
 13   CONTINUE
 15   IF(CABS(SUM1).EQ.0.)SUM1=SUM2
      Z=CONST*SUM1
      RETURN
      END
      SUBROUTINE REFLEF(IS,KWCA,KSCA,IDOM,VT,MODESS,NW,NZS,RLAMDA,
     2NUMAPE,PHZ,T,R)
      COMMON PI,DX,DY,DZ,RLM,D,YHT,ZLEN
      COMPLEX XEXP,S21,ARGY,J,SUM1,SUM2,TERM2,PHZ(NUMAPE),T(NUMAPE)
      COMPLEX VT(MODESS),PSUM,YSUM,F4,CUMPI,HXI,HIMAGE,HXR,R(NUMAPE),P2
      J=(0.,1.)
      B=2.*PI/RLAMDA
      ETA=376.73
      MODES=NW*NZS
      JKL=2
      DO 57 K12=1,KWCA
      DO 57 KKL=1,KSCA
      XO=0.
      YO1=-D/4.-(JKL-1)*D/4.
      YO2=-3.*D/4.+(JKL-1)*D/4.
      ZO=YHT/2.
      DXR=DX
      DZR=YHT
      H=YHT/NW
      HL=ZLEN/(NZS+1)
      CONST1=-1.*100./(B*DX*DZ)
      CONST2=-1.*100./(2.*ETA*(B**2)*DXR*DZR)*2.
C
C****CALCULATE INCIDENT AND IMAGE FIELDS
C
      HXI=(0.,0.)
      HIMAGE=(0.,0.)
      SUM1=(0.,0.)
```

```
      DO 273 MM=1,2
      M=MM-1
      P1=1.-COS(B*RLM)
      EJMPI=CEXP(J*M*PI)
      IF(IDOM.EQ.1) N2=0
      IF(IDOM.EQ.3) N2=1
      Q21=1.-((N2+.5)*RLAMDA/DX)**2
      IF(Q21.GE.0.)S21=CMPLX(SQRT(Q21),0.)
      IF(Q21.LT.0.)S21=-J*SQRT(ABS(Q21))
      ARGY=J*B*(P*DY-YDI)*S21
      EYBS=CEXP(-ARGY)
      TERM2=F1*EJMPI*EYBS*2.
      SUM1=SUM1+TERM2
273   CONTINUE
      NNAP=KKL+(K12-1)*KSCA
      HXI=SUM1*CONST1*PHZ(NNAP)
C
C****CALCULATE REFLECTED FIELD
C
      F2=B*D/2.
      F1=4./(YBT/BW*SIN(B*HL))
      SUM2=(0.,0.)
      F3=(COS(B*HL*(N2+.5)*RLAMDA/DXR)-COS(B*HL))/1.
      PSUM=(0.,0.)
      KN=0
      JLOW=1+MODES*(KKL-1)+(K12-1)*MODES*KSCA
      JUP=JLOW+MODES-1
      DO 771 JN=JLOW,JUP
      KN=1
      X2F=-ZLEF/2.+KN*HL
      F4=VT(JN)*COS(B*(N2+.5)*X2F*RLAMDA/DXR)
      PSUM=PSUM+F4
771   CONTINUE
      P2=F1*F2*F3*PSUM
      Q21=1.-((N2+.5)*RLAMDA/DXR)**2
      IF(Q21.GE.0.)S21=CMPLX(SQRT(Q21),0.)
      IF(Q21.LT.0.)S21=-J*SQRT(ABS(Q21))
      ARGY=-J*B*YDR*S21
      EYBS=CEXP(-ARGY)/S21
      TERM2=P2*EYBS*2.
      SUM2=SUM2+TERM2
      HXR=SUM2*CONST2
      DIF=ABS(YDR-YDT)
      HIMAGE=HXI*CEXP(-2.*J*B*(4-JKL)*D/4.*S21)
      IF(DIF.GT.0.1)GO TO 299
C****CALCULATE VOLTAGE REFL COEFF (MINUS SIGN NEEDED TO CONVERT)
      R(NNAP)=-CEXP(2.*J*B*D/2.*S21)*(HXR+HIMAGE)/HXI
      T(NNAP)=1.+R(NNAP)
      MZMID=(KKCA+1)/2
      MYMID=(KSCA+1)/2
      IF(IS.EQ.2.AND.KKL.GT.MYMID) GO TO 57
      IF(IS.NE.2.AND.K12.GT.MZMID) GO TO 57
      WRITE(6,5571)NNAP
5571  FORMAT(' APERTURE',2X,I3)
      WRITE(6,299)R(NNAP),IDOM
```

```
2244  FORMAT(' REFL COEF=',2F12.5,3X,'TE',I1,'0',2X,'MODE')
      REFMAG=CABS(R(NNAP))
      REFPHA=ATAN2(AIMAG(R(NNAP)),REAL(R(NNAP)))*180./PI
      WRITE(6,7174)REFMAG,REFPHA
7174  FORMAT(' MAGNITUDE REFL COEF=',F8.5,3X,'PHASE REFL COEF=',
     &F8.1,3X,'DEGREES')
      TMAG=CABS(T(NNAP))
      TPHA=ATAN2(AIMAG(T(NNAP)),REAL(T(NNAP)))*180./PI
      WRITE(6,7654)TMAG,TPHA
7654  FORMAT(' TRANSMISSION COEF=',F12.5,3X,F8.1,2X,'DEGS')
999   HXIMAG=CABS(HXI)
      HXIPHA=ATAN2(AIMAG(HXI),REAL(HXI))*180./PI
      HXRMAG=CABS(HXR)
      HXRPHA=ATAN2(AIMAG(HXR),REAL(HXR))*180./PI
      HIMGMA=CABS(HIMAGE)
      HIMGPH=ATAN2(AIMAG(HIMAGE),REAL(HIMAGE))*180./PI
      WRITE(6,5772)HIMGMA,HIMGPH
5772  FORMAT(' HIMAGE MAG=',F11.5,3X,'HIMAGE PHASE=',3X,
     &F10.4,1X,'DEGREES')
      WRITE(6,5777)HXRMAG,HXRPHA
5777  FORMAT(' HXR MAG=',F14.5,3X,'HXR PHASE=',F15.4,3X,'DEGREES')
      WRITE(6,5766)HXIMAG,HXIPHA
5766  FORMAT(' HXI MAG=',F14.5,3X,'HXI PHASE=',F15.4,3X,'DEGREES')
      WRITE(6,5421)
5421  FORMAT(' ***********************************************')
57    CONTINUE
      RETURN
      END
C****CALCULATES EXCITATION MATRIX IN CLOSED FORM
      SUBROUTINE VEQIS2(IDOM,RLAMDA,MODES,NW,NZS,VT)
      COMMON PI,EPS,DYI,DZI,PLMU,DYHI,ZLEG
      COMPLEX CTPS,YFAC1,YFAC2,SZ1,ARGY1,ARGY2,VT(MODES),J,PHZFAC
      COMPLEX SUM1,SUM2,TERM1,TERM2,SS
      B=YHI/2.
      E=2.*PI/RLAMDA
      DL=ZLEG/(NZS+1)
      J=(0.,1.)
      DXR=DXI
      DZR=YHI
      CONST1=-1./(E*DXI*DZI)
      CONST2=4./(YHI/NW*E**2*SIN(E*DL))
      DO 5 I=1,NZS
      DO 5 JJ=1,NW
      SUM1=(0.,0.)
C
C****SEARCH FOR POSSIBLE N1'S
C
      N1=0
      F1=2.*(COS(2.*PI*N1*RLM/DZ1)-COS(E*DL))/(1.-(N1*RLAMDA/DZ1)**2)
      PHZFAC=CEXP(J*PI*DZ2*N1*RLAMDA/DZ1)
      IF (N1.EQ.0) GO TO 7
      SIGAXX=SIN(PI*DZ2*N1*RLAMDA/DZ1)/(N1*RLAMDA/DZ1)
7     SIGAXX=PI*DZ2
      TERM1=F1*PHZFAC*SIGAXX*CONST1*CONST2
      SUM2=(0.,0.)
```

```
C
C****SEARCH FOR POSSIBLE N2'S
C
      IF(IOOP.EQ.1) N2=0
      IF(IOOP.EQ.5) N2=1
      PX=COS(B*HL*RLAMDA/DXI*(N2+.5))-COS(B*HL)
      PX=PX/(1.-(RLAMDA/DXI*(N2+.5))**2)
      XP=-ZLEN/2.+HL*I
      XEXP=COS(B*XP*RLAMDA/DXI*(N2+.5))
      Q21=1.-(N1*RLAMDA/DZI)**2-((N2+.5)*RLAMDA/DXI)**2
      IF(Q21.GT.0.0) S21=CMPLX(SQRT(Q21),0.)
      IF(Q21.LE.0.0) S21=-J*SQRT(ABS(Q21))
      ARGY1=J*B*D*S21
      YFAC1=CEXP(-ARGY1)
      ARGY2=J*B*DYI*S21
      YFAC2=1.-CEXP(-ARGY2)
      TERM2=TERM1*PX*XEXP*YFAC1*YFAC2*2.
88    SUM1=SUM1+TERM2
      VT(JJ)=SUM1
3     CONTINUE
      CNOR=0.
      DO 40 K=1,MODES
      SA=CABS(VT(K))
      IF(SA.GT.CNOR)CNOR=SA
40    CONTINUE
      IF(CNOR.LE.0.)CNOR=1.
      DO 44 K=1,MODES
      SS=VT(K)
      SA=CABS(SS)
      SNOR=SA/CNOR
      PHR=0.
      IF(SA.GT.0.)PHR=ATAN2(AIMAG(SS),REAL(SS))
      PH=57.29578*PHR
      WRITE(6,2)K,SNOR,SA,PH
2     FORMAT(1X,I15,1F10.6,3X,1E15.5,1F10.0)
44    CONTINUE
      DO 4921 K=1,MODES
      WRITE(6,1212)K,VT(K)
1212  FORMAT(' I(',I2,')=',1X,2E15.5)
4921  CONTINUE
      RETURN
      END
C     SUBROUTINE TOEPL
C
C     PROGRAM BY ALAN FENN...OSU-ESL.....
C
      SUBROUTINE TOEPL(IBLT,ND,IDMB,IDM,Z)
C     PURPOSE
C        TO FILL THE FIRST BLOCK ROW OR THE UPPER RIGHT TRIANGLE OF
C        A BLOCK TOEPLITZ MATRIX, FROM KNOWLEDGE OF THE ELEMENTS
C        OF ONLY THE FIRST ROW.
C     REMARKS
C
C     DESCRIPTION OF PARAMETERS
C        IBLT= 1   IF WANT TO FILL FIRST BLOCK ROW (BLTSOL)
```

```
C              0  IF WANT TO FILL UPPER RIGHT TRIANGLE (CROUT)
C         NB     =NUMBER OF BLOCKS IN FIRST "BLOCK ROW".
C                 (NOTE: A "BLOCK ROW" IS A ROW OF TWO OR MORE
C                 TOEPLITZ MATRICES)
C         IDMB   =DIMENSION OF ONE BLOCK.
C         IDM    =DIMENSION OF THE ENTIRE MATRIX.
C         Z      =THE MATRIX TO BE FILLED. (NOTE: UPON ENTERING THE
C                 SUBROUTINE THE FIRST ROW OF Z MUST BE SPECIFIED)
C
C
      COMPLEX Z(IDMB,IDM)
      ND=IDMB
C
C     FILL FIRST BLOCK
C
      DO 1 I=2,ND
      DO 1 J=I,ND
      K=1+J-I
      Z(I,J)=Z(1,K)
1     CONTINUE
      IF(IBLT.EQ.0) GO TO 77
      DO 4 I=1,ND
      DO 4 J=I,ND
      Z(J,I)=Z(I,J)
4     CONTINUE
C
C     FILL REMAINING BLOCKS IN FIRST "BLOCK ROW"
C
77    NUMBL=NB-1
C     FILL UPPER HALF OF EACH BLOCK (FIRST "BLOCK ROW")
      DO 2 IT=1,NUMBL
      NCELM=ND*IT
      IUST=0
      DO 3 IE=2,ND
      IIN=IE+NCELM
      IUST=IUST+1
      NAD=IIN+(ND-1)-IUST
      DO 3 JE=IIN,NAD
      KE=1+JE-IE
      Z(IE,JE)=Z(1,KE)
3     CONTINUE
2     CONTINUE
C
C     FILL LOWER HALF OF EACH BLOCK (FIRST "BLOCK ROW")
      NUOS=ND
      NUMA=NB-1
      DO 10 NTUR=1,NUMA
      NBA=ND-1
      DO 95 NIP=1,NBA
      NTIM=ND-NIP
      DO 11 NTWOT=1,NTIM
      NRSJ=ND*NTUR+NTWOT
      NRSI=NTWOT+NIP
      NLSJ=NRSJ+NIP
      NLSI=NTWOT
```

```
      Z(NRSI,NRSJ)=Z(NLSI,NLSJ)
11    CONTINUE
95    CONTINUE
10    CONTINUE
C     IBLT=0
      IF(IBLT.EQ.1) GO TO 27
C
C     FILL REMAINING BLOCKS OF MATRIX
C
      IARD=0
      LML=IDMB+1
      LMU=IDMB*NB
      DO 66 IAL=LML,LMU
      IARD=IARD+1
      DO 66 JAL=IAL,LMU
      KAL=IARD+JAL-IAL
66    Z(IAL,JAL)=Z(IARD,KAL)
27    RETURN
      END
C     SUBROUTINE BBTOPL
C
C     PROGRAM BY ALAN FENN...OSU-ESL
      SUBROUTINE BBTOPL(NB,IDMB,IDM,NBB,IDMBB,Z)
C        TO FILL THE FIRST DOUBLE-BLOCK ROW OF A DOUBLE-BLOCK TOEPLITZ
C        MATRIX.
C     GIVEN
C        ELEMENTS IN THE FIRST BLOCK ROW OF EACH BLOCK IN THE FIRST
C        DOUBLE-BLOCK ROW.
C     DEFINITIONS
C        A DOUBLE-BLOCK TOEPLITZ MATRIX IS A BLOCK TOEPLITZ MATRIX
C        CONSISTING OF SUB-MATRICES (BLOCKS) WHICH ARE BLOCK TOEPLITZ
C     DESCRIPTION OF PARAMETERS
C        NB     -NUMBER OF BLOCKS IN THE SUB-MATRICES (BLOCK TOEPLITZ)
C        IDMB   -DIMENSION OF THE BLOCKS IN THE SUB-MATRICES (BLOCK
C                TOEPLITZ)
C        IDM    -DIMENSIONS OF THE SUB-MATRICES (BLOCK TOEPLITZ)
C        NBB    -NUMBER OF BLOCKS IN DOUBLE-BLOCK TOEPLITZ MATRIX
C        IDMBB  -DIMENSION OF THE DOUBLE-BLOCK TOEPLITZ MATRIX
C         Z     -THE MATRIX TO BE FILLED    (NOTE: UPON ENTERING THE
C                SUBROUTINE THE FIRST BLOCK ROW OF EACH BLOCK IN THE
C                FIRST DOUBLE-BLOCK ROW OF Z MUST BE SPECIFIED)
C               THAT IS, INITIALLY Z WILL HAVE DIMENSIONS (IDMB,IDMBB).
C               UPON LEAVING THE SUBROUTINE Z WILL HAVE THE NEW
C               DIMENSIONS (IDM,IDMBB)
       COMPLEX Z(IDM,IDMBB)
       NU=IDMB*NB
C     FILL UPPER RIGHT TRIANGLE OF EACH BLOCK TOEPLITZ MATRIX
       DO 77 M=1,NBB
       IARD=0
       LML=IDMB+1
       LMU=NU
       DO 66 IAL=LML,LMU
       IARD=IARD+1
       IALF=IAL+NU*(M-1)
       LMUF=LMU+NU*(M-1)
```

```
      DO 66 JAL=IALF,LMUF
      KAL=IARD+JAL-IAL
      Z(IAL,JAL)=Z(IARD,KAL)
66    CONTINUE
C     FILL LOWER RIGHT TRIANGLE OF EACH BLOCK TOEPLITZ MATRIX
      DO 27 I=1,NP
      DO 27 J=1,NP
      IM=1+NP*(M-1)
      JM=J+NP*(M-1)
      Z(J,IM)=Z(I,JM)
27    CONTINUE
77    CONTINUE
      RETURN
      END
C****THIS SUBROUTINE CALCULATES YHS FOR ARBITARY # OF APERTURES
      SUBROUTINE ZAPCAL(KWCA,KSCA,MODT,MODESS,DWCA,DSCA,YL,ZL,NW,NZ
     2,NMAX,YHS)
      COMPLEX ZAB,YHS(MODT,MODESS)
      HL=ZL/NZ
      DWL=YL/NW
      NZS=NZ-1
      MODES=NW*NZS
      DO 79 IAJ=1,KSCA
      DO 79 JAJ=1,MODES
      ILM=(IAJ-1)*MODES+JAJ
      IF(ILM.GT.1.AND.DSCA.EQ.0)GO TO 9193
      IF(ILM.GT.MODES) GO TO 9193
      SY1=(YL+DSCA)*(IAJ-1)+DWL*(JAJ-1)
      SZ1=0.0
      DO 77 IN=1,KWCA
      DO 77 JN=1,KSCA
      DO 22 K=1,NW
      DO 22 L=1,NZS
      NJ=K+(L-1)*NW+MODES*(JN-1)+MODES*KSCA*(IN-1)
      SY2=(YL+DSCA)*(JN-1)+DWL*(K-1)
      SZ2=(ZL+DWCA)*(IN-1)+HL*(L-1)
      SY=ABS(SY2-SY1)
      SZ=ABS(SZ2-SZ1)
      CALL ZMNPSU(DWL,HL,SY,SZ,NMAX,ZAB)
      YHS(ILM,NJ)=ZAB/3/6.73**2*2.
C     WRITE(3,*)NJ,YHS(1,NJ)
22    CONTINUE
77    CONTINUE
79    CONTINUE
9193  RETURN
      END
C****THIS SUBROUTINE CALCULATES ZMN BY TRANSFORMATION
      SUBROUTINE ZMNPSU(DWL,HL,SY,SZ,NMAX,ZAB)
      COMPLEX TERM,SUM,ZAB,Z,ZMN
      DIMENSION C(171)
C****DWL,SY,SZ,HL ALL IN WAVELENGTHS
      CALL SIMPC(NMAX,C)
      DV=DWL/SQRT(2.)/(NMAX-1)
      CONST=4.*DV/(DWL**2*3.)
      SUM=(0.,0.)
```

```
      DO 5 K=1,NMAX
      VK=SY/SQRT(2.)+DV*(K-1)
      FAC=DVL/SQRT(2.)-ABS(VK-SY/SQRT(2.))
      VK=ABS(VK)*SQRT(2.)
      IF(ABS(VK).LT.0.0001) VK=0.0001
      Z=ZMN(VK,HL,SZ)
      TERM=C(K)*FAC*Z
      SUM=SUM+TERM
5     CONTINUE
      ZAB=CONST*SUM
      RETURN
      END
      COMPLEX FUNCTION ZMN(DL,HL,SL)
      REAL L,LE,LL
      DOUBLE PRECISION DD,DH,DHML,DHPL,DHP2L,DHP3L
      B=6.2831853
      D=DL
      DD=D
      L=HL
      LE=HL
      HC=SL
      BLE=B*LE
      H=ABS(HC)-L
      DH=H
      LL=LE
      HP2L=H+2.0*LL
      HPL=H+LL
      HP3L=H+3.0*LL
      HML=H-LL
      DHML=HML
      DHPL=HPL
      DHP2L=HP2L
      DHP3L=HP3L
      SBL=SIN(BLE)
      CBL=COS(BLE)
      SBH=SIN(B*H)
      CBH=COS(B*H)
      SBHML=SIN(B*HML)
      CBHML=COS(B*HML)
      SBHPL=SIN(B*HPL)
      CBHPL=COS(B*HPL)
      SBHP2L=SIN(B*HP2L)
      CBHP2L=COS(B*HP2L)
      SBHP3L=SIN(B*HP3L)
      CBHP3L=COS(B*HP3L)
      TEMP=DSQRT(DD*DD+DH*DH)+DH
      V1=B*D*D/TEMP
      U1=B*TEMP
      TEMP=DSQRT(DD*DD+DHML*DHML)+DHML
      U0=B*TEMP
      V0=B*D*D/TEMP
      TEMP=DSQRT(DD*DD+DHPL*DHPL)+DHPL
      U3=B*TEMP
      V3=B*D*D/TEMP
      TEMP=DSQRT(DD*DD+DHP2L*DHP2L)+DHP2L
```

```
      U2=B*D*D/TEMP
      V2=B*TEMP
      TEMP=DSQRT(DD*DD+DHP3L*DHP3L)+DHP3L
      U4=B*D*D/TEMP
      V4=B*TEMP
      CALL SICI (SIU0,CIU0,U0)
      CALL SICI (SIU1,CIU1,U1)
      CALL SICI (SIV2,CIV2,V2)
      CALL SICI (SIV4,CIV4,V4)
      CALL SICI (SIU3,CIU3,U3)
      IF (D.LE.0.0) GO TO 80
      CALL SICI (SIV1,CIV1,V1)
      CALL SICI (SIV0,CIV0,V0)
      CALL SICI (SIV3,CIV3,V3)
      CALL SICI (SIU2,CIU2,U2)
      CALL SICI (SIU4,CIU4,U4)
      R=15.0*(CBHML*(CIU0+CIV0-CIU1-CIV1)-SBHML*(-SIU0+SIV0+SIU1-SIV1)+C
     2BHPL*(2.*CIV3+2.*CIU3-CIU2-CIV2-CIU1-CIV1)+SBHPL*(-SIV3+SIU3+SIU2-
     3SIV2-SIU1+SIV1+SIU3-SIV3)+CBHP3L*(-CIU2-CIV2+CIU4+CIV4)+SBHP3L*(SI
     4U2-SIV2-SIU4+SIV4) +2.*CBL*CBH*(-CIV1-CIU1+CIV3+CIU3)+2.*CBL*SBH*(
     5SIV1-SIU1-SIV3+SIU3)+2.*CBL*CBHP2L*(CIV3+CIU3-CIU2-CIV2)+2.*CBL*SB
     6HP2L*(-SIV3+SIU3+SIU2-SIV2))
      X=15.0*(CBHML*(-SIU0-SIV0+SIU1+SIV1)-SBHML*(-CIU0+CIV0+CIU1-CIV1)+
     2CBHPL*(-2.*SIV3-2.*SIU3+SIU2+SIV2+SIU1+SIV1)+SBHPL*(-2.* CIV3+2.*C
     3IU3+CIU2-CIV2-CIU1+CIV1)+CBHP3L*(SIU2+SIV2-SIU4-SIV4)+SBHP3L*(CIU2
     4-CIV2-CIU4+CIV4)+2.*CBL*CBH*(SIV1+SIU1-SIV3-SIU3)+ 2.*CBL*SBH*(CIV
     51-CIU1-CIV3+CIU3)+2.*CBL*CBHP2L*(-SIV3-SIU3+SIU2+SIV2)+2.*CBL*SBHP
     62L*(-CIV3+CIU3+CIU2-CIV2))
      GO TO 90
   80 CONTINUE
      R=15.0*(CBHML*(CIU0-CIU1+ALOG(H /HML))+SBHML*(SIU0-SIU1)+SBHPL*
     2 (2.*SIU3 -SIV2-SIU1)+CBHPL*(2.*CIU3-CIV2-CIU1+ALOG(HP2L/HPL)+
     3ALOG(H /HPL))+CBHP3L*(CIV4-CIV2+ALOG(HP2L/HP3L))+SBHP3L*(SIV4-SIV2
     4 )+2.*CBL*CBH*(CIU3-CIU1+ALOG(H /HPL))+2.*CBL*SBH*(SIU3-SIU1) +
     5 2.*CBL*CBHP2L*(CIU3-CIV2+ALOG(HP2L/HPL))+2.*CBL*SBHP2L*(SIU3-
     6 SIV2))
      X=15.0*(CBHML*(SIU1-SIU0)+SBHML*(CIU0-CIU1+ALOG(HML/H ))+CBHPL*
     2 (SIV2+SIU1-2.*SIU3)+SBHPL*(2.*CIU3-CIV2-CIU1+ALOG(HPL/HP2L)+
     3ALOG(HPL/H ))+CBHP3L*(SIV2-SIV4)+SBHP3L*(CIV4-CIV2+ALOG(HP3L/HP2L)
     4)+2.*CBL*CBH*(SIU1-SIU3)+2.*CBL*SBH*(CIU3-CIU1+ALOG(HPL/H ))+2.*CB
     5L*CBHP2L*(SIV2-SIU3)+2.*CBL*SBHP2L*(CIU3-CIV2+ALOG(HPL/HP2L)))
   90 ZMN=CMPLX(R,X)/(SBL*SBL)
      RETURN
      END
      SUBROUTINE SICI(SI,CI,X)
      Z=ABS(X)
      IF(Z-4.0)1,1,4
    1 Y=(4.0-Z)*(4.0+Z)
      SI=-1.570797E0
      IF(Z)3,2,3
    2 CI=-1.0E38
      RETURN
    3 SI=X*(((((1.753141E-9*Y+1.568988E-7)*Y+1.374168E-5)*Y+6.939889E-4)
     2*Y+1.964882E-2)*Y+4.395509E-1+SI/X)
      CI=((5.772156E-1+ALOG(Z))/Z-Z*(((((1.386985E-10*Y+1.584996E-8)*Y
```

```
2+1.725752E-6)*Y+1.185999E-4)*Y+4.990920E-3)*Y+1.315308E-1))*Z
      RETURN
    4 SI=SIN(Z)
      Y=COS(Z)
      Z=4.0/Z
      U=((((((((4.048069E-3*Z-2.279143E-2)*Z+5.515070E-2)*Z-7.261642E-2)
     1*Z+4.987716E-2)*Z-3.332519E-3)*Z-2.314617E-2)*Z-1.134958E-5)*Z
     2+6.250011E-2)*Z+2.583989E-10
      V=((((((((-5.108699E-3*Z+2.819179E-2)*Z-6.537283E-2)*Z
     1+7.902034E-2)*Z-4.400416E-2)*Z-7.945556E-3)*Z+2.601293E-2)*Z
     2-3.764000E-4)*Z-3.122418E-2)*Z-6.646441E-7)*Z+2.500000E-1
      CI=Z*(SI*V-Y*U)
      SI=-Z*(SI*U+Y*V)
      IF(X)5,6,6
    5 SI=-3.141593E0-SI
    6 RETURN
      END
      SUBROUTINE SIMWC(NMAX,C)
      DIMENSION C(71)
      DO 1 N=1,NMAX
      XNN=FLOAT(N)
      NN=N/2
      TT=XNN/2.
      DIF=TT-FLOAT(NN)
      NC=2
      IF(DIF.EQ.0.) NC=4
      IF(N.EQ.1.OR.N.EQ.NMAX) NC=1
      C(N)=NC
1     CONTINUE
      RETURN
      END
      SUBROUTINE ZFFD(XA,YA,ZA,XB,YB,ZB,D,CTH,STH,CPH,SPH,ET,EP)
      COMPLEX ET,EP,ES,EJA,EJB
      XAB=XB-XA
      YAB=YB-YA
      ZAB=ZB-ZA
      CA=XAB/D
      CB=YAB/D
      CG=ZAB/D
      G=(CA*CPH+CB*SPH)*STH+CG*CTH
      GK=1.-G*G
      ET=(.0,.0)
      EP=(.0,.0)
      IF(GK.LT..001)GO TO 200
      B=XB*STH*CPH+YB*STH*SPH+ZB*CTH
      EJB=CMPLX(COS(B),SIN(B))
      SKD=SIN(D)
      CKD=COS(D)
      CGD=COS(G*D)
      ES=60.*(.0,1.)*EJB*(CKD-CGD)/SKD/GK
      T=(CA*CPH+CB*SPH)*CTH-CG*STH
      P=-CA*SPH+CB*CPH
      ET=T*ES
      EP=P*ES
  200 CONTINUE
```

```
      RETURN
      END
      SUBROUTINE CROUT(C,CJ,ICC,ISYM,IWR,I12,N)
      COMPLEX C(ICC,ICC),CJ(1)
      COMPLEX F,P,SS,T
 1    FORMAT(1H0)
 2    FORMAT(1X,I15,1F10.3,1F15.7,1F10.0)
      IF(I12.NE.1)GO TO 22
      IF(N.EQ.1)CJ(1)=CJ(1)/C(1,1)
      IF(N.EQ.1)GO TO 100
      IF(ISYM.NE.0)GO TO 8
      DO 6 I=1,N
      DO 6 J=I,N
 6    C(J,I)=C(I,J)
 8    F=C(1,1)
      DO 10 L=2,N
 10   C(1,L)=C(1,L)/F
      DO 20 L=2,N
      LLL=L-1
      DO 20 I=L,N
      F=C(I,L)
      DO 11 K=1,LLL
 11   F=F-C(I,K)*C(K,L)
      C(I,L)=F
      IF(L.EQ.I)GO TO 20
      P=C(L,L)
      IF(ISYM.EQ.0)GO TO 15
      F=C(L,I)
      DO 12 K=1,LLL
 12   F=F-C(L,K)*C(K,I)
      C(L,I)=F/P
      GO TO 20
 15   F=C(I,L)
      C(L,I)=F/P
 20   CONTINUE
 22   DO 30 L=1,N
      P=C(L,L)
      T=CJ(L)
      IF(L.EQ.1)GO TO 30
      LLL=L-1
      DO 25 K=1,LLL
 25   T=T-C(L,K)*CJ(K)
 30   CJ(L)=T/P
      DO 38 L=2,N
      I=N-L+1
      I1=I+1
      T=CJ(I)
      DO 35 K=I1,N
 35   T=T-C(I,K)*CJ(K)
 38   CJ(I)=T
      IF(IWR.LE.0) GO TO 100
      CNOR=0.
      DO 40 I=1,N
      SA=CABS(CJ(I))
 40   IF(SA.GT.CNOR)CNOR=SA
```

```
      IF(CNOR.LE.0.)CNOR=1.
      DO 44 I=1,N
      SS=CJ(I)
      SA=CABS(SS)
      SNOR=SA/CNOR
      PH=.0
      IF(SA.GT.0.)PH=57.29578*ATAN2(AIMAG(SS),REAL(SS))
   44 WRITE(6,2)I,SNOR,SA,PH
      WRITE(6,5)
  100 RETURN
      END
C     FILE NAME BLTSOL
      SUBROUTINE BLTSOL(Z,V,PS,NW,NP,IENTRY)
C
C      SUBPROGRAM NO.  K 92
C
C      ***  SEE TECH MEMO 1666 (AP)  ***
C       REQUIRES THE FOLLOWING SUBROUTINES--
C      34    LINEQ
C     K45    MATMLT
C     K46    TRMMLT
C     K37    MULTIP
C     K47    MATVCA
C
      COMPLEX Z(1),V(1),PS(1)
      DIMENSION IA(2)
      GO TO (41,42,43,44),IENTRY
   44 CONTINUE
      IRET=0
      GO TO 1
C     SUBROUTINE SOLVES FOR I THE MATRIX EQUATION  V=ZI  WHERE Z IS
C     A SYMMETRIC BLOCK-TOEPLITZ MATRIX OF ORDER NW*NP.  EACH BLOCK IS
C     OF ORDER NP AND AN NW X NW PARTITIONING IS USED.
C     V IS A SPECIFIED  VECTOR OF LENGTH NW*NP.  ON RETURN FROM BLTSOL
C     I IS STORED IN PLACE OF V.
C     PS IS AN ARRAY FOR SCRATCH STORAGE.
C         STORAGE REQUIREMENTS ARE
C             Z(NW*NP**2)       (I.E.. THE FIRST ROW OF NP X NP BLOCKS)
C           Z MATRIX IS FILLED BY COLUMNS. I.E.. Z((J-1)*NP+1)=Z(1,J)
C             V(NW*NP)
C             PS((2*NW+1)*NP**2)  (FOR TEMPORARY STORAGE)
C     BOTH NP AND NW MUST BE GREATER THAN OR EQUAL TO 2.
C     ALL ARRAYS ARE COMPLEX.
C     CONTENTS OF Z ARE DESTROYED.
C      ENTRY (IENTRY) POINTS ARE AS FOLLOWS..
C    (1) LINSET(Z,PS,NW,NP)   FACTORIZES THE Z MATRIX - STEPS I AND II.
C    (3) NEWRHS (V)  MUST BE PRECEDED BY A CALL TO LINSET.  CAN CALL
C     THIS ENTRY POINT A NUMBER OF TIMES TO SOLVE FOR CURRENT FOR
C     DIFFERENT V BUT THE SAME Z FACTORED BY INITIAL CALL TO LINSET.
C    (2) NEWFAC(Z,PS,NW,NP)  CALLED TO RESET ADDRESSES.  MUST BE CALLED
C     IF PS ARRAY, NW, NP ARE STORED ON TAPE AND REREAD FOR SUBSEQUENT
C     CALLS TO NEWRHS.
C    (4) BLTSOL(Z,V,PS,NW,NP) EQUIVALENT TO CALLS TO LINSET AND NEWRHS.
C     FACTORED ARRAY REMAINS FOR POSSIBLE REUSE BY FURTHER CALLS TO
C     NEWRHS OR PS ARRAY CAN BE SAVED ON TAPE FOR LATER USE.
```

```
C      ENTRY LINSET(Z,PS,NW,NP)
41     CONTINUE
       IRET=1
       GO TO 1
C      ENTRY NEWFAC(Z,PS,NW,NP)
42     CONTINUE
       N=NW-1
       N2=NP**2
       I=NW*N2+N2+1
       J=N2+1
       IF(MOD(N,2)) 2,2,3
C      N EVEN
2      IPHI=J-N2
       IPSI=I
       GO TO 4
C      N ODD
3      IPHI=I-N2
       IPSI=J
4      RETURN
C       ENTRY POINT IF A PREVIOUS CALL MADE TO ALTSOL AND NOW ONLY
C        SPECIFY A NEW RHS
C      ENTRY NEWRHS
43     CONTINUE
       GO TO 46
C
C       CALC  DEL(-1)  AND  PS((0),N)
C
1      N=NW-1
       IF(NW.LT.2) GO TO 100
       IF(NP.LT.2) GO TO 101
       N2=NP*NP
       DO 5 I=1,N2
C      WRITE(3,-)I,Z(I)
5      PS(I)=Z(I)
       CALL LINEQ(PS,NP)
       CALL MATMLT(PS,Z(N2+1),PS(N2+1),NP)
C
C        IA(1) = START ADDRESS IN PS ARRAY OF  PS((M-1),0)
C        IA(2) = START ADDRESS IN PS ARRAY OF  PS((M),0)
C        IA(1)-N2 = START ADDRESS IN PS ARRAY OF DEL(M-2)
C        IA(2)-N2 = START ADDRESS IN PS ARRAY OF DEL(M-1)
C        IST+1 =2*NW*N2 + 1 = START ADDRESS OF AN ADDITIONAL SCRATCH AREA.
C
        IA(1)=N2+1
        IA(2)=NW*N2+N2+1
        IST=2*NW*N2
        N3=N2+N2+1
        MM=0
C
C        ITERATE ON M=1,2,... N.  FOR M=N, ONLY CALC  DEL (M-1)
        DO 45 M=1,N
        I0=IA(1)+MM
        MM=MM+N2
        I1=IA(2)+MM
C         I0 IS START ADDRESS OF PS((M-1),M-1)
```

```
C        I1 IS START ADDRESS OF PS((M),M)
C
C        CALC DEL(M-1)
      CALL MATMLT(PS(I0),PS(I0),PS(IST+1),NP)
      IJ=IST
      DO 20 J=1,NP
      DO 20 I=1,NP
      IJ=IJ+1
      PS(IJ)=-PS(IJ)
20    IF(I.EQ.J) PS(IJ)=PS(IJ)+1.
      CALL LINEQ(PS(IST+1),NP)
      I0=IA(1)-N2
      I01=IA(2)-N2
      CALL MATMLT(PS(IST+1),PS(I0),PS(I01),NP)
      IF(M.EQ.N) GO TO 50
C
C        CALC PS((M),M)
      MZZ=MZ
      MS=IA(1)
      IJ=IST
      DO 25 I=1,N2
      IJ=IJ+1
      PS(IJ)=Z(MZZ)
25    MZZ=MZZ+1
      MZZ=MZ-N2
      DO 30 IS=1,M
      CALL TRMMLT(PS(MS),Z(MZZ),PS(IST+1),NP)
C          TRMMLT ACCUMULATES   -TRANSP(PS(MS))*Z(MZZ)
      MS=MS+N2
30    MZZ=MZZ-N2
      MZ=MZ+N2
      CALL MATMLT(PS(I01),PS(IST+1),PS(I1),NP)
C        CALC PS((M),R) FOR  R=0,1,...M-1.  (IK=R)
      I0R=IA(1)
      I1R=IA(2)
      IMR=I0
      DO 40 IR=1,M
      CALL MATMLT(PS(IMR),PS(I1),PS(IST+1),NP)
      IMR=IMR-N2
      IJ=IST
      DO 40 I=1,N2
      PS(I1R)=PS(I0R)-PS(IJ+1)
      IJ=IJ+1
      I1R=I1R+1
40    I0R=I0R+1
      I=IA(1)
      IA(1)=IA(2)
45    IA(2)=I
C
C        HAVE FINISHED ITERATION OF PS. NOW PUT PHI(R) INTO PS(IA(2))
50    IPHI=IA(2)-N2
      IPSI=IA(1)
      I0R=IA(1)
      I1R=IA(2)
      DO 60 I=1,N
```

```
      CALL MULTTR(PS(IPHI),PS(IOR),PS(I1R),NP)
      IOR=IOR+N2
60    I1R=I1R+N2
C
C      PUT PHI(-1) IN PS(IPHI)
      J=IPHI
      DO 65 I=1,N2
      PS(J)=-PS(J)
65    J=J+1
C
C   NOW HAVE   PHI(S), S=-1,0,1... N-1  STARTING AT PS(IPHI)
C   AND        PSI(S), S=0,1....   N-1 STARTING AT PS(IPSI)
C
C      FORM A AND B IN  Z ARRAY
      IF(IRET.NE.0) RETURN
68    IB=NW*NP+1
      IC=1
      J=2*NW*NP
      DO 70 I=1,J
70     Z(I)=(0.,0.)
      IV=1
      DO 80 J=1,N
      JR=NW-J+1
      I1S=IPHI
      I2S=IPHI+ N*N2
      IVS=IV
      DO 75 I=1,NP
      JENTRY=1
      CALL MATVCA(PS(I1S),V(IVS),Z(IC),NP,JENTRY)
      CALL MATVCA(PS(I2S),V(IVS),Z(IB),NP,JENTRY)
      I1S=I1S+N2
      I2S=I2S-N2
75    IVS=IVS+NP
      IV=IV+NP
      IC=IC+NP
80    IB=IB+NP
C      NOW CALCULATE I IN V LOCATIONS.
      J=NW*NP
      DO 85 I=1,J
85    V(I)=-Z(I)
C
      IV=NP+1
      IC=1
      IB=IV+J
      DO 95 IR=1,N
      I1S=IPSI
      I2S=(N-1)*N2+IPSI
      ICS=IC
      IBS=IB
      DO 90 IS=1,IR
      JENTRY=1
      CALL MATVCA(PS(I1S),Z(ICS),V(IV),NP,JENTRY)
      JENTRY=2
      CALL MATVCA(PS(I2S),Z(IBS),V(IV),NP,JENTRY)
      I1S=I1S+N2
```

```
      I2S=I2S-N2
      ICS=ICS-NP
90    IBS=IBS-NP
      IV=IV+NP
      IC=IC+NP
95    IB=IB+NP
      RETURN
C       ERROR RETURNS
100   WRITE(6,1000) NW
      RETURN
101   WRITE(6,1001) NP
      RETURN
1000  FORMAT(///10X,27HILLEGAL CALL TO BLTSOL, NW=, I6)
1001  FORMAT(///10X,27HILLEGAL CALL TO BLTSOL, NP=,I6)
      CALL EXIT
      END
C     SUBROUTINE NO. 854
C     INVERSION OF COMPLEX MATRIX C, OF ORDER LL.  INVERSE IS RETURNED IN
C     PLACE OF C
      SUBROUTINE CINFQ(C,LL)
      COMPLEX C(1),STOR,STO,ST,S
      DIMENSION LR(77)
      COMPLEX X
      CABQ(X)=REAL(X)*REAL(X)+AIMAG(X)*AIMAG(X)
      DO 20 I=1,LL
      LR(I)=I
20    CONTINUE
      M1=0
      DO 18 M=1,LL
      K=M
      DO 2 I=M,LL
      K1=M1+I
      K2=M1+K
      IF(CABQ(C(K1))-CABQ(C(K2))) 2,2,6
6     K=I
2     CONTINUE
      LS=LR(M)
      LR(M)=LR(K)
      LR(K)=LS
      K2=M1+K
      STOR=C(K2)
      J1=0
      DO 7 J=1,LL
      K1=J1+K
      K2=J1+M
      STO=C(K1)
      C(K1)=C(K2)
      C(K2)=STO/STOR
      J1=J1+LL
7     CONTINUE
      K1=M1+M
      C(K1)=1./STOR
      DO 11 I=1,LL
      IF(I-M) 12,11,12
12    K1=M1+I
```

```
      ST=C(K1)
      C(K1)=(0.,0.)
      J1=0
      DO 10 J=1,LL
      K1=J1+I
      K2=J1+M
      C(K1)=C(K1)-C(K2)*ST
      J1=J1+LL
10    CONTINUE
11    CONTINUE
      M1=M1+LL
18    CONTINUE
      J1=0
      DO 9 J=1,LL
      IF(J-LR(J)) 14,8,14
14    LRJ=LR(J)
      J2=(LRJ-1)*LL
21    DO 13 I=1,LL
      K2=J2+I
      K1=J1+I
      S=C(K2)
      C(K2)=C(K1)
      C(K1)=S
13    CONTINUE
      LR(J)=LR(LRJ)
      LR(LRJ)=LRJ
      IF(J-LR(J)) 14,8,14
8     J1=J1+LL
9     CONTINUE
      RETURN
      END
C     SUBROUTINE NO. H55
      SUBROUTINE MATMLT(A,B,C,NP)
C      CALCULATES C=A*B.  A,B,C ARE NP X NP MATRICES OF COMPLEX NUMBER.
      COMPLEX A(1),B(1),C(1),D
      IJ=0
      L=1
      DO 15 J=1,NP
      DO 10 I=1,NP
      IJ=IJ+1
      D=(0.,0.)
      KJ=L
      IK=I
      DO 5 K=1,NP
      D=D+A(IK)*B(KJ)
      IK=IK+NP
5     KJ=KJ+1
10    C(IJ)=D
15    L=L+NP
      RETURN
      END
C     SUBROUTINE NO. H56
      SUBROUTINE TAMMLT(A,B,C,NP)
C      ACCUMULATES IN C      -TRANS P(A)*B
      COMPLEX A(1),B(1),C(1),D
```

```
      IJ=0
      L=1
      DO 15 J=1,NP
      M=1
      DO 10 I=1,NP
      IJ=IJ+1
      D=(0.,0.)
      KI=M
      KJ=L
      DO 5 K=1,NP
      D=D+A(KI)*B(KJ)
      KI=KI+1
    5 KJ=KJ+1
      M=M+NP
   10 C(IJ)=C(IJ)-D
   15 L=L+NP
      RETURN
      END
C     SUBROUTINE NO. H57
      SUBROUTINE MULTTR(A,B,C,NP)
C      CALCULATES C=A*TRANSP(B)
      COMPLEX A(1),B(1),C(1),D
      IJ=0
      DO 10 J=1,NP
      DO 10 I=1,NP
      IJ=IJ+1
      D=(0.,0.)
      IK=I
      JK=J
      DO 5 K=1,NP
      D=D+A(IK)*B(JK)
      IK=IK+NP
    5 JK=JK+NP
   10 C(IJ)=D
      RETURN
      END
C     SUBPROGRAM H47
      SUBROUTINE MATVCA(A,B,C,N,JENTRY)
C
C      POSITIVE ACCUMULATION OF  A*B IN C.  WHERE A IS AN N X N MATRIX,
C      B IS AN N-VECTOR. C IS AN N-VECTOR.  ALL ARE COMPLEX
      COMPLEX A(1),B(1),C(1),D
      GO TO (32,33),JENTRY
   32 IGO =1
      GO TO 1
   33 CONTINUE
C      NEGATIVE ACCUMULATION - SYMBOLS AS ABOVE
      IGO=2
    1 DO 10 J=1,N
      D=(0.,0.)
      IJ=J
      DO 5 I=1,N
      D=D+A(IJ)*B(I)
    5 IJ=IJ+N
      GO TO (6,7),IGO
```

```
6       C(J)=C(J)+U
        GO TO 10
7       C(J)=C(J)-U
10      CONTINUE
        RETURN
        END
```

```
CENT TO CENT E-PLANE SPACING=     .2540  WAVLGTHS
CENT TO CENT H-PLANE SPACING=     .5714  WAVLGTHS

***PIECEWISE SINUSOIDAL-UNIFORM EXPANSIONS ***
      ...PROGRAM FARRAY...BY ALAN FENN...

NMAX=  71   FREQUENCY=  .23760E 10   (A/B)=      2.250

YL=  .2540 WAVLGTHS   ZL=  .5714 WAVLGTHS      NW=   7   NZ=   2

**FIRST ROW OF HALF-SPACE ADMITTANCE MATRIX (MHOS)

YHS(1,  1)=  .15688E -2   .17856E -2
YHS(1,  2)=  .15405E -2   .89043E -3
YHS(1,  3)=  .14799E -2   .47002E -3
YHS(1,  4)=  .13887E -2   .14076E -3
YHS(1,  5)=  .12699E -2 -.11361E -3
YHS(1,  6)=  .11277E -2 -.32914E -3
YHS(1,  7)=  .96658E -3 -.50223E -3
YHS(1,  8)=  .79198E -3 -.63477E -3
YHS(1,  9)=  .60053E -3 -.72799E -3
YHS(1, 10)=  .42503E -3 -.76327E -3
YHS(1, 11)=  .24425E -3 -.80285E -3
YHS(1, 12)=  .72662E -4 -.78841E -3
YHS(1, 13)= -.84746E -4 -.74426E -3
YHS(1, 14)= -.22363E -3 -.67414E -3
YHS(1, 15)= -.34044E -3 -.58270E -3
YHS(1, 16)= -.43256E -3 -.47505E -3
YHS(1, 17)= -.49835E -3 -.35654E -3
YHS(1, 18)= -.53722E -3 -.23262E -3
YHS(1, 19)= -.54957E -3 -.10864E -3
YHS(1, 20)= -.53680E -3   .10364E -4
YHS(1, 21)= -.50118E -3   .11985E -3
YHS(1, 22)=  .41549E -3   .19772E -3
YHS(1, 23)=  .40405E -3   .10162E -3
YHS(1, 24)=  .37934E -3   .13377E -4
YHS(1, 25)=  .34240E -3 -.65205E -4
YHS(1, 26)=  .29477E -3 -.13245E -3
YHS(1, 27)=  .23842E -3 -.18690E -3
YHS(1, 28)=  .17569E -3 -.22747E -3
YHS(1, 29)=  .10915E -3 -.25348E -3
YHS(1, 30)=  .41527E -4 -.26474E -3
YHS(1, 31)= -.24434E -4 -.26161E -3
YHS(1, 32)= -.86094E -4 -.24403E -3
YHS(1, 33)= -.14102E -3 -.21607E -3
YHS(1, 34)= -.18711E -3 -.17684E -3
YHS(1, 35)= -.22265E -3 -.12941E -3
YHS(1, 36)= -.24143E -3 -.76240E -4
YHS(1, 37)= -.25769E -3 -.19963E -4
YHS(1, 38)= -.25631E -3   .36729E -4
YHS(1, 39)= -.24269E -3   .91175E -4
YHS(1, 40)= -.21773E -3   .14091E -3
YHS(1, 41)= -.18283E -3   .18571E -3
YHS(1, 42)= -.13960E -3   .21773E -3
YHS(1, 43)= -.47767E -4   .34495E -4
```

YHS(1, 44)=	-.47203E -4	.35135E -4
YHS(1, 45)=	-.45942E -4	.36512E -4
YHS(1, 46)=	-.43946E -4	.38559E -4
YHS(1, 47)=	-.41158E -4	.41168E -4
YHS(1, 48)=	-.37517E -4	.44197E -4
YHS(1, 49)=	-.32962E -4	.47460E -4
YHS(1, 50)=	-.27450E -4	.50770E -4
YHS(1, 51)=	-.20957E -4	.53865E -4
YHS(1, 52)=	-.13501E -4	.56494E -4
YHS(1, 53)=	-.51427E -5	.58389E -4
YHS(1, 54)=	.40065E -5	.59279E -4
YHS(1, 55)=	.15766E -4	.58911E -4
YHS(1, 56)=	.23914E -4	.57059E -4
YHS(1, 57)=	.34163E -4	.53540E -4
YHS(1, 58)=	.44178E -4	.48231E -4
YHS(1, 59)=	.5[illegible]90E -4	.41076E -4
YHS(1, 60)=	.62003E -4	.32105E -4
YHS(1, 61)=	.69019E -4	.21434E -4
YHS(1, 62)=	.74252E -4	.92660E -5
YHS(1, 63)=	.77351E -4	-.40889E -5

PHI1= 61.0452 DEGREES

**SELF BLOCK (Y11) OF WAVEGUIDE-ADMITTANCE MATRIX (MHOS)

YWG(1,1)=	.17017E -2	.12934E -2
YWG(1,2)=	.17017E -2	.45340E -3
YWG(1,3)=	.17017E -2	-.15786E -4
YWG(1,4)=	.17017E -2	-.27926E -3
YWG(1,5)=	.17017E -2	-.44536E -3
YWG(1,6)=	.17017E -2	-.54389E -3
YWG(1,7)=	.17017E -2	-.58781E -3
YWG(2,2)=	.17017E -2	.82422E -3
YWG(2,3)=	.17017E -2	.19148E -3
YWG(2,4)=	.17017E -2	-.18429E -3
YWG(2,5)=	.17017E -2	-.37624E -3
YWG(2,6)=	.17017E -2	-.46928E -3
YWG(2,7)=	.17017E -2	-.54389E -3
YWG(3,3)=	.17017E -2	.65656E -3
YWG(3,4)=	.17017E -2	.92423E -4
YWG(3,5)=	.17017E -2	-.22736E -3
YWG(3,6)=	.17017E -2	-.37624E -3
YWG(3,7)=	.17017E -2	-.44536E -3
YWG(4,4)=	.17017E -2	.61849E -3
YWG(4,5)=	.17017E -2	.92943E -4
YWG(4,6)=	.17017E -2	-.18344E -3
YWG(4,7)=	.17017E -2	-.27770E -3
YWG(5,5)=	.17017E -2	.65656E -3
YWG(5,6)=	.17017E -2	.19149E -3
YWG(5,7)=	.17017E -2	-.15786E -4
YWG(6,6)=	.17017E -2	.82422E -3
YWG(6,7)=	.17017E -2	.45340E -3
YWG(7,7)=	.17017E -2	.12934E -2

**FIRST ROW OF TOTAL ADMITTANCE MATRIX (MHOS)

```
Y(1,  1)=  .32702E -2   .50790E -2
Y(1,  2)=  .32422E -2   .13438E -2
Y(1,  3)=  .31610E -2   .45424E -3
Y(1,  4)=  .30904E -2  -.15050E -3
Y(1,  5)=  .29716E -2  -.55897E -3
Y(1,  6)=  .28254E -2  -.87305E -3
Y(1,  7)=  .26683E -2  -.10900E -2
Y(1,  8)=  .79190E -3  -.63477E -3
Y(1,  9)=  .60953E -3  -.72799E -3
Y(1, 10)=  .42503E -3  -.76327E -3
Y(1, 11)=  .24425E -3  -.80253E -3
Y(1, 12)=  .72662E -4  -.78841E -3
Y(1, 13)= -.84746E -4  -.74426E -3
Y(1, 14)= -.22363E -3  -.67414E -3
Y(1, 15)= -.34044E -3  -.56270E -3
Y(1, 16)= -.43256E -3  -.47505E -3
Y(1, 17)= -.49835E -3  -.35654E -3
Y(1, 18)= -.53722E -3  -.23262E -3
Y(1, 19)= -.54957E -3  -.10064E -3
Y(1, 20)= -.55[illegible]E -3   .10564E -4
Y(1, 21)= -.50119E -3   .11983E -3
Y(1, 22)=  .41549E -3   .19772E -3
Y(1, 23)=  .40405E -3   .10162E -3
Y(1, 24)=  .37934E -3   .13377E -4
Y(1, 25)=  .34240E -3  -.65205E -4
Y(1, 26)=  .29477E -3  -.13245E -3
Y(1, 27)=  .23842E -3  -.18690E -3
Y(1, 28)=  .17560E -3  -.22747E -3
Y(1, 29)=  .10915E -3  -.25348E -3
Y(1, 30)=  .41527E -4  -.26474E -3
Y(1, 31)= -.24434E -4  -.26161E -3
Y(1, 32)= -.86094E -4  -.24403E -3
Y(1, 33)= -.14162E -3  -.21607E -3
Y(1, 34)= -.18711E -3  -.17684E -3
Y(1, 35)= -.22265E -3  -.12941E -3
Y(1, 36)= -.24641E -3  -.76240E -4
Y(1, 37)= -.25769E -3  -.19963E -4
Y(1, 38)= -.25631E -3   .36725E -4
Y(1, 39)= -.24269E -3   .91175E -4
Y(1, 40)= -.21773E -3   .14091E -3
Y(1, 41)= -.16283E -3   .18371E -3
Y(1, 42)= -.13980E -3   .21773E -3
Y(1, 43)= -.47767E -4   .34495E -4
Y(1, 44)= -.47263E -4   .35135E -4
Y(1, 45)= -.45942E -4   .36512E -4
Y(1, 46)= -.43946E -4   .38559E -4
Y(1, 47)= -.41156E -4   .41168E -4
Y(1, 48)= -.37517E -4   .44197E -4
Y(1, 49)= -.32962E -4   .47468E -4
Y(1, 50)= -.27450E -4   .50770E -4
Y(1, 51)= -.20957E -4   .53865E -4
Y(1, 52)= -.13501E -4   .56494E -4
```

```
Y(1, 53)= -.51427E -5   .58389E -4
Y(1, 54)=  .40035E -5   .59279E -4
Y(1, 55)=  .15766E -4   .58911E -4
Y(1, 56)=  .25914E -4   .57059E -4
Y(1, 57)=  .34166E -4   .55540E -4
Y(1, 58)=  .44178E -4   .48231E -4
Y(1, 59)=  .55590E -4   .41076E -4
Y(1, 60)=  .62003E -4   .32105E -4
Y(1, 61)=  .69019E -4   .21034E -4
Y(1, 62)=  .74252E -4   .92698E -5
Y(1, 63)=  .77251E -4  -.40009E -5


SCAN ANGLE IN DEGREES (W.R.T. ARRAY NORMAL)=    0.00000

EXCITATION MATRIX (AMPS)  TE10  MODE

 *****E-PLANE SCAN*******
    1  1.000000              .319E  0         99.
    2  1.000000              .319E  0         99.
    3  1.000000              .319E  0         99.
    4  1.000000              .319E  0         99.
    5  1.000000              .319E  0         99.
    6  1.000000              .319E  0         99.
    7  1.000000              .319E  0         99.
I( 1)=       -.50057E -1      .31464E  0
I( 2)=       -.50057E -1      .31464E  0
I( 3)=       -.50057E -1      .31464E  0
I( 4)=       -.50057E -1      .31464E  0
I( 5)=       -.50057E -1      .31464E  0
I( 6)=       -.50057E -1      .31464E  0
I( 7)=       -.50057E -1      .31464E  0

PHASE SHIFT (IN DEGREES) BETWEEN APERTURES=   0.00000

    1      1.000      .3186011       99.
    2      1.000      .3186011       99.
    3      1.000      .3186011       99.
    4      1.000      .3186011       99.
    5      1.000      .3186011       99.
    6      1.000      .3186011       99.
    7      1.000      .3186011       99.
    8      1.000      .3186011       99.
    9      1.000      .3186011       99.
   10      1.000      .3186011       99.
   11      1.000      .3186011       99.
   12      1.000      .3186011       99.
   13      1.000      .3186011       99.
   14      1.000      .3186011       99.
   15      1.000      .3186011       99.
   16      1.000      .3186011       99.
   17      1.000      .3186011       99.
   18      1.000      .3186011       99.
   19      1.000      .3186011       99.
   20      1.000      .3186011       99.
```

21	1.000	.3186011	99.
22	1.000	.3186011	99.
23	1.000	.3186011	99.
24	1.000	.3186011	99.
25	1.000	.3186011	99.
26	1.000	.3186011	99.
27	1.000	.3186011	99.
28	1.000	.3186011	99.
29	1.000	.3186011	99.
30	1.000	.3186011	99.
31	1.000	.3186011	99.
32	1.000	.3186011	99.
33	1.000	.3186011	99.
34	1.000	.3186011	99.
35	1.000	.3186011	99.
36	1.000	.3186011	99.
37	1.000	.3186011	99.
38	1.000	.3186011	99.
39	1.000	.3186011	99.
40	1.000	.3186011	99.
41	1.000	.3186011	99.
42	1.000	.3186011	99.
43	1.000	.3186011	99.
44	1.000	.3186011	99.
45	1.000	.3186011	99.
46	1.000	.3186011	99.
47	1.000	.3186011	99.
48	1.000	.3186011	99.
49	1.000	.3186011	99.
50	1.000	.3186011	99.
51	1.000	.3186011	99.
52	1.000	.3186011	99.
53	1.000	.3186011	99.
54	1.000	.3186011	99.
55	1.000	.3186011	99.
56	1.000	.3186011	99.
57	1.000	.3186011	99.
58	1.000	.3186011	99.
59	1.000	.3186011	99.
60	1.000	.3186011	99.
61	1.000	.3186011	99.
62	1.000	.3186011	99.
63	1.000	.3186011	99.

****

VOLTAGE MATRIX (RESPONSE) TE10 MODE

1	1.000	22.3316082	71.
2	.534	11.9248413	91.
3	.480	10.7169987	101.
4	.467	10.4274963	109.
5	.477	10.6615696	115.
6	.503	11.2421441	120.
7	.664	14.8276128	135.
8	.352	7.8573780	81.

9	.412	9.1996084	112.
10	.430	9.6045152	116.
11	.435	9.7062589	117.
12	.430	9.6036128	116.
13	.412	9.1994382	112.
14	.352	7.8534521	81.
15	.664	14.8326265	135.
16	.503	11.2422465	120.
17	.477	10.6632954	115.
18	.467	10.4253453	109.
19	.480	10.7190502	101.
20	.534	11.9254309	91.
21	1.000	22.3290692	71.
22	.956	21.3592122	69.
23	.466	10.3974667	94.
24	.419	9.3657269	106.
25	.416	9.2933434	115.
26	.436	9.7450788	122.
27	.474	10.5941855	128.
28	.683	15.2596137	141.
29	.256	5.7062409	83.
30	.368	8.2233884	122.
31	.396	8.8326152	126.
32	.403	8.9955467	127.
33	.395	8.8318479	126.
34	.368	8.2232488	122.
35	.255	5.7030675	83.
36	.684	15.2640864	141.
37	.474	10.5940675	128.
38	.436	9.7449443	122.
39	.416	9.2935343	115.
40	.419	9.3667916	106.
41	.466	10.3980668	94.
42	.956	21.3576006	69.
43	1.000	22.3316082	71.
44	.534	11.9249413	91.
45	.480	10.7169587	101.
46	.467	10.4274963	109.
47	.477	10.6615695	115.
48	.503	11.2421441	120.
49	.664	14.8276125	135.
50	.352	7.8573780	81.
51	.412	9.1996084	112.
52	.430	9.6045152	116.
53	.435	9.7062589	117.
54	.430	9.6036128	116.
55	.412	9.1994382	112.
56	.352	7.8563520	81.
57	.664	14.8326265	135.
58	.503	11.2422465	120.
59	.477	10.6632954	115.
60	.467	10.4253453	109.
61	.480	10.7190502	101.
62	.534	11.9254309	91.
63	1.000	22.3290692	71.

```
APERTURE    1
REFL COEF=      -.09019        .05977   TE10  MODE
MAGNITUDE REFL COEF=  .10820   PHASE REFL COEF=    146.5    DEGREES
TRANSMISSION COEF=          .91177          3.8  DEGS
HIMAGE MAG=      4.07293   HIMAGE PHASE=        24.5887   DEGREES
HXR MAG=         3.71356   HXR PHASE=         -151.6527   DEGREES
HXI MAG=         4.07293   HXI PHASE=          173.4902   DEGREES
*************************************************
APERTURE    2
REFL COEF=      -.35270        .08136   TE10  MODE
MAGNITUDE REFL COEF=  .36197   PHASE REFL COEF=    167.0    DEGREES
TRANSMISSION COEF=          .65239          7.2  DEGS
HIMAGE MAG=      4.07293   HIMAGE PHASE=        24.5887   DEGREES
HXR MAG=         2.65714   HXR PHASE=         -140.2475   DEGREES
HXI MAG=         4.07293   HXI PHASE=          173.4902   DEGREES
*************************************************
APERTURE    3
REFL COEF=      -.09017        .05977   TE10  MODE
MAGNITUDE REFL COEF=  .10819   PHASE REFL COEF=    146.5    DEGREES
TRANSMISSION COEF=          .91179          3.8  DEGS
HIMAGE MAG=      4.07293   HIMAGE PHASE=        24.5887   DEGREES
HXR MAG=         3.71365   HXR PHASE=         -151.6525   DEGREES
HXI MAG=         4.07293   HXI PHASE=          173.4902   DEGREES
*************************************************
APERTURE    4
REFL COEF=      -.18063        .11794   TE10  MODE
MAGNITUDE REFL COEF=  .21572   PHASE REFL COEF=    146.9    DEGREES
TRANSMISSION COEF=          .82781          8.2  DEGS
HIMAGE MAG=      4.07293   HIMAGE PHASE=        24.5887   DEGREES
HXR MAG=         3.37163   HXR PHASE=         -147.2206   DEGREES
HXI MAG=         4.07293   HXI PHASE=          173.4902   DEGREES
*************************************************
APERTURE    5
REFL COEF=      -.46799        .16540   TE10  MODE
MAGNITUDE REFL COEF=  .49636   PHASE REFL COEF=    160.5    DEGREES
TRANSMISSION COEF=          .55712         17.3  DEGS
HIMAGE MAG=      4.07293   HIMAGE PHASE=        24.5887   DEGREES
HXR MAG=         2.26915   HXR PHASE=         -138.1413   DEGREES
HXI MAG=         4.07293   HXI PHASE=          173.4902   DEGREES
*************************************************
APERTURE    6
REFL COEF=      -.18061        .11794   TE10  MODE
MAGNITUDE REFL COEF=  .21571   PHASE REFL COEF=    146.9    DEGREES
TRANSMISSION COEF=          .82783          8.2  DEGS
HIMAGE MAG=      4.07293   HIMAGE PHASE=        24.5887   DEGREES
HXR MAG=         3.37171   HXR PHASE=         -147.2206   DEGREES
HXI MAG=         4.07293   HXI PHASE=          173.4902   DEGREES
*************************************************

APERTURE ADMITTANCES (MHOS)

Y0=     .12851E -2  .00000E  1
APERTURE   1   APERTURE ADMITTANCE=   .15277E -2 -.18478E -3
APERTURE   2   APERTURE ADMITTANCE=   .26237E -2 -.40129E -3
APERTURE   3   APERTURE ADMITTANCE=   .15276E -2 -.18479E -3
```

```
APERTURE    4    APERTURE ADMITTANCE=  .17890E -2 -.44231E -3
APERTURE    5    APERTURE ADMITTANCE=  .31204E -2 -.13695E -2
APERTURE    6    APERTURE ADMITTANCE=  .17079E -2 -.44231E -3
APERTURE    7    APERTURE ADMITTANCE=  .15277E -2 -.18478E -3
APERTURE    8    APERTURE ADMITTANCE=  .26257E -2 -.49129E -3
APERTURE    9    APERTURE ADMITTANCE=  .15276E -2 -.18479E -3

NMAX=  71    FREQUENCY=  .23760E 10    (A/B)=      2.250

Y1=  .2540 WAVLGTHS    Z1=  .5714 WAVLGTHS        NY=   7    NZ=    2

# OF WEAK-COUPLED APERTURES=   3    DWCA=   0.00000 WAVLGHTS
# OF STRONG-COUPLED APERTURES=   3    DSCA=   0.00000 WAVLGHTS
```

REFERENCES

1. L. Stark, "Microwave Theory of Phased-Array Antennas - A Review," Proc. IEEE, Vol. 62, No. 12, p. 1161-1701, December 1974.

2. N. Amitay, V. Galindo, and C. P. Wu, Theory and Analysis of Phased Array Antennas, New York, N.Y.; John Wiley and Sons, Incorporated, 1972, p. 4.

3. Ibid., pp. 149-154.

4. J. D. Kraus, Antennas, McGraw-Hill Book Company, Incorporated, 1950, pp. 66-67.

5. N. Amitay, V. Galindo, and C. P. Wu, op. cit., p. 3.

6. R. F. Harrington and J. R. Mautz, "A Generalized Network Formulation for Aperture Problems," Scientific Report No. 8 on Contract F19628-73-C-0047 with A. F. Cambridge Research Laboratories, Report AFCRL-TR-75-0589, November 1975.

7. G. A. Thiele, "Wire Antennas," Chapter 2 of Computer Techniques for Electromagnetics, R. Mitra, Ed., Pergamon Press, London, 1973.

8. R. F. Harrington, Field Computation by Moment Methods, New York, N.Y., The Macmillan Company, 1968.

9. R. F. Harrington, Time-Harmonic Electromagnetic Fields, New York, N. Y., McGraw-Hill Book Company, 1961, pp. 106-110.

10. G. A. Thiele, op. cit., pp. 16-17.

11. E. C. Jordan and K. G. Balmain, Electromagnetic Waves and Radiating Systems, Englewood Cliffs, New Jersey, Prentice-Hall, Inc., 1968, pp. 517-519.

12. N. N. Wang, J. H. Richmond, and M. C. Gilreath, "Sinusoidal Reaction Formulation for Radiation and Scattering from Conducting Surfaces," IEEE Trans. on Antennas and Propagation, Vol. AP-23, pp. 376-382, May 1975.

13. J. R. Mautz and R. F. Harrington, "Transmission from a Rectangular Waveguide into Half Space Through a Rectangular Aperture," Technical Report TR-76-5, May 1976, Syracuse University, Department of Electrical and Computer Engineering.

14. M. Cohen, T. Crowley, and C. Levis, "The Aperture Admittance of a Rectangular Waveguide Radiating into Half-Space," Antenna Laboratory Report ac 21114 S.R. No. 22, The Ohio State University, 1953.

15. J. R. Mautz and R. F. Harrington, op. cit.

16. R. C. Hansen (ed.), Microwave Scanning Antennas, Vol. II: Array Theory and Practice, Academic Press, New York, 1966, pp. 315-322.

17. A. A. Oliner and G. H. Knittel (ed.), Phased Array Antennas, Artech House, Inc., Dedham, Massachusetts, 1972, pp. 107-112.

18. D. H. Sinnott, "Matrix Analysis of Linear Antenna Array of Equally Spaced Elements," IEEE Trans. on Antennas and Propagation, Vol. AP-21, p. 385, May 1973.

19. G. A. Watson, "An Algorithm for the Inversion of Block Toeplitz," Journal of the Association for Computing Machinery, Vol. 20, No. 3, July 1973, pp. 409-415.

20. A. J. Fenn and G. A. Thiele, "A Moment Method Technique for Probe-Fed Cavity-Backed Slot Antennas," Report 4091-3, March 1976, The Ohio State University ElectroScience Laboratory, Department of Electrical Engineering; prepared under Contract N00014-75-C-0313 for Office of Naval Research. pp. 96-98.

21. P. H. Sinnott, "An Improved Algorithm for Matrix Analysis of Linear Antenna Arrays," Australian Defence Scientific Service, Weapons Research Establishment, Adelaide, South Australia, WRE-TECH. NOTE-1066(AP).

22. N. Amitay, V. Galindo, and C. P. Wu, op. cit., pp. 135-139.

23. Ibid, p. 150.

24. L. Stark, op cit., p. 1670.

25. G. A. Thiele and T. H. Newhouse, "A Hybrid Technique for Combining Moment Methods with the Geometrical Theory of Diffraction," IEEE Trans. on Antennas and Propagation, Vol. AP-23, No. 1, January 1975.

26. B. A. Munk, G. A. Burrell, and T. W. Kornbau, "A General Theory of Periodic Surfaces in Stratified Dielectric Media," Report 784346-1, November 1977, The Ohio State University ElectroScience Laboratory, Department of Electrical Engineering; prepared under Contract F33615-76-C-1024 for Aeronautical Systems Division, Wright-Patterson Air Force Base, Ohio. AFAL-TR-77-219.

27. C. H. Walter, Traveling Wave Antennas, New York, N. Y.; Dover Publications, Incorporated, 1970, p. 22.

28. N. Amitay, V. Galindo, and C. P. Wu, op cit., pp.37-40.

29. A. Papoulis, The Fourier Integral and Its Applications, New York, N.Y., McGraw-Hill Book Company, 1962, pp. 47-49.

30. H. Bateman, "Tables of Integral Transforms," Vol. I, McGraw-Hill, 1954, sec. 1.13 formula (42) for $\nu = 1/2$.

31. A. Papoulis, op cit., p. 15.

32 H. Bateman, op cit., sec. 1.13 formula (42) for $\nu = 0$.

33. Ibid., sec. 1.13 formula (43).

34. R. F. Harrington, Time-Harmonic Electromagnetic Fields, op. cit., p. 450.

35. Ibid.

36. S. M. Selby, CRC Standard Mathematical Tables, 19th Edition, The Chemical Rubber Co., 1971, p. 438.

37. J. H. Richmond and N. Wang, "Sinusoidal Reaction Formulation for Scattering by Conducting Bodies of Arbitrary Shape," Short Course on Application of GTD and Numerical Techniques to the Analysis of Electromagnetic and Acoustic Radiation and Scattering, September 8-12, 1975, Vol. 2, The Ohio State University.

38. S. A. Schelkunoff and H. T. Friis, Antennas Theory and Practice, J. Wiley and Sons, 1952, p. 298, Equation (100) and p. 366, Equation (26).

39. S. A. Schelkunoff, op. cit., p. 366.

40. C. H. Walter, op. cit., p. 22.

41. Ibid, p. 23.

42. Ibid, p.23.

43. D. Castello and B. A. Munk, "Table of Mutual Impedance of Identical Dipoles In Echelon," Report 2382-1, October 1967, The Ohio State University ElectroScience Laboratory, Department of Electrical Engineering; prepared under Contract F33615-67-C-1507 for Air Force Avionics Laboratory, Wright-Patterson Air Force Base, Ohio. (AD 822013)

44. J. H. Richmond, "Computer Analysis of Three-Dimensional Wire Antennas," Report 2708-4, December 1969, The Ohio State University ElectroScience Laboratory, Department of Electrical Engineering; prepared under Contract DAAD05-69-C-0031 for Ballistic Research Laboratory.

45. Z. D. Popovic and B. D. Popovic, "Transformation of Double Integrals Appearing in Variational Formulation of Cylindrical Antenna Problems," publications De la Faculte Dielectrotechnique de L'Universite A. Belgrade, Serie: Electronique, Telecommunications Automatique, No. 64, 1971.

46. M. R. Spiegel, Advanced Mathematics for Engineers and Scientists, McGraw-Hill Book Co., New York, 1971, pp. 127-128.

47. A. Ralston, A First Course In Numerical Analysis, McGraw-Hill Book Co., New York, 1965, pp. 117-119.

48. B. A. Munk, G. A. Burrell, and T. W. Kornbau, op cit., pp. 17-19.

49. S. A. Schelkunoff and H. T. Friis, op cit., p. 366.

50. R. F. Harrington, Time-Harmonic Electromagnetic Fields, op. cit., p. 99.

51. A. J. Fenn and G. A. Thiele, op cit., p. 23.

52. R. E. Collin, Foundations for Microwave Engineering, McGraw-Hill Book Co., New York, 1966, pp. 183-187.

53. R. E. Collin, Field Theory of Guided Waves, McGraw-Hill Book Co., New York, 1960, pp. 258-271.

54. M. Becker, The Principles and Applications of Variational Methods, MIT Press, Cambridge, Massachusetts, 1964, pp. 10-11.

55. R. F. Harrington, Field Computation by Moment Methods, op. cit., p. 18.